Analytical and Numerical Analysis of the Shear Tension Critical Prestressed Beams

Maciej J. Kraczla

Master of Science Thesis

TU Delft Delft University of Technology

Analytical and Numerical Analysis of the Shear Tension Critical Prestressed Beams

Master of Science Thesis

For the degree of Master of Science in Structural Engineering, Concrete Structures at Delft University of Technology

Maciej J. Kraczla

November 14, 2016

Faculty of Civil Engineering and Geosciences · Delft University of Technology

Delft University of Technology
Department of
Structural and Building Engineering, Concrete Structures

The undersigned hereby certify that they have read and recommend to the Faculty of Civil Engineering and Geosciences for acceptance a thesis entitled

Analytical and Numerical Analysis of the Shear Tension Critical Prestressed Beams

by

Maciej J. Kraczla

in partial fulfillment of the requirements for the degree of

Master of Science in Structural Engineering, Concrete Structures

Dated: November 14, 2016

Supervisor(s):

Prof. dr. ir. D.A. Hordijk

Dr. ir. C. van der Veen

Dr. ir. M.A.N Hendriks

Ir. M.A. Roosen

Ir. L.J.M. Houben

Acknowledgements

First of all, I would like to express my sincere gratitude to my direct supervisors, Ir. M.A. Roosen and Dr. ir. M.A.N. Hendirks, for showing genuine interest in the project, for time and energy they dedicated and for providing me with invaluable knowledge whenever it was necessary.

Furthermore, I would like to thank Dr. ir. C. van der Veen who suggested the project that aligned with the primary interest of mine in the field of bridge engineering. Submitting this thesis after several months of work, I still consider it as a really good choice.

I would also like to offer my appreciation to Prof. dr. ir. D.A. Hordijk who has overseen the overall process providing a valuable assistance upon completion of the project.

Finally, I would like to thank my family and friends for their support during this, difficult at times, chapter of my life.

Delft, University of Technology
November 14, 2016

Maciej J. Kraczla

Abstract

Numerous structures constructed in 60's and 70's are now reaching their design service life and require reassessment to assure safety of users, reliability and economical exploitation. As a consequence, an adequate structural assessment of existing bridges has recently become a major subject of scientific work commissioned by the authorities in charge.
The bridges designed according to then biding codes are often deemed to be structurally deficient when re-evaluated with more restricting current design provisions. At the same time, it is often in conflict with the reality as many of the structures still continue in operation displaying no perceptible deterioration of state nor fatigue. The challenge therefore is to develop more refined models to evaluate the structural behaviour and possible reserves of capacity accounting for the actual condition of the bridge under investigation.
One of the potential deficiencies is related to the shear tension failure in thin-webbed post-tensioned T-girders which is the item of the this dissertation. The study comprises of two major parts. In the first part, the thesis investigates an ability of the shear provisions for reinforced concrete structures as given in the following codes: Canadian Standard Association (CSA), the fib Model Concrete 2010 (MC2010), the Eurocode 2 (EC2) and the RBK 1.1 (Richtlijnen Beoordeling Kunstwerken) to adequately address shear tension critical members. The predictions from codes are calculated for the three selected benchmark continuous I-beams tested in destructive laboratory tests as a part of the research on the influence of axial load and prestress on the shear strength of web-shear critical reinforced concrete elements at the University of Toronto. Out of three selected beams of interest subjected to approximately the same prestressing force, two contained a varying amount of reinforcement equal to twice and four times the minimum amount shear reinforcement as specified by the CSA code and one containing no stirrups in the test region. From the comparison of codes it was concluded that shear previsions relating shear resistance to the strain state of the considered section (CSA and MC2010) provide good predictions for members furnished with stirrups but inaccurately evaluate shear resistance for members without shear reinforcement being overly conservative. For this case, the empirical formulation according to the EC2 with mean characteristics applied resulted in the best estimate.
In the second part of the study, an attempt to reproduce the tests of the benchmark beams numerically was undertaken. The simulation according to the highest level of approximation

as classified in the MC2010 was performed through a series of nonlinear finite element analyses. Sensitivity analyses with the diverse variables such as: crack models, shear retention functions, iterative methods and convergence norms were studied to determine their influence on the ultimate shear strength and competence to recreate the observed in tests performance; i.e. the failure mechanism and crack pattern. From the conducted analyses, it was concluded that satisfactory crack pattern as well as magnitudes of shear resistance can be obtained for all treated specimens. The thesis was completed with considerations regarding the most appropriately performing constitutive model to simulate shear tension failure mechanism for the cases of benchmark tests. For the considered cases of shear tension critical beams, models with the rotating crack, energy convergence norm in combination with force or displacement convergence norm and the modified Newton-Raphson iterative method are recommended.

Table of Contents

List of Figures

List of Tables

Chapter 1

Introduction

Following the reconstruction after the Second World War, the Netherlands entered the period of economic expansion with the beginning dated back to 1950s. This prosperous period left a mark on the Dutch infrastructure network. A number of vehicles increased substantially and this consequently triggered a need for enhanced roads network resulting in numerous infrastructural investments. Figure 1-1 shows the growth of the motorway network in the Netherlands (in kilometres). Many of existing nowadays bridges were originated in the 60's and 70's and are located in highways lines. The bridges were design in accordance with then binding standards with a predicted service life of 50 years and hence they are now reaching the end of their working life. Many bridges require reassessment and some rehabilitation to assure safety for users, reliability and economical exploitation. Such reassessment is currently one of the most common project type commissioned by the Ministries of Transportation and Infrastructure in many countries and it is no different in the Netherlands.

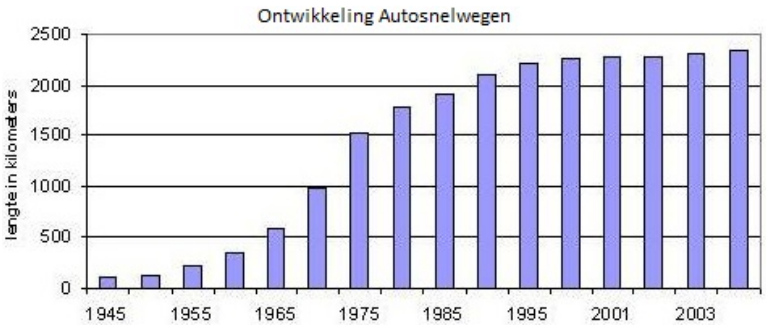

Figure 1-1: Growth of the motorway network in the Netherlands [1]

The common standards cover the procedures for new structures. Because the procedures of assessment of existing structures differ from those for new structures, the existing bridges require often an application of more refined methods. The difficulty lies in a lack of reliability of the actual state of structures and used material properties. In addition, the current standards impose more sever requirements by an application of higher traffic loads and partial safety factors on both action side as well as strength of materials [16]. For these reasons some of existing structures may not meet the requirements of the design for new structures and hence deemed to be structurally deficient. This however may be in conflict with the reality as they may still comply with the performance requirements and be adequate to continue in operation. In this context, the shear strength is one of the major concerns.

1-1 Background information

In many designs, the governing aspect dictating the section dimensions is generally not the shear phenomenon. It is however well known that a shear failure requires special attention. It is a failure mechanism, which comes from a low degree of redundancy in beam elements, is sudden and therefore a minimum amount of shear reinforcement should be provisioned. An element subjected to a certain load can display two types of cracking, namely flexural cracking and shear tension cracking. The cracking occurs when the principal tensile stresses in the considered section exceed the tensile strength of the concrete. The principal tensile stresses act perpendicular/normal to the principal compressive stresses, thus these paths can be a representation of the directions of crack development. Depending on a crack type and aspects contributing the cracks development (a region of crack occurrence, a cross section type and geometry etc.), two main failure mechanisms can be distinguished. *The diagonal tension shear failure* depicted in Figure 1-2a which is originated from the flexural cracks nearest the support (where the shear force is the greatest). The flexural cracks develop into the inclined shear-flexure crack and propagate further till the failure mechanism occurs. As a vast majority of beam elements fail in this manner, it is therefore a very common failure mechanism. The second failure mechanism is related to shear tension cracking, hence called *the shear tension failure*, Figure 1-2b. This very brittle failure type appears in beams with thin webs in regions where shear force is large compared to bending moment (e.g. a point of contraflexure or in a vicinity of a support).
In prestressed concrete members, the prestressing delays the formation of any crack type. Another effect of prestressing is that after tensile stress σ_1 reaches the tensile strength of concrete, the crack tend to be more inclined to horizontal. In an ordinary reinforced element such behaviour would be advantageous for the shear strength as a higher number of shear links cross the crack and is involved in load carrying. Nevertheless, for poorly reinforced against shear forces elements the effect of prestressing has yet to be examined.

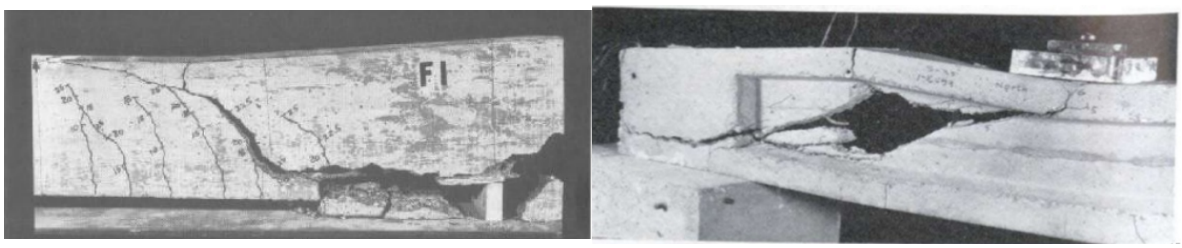

(a) Diagonal flexure-shear failure

(b) Web shear failure in tension shear

Figure 1-2: Typical shear failure mechanisms of reinforced concrete

1-2 Aim of the Study

In the past in the Netherlands about 150 bridges were built with post-tensioned T girders. The design was developed according to the RVB 1962 and RVB 1967 standards. When compared with ECs in which the traffic loads are increased and the partial safety factors are applied, there is a possibility that the old bridges do not meet reliability requirements. In order to evaluate the factual shear capacity, it is necessary to have a refined method accurately

assessing the shear resistance at hand. The objective of this thesis is therefore to investigate which of the available shear provisions is able to evaluate the tension shear critical the most accurately.
The benchmark beams used in this study serving as an indicator of the models correctness are thin-webbed reinforced concrete I-beams subjected to the destructive laboratory test at the University of Toronto. The research was conducted to investigate the influence of an axial load and prestressing on the shear resistance of web-shear critical reinforced concrete elements. The methods used in that research were the shear provision from American Concrete Institute (ACI) and Canadian Standard Association (CSA) which are two major models for shear design commonly applied in North America. The results of the experimental research indicated that the CSA code provides better predictions for shear strength of the web-shear critical reinforced concrete members subjected to combined axial force and shear force than the ACI code [13]. Consequently, the ACI code will not be treated in this study. For the sake of a better comparison, the analytical solution in this study employs three additional standards: the Eurocode 2 (EC2), the fib Model Code for Concrete Structures 2010 (MC2010) and the RBK 1 (Richtlijnen Beoordeling Kunstwerken). The analytical solution will be computed using parameters of the members tested in the PhD dissertation (hence the as-built dimensions and mean material properties) and validated with the test results. The scope of the study includes also numerical analysis on models of beams LB6, LB10 and LB11. In this part, an ability to implement numerical methods to simulate the tension shear failure and their compatibility with the results of destructive laboratory tests are investigated.

1-3 Outline of the Study

The report contains five principal parts:

1. Literature study (Chapter 2)
2. Description of the experimental study of the benchmark beams conducted at the University of Toronto (Chapter 3)
3. Analytical analysis (Chapter 4)
4. Numerical analysis (Chapter 5)
5. Conclusions and recommendations (Chapter 6)

The intention of the first part is to familiarize the reader with general aspects related to shear in concrete structures i.e. cracking and shear transfer after cracking. Moreover, the background of the applied shear provisions is introduced and thoroughly explained (the RBK 1.1 is excluded from the consideration, yet applied in the second part of the report). In the subsequent chapter, the experimental research on the influence of axial force and prestressing on the web-shear critical beams is summerized. The summary pays special attention to the post-tensioned beams LB6, LB10 and LB11 containing a varying amount of shear reinforcement across the tested span. The approaches demonstrated in the foregoing Chapter 2 are implemented in Chapter 4 with mean values of material properties applied. Such a measure is undertaken due to the predictions of the factual shear resistance being of the primary interest

rather than the design or characteristic resistances. The results are collated and compared to support a conclusive recommendation regarding the most appropriate approach (under given circumstances). Last but not least, an attempt to reproduce the experimental results from the test site using finite element analysis is made in Chapter 5. The objective of this part was to study different shear behaviours (crack models and shear retention functions) within the total strain based crack model by means of variable iterative procedure configurations. The report is concluded with a summary of the results and observations and further research recommendations.

Chapter 2

Literature Study

In design of structural elements for moment and axial loads, engineers can make use of available general and rational method called the "plane sections" theory. With this method it is possible to predict both the flexural strength and the complete load-deformation response of reinforced concrete elements. The theory has proved its validity and therefore there is little disagreement in different design codes on the design of the flexural strength or the required amount of reinforcement needed to ensure ductile flexural behaviour [17]. In contrast to flexure, there is substantial disagreement on how to design reinforced concrete members to ensure ductile shear behaviour. Over the years different methods have been proposed. Upon the lack of universally agreed model for shear behaviour, codes of practise propose complex, restricted or purely empirical equations for estimation of shear strength. In addition to that they tend to be conservative imposing more sever safety requirements which leads to their inapplicability for evaluation of existing structures. An ability to adequately address shear resistance of existing bridges which are often deemed to be structurally deficient emphasized the need for more suitable shear design provision and triggered more researches on this subject.

Good understanding of shear behaviour of concrete structures is essential to properly design members against shear failure. Therefore, this section will provide a reader with general information about shear. A review of shear design in codes of practise further used in the analytical solution will be introduced and explained. Although the shear problems in this chapter will be treated globally, it should be borne in mind that the web-shear failure constitutes the key interest of this study.

2-1 Cracking in concrete

In Figure 2-1 a small segment at the level of neutral axis of a beam subjected to certain loading is illustrated. From the vertical equilibrium, there appear to be two vertical opposite stresses acting on either side of the segment which tend to rotate the segment clockwise. To prevent from this rotation and to obtain the overall equilibrium, two additional balancing stresses are required on horizontal faces of the segment. The forces corresponding to those four stresses

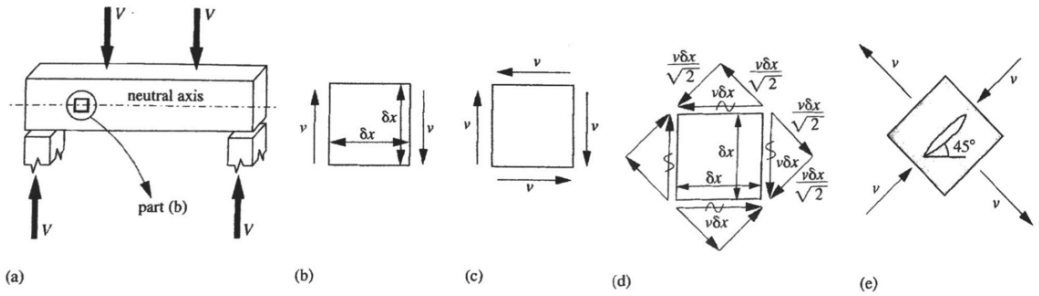

Figure 2-1: Stress in a segment of concrete; a) a beam subjected to four point bending; b) and c) shear stresses in a concrete segment; d) stress resolution; e)stresses in the principal directions [2]

can be resolved into components at the 45 degrees angle as depicted in Figure 2-1(d). Now, it can be observed that a total compressive force $\sqrt{2}v\delta x$ in one direction and a total tensile force of the same magnitude in the other. These forces divided by the length on which they are acting, which is the diagonal of the segment $\sqrt{2}\delta x$, result in stresses $\sqrt{2}v\delta x/\sqrt{2}\delta x = v$. Such stresses are called the principal stresses and are of great importance as far as cracking is concerned. The principal stresses therefore are defined as the normal stresses on the face oriented in such a way that shear stress vanishes. From 2-1(e) it can be seen that such tensile stresses are a cause of the crack at 45 degrees to the horizontal. It is important to note that cracking occurs when the principal tensile stresses exceed the tensile strength of concrete. For the segments not in line with the neutral axis, additional axial stresses as a result of bending moment should be accounted for. Also for prestressed members, axial stresses have an impact on diagonal cracking.

First type of cracking called web-shear cracking occurs in a section where shear stresses prevail. It is not a very common type of cracking but can appear in sections near a point of contraflexure which is where bending moment is negligible and shear force predominates or in members with thin webs and a limited amount of shear reinforcement (often considered as elements without shear links) such as for example T or I girders. The distinctive features of this type of cracking are cracks propagating from the level in a close proximity of the neutral axis. Another type of cracking is called flexural cracking. For the segment located at the bottom of a member, shear stress in an extreme bottom fibre equal 0 while bending normal stresses have the maximum value. As a result, the principal stresses act normal to the vertical plane. It was previously shown that there exist two limits. For the segment at the level of neutral axis (for 0 bending stress and the maximum shear stress) crack inclines at the angle of 45 degrees, Figure 2-2(b) while for pure bending stresses and the extreme bottom fibre a crack appears at the angle of 90 degrees. In the segment between the neutral axis and the bottom of the member, a combination of bending and shear stresses is acting on the element and therefore the crack will develop with an inclination of between 45 and 90 degrees, Figure 2-2(d). At any point/segment of a beam, an inclination of principal stresses can be determined through the Mohr's Circle. It can be well represented by means of stress paths through the member, Figure 2-3, where the dashed lines are the trajectories along which cracks will tend to develop. It is clear that the inclination of the crack will decrease towards the neutral axis as the shear stress become larger and the axial stresses from bending approach 0. The stress paths however are only an indication and it is by no means in agreement with the crack patterns developed in practice. Such a model does not account for many aspects such as for

example redistribution of the shear stresses which occurs when cracks are formed.

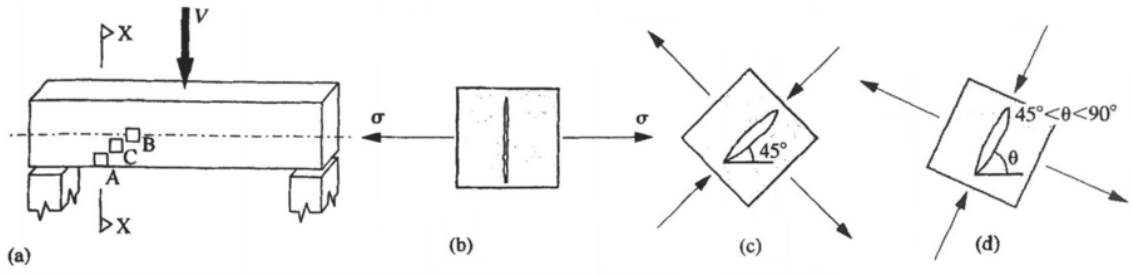

Figure 2-2: Principal stresses in individual locations a) beam with segments' locations; b) segment A principal stress; c) segment B; d) segment C [2]

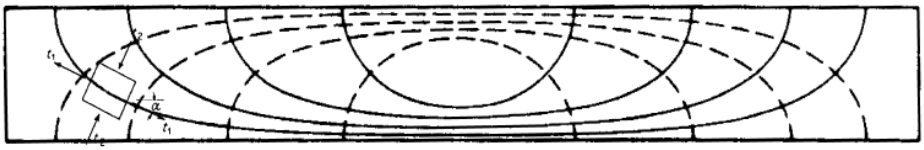

Figure 2-3: Principal stress trajectories

From the stress paths in Figure 2-3, one can see that for a member in shear and bending, the cracks are curved with a slope ranging from 45 at the neutral axis – pure shear, to 90 degrees at the extreme fiber due to pure bending. This form of cracking is called shear-flexure cracking. The vast majority of reinforced and prestressed members crack in flexure so before the tensile stresses at the neutral axis exceed the tensile strength of concrete. It is thus the most common type of cracking and in the most severe cases a cause of failure [2].
The advantage of prestressing concrete members is a reduction or elimination of tensile stresses at the serviceability limit state. At the ultimate limit state, when the applied loads are significantly larger, the tensile principal stresses can reach the tensile strength of concrete resulting in cracks. Nevertheless, the benefit of prestressing is that the load at which cracking forms is increased. Prestressing has also an influence on the angle of crack formation and a crack width. In Figure 2-4, the chosen segment B at the centroid from Figure 2-2 subjected to horizontal compression stresses and shear stresses due to applied loading is considered. The effect of prestressing can be explained using a simple Mohr's circle. When the segment B is subjected to pure shear τ, the principal tensile stresses act at 45 deg. When the axial force is not equal zero the reduction of principal tensile stress occurs. In addition, if the crack materialize its inclination is flattened and forms at the angle between 0 and 45 degrees. The lowered angle has in general a beneficial effect on the shear strength of members because the crack is such a situation crosses a higher number of shear links thus effectiveness of transverse reinforcement is increased. Please note that in case of I-beams the maximum principal tension may not occur at the controidal axis where the shear stress is the greatest but instead,it may arise at the flange-web junction. In this location shear stresses are slightly lower but the crack formation is aided by external bending.

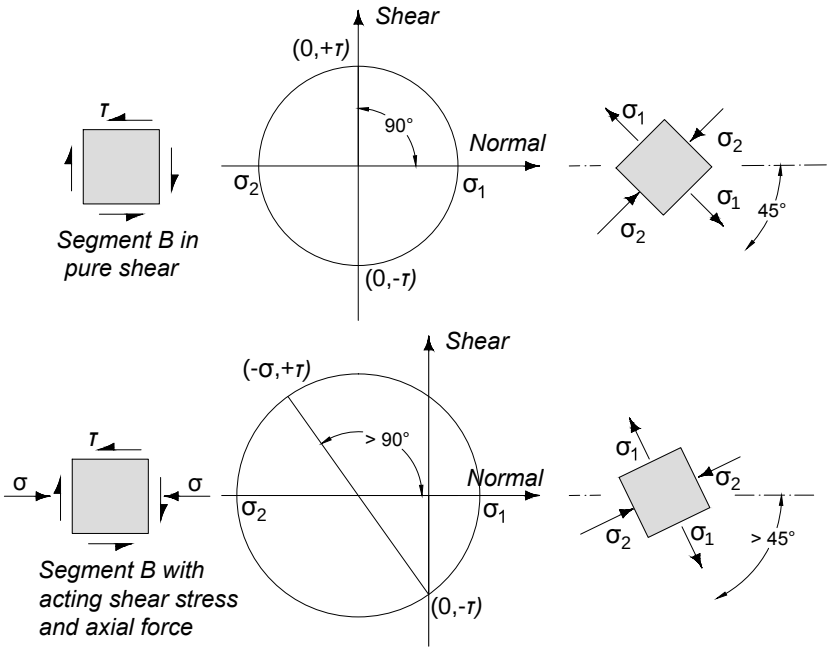

Figure 2-4: Effect of prestress on an angle of principal stresses in a beam; reproduced from [3]

2-2 Mechanism of Shear Transfer After Diagonal Cracking

Prior to cracking of concrete, shear in the beam's web is carried by diagonal compressive stresses at a certain angle of inclination complemented with perpendicular to them diagonal tensile stresses. The steels bars (if present) have a negligible effect on the behaviour of reinforced concrete element. For such a concrete element (without inclusion of steel bars), the principal stresses coincide with the applied principal stresses. Once the tensile strength of concrete is reached, cracks form and the ability of concrete to transmit principal tensile stresses is substantially reduced (for the cracks width greater than 0.05 mm significant transmission does not occur [18]) and unless a member is sufficiently reinforced, failure may develop. The purpose of such reinforcement is therefore to carry shear. In the case of an element reinforced with a different amount of reinforcement in two directions, the principal coordinate of the concrete element will deviate from the applied principal stresses coordinate of the RC element. The deviation will increase under the shear stress increase until the maximum angle is reached which relates to the yielding of the steel [9]. To elaborate further the mechanism, a reference to the possible stress fields given in the [4] can be made. The stress fields depicted in Figure 2-5 are related to the behaviour of reinforced concrete before and after a crack onset. Before cracking the principal stresses in both compression and tension are equally engaged in resisting the shear. After cracking however, under the assumption that tensile stresses in concrete decline to zero, the concrete diagonals have to take over the part previously carried by principal tensile stresses, thus principal compressive stresses double in the value. If the beam is appropriately reinforced, the imbalance is redistributed with longitudinal reinforcement in tension balancing the longitudinal component of the diagonal compression and the web reinforcement balancing the transverse component of the diagonal compression Figure 2-5 (b).

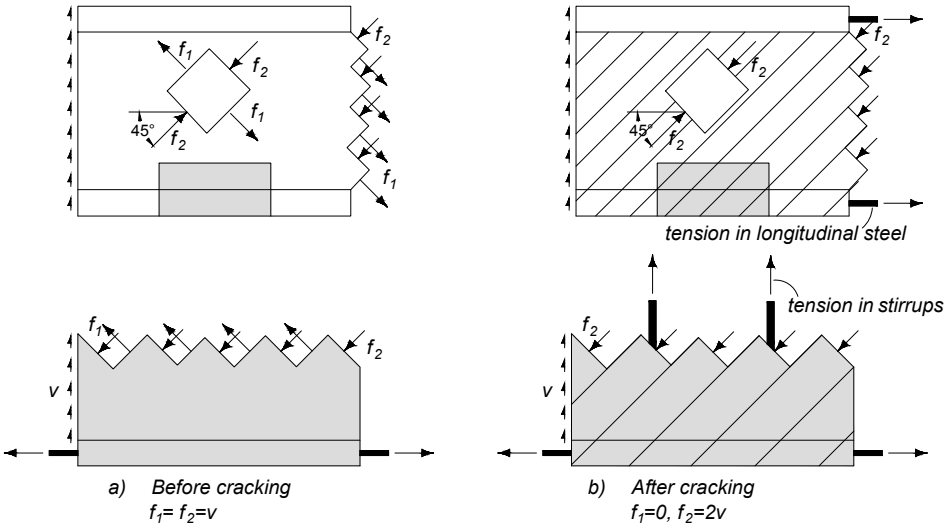

Figure 2-5: Stress field before and after cracking in a reinforced element; reproduced from [4]

In normal strength concrete, the strength of aggregates is typically higher than the strength of harden cement paste. In the system consisting of the aggregate particles and the matrix, the interface between cement and aggregate (the interfacial transition zone of high porosity) is normally regarded as the weakest link [19]. Because of this, the cracks cross the cement paste but instead intersecting further the aggregate particles, the cracks propagate along the edges of the particles creating a rough surface, Figure 2-6 [5]. Such protruding aggregates, by means of interlocking one another, generate shear stresses when the relative tangential displacement occurs [20]. This is however only true for regular or low strength concrete. The capacity of aggregate interlock is reduced for concretes with lightweight aggregate and high strength concrete. In the lightweight concrete, as the result of the low strength of aggregate, the crack runs through the particles. Similarly in the later case, due to the high strength of concrete, the crack proceeds through the matrix as well as the aggregate particles. Another load carrying mechanism is dowel action of longitudinal reinforcement. It is defined as an ability of reinforcing bars to transfer forces in the direction perpendicular to their axes. The dowel action occurs upon a crack surface slip which is counteracted by crossed reinforcement. Lastly, the shear can be carried in the uncracked compression zone of a member.

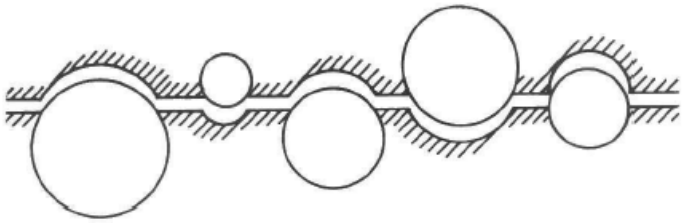

Figure 2-6: Crack surface in cracked concrete [5]

2-3 Shear Models

2-3-1 The 45 Degree Truss Model

The first truss model with parallel chords was proposed by Ritter. The truss is composed of diagonal compressive struts inclined at the angle of 45 degrees, the transverse tension ties, the top compression chord and bottom tension chord. Later in 1902, the model with discrete diagonal compressive struts was undermined by Mörsch who claimed that the diagonal compression is transferred through a continuous field resisting shear. The 45-degree model comprises of three assumptions: the tensile stresses in the cracked concrete are neglected; the diagonal compression stress coincides with the crack angle and after cracking the angle remains at 45 degrees; the contribution of the top and bottom chords in resisting shear is neglected and shear stressed are uniformly distributed over an effective shear area ($b_w * d$).

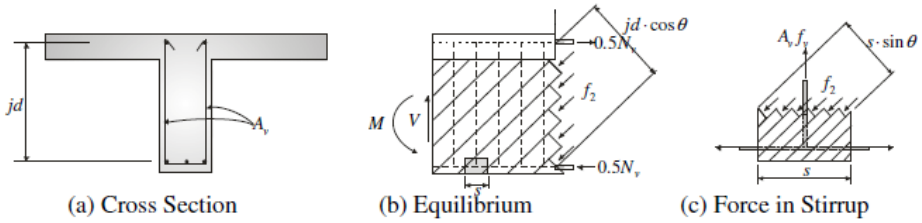

Figure 2-7: Free body diagram for the equilibrium derivation [6]

From the 2-7 (b) and (c), it can be seen that the total diagonal compressive force, f_2:

$$f_2 b_w d/\sqrt{2} = \sqrt{2}V \quad \text{thus} \quad f_2 = 2V/b_w d \tag{2-1}$$

The vertical component of the diagonal compressive force $f_2 b_w s/\sqrt{2}$ in Figure 2-7(c) has a vertical component equal $f_2 b_w s/2$ which has to be balanced by the force in stirrups. Substituting f_2 from equation 2-1 to $f_2 b_w s/2$ gives:

$$\frac{A_v f_v}{s} = \frac{V}{d} \tag{2-2}$$

with $A_s f_v$ being the cross-sectional area of stirrups and tensile stress in the stirrups. The additional force in the longitudinal reinforcement due to shear is:

$$N_v = V \tag{2-3}$$

With the equation 2-1 the compressive stress in the web can be checked while the equation 2-2 enables to determine the required areas and spacing of stirrups. The 45 degrees angle of inclination, which was also recognized by Mörsch, gives conservative estimations because in the members containing usual amounts of shear reinforcement the shear cracks form at the angle much smaller angle. In addition, for members with a little amount of reinforcement, the contribution of concrete is far from negligible.

2-3-2 Variable-Angle Truss Model

The variable-angle truss model is based on the same rules as the previous truss model. To account for the fact that the angle θ is typically less than 45 degrees for some cases, such as e.g. prestressed members, the model was modified. In a similar manner, for the equilibrium in Figure 2-7, the equations for the principal compressive stress 2-4, the tensile force in the longitudinal reinforcement due to shear 2-5 and the tensile force in the stirrups 2-6 can be derived:

$$f_2 = \frac{V}{b_w d \sin\theta \cos\theta} = \frac{V}{b_w d}(\tan\theta + \cot\theta) \tag{2-4}$$

$$N_v = A_l f_l = V \cot\theta \tag{2-5}$$

$$A_v f_v = f_2 b_w s \sin^2\theta \quad \text{or subtituting for } f_2 \quad \mapsto \quad \frac{A_v f_v}{s} = \frac{V}{d}\tan\theta \tag{2-6}$$

For the given shear load, there are four unknowns (i.e. the principal compressive stress f_2, the tensile force in the longitudinal reinforcement N_v, the stress in the stirrups f_v and the inclination of the principal stresses θ) and only three equilibrium equations. To solve the problem, two plasticity-based methods have been developed. The plasticity-based methods are referred as the approaches which consider the mechanism of failure to solve a set of equations 2-4, 2-5, 2-6. The first of these methods, assumes that in the ultimate limit state the stirrups yield and the concrete in compressive diagonals reaches an effective concrete compressive strength [4]. With these assumptions, V and θ can be found by solving simultaneously equations 2-4 and 2-6. In the second approach, it is assumed that both the longitudinal and transverse reinforcement yield and subsequently with (2-5–2-6), V and θ can be determined. The recommended effective concrete compressive strength is $0.6f_c^{'}$.

2-3-3 Compression Field Theory and Modified Compression Field Theory

Compression Field Theory

The Compression Field Theory is a smear crack continuum mechanics modelling approach [6] in which cracked concrete is treated as a new material with its own stress-strain characteristics. The word smeared in this context refers to the strains expressed in average terms thus the strains are smeared over a base lengths equal at least the crack spacing. The formulation of the approach comprises of the equilibrium equations of external forces with internal forces, the compatibility equations relating strains in the reinforcement and strains in the concrete and lastly the constitutive relationships linking the average strains and average stresses for the reinforcement and concrete. The equilibrium conditions result from balancing the applied external forces on a RC element and stresses arose in the concrete and the reinforcing steel. The sum of the forces in each direction and shear forces equals to zero. The compatibility conditions assume that (provided that steel is properly anchored in the concrete and the rebars are perfectly bonded) the deformation of concrete is accompanied by an identical deformation in the reinforcement. The same condition applies to strains in the reinforcement and concrete. In the second assumption, the angle of inclination of the principal stresses coincides with the angle of inclination of the principal strains hence it is a rotating crack concept. The compatibility conditions are essentially derived from the three compatibility equations of the rotating angle theories which are fully elaborated in [9]. The stress-strain relationship of the concrete in e.g. a cracked web of a beam differs from the relationship

obtained with standard compression tests on a concrete cylinder. Therefore in the CFT, depending on the actual strain condition to which concrete elements is subjected, the "new" stress state is calculated. Moreover, the diagonally cracked web is subjected to significant tensile strains which in turn results in the concrete being weaker and softer than the concrete in a cylinder in which the only existing tensile strains come from Poison's effect [4]. Such a detrimental impact of the principal tensile strains on the stiffness and strength of concrete in compression is called compression softening [6]. It can be seen in Figure 2-13 (h) stress-strain relationship for concrete in compression that principal compressive stresses f_2 are indeed a function of the corresponding principal compressive strain ε_2 as well as the principal tensile strain ε_1 and that the principal tensile strain decreases the maximal concrete strength. In conclusion, employing the equilibrium, compatibility and constitutive relationships of CFT enables determination of the complete load-deformation response of a member subjected to shear.

Modified Compression Field Theory

The compression field theory assumes that after concrete has cracked, the principal tensile stress is equal to zero. For this reason, CFT overestimates deformations and provides conservative results. In reality, which was found by Vecchio and Collins in the tests on RC panels subjected to pure shear, the residual tensile stresses exist in the concrete between two adjacent cracks which in turn can significantly contribute and increase the ability of concrete to resist the shear. It essentially means that shear after cracking is not carried solely by reinforcement but instead by a combination of the concrete and steel contributions (concrete stiffening). To account for this, the Modified Compression Field Theory was developed which explicitly considers a residual post-peak tensile capacity of reinforced concrete.

The mechanism of the shear transfer in a panel subjected to shear is shown in Figure 2-8 (b)

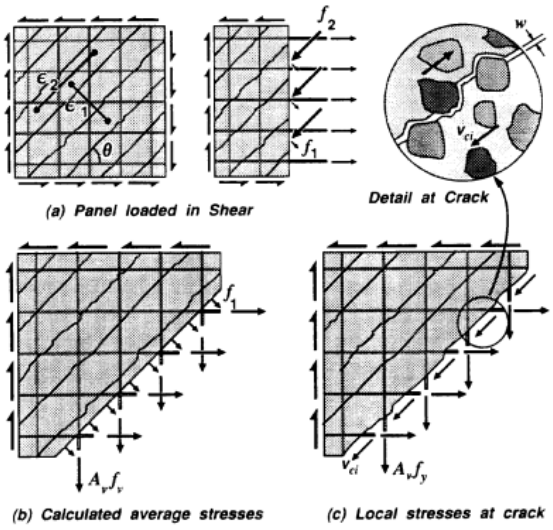

Figure 2-8: Reinforced concrete panel subjected to shear [7]

and (c) – average stresses between the cracks and local stresses at the crack location respectively. These two sets of stresses are statically equivalent (their resultants are equal). Because of this, the stresses between two sets impart. It means that the loss of tensile stresses in the concrete at the crack location must result in an increase of steel stresses at the crack or, when

the reinforcement yielded due to excessive stresses in shear stresses on the crack interface (aggregate interlock) .The effectiveness of such a shear transfer across the crack depends on the crack width [7].
It was already mentioned that the CFT considers the "actual" strain state. So does the MCFT. In [7], it is explained that the average principal tensile strain ε_1 in the cracked concrete serves as a "damage indicator" that controls the average tensile stress f_1 in the cracked concrete (eq. 14 Figure 2-13), the ability of the diagonally cracked concrete to carry compressive stresses f_2 (eq. 13 Figure 2-13), and the shear stress that can be transmitted across the crack v_{ci} through relating it to the crack width (eq. 9 and 15 Figure 2-13).
The stress-strain relationship for concrete in tension can be seen in Figure 2-13 i). The average tensile stresses after cracking can be calculated from the equation (14) in this figure. This expression is related to the second branch (tension softening due to the gradual loss of concrete integrity) of the stress-strain diagram Figure 2-13 (i). For the substantial values of the principal tensile strains, the average tensile stress f_1 is limited by the yielding of the reinforcement at the crack and shear stress v_{ci} on the crack that can be transferred across cracks. The maximum shear stress v_{ci} that can be transmitted across the crack was defined from the experimental test data of Walraven and is expressed with the equation 15 in Figure 2-13. It is a function of crack width w and the aggregate size a. The third branch of the Figure 2-13 (i) describes the limit value of f_1 against "crack slipping failure" which is when stirrups have reached the yield stress and the shear transfer depends on the aggregate interlock according to [7]:

$$f_1 = v_{ci} \tan\theta \tag{2-7}$$

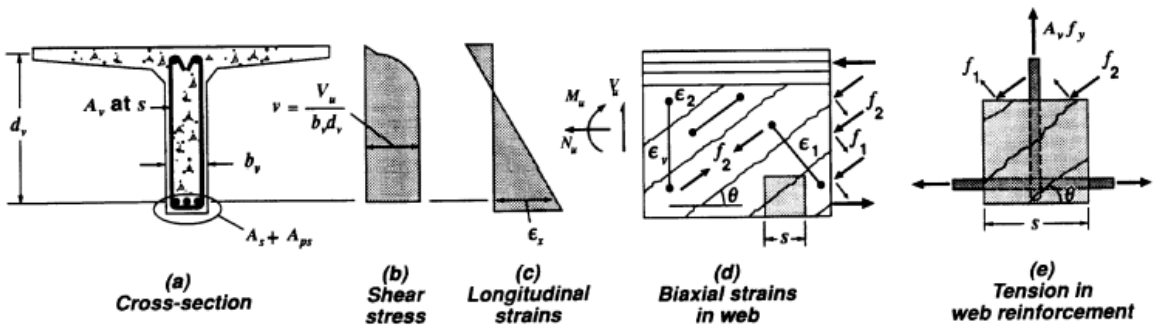

Figure 2-9: Beam subjected to shear, moment and an axial load [7]

The nominal shear strength given with:

$$V = V_c + V_s + V_p = f_1 b_w d_v cot\theta + \frac{A_v f_v}{s} d_v \cot\theta + V_p \tag{2-8}$$

Equation 2-8 is derived from the average stresses equilibrium (Equation (3) in Figure 2-13) in the form of $f_2 = v(\tan\theta + \cot\theta) - f_1$ substituted into the expression for the unbalanced vertical component that must be taken over by the stirrups(Figure 2-9 (e)):

$$A_v f_v = (f_2 sin^2\theta - f_1 cos^2\theta) b_w s \tag{2-9}$$

Combining Equation 2-8 with the expressions for the aggregate interlock the nominal shear resistance can be written as:

$$V = \beta\sqrt{f'_c} b_v d_v + \frac{A_s f_y}{s} d_v \cot\theta + V_p \tag{2-10}$$

Where:

$$\beta = \frac{0.33 \cot \theta}{1 + \sqrt{500\varepsilon_1}} \leq \frac{0.18\sqrt{f'_c}}{0.3 + \frac{24w}{a+16}} \tag{2-11}$$

The MCFT procedure to calculate the concrete tensile stress factor β and an angle of struts inclination θ is iterative and can be adopted for hand calculations provided that some simplifying assumptions are made. Due to the fact that under a combination of shear and moment longitudinal strain ε_x varies over the depth of the section, the angle of inclination θ also varies being steeper in a tension zone and flatter in a compression zone. In Figure 2-9 (b) the shear stresses are shown. They are assumed to be uniformly distributed over the effective depth. Moreover, the stresses and strains are considered at only one level and the longitudinal strain ε_x at this level is used to determine an angle θ which is assumed to remain the same over the whole depth of the web [4]. The determination of the longitudinal strain is illustrated in Figure 2-10. While it is conservative to compute the longitudinal strain in the

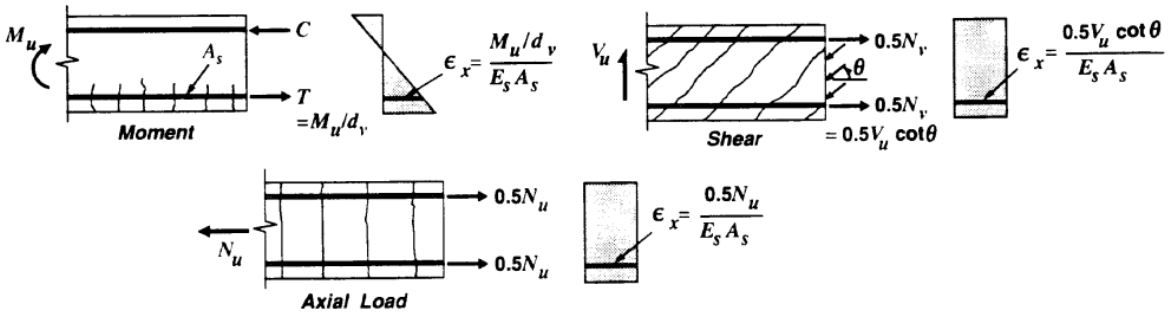

Figure 2-10: Determination of strain ε_x for nonprestressed beam [7]

level of longitudinal reinforcement (increased ε_x will result in decrease of the shear capacity), the members with shear reinforcement are considered to have an ability to redistribute shear stresses from the locations where strains are the greatest to the location less highly strained. Because of this redistribution, [4] suggests that it is reasonable to use the longitudinal strains at the mid-depth of the web. Members without web reinforcement have a limited capacity to redistribute the stresses hence the longitudinal strains should be taken as the strain in the flexural tension reinforcement:

$$\varepsilon_x = \frac{M_u/d_v + 0.5N_u + 0.5V_u \cot\theta - A_{ps}f_{po}}{E_s A_s + E_p A_{ps}} \tag{2-12}$$

The formula above considers a member with applied prestressing and the reinforcement on the flexural tension side of the member. For the case where the longitudinal strains are considered at the mid-depth level, the denominator should be multiplied by the factor of two. In Equation 2-12, the stiffness of the concrete, for strains larger than zero, is not taken into account. It is reasonable for the sections in tension. When however a section in compression is treated, exclusion of the concrete stiffness would overestimate calculated strains (strains are negative when in compression). For this reason, for the compressive strains, the MCFT takes conservatively ε_x as equal to zero. Because the nominal strength is dependent on the "damage indicator" ε_1, it is ε_1 where the remaining strains should be related to. Through the average strain compatibility, equations (6) and (7) Figure 2-13, the following can be obtained:

$$\varepsilon_1 = \varepsilon_x + (\varepsilon_x - \varepsilon_2)\cot^2\theta \tag{2-13}$$

Including further (3) Figure 2-13 conservatively taken as:

$$f_2 = v(\tan\theta + \cot\theta) \tag{2-14}$$

and the equation (13) Figure 2-13 assuming that at the peak stress the compressive strain is $\varepsilon_c^{'}$ 0.002, the principal tensile strains can be expressed as:

$$\varepsilon_1 = \varepsilon_x + \left[\varepsilon_x + 0.002\left(1 - \sqrt{\frac{v}{f_c'}(\tan\theta + \cot\theta)(0.8 + 170\varepsilon_1)}\right)\right]\cot^2(\theta) \tag{2-15}$$

With a known value of ε_1 and an angle of inclination θ, the tensile stress factor β can be calculated as shown in Equation 2-11. To further simplify calculations, the method provides an engineer with a table with use of which, the values of β and θ for calculated $v/f_c^{'}$ and ε_x can be obtained. The values of θ in the table were derived assuming crack spacing of 300mm and were chosen to ensure that stirrups yield and crushing of the concrete struts do not occur. The procedure of the shear design along with solved examples is given in textbook [4].
As far as members without shear reinforcement are concerned, the shear strength is governed by the crack width calculated with Equation 9 Figure 2-13. Where no stirrups were provided, the crack spacing is larger and so is the crack width, Figure 2-11. Therefore, following the

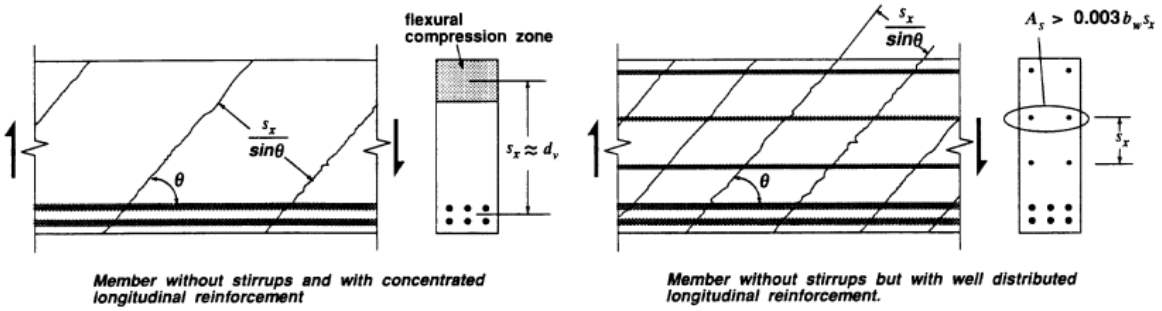

Figure 2-11: Assumed determination of spacing for members without shear reinforcement [7]

above instructions (for members with shear reinforcement) would result in an overestimation of the shear strength. The maximum shear capacity i.e. the largest value of β can be obtained by setting the concrete shear resistance V_c:

$$V_c = \frac{0.33\sqrt{f_c'}}{1 + \sqrt{500\varepsilon_1}}\cot\theta b_v d_v \tag{2-16}$$

to the value limiting the ability of diagonal cracks to transmit the shear stress:

$$V_c \leq \frac{0.18\sqrt{f_c'}}{0.3 + [24/(a+16)](\varepsilon_1 s_x/\sin\theta)} b_v d_v \tag{2-17}$$

After rearranging, the angle at the maximum shear can be found with:

$$\theta = \tan^{-1}\left(\frac{0.568 + 44\varepsilon_1 s_x/[(a+16)\sin\theta]}{1 + \sqrt{500\varepsilon_1}}\right) \tag{2-18}$$

Finally, the principal tensile strain is calculated from the equation (13) Figure 2-13, eq. 2-16 and noticing from the Mohr's circle that $f_2 = v \cot\theta$, thus:

$$\varepsilon_1 = \varepsilon_x(1+\cot^2\theta) + 0.002\left(1-\sqrt{1-\frac{0.33\cot^2\theta(0.8+170\varepsilon_1)}{\sqrt{f_c'}(1+\sqrt{500\varepsilon_1})}}\right)\cot^2\theta \tag{2-19}$$

With ε_x calculated at the level of the longitudinal reinforcement in the flexural tensile part. An iterative procedure explained in [21] is necessary to determine ε_x, ε_1 and θ. In order to simplify the calculation, Collins and Mitchell tabulated the solutions of Equations 2-18 and 2-19 in a form of a table for the concrete compressive strength $f_c^{'} = 35MPa$ and a=19mm with variable ε_x and a crack spacing s_x. It is explained in [21] that the solutions are not strongly influenced by concrete strength and can be corrected for a different aggregate size hence can be used for all designs of members without shear reinforcement. It is important to mention that the size effect plays an important role. The crack spacing will increase as the member size increases resulting in a reduced shear strength.

In the members subjected to shear, the shear force causes the additional tension in the longitudinal reinforcement in the flexural tensile side. For a considered section with no bending moment such as e.g. the section near the support, Figure 2-12, the tensile force that is generated by shear is (the contribution of the aggregate interlock is assume to be negligible):

$$T = \left(\frac{V_u}{\phi} - 0.5V_s\right)\cot\theta \tag{2-20}$$

For sections subjected to combined shear force, bending moment and an axial force, to avoid yielding of the longitudinal reinforcement on the flexural tension side, the following relation must be satisfied:

$$A_s f_y + A_{ps} f_{ps} \leq \frac{M_u}{\phi d_v} + 0.5\frac{N_u}{\phi} + \left(\frac{V_u}{\phi} - 0.5V_s - V_p\right)\cot\theta \tag{2-21}$$

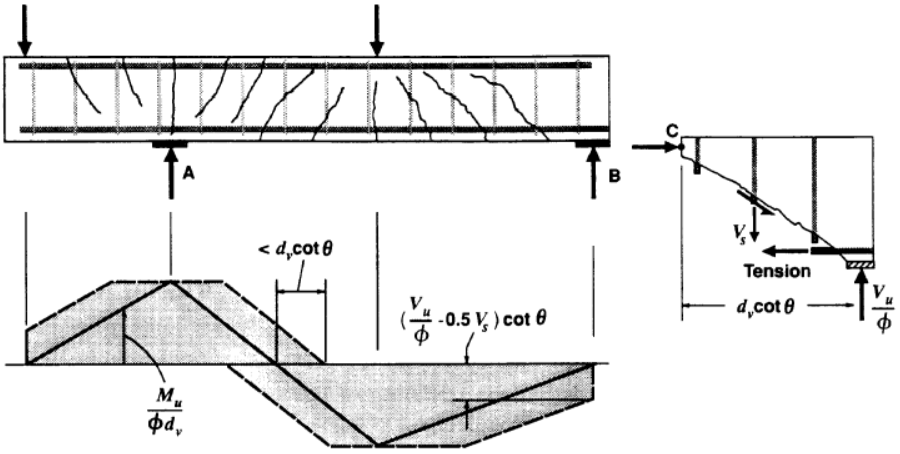

Figure 2-12: Influence of shear on forces in the longitudinal reinforcement [7]

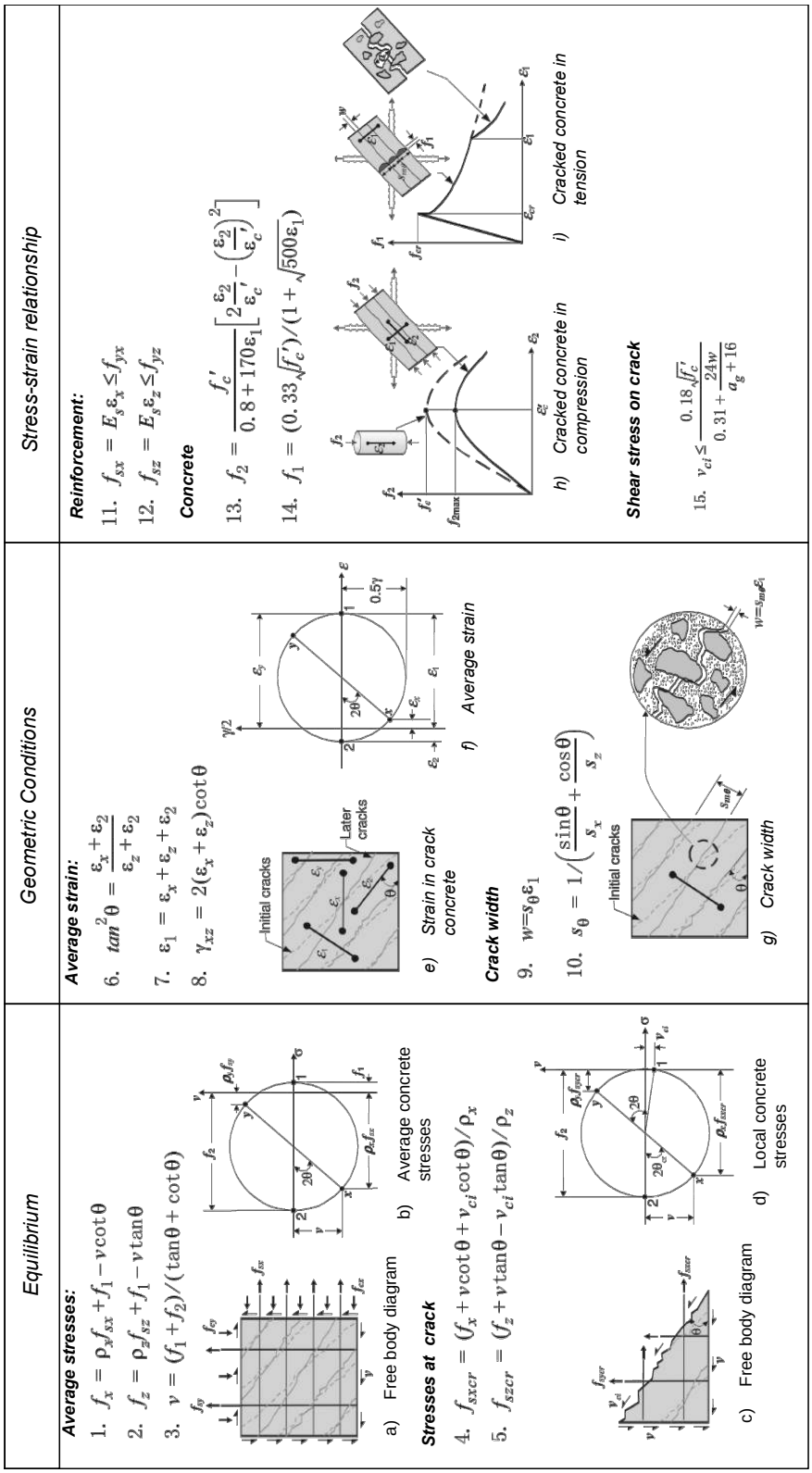

Figure 2-13: Description of Modified Compression Field Theory

2-4 Codes of Practice

In the previous section, a general background of the shear transfer mechanisms before and after cracking was briefly explained. Moreover, different approaches such as the variable strut inclination approach and the MCFT were introduced. This will further serve better understanding of how these approaches were adapted in the contemporary codes which are treated in this section. The shear provisions according to the following standards are of interest: Eurocode 2, fib Model Code 2010, the 2004 Canadian Standards Association A23.3 and RBK 1.1.

2-4-1 Eurocode 2

Prestressed Members Without Shear Reinforcement

While considering a prestressed element without shear reinforcement two main regions should be distinguished. Depending on the region, the EC2 suggests different measures. The first region (called here the area A in Figure 2-14) is largely uncracked in flexure (high V, small M) with a failure location near the beam supports. The criteria for the determination of the shear capacity are permissible tensile stresses in the principal direction caused by interaction between the compressive stress from prestressing, the shear stress caused by the applied load and stresses due to bending moment. In the EC2, the stresses are designed on the elastic basis. In the region A, Figure 2-14, cracks originate in the web where principal tensile stresses exceeded the concrete tensile strength. In members where no reinforcement is applied, cracking will lead to failure. This type of failure is called tensile splitting shear failure [8]. The second region cracked in flexure is (area B) located away from the supports for a simply supported beam as well as for continuous beams, at the internal supports, where both moderate V and M are present. The shear capacity in regions cracked in flexure is designed based on an empirical formula developed based on numerous tests. The elements are deemed to be cracked in flexure if the flexural tensile stress in the extreme fibre is greater than $\frac{f_{ctk,0.05}}{\gamma_c}$.

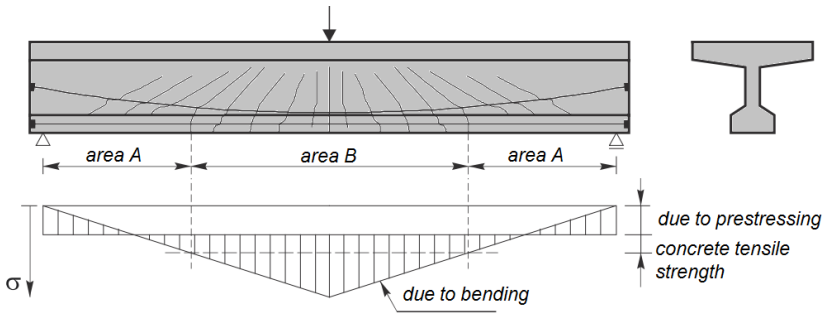

Figure 2-14: Crack pattern in a prestressed beam and the stresses in the bottom part [8]

Region 1

The equation 6.4 from EC2 [22] can be found making a use of the Mohr's circle, Figure 2-15 [9] – formula for the stress σ_I in the principal direction equated to the concrete tensile strength and the expression for shear stresses in a considered section.

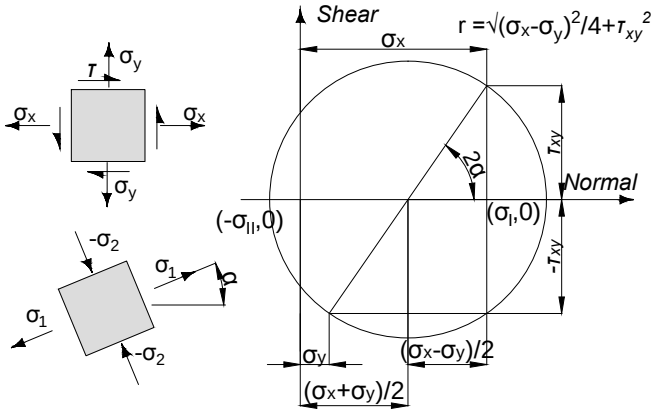

Figure 2-15: Graphical expression of principal stresses; [9]

$$\sigma_I = \frac{\sigma_x}{2} + \sqrt{\frac{\sigma_x^2}{4} + \tau_{xy}^2} = f_{ctd} \tag{2-22}$$

$$\tau_{xy} = \frac{V_{Ed} S_c}{b_w I_c} \tag{2-23}$$

After transformations of the above formulas, the shear tension resistance 6.4 in the EC2 is given as:

$$V_{Rd,c} = \frac{I b_w}{S_c} \sqrt{(f_{ctd}^2) + \alpha_l \sigma_{cp} f_{ctd}} \tag{2-24}$$

in the case of compression σ_x is negative. The formula 6.4 from EC2 $V_{Rd,c}$ can be only applied in prestressed single span members in the regions uncracked in bending. In the members with the width changing over the height, the maximum principal stress should be also checked in the axis other than the centroidal axis. In the equation 2-24, α_l takes into account the transition length; relevant in the case of pre-tensioned elements where the prestressing force is transmitted to concrete by bond. 6.2.2(3) in EC2 provisions that it is not required to calculate the shear resistance for the cross-sections that are nearer to the support than the point which is intersection of the elastic centroidal axis and a line inclined from the inner edge of the support at an angle of 45 degrees.

Region 2

The design value for the shear resistance of the region cracked in flexure (area B in the Figure 2-14) is given by EN 1992-1-1; (6.2.a) and (6.2.b) from [22]:

$$V_{Rd,c} = [C_{Rd,c} k (100 \rho_l f_{ck})^{\frac{1}{3}} + k_1 \sigma_{cp}] b_w d \tag{2-25}$$

The formula takes into account the most relevant factors for the members' shear strength such as the concrete strength, longitudinal reinforcement ratio and a height of the cross section. It can be seen that the expression 2-25 also takes into account effect of prestressing. It origins from the assumption that the shear behaviour of a prestressed beam can be regarded as a reinforced beam after decompression moment (bending moment that reduces stresses from prestressing in a beam to zero) has been reached; thus:

$$V_{Rd,c} = V_c + V_p \tag{2-26}$$

where V_c is the shear resistance of a non-prestressed beam and V_p is the contribution of prestressing force to the shear resistance. The derivation of the expression 2-24 can be found below.
In Figure 2-16, a prestressed beam with reduced normal stresses at the bottom side is depicted. The reduction of initially compressive stresses in the whole section from prestressing is caused due to action of bending moment. The magnitude of this so-called decompression bending moment M_0 can be calculated as follows:

$$\sigma_{cb} = -\frac{P_m}{A_c} - \frac{P_m e_p}{W_{cb}}$$

$$M_0 = \sigma_{cb} W_{cb} = F_p \left(\frac{W_{cb}}{A_c} + e_p \right) = F_p \left(\frac{1}{6} h + e_p \right) = V_p a.$$

Proceeding considerations, in most tests on shear critical beams the ratios e_p/h is about 0.35. Under this assumption and the assumption that for a rectangular cross section $d = 0.85h$, the contribution of prestressing force to the shear resistance is: $V_p = \frac{0.61 F_p}{a/d}$.
Moreover, in most tests on shear critical beams a/d varies between 2.5 and 4 which gives: $V_p = 0.15F_p$ to $V_p = 0.25F_p$ or $V_p = 0.15\sigma_{cp}bd$ to $V_p = 0.25\sigma_{cp}bd$.
It can be seen therefore that k_1 in expression 2-24 is a coefficient of an increase of shear capacity relative to a reinforced beam due to an application of prestressing. The recommended safe lower bound value suggested in [8] is 0.15. The coefficient k_1 can only be applied in prestressed members without shear reinforcement.

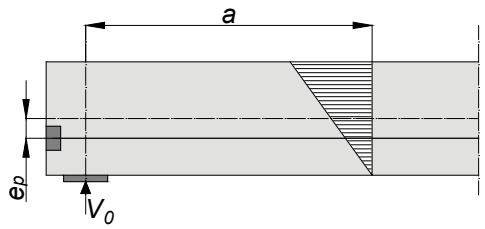

Figure 2-16: Calculation of the contribution V_p from prestressing to shear resistance [10]

The expression 2-24 indicates that when a value of reinforcement ratio goes to zero, the shear resistance also approaches zero. For this reason the minimum value of shear resistance is derived. For the position of a point load in a distance $a < 2.5d$, the shear capacity of a beam increases due to the arc action. For the position of $a = 2.5d$ which is the most unfavourable for a beam, the 5% lower limit for the shear resistance is obtained with:

$$V_{uk} = 0.15k(100\rho_l f_{cm})^{1/3} b_w d$$

The bending moment at this location is:

$$M_{uv} = 2.5dV_{uk} = 0.375k(100\rho_l f_{cm})^{1/3} b_w d^2$$

When equated to the yielding bending moment $M_{uf} = 0.9d(\rho_l bd) f_{yk}$, taking $f_{yk} = 500MPa$, results in the reinforcement ratio below which shear failure will not occur:

$$\rho_l = 0.00024k^{3/2}(f_{cm})^{0.5} \frac{b_w}{b}^{3/2}$$

Substituting this value to the expression 2-24 and replacing f_{cm} with f_{ck} and taking $b_w/b = 1$ results in:

$$\nu_{min} = 0,035k^{3/2}f_{ck}^{1/2}$$

Accounting for the positive impact of prestressing force results in the expression:

$$V_{Rd,c} = (\nu_{min} + k_1\sigma_{cp})b_w d \tag{2-27}$$

where: $k = 1 + \sqrt{200/d} \leq 2.0; d$ in mm is a size-effect coefficient; ρ_l is a longitudinal reinforcement ratio based on the effective depth $\rho_l = \frac{A_{sl}}{b_w d} \leq 0.02$; b_w the smallest width of the cross-section in the tensile area; σ_{cp} the axial stress due to prestressing, note: $\sigma_{cp} = \frac{N_{Ed}}{A_c} \leq 0.2f_{cd}$; A_c is the cross-sectional area of concrete; f_{cd} is cylinder compressive strength of concrete; $C_{Rd,c}$ is the coefficient with recommended value 0,12 (König and Fisher 1995, from [10]), the Dutch Annex EN 1992-1-1.

6.2.2(6) explains that for members with loads applied on the upper side within a distance $0.5d < a_v < 2d$ from the edge of a support, the contribution of this load to the shear force V_{Ed} can be multiplied by $\beta = a_\rho/2d$ as the result of an arch action. In addition, within the distance d from the face of the support, it is not required to check the design value of the shear force V_{Ed}, however this shear force must be less than $V_{Rd,max}$ from:

$$V_{Ed} \leq 0.5b_w dv f_{cd} \quad \text{with} \quad \upsilon = 0.6\left[1 - \frac{f_{ck}}{250}\right] \tag{2-28}$$

Prestressed members with shear reinforcement

Members in which the shear resistance is lower than the value of shear force, must be provided with shear reinforcement. In the EC2, members with shear reinforcement are designed with the variable angle truss model with no contribution of concrete to the shear resistance. It is so because the model conservatively assumes that the angle of the shear cracks are parallel to the diagonal compression and as the result no shear friction on the crack interface exists [23]. The contribution of the uncracked compression zone of a member is neglected as well. The capacity of each vertical member follows from the strength of shear reinforcement within the length of $0.9dcot\theta$ (with $0.9d = z$), hence the shear resistance:

$$V_{Rd,s} = \frac{A_{sw} z f_{ywd} \cot\theta}{s} \tag{2-29}$$

From the results of the experiments it was concluded that crack patterns is dependent on the amount of applied reinforcement. The manner in which beams fail adapts to the amount of reinforcement hence the lower inclination of the cracks corresponds to a smaller amount of stirrups. In other words when shear reinforcement yields, the compression struts rotate lowering the angle (a new state of equilibrium is reached, or not at failure) and consequently more stirrups become intersected and activated to carry the load. Such a rotating mechanism increases however compression stresses in the struts and can proceed until crushing of the concrete occurs [23], [8]. The limit value is dictated by:

$$V_{Rd,max} = \frac{b_w z \sigma_{cd}}{\cot\theta + \tan\theta} \quad \text{where} \quad \sigma_{cd} = \alpha_{cw}\nu_1 f_{cd} \tag{2-30}$$

α_{cw} is a coefficient taking into account the state of stress in the compression strut; EN 1992-1-1 cl.6.2.3 eq. (6.11.aN), (6.11.bN) and (6.11.cN); ν_1 is a strength reduction factor for concrete cracked in shear which can be found from EN 1992-1-1 eq. (6.10.aN), (6.10.bN) or (6.6N) otherwise.
The range of θ values can be derived from the equilibrium plasticity truss model theory assuming that the maximum possible shear capacity can be found when crushing of the concrete and yielding of the shear reinforcement occur simultaneously, thus when $V_{Rd,s} = V_{Rd,max}$. The recommended limiting values for $cot\theta$ are: $2.5 \leq \cot\theta \leq 1 \quad (21.8° \leq \theta \leq 45°)$.
The prescribed range of angles according to the equilibrium plasticity truss model is derived by combining expressions 2-4 and 2-6 hence assuming that yielding of transverse steel occurs in parallel with crushing of concrete as follow:

$$f_2 = \frac{V}{b_w d \sin\theta \cos\theta} \longrightarrow v = f_{c1} \sin\theta cos\theta \quad \text{where} \quad f_{c1} = \nu f_2 \quad and \quad f_2 = f_c \tag{2-31}$$

$$A_v f_v = f_2 b_w s \sin^2\theta \longrightarrow \rho_v f_y = f_{c1} sin^2\theta \quad \text{with} \quad \rho_v = A_v/b_w s \tag{2-32}$$

to eliminate dependence on the angle θ, $sin^2\theta = \rho_v f_y / f_{c1}$ is substituted to 2-31 and including $cos^2\theta + sin^2\theta = 1$ results in:

$$v^2 = f_{c1}\rho_v f_y \left(1 - \frac{\rho_v f_y}{f_{c1}}\right) \longrightarrow v = \sqrt{\rho_v f_y (f_{c1} - \rho_v f_y)} \tag{2-33}$$

The balanced condition 2-33 can be represented graphically by a semicircular curve in $v/f_{ce} - -\Psi$ coordinated system presented in Figure 2-17 dictated by the formula:

$$\frac{v}{f_{c1}} = \sqrt{\Psi(1-\Psi)} \longrightarrow \left(\frac{v}{f_{c1}}\right)^2 + (\Psi - 0.5)^2 = 0.5^2 \quad \text{where} \quad \Psi = \frac{\rho_v f_y}{f_{c1}} \tag{2-34}$$

Additionally by equating equations 2-29 and 2-30 the following relation can be obtained:

$$\frac{A_{sw} z f_{yw} \cot\theta}{s} = \frac{b_w z f_{c1}}{\cot\theta + \tan\theta} \longrightarrow \Psi = \frac{1}{\cot^2\theta + 1} \longrightarrow \tan\theta = \sqrt{\frac{\Psi}{1-\Psi}} \tag{2-35}$$

It is found that for Ψ in the range of 0 and 0.5, the angle θ runs from 0 to 45°. For $\Psi > 0.5$ Eurocode 2 assumes $\theta = 45° = const.$ On the other side of the spectrum, the cut-off limit is $\cot\theta = 2.5$ so $\theta = 22°$.

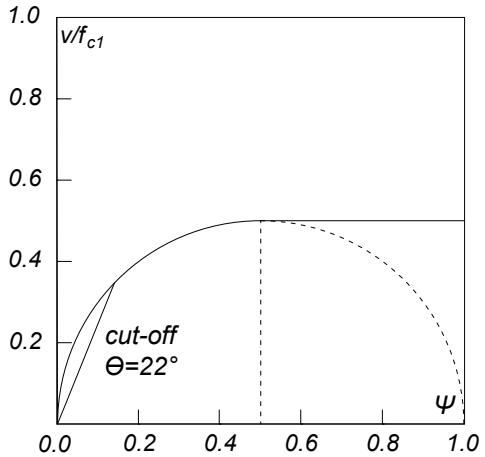

Figure 2-17: Graphical representation of the angle limits according to EC2; reproduced from [10]

2-4-2 *fib* Model Code 2010

The fib Model Code 2010 procedures for shear analysis in members with and without reinforcement are developed from observation of physical-mechanical models. It can be considered as advancement when compared to the preceding Model Code 1990 in which shear provision was based on empirical relationships for members without shear reinforcement and on a truss model for members with shear reinforcement. Furthermore, the new code incorporates an approach called "levels of approximation" (LoA). The concept of the LoA is to provide an engineer with different design models depending on the level of detail needed at the stage of calculations (e.g. preliminary design or detailed design) and importance of the structural member [24] or where not all the details are well defined [25]. The individual LoA are derived from a single physical model and the refinement of the design can be adapted with an application of simplifications. This means that lower LoA can be derived from the higher levels after introduction of appropriate conservative approximations [11]. The fib Model Code 2010 distinguishes four levels of approximation for members with shear reinforcement. The Level III constitutes the base model with the Level II and Level I models being simplified derivatives. As far as members without shear reinforcement are concerned, the Level II model provides the base model, with Level I being a simplification. The highest levels of approximation are Level IV for members with and Level III for element without shear reinforcement. In this case the strength is determined by numerical modelling and it is suggested that great care must be paid to the validation of models [24].

Codes Provisions

The base of the fib Model Code 2010 shear provisions is the Simplified Modified Compression Field Theory (SMCFT). The shear resistance V_{Rd} in the section (called the controlled section) $z = 0.9d$ away from the support (or at other locations if decisive) is determined as a combination of steel and concrete contributions:

$$V_{Rd} = V_{Rd,s} + V_{Rd,c} \geq V_{Ed} \tag{2-36}$$

The procedure of fib Model Code 2010, as the representative parameter, takes the value of the strain ε_x at the mid-depth of the effective shear section. The effective shear depth z in a reinforced member can be assumed to be $0.9d$ while for a prestressed member it is the distance from the resultant of the compressive chord force F_c to the resultant of forces F_t and ΔF_p (see Figure 2-19).
The strain ε_x is obtained from equilibrium of a section of a beam as shown in Figure 2-19:

$$F_{top} = \frac{M}{z} + \frac{V}{2}\cot\theta + N\left(\frac{1}{2} \pm \frac{\Delta e}{z}\right) \tag{2-37}$$

In derivation of the strain parameter two assumptions/simplifications apply. Introducing the first simplification mentioned in [24], it is possible to avoid dependence of strain ε_x on a variable θ which otherwise would induce a need for double iterative calculations to determine strain parameter. Instead, it is conveniently assumed that $V/2\cot\theta \approx V$.
Furthermore, with the conservative assumption that the compressive chord strain is 0, the

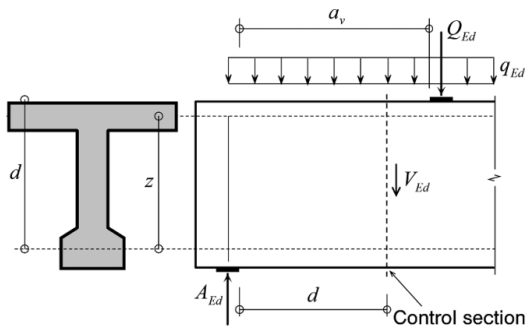

Figure 2-18: Definition of the control section [11]

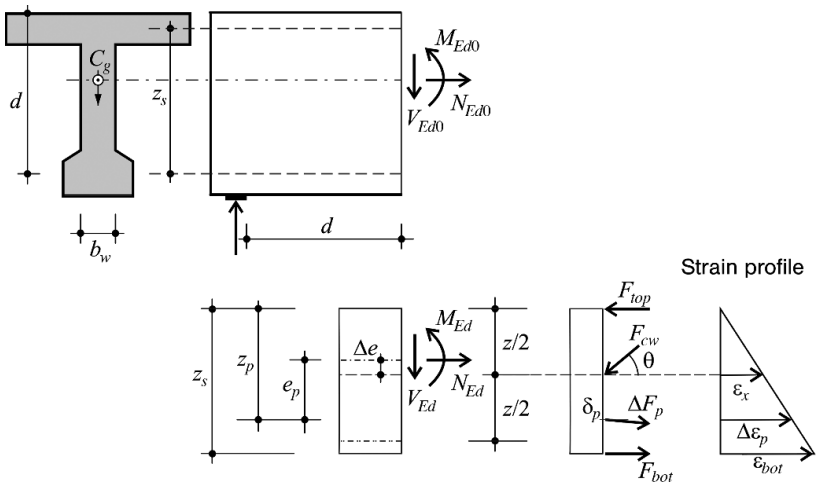

Figure 2-19: Definition of the sectional forces acting of the control section [11]

final form of strain at the mid-depth for members prestressed with bonded tendons can be found with the equation:

$$\varepsilon_x = \frac{\frac{M_{Ed}}{x} + V_{Ed} + N_{Ed}\frac{z_p - e_p}{z}}{2\left(\frac{z_s}{z}E_s A_s + \frac{z_p}{z}E_p A_p\right)} \tag{2-38}$$

with definitions according to Figure 2-19. The assumption of the zero strain value in the compressive chord is not far-fetched as the expression for compressive strain, similar to 2-38, would contain stiffness of uncracked concrete in the denominator which significantly reduces the value of strain.
Additionally the following conditions apply [11]:

- M_{Ed} and V_{Ed} must be taken as positive quantities and N_{Ed} as positive for tension and negative for compression
- It is permissible to use a value of ε_x that is greater than half the yield strain of the longitudinal bars $\varepsilon_{sy}/2$ but a more detailed cross-sectional analysis must be undertaken. The strain ε_x must not exceed 0.003.
- If the value of ε_x is negative it must be taken as zero

- For sections closer than d to the face of the support, the value of ε_x taken at d from the face of the support may be used.
- when calculating A_s and A_p, the area of bars that are terminated less than their development length from the section under consideration must be reduced in proportion to their lack of full development
- If the axial tension is large enough to crack the flexural compression face of the section, the calculated value of ε_x must be multiplied by a factor of 2.0.

In [11] sectional forces accounting for prestressing are taken as:

$$M_{Ed} = M_{Ed0} + M_{Pd} \tag{2-39}$$

$$N_{Ed} = N_{Ed0} + F_p \cos \delta_p \tag{2-40}$$

$$V_{Ed} = V_{Ed0} + F_p \sin \delta_p \tag{2-41}$$

Where M_{Pd} is the designed bending moment due to prestressing which includes a possible moment resulting from static indeterminacy.

Members without shear reinforcement (2 levels of approximation)

In the design of members without shear reinforcement, the stirrups contribution $V_{Rd,s}$ in the main equation 2-36 for the shear resistance, is set to 0. The shear resistance attributed to concrete is calculated with:

$$V_{Rd,c} = k_v \frac{\sqrt{f_{ck}}}{\gamma_c} b_w z f_{ck} \text{ in MPa} \tag{2-42}$$

The value of $\sqrt{f_{ck}}$ cannot be taken as greater than 8MPa. It accounts for the fracture surface passing through aggregates and the large scatter of the observed results. As explained in the section devoted to the mechanism of shear transfer after onset of cracking, this behaviour is typical for members with higher classes of concrete strength and lightweight aggregate concretes.

For *level II approximation*, the design shear resistance is determined with (z in mm):

$$k_v(II) = \frac{0.4}{1 + 1500\varepsilon_x} \frac{1300}{1000 + k_{dg} z} \tag{2-43}$$

This parameter includes "strain parameter" ε_x, the size effect and the effect of aggregate size. In members without shear reinforcement, the shear resistance is influenced by the maximum size of aggregate. For concrete with a different maximum size of aggregate than $d_g = 16mm$, the value k_{dg} may be calculated with:

$$k_{dg} = \frac{32}{16 + d_g} \geq 0.75 \tag{2-44}$$

For concrete strength more than 70MPa and lightweight concrete, the variable d_g in the formula for k_{dg} should be set to 0 as in this case cracks pass through aggregate and aggregate interlock cannot be accounted for [24].

The *level I approximation* is derived from the more general level II. The equation 2-43 is simplified to

$$k_v(I) = \frac{180}{1000 + 1.25z} \tag{2-45}$$

by setting k_{dg} in 2-44 to 1.25 (assuming a maximum aggregate size >9.6mm) and ε_x to 0.00125 ($\varepsilon_x \approx \frac{f_{yk}}{2E_s}$) which corresponds to half the yield strain for a reinforcing bar with $f_{yk} = 500MPa$

Members with shear reinforcement (3 levels of approximation)

Members with shear reinforcement are defined as those which meet the demand for the minimum shear reinforcement according to:

$$\rho_w \geq 0.08\frac{\sqrt{f_{ck}}}{f_{yk}} \quad f_{ck} \text{ and } f_{yk} \text{ in MPa} \tag{2-46}$$

Otherwise the members should be treated as without shear reinforcement.
The general equation 2-36, consists of the shear resistance from stirrups calculated with:

$$V_{Rd,s} = \frac{A_{sw}}{s_w} z f_{ywd} \cot\theta \tag{2-47}$$

and the component of the concrete resistance which is considered differently depending on the LoA. While levels I and II disregard the concrete contribution to the total shear resistance, in the level III concrete contribution is added with the angle of inclination of compressive struts $\theta = \theta_{min}$.

Table 2-1: Summary of shear resistance for the individual levels of approximation

LoA I - represents a variable angle truss model approach	$V_{Rd} = V_{Rd,s} \leq V_{Rd,max}$
LoA II - represents a variable angle truss model approach	
LoA III - based on the SMCFT	$V_{Rd} = V_{Rd,s} + V_{Rd,c}$ $V_{Rd} \leq V_{Rd,max}(\theta_{min})$ If $V_{Rd} \geq V_{Rd,max}(\theta_{min})$ then V_{Rd} from LoA II

For all LoA, the upper limit of the shear strength intended to prevent from web crushing failures is calculated with :

$$V_{Rd,max} = k_c \frac{f_{ck}}{\gamma_c} b_w z \sin\theta \cos\theta \tag{2-48}$$

where k_c is the strength reduction factor $k_c = k_\varepsilon \eta_{fc}$. The strength reduction factor in turn includes a factor to account for the strain effect k_ε and a brittleness factor η_{fc} which reduces the strength for concretes with $f_{ck} > 30MPa$. Concretes with an increase strength according to the foregoing relationship typically exhibit more brittle failure behaviour. The brittleness factor is calculated with:

$$\eta_{fc} = \left(\frac{30}{f_{ck}}\right)^{\frac{1}{3}} \leq 1.0 \quad f_{ck} \text{ in MPa} \tag{2-49}$$

The strain effect for LoA I is taken as $k_\varepsilon = 0.55$. For LoA II and III:

$$k_\varepsilon = \frac{1}{1.2 + 55\varepsilon_1} \leq 0.65 \tag{2-50}$$

with

$$\varepsilon_1 = \varepsilon_x + (\varepsilon_x - \varepsilon_2)\cot^2\theta$$

from the average strain compatibility of MCFT (eq. 6 and 7 in Figure 2-13). From [24], an adequate approximation for negative strain $-\varepsilon_2$ may be taken as the concrete peak strain $\varepsilon_{c0} = 0.002$.

The possible angle of the strut is in the range $\theta_{min} < \theta < 45\,\text{deg}$. The values of θ_{min} depend on the LoA; in [11] the following values are presented:

- Level I with the fixed values of the minimal inclination of the compressive stress field:
  $\theta_{min} = 25°$ for members with significant axial compression or prestress;
  $\theta_{min} = 30°$ for reinforced concrete members;
  $\theta_{min} = 40°$ for members with significant axial tension
- Levels II and III θ_{min} is a function of strains at the mid-depth:

$$\theta_{min} = 20° + 10000\varepsilon_x \tag{2-51}$$

The contribution of concrete in Level III is taken into account through equation 2-42 with:

$$k_v = \frac{0.4}{1 + 1500\varepsilon_x}\left(1 - \frac{V_{Ed}}{V_{Rd,max}\theta_{min}}\right) \tag{2-52}$$

Here again, the value of $\sqrt{f_{ck}}$ must not be greater than 8MPa. In the equation 2-48, the effective web width b_w in the case of prestressing tendons with duct diameters $\phi_D \geq \frac{b_w}{8}$ follows from:

$$b_{w,nom} = b_w - k_D \sum \phi_D \tag{2-53}$$

Where $\sum \phi_D$ is the most unfavourable prestressing tendon configuration. The value k_d varies depending on the type of material of the duct and whether it is grouted or not. The values from [11]: grouted steel ducts $k_D = 0.5$; grouted plastic duct $k_D = 0.8$; ungrouted duct: $k_D = 1.2$.

2-4-3 2.1.3. 2004 Canadian Standards Association (CSA) A23.3 Shear Design Provision for Reinforced and Prestressed Concrete Structures

Fully based on [12] with a similar structure.
The 2004 shear design provision was an answer to an attempt of harmonizing the two previous independent methods for shear design: the simplified method which was derived from the empirical method of the American Concrete Institute code and the second rationally based shear design method developed by Michael P. Collins called the general method. It was reported in [12] that those two methods at times could cause incompatibilities. Members calculated with one method and considered as safe could be deemed as unsafe by the other method.
The idea of harmonization consisted of an application of one or two physical assumptions so that the general method would mathematically be reduced to the simplified method. In this way incompatibilities would be disposed and the code would become more transparent for a user.

Basis of the general shear design method

The 2004 shear design provision is based on the Modified Compression Field Theory for reinforced concrete element subjected to shear. In Figure 2-20 the free body diagram of concrete flexural members with a diagonal shear crack running through stirrups legs, the longitudinal reinforcement and the flexural compression area is shown. According to the CSA code, in such members the bending moment at the critical shear section is carried by coupled compression force in concrete and a tension force in the longitudinal reinforcement; C and F_{lt} respectively. As usual, the shear behaviour is more complex and here is assumed to be carried by the following: the vertical forces in the yielding stirrup legs that are intersected by the crack, the aggregate interlock stress v_c, the vertical component of prestressing force V_p and shear stresses in the concrete flexural compressive zone. It is also noted that an additional resistance can be obtained from the dowel action. This however is ignored in the MCFT thus the CSA does not considered it as well.

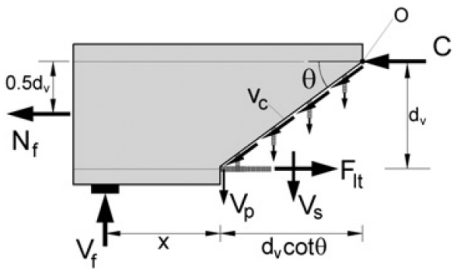

Figure 2-20: Basic shear mechanism of the CSA method [12]

Another assumption in the shear model refers to the aggregate interlock. It concludes that the aggregate interlock resistance of the complex crack geometry can only be represented across the entire crack surface by the aggregate interlock resistance estimated at one depth. The third assumption is related to the members without shear reinforcement and states that because the resistance of the cracked regions is lower than that of the compression region thus the former would be governing.

The shear strength of a member in the CSA code is considered as a combination of individual contributions in a section: the concrete component in a form of the aggregate interlock V_c, the steel component from the shear links crossed by the diagonal crack and the vertical component from prestressing. The resistance thus is calculated from:

$$V_r = V_c + V_s + V_p \tag{2-54}$$

$$\frac{V_r}{b_w d_v} = \phi_c \lambda \beta \sqrt{f_c'} + \frac{A_v \phi_s f_y}{b_w s} \cot\theta + V_p \leq 0.25 \phi_c f_c' + V_p \tag{2-55}$$

where b_w is the web width, $d_v = 0.9d$ is the flexural lever arm in the beam, ϕ_c is the resistance factor for concrete, λ is a factor to account for low-density concrete, β is a factor to account for aggregate interlock in concrete members, f_c' is the concrete cylinder strength, A_v is the area of transverse reinforcement, ϕ_s is the resistance factor for the reinforcing steel, f_y is the yield strength of reinforcement, s is the spacing of the shear reinforcement, θ is the angle of average principal compression in the beam with respect to the longitudinal axis.

The equation 2-55 is limited by the maximum shear strength, which is based on the crushing capacity of the concrete struts. The value $d_v = 0.9d$ is related to the shear stresses in the cross section. It is known that shear stresses at the top and the bottom surface of the section approach zero. The exclusion of the resistance in those parts of the section corresponds better to the reality and hence the value of d is reduced. The further precaution of $\sqrt{f'_c}$ not to be taken as greater than 8MPa is related to the smoother crack surface when the rupture passes through the aggregate. It is typical for members with high strength concrete.

To define the remaining variables β and θ in the equation 2-55, the required main parameters are: the normalized shear stress ν/f'_c, longitudinal strain ε_x and effective crack spacing s_{ze}. They are elaborated below.

Longitudinal strain parameter

To account for all the geometrical and loading effect such as percentage of reinforcement, applied moment, shear and axial force, prestressing etc. the CSA code uses the longitudinal strain parameter. The concept of the strain parameter as explained in [12] is that the larger it is, the wider crack becomes, hence the lower the aggregate interlock and consequently V_c. Such a decrease of strength with an increased value of longitudinal strains is called strain effect. The longitudinal strain is to be calculated at the mid-depth of a section. It is a conservative approximation. The strain in the concrete in flexural compression, due to the high stiffness of concrete, is small thus can be assumed to be equal to zero. In this way, the strain in the mid-depth is the half of the strain in flexural tensile reinforcement.

$$\varepsilon_x = \frac{\frac{M_f}{d_v} + V_f + 0.5N_f - A_p F_{p0}}{2(A_s E_s + A_p E_p)} \tag{2-56}$$

Where M_f is the factored applied moment (M_f and V_f should be always taken as positive), N_f is factored applied axial force (tension positive), A_p is the area of prestressed flexural tendon, f_{p0} is the stress in the prestressed reinforcement when the strain in the surrounding concrete is zero, A_s is the area of main flexural reinforcement, E_s is the Young's modulus of the reinforcement, and E_p is the Young's modulus of the prestressed reinforcement.

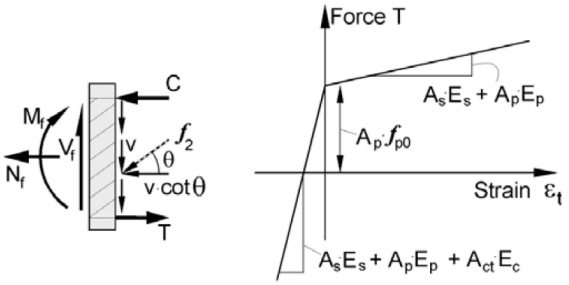

Figure 2-21: Development of the longitudinal strain parameter equation

The equation 2-56 can be derived from the section of a beam with external forces on the left and resolved internal forces on the right (Figure 2-21). From the equilibrium about the compressive force C, the force in the longitudinal reinforcement can be found. To get rid of the dependence on the angle of inclination of struts θ , the conservative assumption $0.5 \cot \theta \approx 1$ which slightly overestimates the impact of shear on the force T is applied. The force T is then

converted to strain from the relation presented in Figure 2-21. From the strain-force relation, two important aspects can be noted. Firstly, the offset caused by the prestressing force which increases the cracking force occurs in the member. Another is the stiffness of the concrete part in the tension zone which no longer has an impact on strain once the concrete member is cracked (A_{ct} is the area of concrete on the flexural tension side of the member and E_c is the uncracked elastic stiffness of the concrete). The final value of the strain term must not be taken as less than $-0.2 * 10^{-3}$. The last provision mentioned in the code's background is in the case of the applied forces of such a magnitude that the flexural compression zone cracks. When it occurs, the equation 2-56 is not conservative anymore and to account for this, the mid-depth strain can be calculated as an average of the top and bottom chord strains, or the results from 2-56 may be doubled.

In conclusion, the longitudinal strain parameter indicates what is the relation between the demand on the reinforcement and the reinforcement in a member. The higher the demand, the larger the crack width, unless prestressing or an axial compression is applied which would significantly diminish the strain effect and it would result in a higher shear strength. On the other hand, in the case of the axial tensile force or high moment, the shear strength is decreased.

Effective crack spacing parameter

It was earlier mention that the aggregate interlock, and at the same time V_c , depends on a crack width in a member. The crack width can be calculated as the value of strain in the direction perpendicular to the crack multiplied by the average crack spacing in the same direction. From the researches conducted by Kuchma and Collins, Shioya, Lubell and Bentz and Buckley, it was concluded that the crack pattern is consistent and proportional with an increased depth of a member. It means that for members subjected to the same shear stresses and therefore the same strain, the beam of a larger depth would display the larger crack spacing and thus the crack width. This phenomenon is called the size effect in shear. While for the members reinforced in the transverse direction with shear links, the crack width can be control (such members are not expected to display a meaningful size effect), the size effect is of a huge importance for members without shear reinforcement. The crack spacing varies depending on the element type. For members without shear reinforcement the crack spacing is assumed to be $d_v = 0.9d$ while for members with shear reinforcement the crack it is no more than 300mm.

The aggregate interlock depends not only on the crack width but also an aggregate size. The increased roughness of the crack surface results in the higher resistance to shear. In the CSA code it is taken into account by a simple aggregate size correction to the crack spacing. It is calculated according to the formula:

$$s_{ze} = \frac{s_z 35}{15 + a_g} \leq 0.85 s_z \tag{2-57}$$

The CSA provision for the higher concrete strength: as concrete strengths increase from 60 to 70 MPa, it is recommended that the aggregate size used in the equation for s_{ze} be reduced linearly from the specified size to zero. The nominal value of aggregate size is 20mm.

Relating shear parameters to shear strength

In the 2004 CSA code shear provision, the equations for β and θ are related to the above explained parameters ε_x and s_{ze}.

The following equations 2-59–2-63 can be applied provided that a flexural failure will not occur before a shear failure. The flexural failure is determined by the sufficient flexural capacity of the longitudinal reinforcement to permit the shear failure; according to the Figure 2-20, by taking the moment equilibrium about the point O, the force in the longitudinal reinforcement at the position x:

$$F_{lt} \geq \frac{M_f}{d_y} + 0.5N_f + (V_f - 0.5V_s - V_p)\cot\theta \tag{2-58}$$

Development of the β equation

The final form of β to account for concrete component to shear resistance in the general equation 2-55 of the CSA general method is:

$$\beta = \frac{0.4}{1 + 1500\varepsilon_x}\frac{1300}{1000 + s_{ze}} \tag{2-59}$$

The development of β begins with a relationship for aggregate interlock. The maximum aggregate interlock that may be resisted for a given crack width is:

$$v_{ci} = \frac{0.18\sqrt{f'_c}}{0.31 + 24w/(16 + a_g)} \tag{2-60}$$

By means of an iterative procedure of the MCFT the diagonal crack width w (in mm) at the moment of failure can be obtained. The result of the analysis is plotted in Figure 2-22 for the effective crack spacing of 300 mm and concrete cylinder strengths of 20 and 100 MPa. The figure shows that with the increase longitudinal strain, the crack width increases as well. The minimum diagonal crack width is predicted for the negative compression strain for example due to prestressing. This is a result of principal tensile strain at least $0.2 * 10^{-3}$ for all analyses and therefore all analyses consider the strength in already cracked concrete. Next, the equation 2-60 is simplified to 2-61 by limiting strain values to 0.001 and an application of the simplified equation for the crack width to the equation from the MCFT:

$$v_{ci} = \frac{0.4\sqrt{f'_c}}{1 + 1500\varepsilon_x} \tag{2-61}$$

The strain limit value of 0.001 comes from the consideration that steel with $f_{yd} = 400MPa$ is the most commonly used in Canada and therefore at the failure, the strains at the mid-depth are equal to: $\varepsilon_x = \frac{f_{yd}}{2E_s} = 1.0 * 10^{-3}$.

From Figure 2-22, it can be seen that the negative strain values smaller than $-0.2*10^{-3}$ would result in the negative crack width, thus the equations of the general method should not be used lower values than this. The linear simplified equation for the crack width $w = 0.2 + 1000\varepsilon_x$ diverges for higher values of strain as compared to the MCFT analysis. The crack widths are overestimated and consequently, the predicted shear strengths for those values of strain are conservative.

The second multiplier in the equation 2-60 accounts for different member depths and aggregate sizes. It was obtained from the iterative process with different effective crack spacings and further the results are normalized by dividing them with the results from the iterative process for $s_{ze} = 300mm$. The reference [12] explains that such a relation was chosen because it is

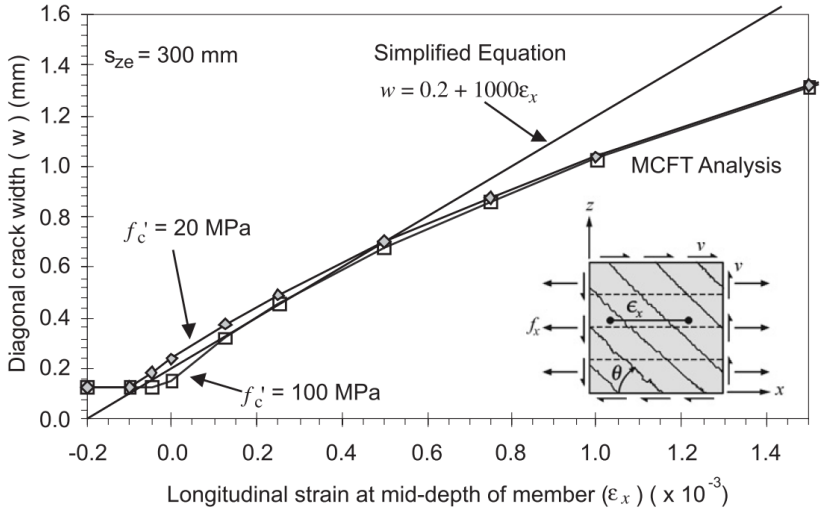

Figure 2-22: Longitudinal strain and the diagonal crack width relation [12]

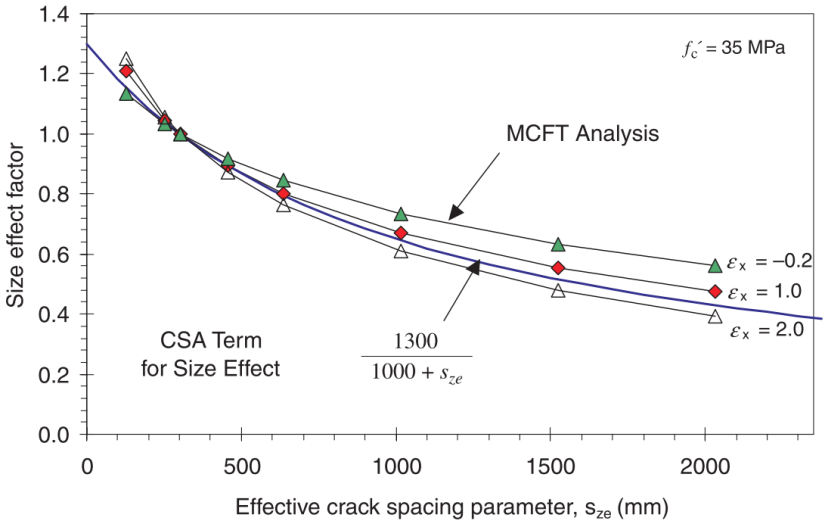

Figure 2-23: Size effect factor [12]

close to the lower bound of the data from the MCFT across the size range and it is similar to the size factor used in the 1994 CSA simplified method. The chart in Figure 2-23 indicates that the size effect is underestimated for large members (prestressed) without stirrups and slightly overestimated for small reinforced members.

An angle of inclination θ of principal strains to x-axis

Redistribution of shear stresses by mechanism of a plastic truss in concrete reinforced in both longitudinal and transverse directions at different angles is possible provided that certain assumptions are fulfilled:

- concrete inclined compressive struts must be able to resist the applied load without crushing,

- stirrups are able to yield

The above assumptions, similarly as in the other codes, are the lower and upper limit respectively. The angle θ should be taken as higher than the lower limit dictated by crushing of concrete and lower than the upper limit controlled by the yield of reinforcement. The Figure 2-24 from [12] shows that limits calculated based on the equations of the MCFT. It can be observed that with increasing longitudinal strains, the permissible angles range also increases. The CSA code fits a linear equation for θ between the lower and upper limits that meet the requirements for a shear resistance of $v = 0.25 f_c^{'}$:

$$\theta = 29\,\mathrm{deg} + 7000\varepsilon_x \tag{2-62}$$

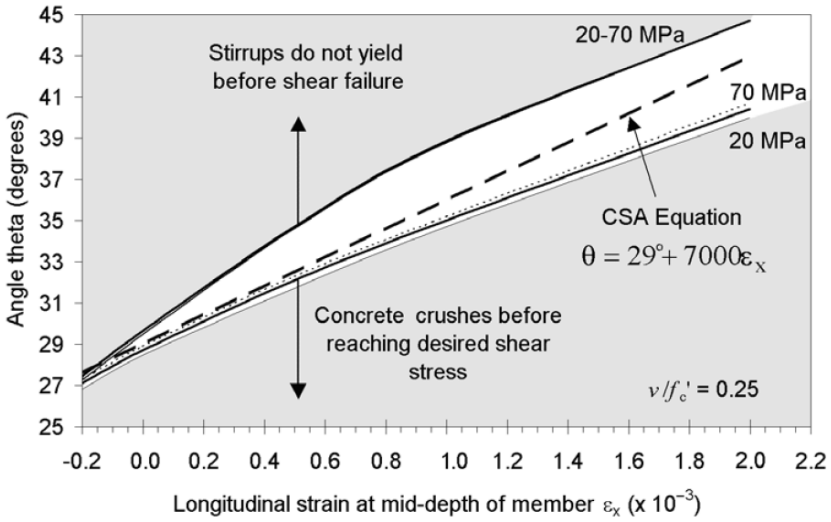

Figure 2-24: Limits on the angle θ for higher shear loading [12]

In the paper of the CSA code development, the equation 2-62 is claimed to be appropriate for members with stirrups and can be conservative for large members without shear links. As the result, the CSA code modifies it by adding the adjustment from curve fitting to the MCFT results, for checking the anchorage requirements:

$$\theta = (29\,\mathrm{deg} + 7000\varepsilon_x)(0.88 + \frac{s_{ze}}{2500}) \tag{2-63}$$

Validation with the MCFT

In Figure 2-25 the prediction of the strength development from plasticity with employed equations of the MCFT are presented. The equation for the shear strength is derived from the equilibrium based equations $f_z = \rho_z f_{sz} + f_1 - v\tan\theta$, $v = (f_1 + f_2)/(\tan\theta + \cot\theta)$ [17] with applied additional assumptions: tension stiffening f_1 can be ignored, the stress-strain relationships will be ignored and the maximum compressive stress in the concrete f_2 is assumed to be a constant percentage of the concrete cylinder strength; clamping stress f_z is assumed to be zero. The resulting equation for the shear strength of a member with

transverse steel that is yielding but the stresses in longitudinal steel do not reach the yield stress is (see also equation 2-33):

$$v = \sqrt{\rho_z f_y (f_2 - \rho_z f_y)} \tag{2-64}$$

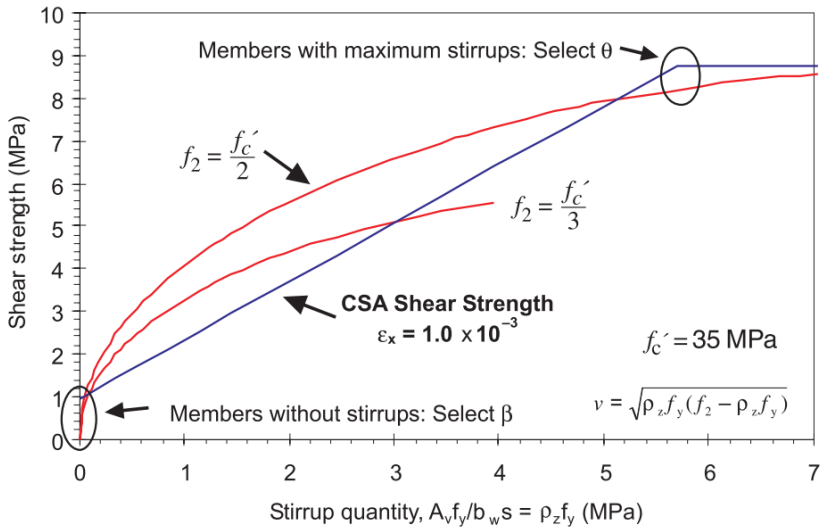

Figure 2-25: Shear strength by plastic analysis [12]

It can be seen that according to the equilibrium based equation 2-64 for the shear strength, with increased stirrups quantity, the shear strength is also increased. The increase is not linear and for different assumed concrete cylinder strengths, different shear strengths are obtained. Conversely, the general method of the CSA code, between the limits, predicts a linear increase of the shear strength for a constant longitudinal strain ε_x . The argumentation for this is the fact, the equations 2-59 and 2-63, for a constant strain in the mid-depth, stay constant and therefore the linear increase of strength is possible. It is also explained that the assumption of the constant strain is not unrealistic for members failing in flexure which would have the same longitudinal strain at the mid-depth for one type of steel ($f_{yd}/2E_s$). The limits here are the shear strength of the members without shear reinforcement and the top limit for the members heavily reinforced with stirrups. The second limit is constrained by crushing of concrete with a threshold of $0.25f_c^{'}$ given in the equation 2-55. It is notable, that as the plots of the actual shear strength are concave downwards, the linear code function will give a conservative results for all quantities of stirrups.

2-4-4 Summary

Different general methods of computing shear strength of members containing and without stirrups have been presented. As the report regards tension shear failure, the evaluation pays special attention to this failure mechanism. The first mentioned approach for members with shear reinforcement was the EN 1992-1-1:2004. According to the EC2, failure occurs when the principal tensile stresses in the web in the region uncracked in flexure calculated with the expression 2-24 reach the tensile strength of concrete. This method, when the code's commentary is strictly followed, has a limited application as it is only suitable for single span

beams. The code suggests that a member has no residual resistance after an onset of a crack resulting from exceeding the tensile strength of concrete. Typically, the tension shear crack appears in the mid-depth of a element's web. The uncracked concrete might still contribute to load carrying as well as flanges through the so-called clamping effect; it was proven in [13] that such a clamping effect is advantageous for the ultimate shear resistance. It is further questionable as there exist additional potential sources of shear resistance such as aggregate interlock resistance, dowel action of longitudinal reinforcement or a shear contribution of compression zone which are not taken into account. As far as the expression for the tension shear resistance from the EC2 is concerned, no influence of shear reinforcement is accounted for. An application of the minimum shear reinforcement or effective shear reinforcement could possibly increase shear capacity and ensure a ductile failure after cracking. Even a small amount of shear reinforcement might turn out to be effective. It is especially relevant for prestressed beams in which prestressing reduces an angle of crack inclination and thus more stirrups can be intersected.

The fib Model Code 2010 and the CSA shear provision are somewhat similar as both are based on Simplified Modified Compression Field Theory (SMCFT) for members without shear reinforcement and only fib Model Code 2010 for members with stirrups combines a general stress field approach with SMCFT [24]. Both methods provide an engineer with a general more refined method which can be reduced to a simplified method(s) with an application of simplifying assumptions. In the fib Model Code 2010, it is known as the Levels-of-Approximation approach.
In contrast to the EC2 methods (limiting principal tensile stresses for a region uncracked in flexure, the empirical expression for regions cracked in flexure in members without stirrups and the variable angle truss model for members with stirrups), the methods in Model Code and the CSA code use a strain condition in the web hence there is no distinction between different methods for different types of cracking (a flexural shear crack and a shear tension crack). It can be considered as a drawback as the nature of the governing failure mechanism remains unknown making the analysis ambiguous.
The first difference as compared to the CSA code method is the way in which the equilibrium is considered. For the case in which an external axial force is applied, in the CSA the force is located at the depth of a half of an effective shear depth d_v. Conversely, in the MC 2010 an external axial force is applied in the center of gravity, therefore calculating the strain ε_x from the moment equilibrium about the center of compression zone, this force acts on a certain eccentricity (see Figures 2-20 and 2-19 for comparison). For both cases the longitudinal strain is calculated at the level a half the depth of the effective shear depth from the reinforcement and tendon axes. In the equilibrium, similar as previously, to avoid iterations shear force term is approximated as $V/2cot\theta = V$.

The shear resistance according to the General Method of the CSA shear provision and the Level III Approximation is determined as a summation of concrete and stirrups contributions. Whereas the shear resistance attributed by stirrups does not require explanation, the concrete part differs slightly. The first factor in the expression for β and k_v, namely $\frac{0.4}{1+1500\varepsilon_x}$ is the same for both methods. It origins from the maximum aggregate interlock as specified in the MCFT and the simplified equation for the crack width (Figure 2-22). The second factor in the CSA code $\frac{1300}{1000+s_{ze}}$ as mentioned earlier is a curve fitting extension to account for different member depths and aggregate sizes. In the case of the MC10, the second component

$\left(1 - \frac{V_{Ed}}{V_{Rd,max(\theta_{min})}}\right)$ limits the concrete contribution to the total resistance by relating the applied shear load to the crushing at the minimum inclination. From [11], the value of $k_v \geq 0$ hence when the applied load exceeds the shear strength limited by crushing of concrete given by $V_{Rd,max(\theta_{min})}$, the concrete contribution cannot be taken into account. This however does not mean that the design is not possible. By increasing an angle of struts inclination and thus the amount of shear reinforcement needed, shear resistance defined by stirrups alone (Level II Approximation) can meet the limits of crushing of concrete $V_{Rd,max}$ and θ explicitly limited by $\theta_{min} < \theta < 45°$. Here, another difference arises. In the CSA code, the angle of inclination θ is defined with a use of a value of a strain factor ε_x (as depicted in Figure 2-24) while the MC10 allows an engineer to choose a value of θ within the limits specified above.
In the MC 2010, members with the amount of reinforcement lower than specified as the minimum, thus without reinforcement, a transition is made to expression 2-59 in which only the coefficient for aggregate size is slightly different. This is why it is crucial to check if the provided amount of shear reinforcement in an element is higher than minimum; when the amount is lower, the failure mechanism changes and different aspects start to play an important part such as for example the member size. In members containing a sufficient quantity of shear reinforcement, the member size effect is not expected to be significant [12].

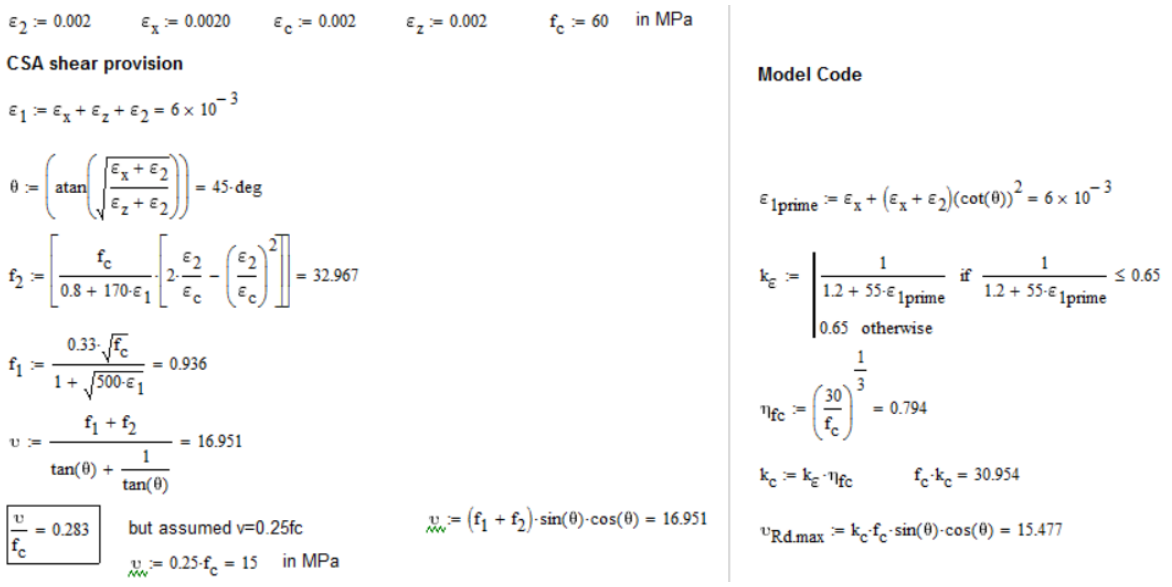

Figure 2-26: Crushing of concrete struts according to CSA and MC2010

Both methods have the shear strength cut-off limits. For the MC10, the limit is related to crushing of concrete struts at the angle of 45 degrees, expressed with equation 2-48. In 2-48, the concrete strength is reduced by a factor for the strain effect and a brittleness factor. The maximum shear stress according to the CSA is derived using the MCFT equations from Figure 2-13. Under the assumption that at the failure the transverse reinforcement yields while concrete crushes in compression, the conservative assumption of the shear strength $0.25f_c^{'}$ was made. Due to this simplification, from Figure 2-26, it can be seen that the CSA code gives a more conservative limit of the failure shear stress than MC10.

The allowable range of the strain effect parameter in both methods does not exactly match. The longitudinal strain must not exceed the value of 0.003 for the either case. The permissible minimum values of strain are $-0.2 \cdot 10^{-3}$ and 0 for the CSA code and MC10 respectively. Typically, for a section in high compression, due to for example prestressing, while calculating longitudinal strain the stiffness of the concrete should be included in the denominator. Neglecting the stiffness of concrete would result in an overestimated negative strain value and consequently in an overestimated shear strength. Therefore, the assumption of the 0 value of the longitudinal strain for a section in compression adapted by the MC10 is conservative.

Chapter 3

Study of the Influence on the Shear Strength of Web-Shear Critical Reinforced Concrete Elements

3-1 General Information

This chapter contains summarized information on the experimental research *"Influence of Axial Load and Prestress on the Shear Strength of Web-Shear Critical Reinforced Concrete Elements"* conducted by Liping Xie at the University of Toronto [13].

Purpose of the study
The basis for a comparison of different design codes are experimental results from the study of Liping Xie on eleven I-shaped reinforced concrete beams subjected to different combinations of axial and shear force. The study investigated the influence of axial load, prestress and an amount of stirrups on the shear strength of web-shear critical reinforced concrete elements and related the results to the predictions from the commonly used design codes; i.a. the ACI code, the CSA code and the EC2.

Test setup
The test setup was chosen to simulate the conditions of a continuous beam near the point of inflection, as illustrated in Figure 3-1. In this study, the point of inflection which corresponds to the point where bending moment becomes zero is accompanied by a region of constant shear force. Such a static scheme with double bending was obtained with the use of the Balwin machine and a spreader beam applying the load in a way that the ratio between loads at the eastern and western loading plate equals 1.8. The positions of the supports along with loading plates are depicted in the Figure 3-1. This scheme has an additional advantage over tests on simply supported beams under three or four points bending for which the critical web-shear sections are located in the disturbed region close to a support. This in turn may enhance the shear strength by strut-action [13]. The highest values of the shear force were located outside of the test region whereas the hogging bending moment at the support.

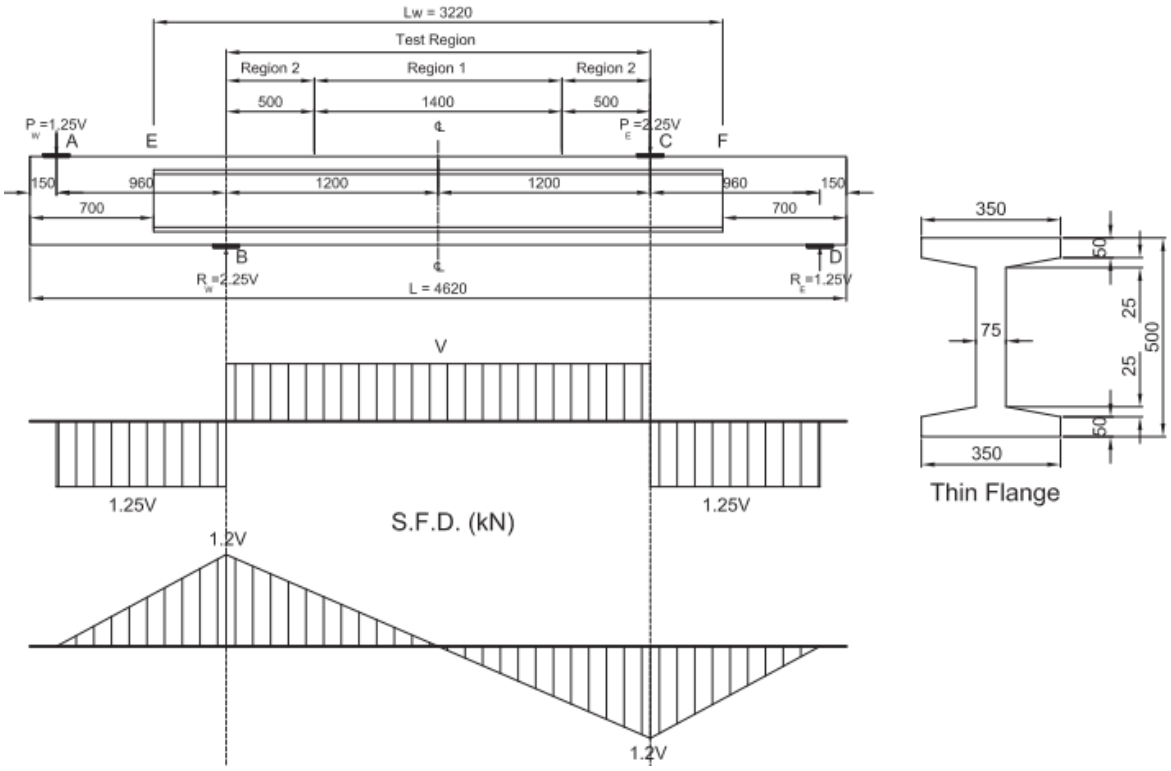

Figure 3-1: Test setup [13]

Specimens

The tested beams consisted of two parts: the middle I-shaped part 3220mm long and the 700 mm long diaphragm blocks at each end of the beams. The specified height of all beams was 500mm. The specified web thickness of 75 mm was the same for beams while the flange thickness varied depending on the test group: 75mm thick flanges for the first group and 50mm for the group with thin flanges. The group 1 (thick flange) comprised of beams LB1-LB5 under different axial loading with the LB1 in high compression (-800kN) and LB5 in high tension (500kN). The axial force in beams LB2 till LB5 ranged -800, -400, 250, 500 kN. The second group consisted of beams LB6-LB11 in axial compression with the highest force for LB6 decreasing for the subsequent beams till LB9 (0 axial force). The beams LB6, LB10 and 11 reinforced with a different amount of stirrups were subjected to the same compressive force. The objective of a such division was to investigate the impact of the compressive/tensile force and a different flange thickness in beams LB1-LB9 and a varying (increased) amount of shear reinforcement in beams LB6, LB10, LB11 on the shear tension resistance.

For the comparison of designers' codes, three thin flange beams were chosen: LB6, LB10, LB11. The selected beams can be also classified as the beams with a normal amount of stirrups for LB6, an increased amount of stirrups for LB10 and a beam without stirrups in the Region 1 of the test setup. The amount of longitudinal reinforcement for the beams is the same. With such selection, the intention is to examine shear capacity of the beams with and without shear reinforcement with respect to different design approaches in common codes and refer the results to the benchmark tests.

Reinforcement Layout for the Beams LB6, LB10 and LB11

To ensure the intended web-shear failure mode within the region 1 while avoiding a premature failure in other parts of the beams, an extra amount of shear reinforcement was provided in the regions of the high shear force – outside of the test region. The layout of the transverse reinforcement in those location was identical for all beams, namely 10M deformed bars spaced at 125mm. This amounts for about three times the quantity of the shear reinforcement in the Region 1. In addition to that, to prevent the flexure-shear failure at the support (region 2) where high bending moments act, an additional amount of stirrups was applied. For all beams these are wires D4 spaced 87.5 mm. In the case of LB10, wires D4 are spaced 87.5 mm throughout the whole test region. Stirrups in the Region 1 for the beam LB6 are reduced twofold as compared to the Region 2; these are wires D4 spaced 175mm apart. As opposed to the LB6 and LB10, the beam LB11 has no stirrups in the Region 1. Further, in order to ensure that flexural failures would not control nor the rebars yield, a sufficient amount of the longitudinal reinforcement was applied. It consisted of four rebars M15 in each flange. The reinforcement layout is shown in Figures 3-2, 3-3, 3-4.
The beams were prestressed through post-tensioning of two unbonded one-inch high strength smooth bars embedded in conduit ducts and greased to reduce friction losses. The clearance between the duct and prestressing smooth bars was only 1.5mm. The prestressing force was introduced to the test region by means of solid diaphragm concrete blocks at both ends. The prestressing bars as well as the longitudinal rebars are symmetrical with respect to the elements' centroidal axes. Lastly, the D4 cross ties were applied parallel to the longitudinal reinforcement. The function of the cross ties was to hold the bars in place during casting and resist any tendency of longitudinal splitting in flanges.

Method of Prestressing

Prestressing was applied from one end only. The smooth bars were longer than the specimens. The protruding part at one end was fixed to steel plates using nuts and connected to the jacking apparatus at the other. The force was applied by stressing the bar at one end while the steel plates were reacting at the anchored end. After prestressing achieved the desired magnitude, the nuts were tightened to maintain the force.

3-2 Observations of Tests

To bring up the behaviour of specimens in different loading conditions, the general observation of the tested beams will be given.
Each beam before failing developed a crack pattern with numerous cracks. The crack pattern was related to the axial loading and the amount of shear reinforcement. It could be noted that where the amount of shear reinforcement was increased, the crack distribution was improved. The beams with the double shear reinforcement required by the CSA code tend to display solely web-shear cracks. Where the amount of the minimum shear reinforcement was increased four times, as in the case of the beam LB10, both web-shear and flexure-shear cracks developed. The amount of axial compression influenced the sequence of the cracks' development. For the specimens subjected to moderate to no compression, for the low value of shear force the onset of flexural cracks in the locations with high bending moment was

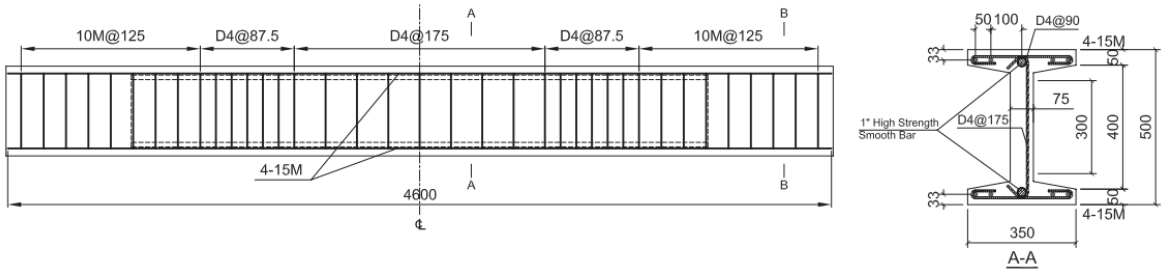

Figure 3-2: Shear reinforcement in the beam LB6 [13]

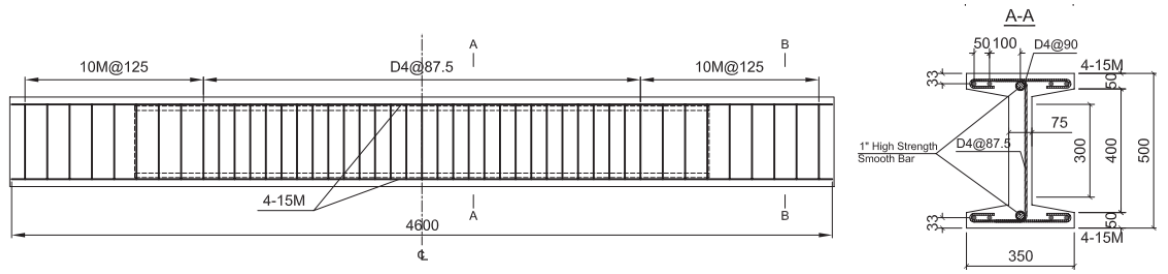

Figure 3-3: Shear reinforcement in the beam LB10 [13]

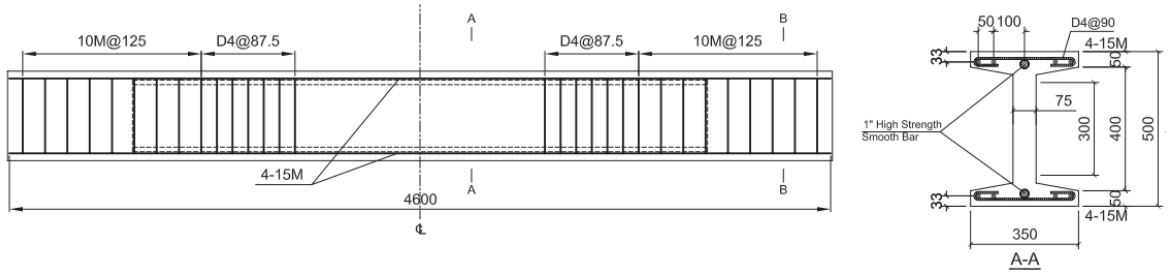

Figure 3-4: Shear reinforcement in the beam LB11 [13]

observed. The cracks later (at the increased shear force) tended to develop into flexure-shear cracks accompanied with the appearance of new, web-shear cracks. For all the specimens, at failure, one web-shear crack developed into the critical shear crack.
The web-shear cracking usually appear at the distance of d_v from one end of the test region and tended to develop towards the mid-span of the beam. The failure mechanism was abrupt. Where shear reinforcement was applied in the whole test region, thus except for the beam LB11, the failure mechanism was related to the rupture of consecutive stirrups and sliding along the surface of the critical web-shear crack. Beams subjected to high compression and shear force tended to expand transversely. As the result, it could be observed that the beams with thick flanges demonstrated higher resistance due to the restraining action – the clamping effect. The clamping effect turned out to affect the resistance more than the amount of longitudinal reinforcement. In the beams with a moderate and high amount of shear reinforcement combined with high axial compression, opening of the critical web-shear crack was followed by flange buckling due to the sudden release of compressive strain energy after the web failed.

From the readings of the load cells it was concluded that the prestressing was successfully transferred from one end of the beam to another. The values of axial compression for beam

LB6, LB10 and LB11 are listed in table 3-1. It can be seen that the loading variation was small and thus the load was maintained at the same level and therefore the average value can be used for further study as representative. It is also noticed that the ratio of the load at the east and the west end of the spreader beam was fairly constant in the range of $P_E/P_W = 1.74/1.86$. In Table 3-2 the cracking and ultimate shear forces are presented with the corresponding values of shear stresses.

Table 3-1: Axial forces for the specimens LB6, LB10, LB11

Specimen	**LB6**	**LB10**	**LB11**
N_{min} [kN]	-793	-810	-809
N_{max} [kN]	-808	-853	-811
N_{avg} [kN]	-797	-822	-809

Table 3-2: Summary of the test results for beams

Specimen	N [kN]	f_{pc} [MPa]	V_{cr-exp} [kN]	v_{cr-exp} [MPa]	V_{u-exp} [kN]	v_{u-exp} [MPa]	θ_{exp} [deg]
LB6	-797	-10.88	148.1	4.77	155.8	5.01	21-35
LB10	-822	-11.16	138.1	4.38	215	6.83	21-29
LB11	-809	-10.97	143.7	4.56	142.8	4.53	21-35
$f_{pc} = N/A_g$ $v_{cr-exp} = \frac{V_{cr-exp}}{b_w d_v}$, where V_{cr-exp} is inclined web-shear cracking force $v_{u-exp} = \frac{V_{u-exp}}{b_w d_v}$,where V_{u-exp} is the ultimate shear force							

3-3 Detailed Observation of Beams LB6, LB10, LB11

3-3-1 Beam LB6

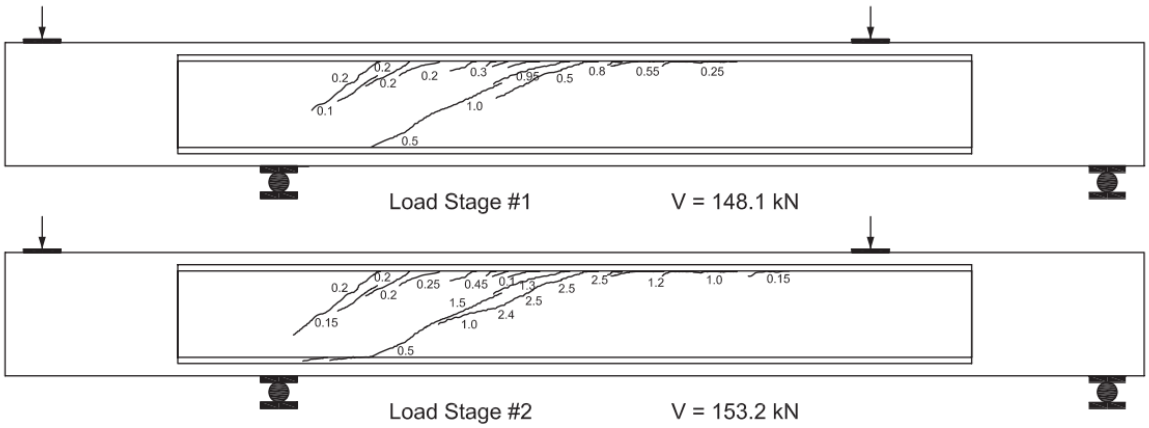

Figure 3-5: Crack pattern for load stage 1 and 2 [13]

Beam LB6 was loaded with the average axial compression of 797 kN. At the cracking shear load of $V = 148.1kN$, the first set of web-shear cracks together with secondary cracks at the joint of the flange and the web appeared. The inclination of the web-shear cracks was between 27° and 36° while the maximum crack width was 1 mm. Further increase of the shear force resulted in widening of the existing cracks and propagation of the horizontal cracks along the junction of the flange and the web towards the loading point. The crack pattern for the cracking shear force and at 98 % of the ultimate shear force is illustrated in Figure 3-5. The failure occurred at the shear force of $155.8kN$ due to opening of the critical shear crack and buckling of the top and bottom flanges, Figure 3-6. The inclination of the critical crack was 25°.

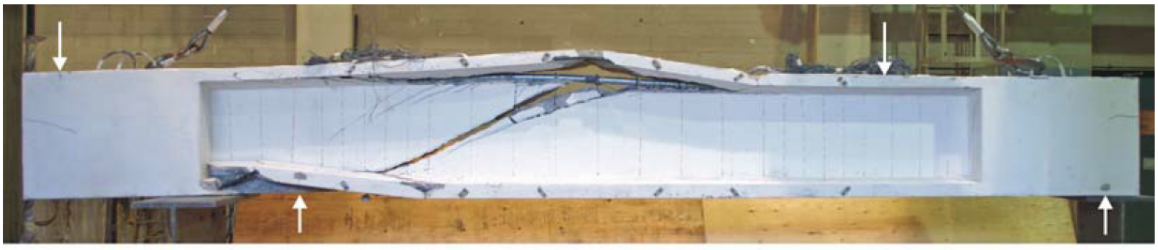

Figure 3-6: Failure of beam LB6 [13]; $A_s = 934mm^2$, $N = -797kN$, $V_u = 155.8kN$, $s = 175mm$

3-3-2 Beam LB10

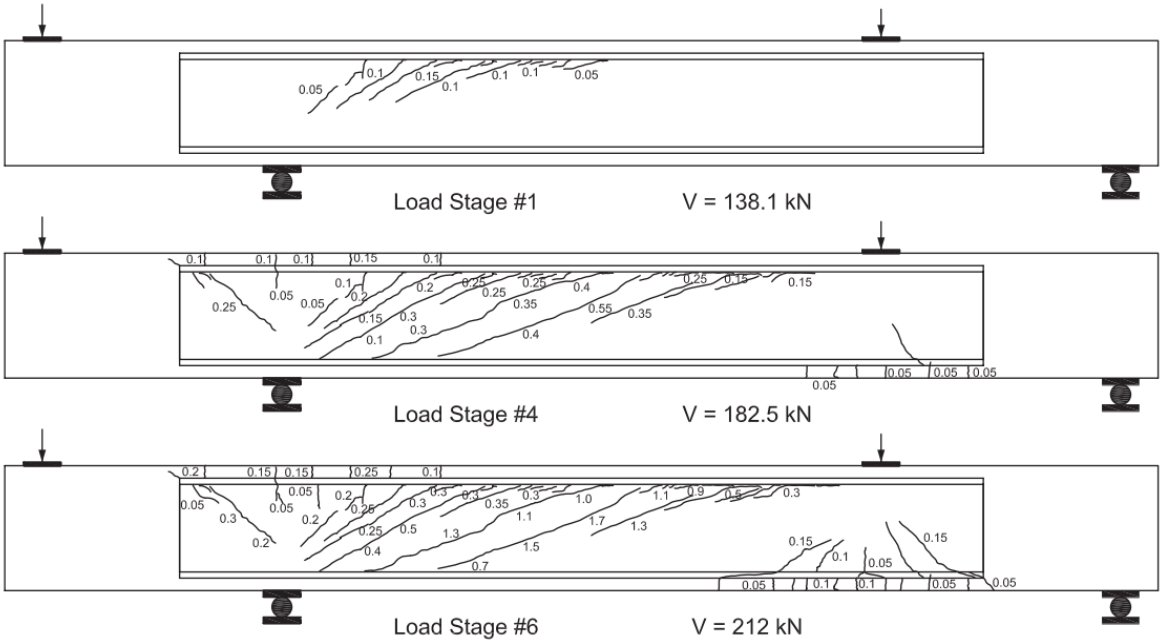

Figure 3-7: Crack pattern for load stage 1, 4 and 6 [13]

The beam LB10 was loaded with the average axial compression of $822kN$. The first set of web-shear appeared at the load of $138.1kN$ before occurrence of any flexural cracks. The

average inclination of cracks was about 25°. The cracks were initiated in the junction of the flange and the web. At the subsequent loading stages more almost parallel web-shear cracks appeared together with some flexural and flexure-shear cracks over the left support and under the right loading point. As the specimen was reinforced with stirrups at the same spacing of 87.5mm in both region 1 and 2, Figure 3-3, a well distributed crack pattern could be observed, Figure 3-7. At failure, the specimen reached the maximum shear force of 215 kN. The failure occurred due to opening of the critical web-shear crack and buckling of the top and bottom flanges as shown in Figure 3-8. The inclination of the failure shear crack was 20°.

Figure 3-8: Failure of beam LB10 [13]; $A_s = 934mm^2$, $N = -822kN$, $V_u = 215kN$, $s = 87.5mm$

3-3-3 Beam LB11

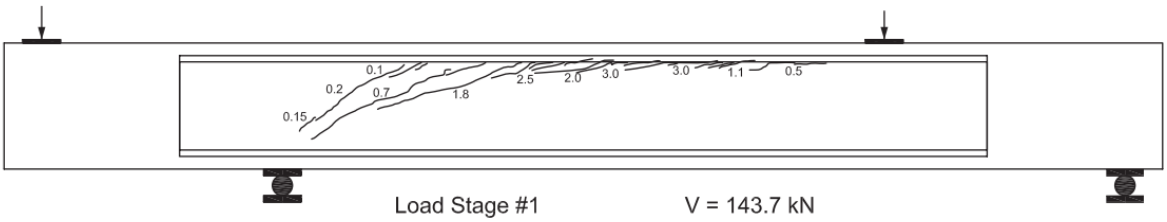

Figure 3-9: Crack pattern for load stage 1 [13]

The beam was loaded with the axial compression of $809kN$. At the load $143.7kN$, the multiple web-shear cracks developed with inclination between 16 and 35°. The widest cracks of 3mm appeared at the junction of the flange and the web propagating towards the right loading point, Figure 3-9. The beam failed at the shear force of $142.8kN$ in an unusual fashion with most of the web remaining uncracked and the critical crack at the junction of the flange and the web. In Figure 3-10, crushing and spalling of concrete close to the right loading point can be seen. Insufficient distribution of cracks before failure could be assigned to the lack of stirrups in the region 1 of the specimen, Figure 3-4.

Figure 3-10: Failure of the bean LB11 [13]; $A_s = 934mm^2$,$N = -809kN$, $V_u = 142.8kN$

3-4 General Findings for the Beams in Compression

From the test on beams in compression the following findings can be drawn:

- Axial compression increases the cracking strength and the shear strength of reinforced concrete beam
- The behaviour at failure of beams in high compression was more brittle than of those subjected to lower compression
- Adding more stirrups improves the shear capacity of beams but did not improve ductility of specimens
- Axial compression increases the post cracking shear capacity as the result of more stirrups being intersected by less inclined cracks.

Chapter 4

Analytical Solution

4-1 Introduction

The theoretical approaches for calculating shear resistance can be divided into two groups. The first group equates the shear strength of a member to a sum of steel and concrete contributions; with the latter contribution by means of the factor to account for aggregate interlock in concrete through strain effect parameter and member size (General Method CSA A23.3.2004 and MC2010 LoA III). Both contributions are also determined with an explicitly defined angle of average principal compressive stress field. The second group addresses shear resistance with expressions applicable depending on the failure mechanism and an amount of shear reinforcement. Methods from this group allow a designer to select a value of an angle of concrete struts for members with shear reinforcement within the limits or implicitly from the Mohr's stress circle (for the splitting tension shear failure).[1]
In this chapter results of calculations for shear resistance of the benchmark beams LB6, LB10 and LB11 are presented. The beams are calculated using expressions from the codes outlined in Chapter 2 Literature Study to check which of the approaches provides the most accurate and comprehensible outcome.

4-2 General Input

To evaluate the specimens as accurately as possible the as-built dimensions and properties of sections were used; and corrected where necessary. The correction concerned solely values of statical moment of area. The geometries and the mass properties used in the calculations are shown in Table 4-1.

The properties of SCC concrete used in the experiment were obtained from the full stress-strain response of the concrete samples tested in compression at 7-day, 14-day, 28-day and at

[1]The flexural shear resistance acc. to the RBK 1.1 combines resistances of both concrete and steel. The expressions are modified versions of the EC2 and the results are analysed as in the case of the EC2

Table 4-1: As-built dimensions

Specimen	LB6	LB10	LB11
$h[mm]$	506	506	506
$b_w[mm]$	73	74	74
$b_{fbot}[mm]$	350	350	350
$h_{fbot}[mm]$	55	50	49
$b_{ftop}[mm]$	350	351	352
$h_{ftop}[mm]$	51	56	57
$h_1 \& h_2$	25		
$d[mm]$	473	473	473
$d_v[mm]$	426	626	426
$A_g[mm^2]$	73225	73670	73740
$A_{ct}[mm^2]$	36265	36650	37597
$I_g[mm^4]$	2.55	2.56	2.56
$Q_{cen}[mm^3]$	6.323	6.346	6.350
$y_{0top}[mm]$	256	248	247
$y_{0bot}[mm]$	250	258	259
$A_{stop}[mm^2]$	934		
$A_{sbot}[mm^2]$	934		
$A_v[mm^2]$	24.2		
$s^*[mm]$	175	87.5	-
$\rho_y = \frac{A_s}{b_w s}[\%]$	0.1894	0.374	-
$N[kN]$	-797	-822	-809

*) values for region 1 only

the test day. More detailed information available in [13]. The material properties from tests used in the calculations are listed in Table 4-2.

Table 4-2: Concrete properties for analytical solution

Specimen	28-days [MPa]	At test [MPa]	E_c	$f_t = 0.33\sqrt{f'_c}$ [MPa]	$\epsilon_c[m\varepsilon]$
LB1	56.2	63.5	40300	2.63*	2.47
LB10-11	59.2	62.3	37900	2.60*	2.27

**Note: the concrete tensile strength was not a measured value. It is calculated from the measured concrete compressive strength. Different tensile strengths are applied for the calculations according to the EC2 (mean concrete tensile strength)*

The properties of reinforcing steel and 1 inch high strength smooth bars resulted from coupon tests on 18 inch long sample bars are listed in Table 4-3.

For the specimens which contained a varying amount of stirrups along the length, the function taking into account the variation of stirrups was applied (Figure 4-1). Such a proportioning of transverse reinforcement is supported by C8.9.3.9 in the Commentary to the CSA shear provision [26]. It argues that a shear failure caused by yielding of stirrups involves yielding of transverse reinforcement over a certain length. At locations where the spacing of stirrups changes, no abrupt but rather a gradual change in shear strength occurs. The gradual dif-

Table 4-3: Steel properties for analytical solution

Size	$d_b[mm^2]$	$A_s[mm^2]$	$f_y[MPa]$	$f_u[MPa]$	$\varepsilon_y[m\varepsilon]$	$\varepsilon_u[m\varepsilon]$	$E_s[MPa]$	$E_s[MPa]$
D4	5.72	24.2	529	581	2.65	40	195800	1392
10M	11.3	100	431	571	2.16	140	201880	-
15M	16.0	200	409	671	2.05	130	201100	-
1 inch bar	25.4	507	972	1074	-	-	199400	-

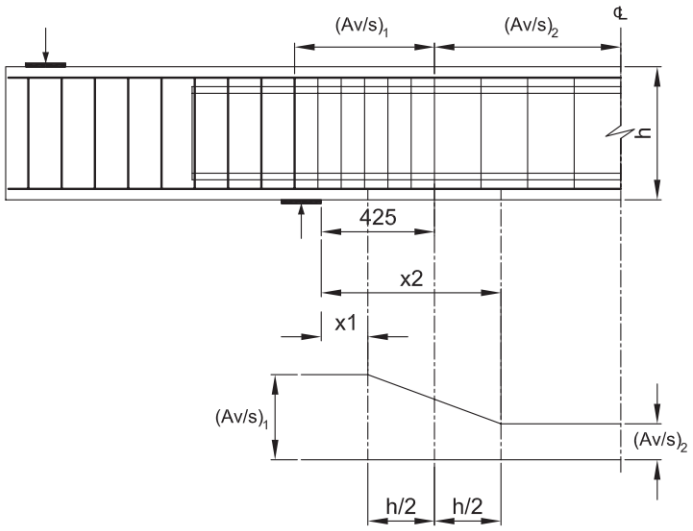

Figure 4-1: Variation of stirrups [13]

ference in capacity spreads over $h/2$ from an end of a region with spacing s_1 to $h/2$ of the beginning of a region with spacing s_2, Figure 4-1.

Depending on the location of the considered section, the effective amount of stirrups per meter of length was calculated with equation 4-1:

$$\frac{A_v}{s} = \begin{cases} \left(\frac{A_v}{s}\right)_1 & \text{for } x \leq 0 \\ \left(\frac{A_v}{s}\right)_1 - \left[\left(\frac{A_v}{s}\right)_1 - \left(\frac{A_v}{s}\right)_2\right]\left(\frac{x-x_1}{x_2-x_1}\right) & \text{for } x_1 < 0 < x_2 \\ \left(\frac{A_v}{s}\right)_2 & \text{for } x \geq x_2 \end{cases} \tag{4-1}$$

where $x_1 = 425 - \frac{h}{2}[mm]$ and $x_2 = 425 + \frac{h}{2}[mm]$.

4-3 Analytical Solution CSA A23.3 2004

The recommendations of the CSA code in case of a member containing a constant amount of stirrups specify to check the critical section located at the distance d_v from the edge of support. The specimens LB6 and LB11 tested in the research program contained a varying amount of stirrups per running meter of length. Consequently, shear resistance has to be checked at different locations in order to determine the critical section. For the beam LB10 which contained a uniform spacing of the stirrups calculations were conducted at diverse

locations as well. Only after this, it could be concluded that the critical section indeed is found at d_v from the edge. In the analytical solution checked locations start at d_v from the edge for the first section and subsequently increase by the increment of 25 mm for the further located sections. The calculation of the shear resistance according to the CSA Code requires an iterative procedure as shown in the flow chart, Figure 4-2.

4-3-1 Shear Resistance of the Critical Sections

Refer also to Appendix A for all results and Mathcad calculations

Analysis of the Critical Section in the Beam LB6

In this section exemplary calculations for the critical section of the beam LB6 are carried out. The as-built dimensions as well as the concrete properties measured at test are used.

The procedure requires iterations to determine the shear resistance of the considered section. However, the critical section location is also unknown. Consequently, a number of sections have to be checked. Because calculations in this section serve only as an example, they are performed for the already known location of the critical cross-sections(located at $\boldsymbol{x=0.675m}$ *from the face of the supporting plate) and the value of shear resistance* $\boldsymbol{V_f = 159.23kN = V_{f,trial}}$.

To find bending moment from the self-weight, the reaction forces at the supports have to be determined. The beam consists of two sections with different areas: the diaphragm block and the I shaped region, Figure 3-1.

The uniformly distributed load from the block:
$q_{Eg1} = h * b_{ftop} * \gamma_{concrete} = 0.506m * 0.35m * 25kN/m^3 = 4.4275kN/m$
Uniformly distributed load from the I shaped section:
$q_{Eg2} = A_g * \gamma_{concrete} = 0.0732m^2 * 25kN/m^3 = 1.831kN/m$

The reaction force at the west support from the vertical force equilibrium:
$0.70m * q_{Eg1} * 4.120m + 3.220m * q_{Eg2} * (\frac{3.220m}{2} + 0.550m) + 0.550m * q_{Eg1} * \frac{0.550m}{2} - \frac{(0.150m)^2}{2} * q_{Eg1} - R_A * 3.360m = 0 \longmapsto R_A = 0.9m * q_{Eg1} + 2.07m * q_{Eg2} = 7.774kN$

The bending moment:
$M_{Eg}(x = 0.675m) = 0.7m*q_{Eg1}*(0.350m+0.410m+x)+(0.41m+x)*q_{Eg2}*(\frac{0.41m+x}{2})-R_A*x = 0.277kNm$
The shear force from the self-weight:
$V_{Eg}(x = 0.675m) = -\frac{d}{dx}(0.7m*q_{Eg1}*(0.350m+0.410m+x)+(0.41m+x)*q_{Eg2}*(\frac{0.41m+x}{2})-R_A*x) = 2.689kN$

The amount of shear reinforcement at the critical section from the equation 4-1:
$A_v/s = 139.1mm^2/m$

The effective shear depth is defined as $d_v = max(0.72h, 0.9d) = max(364mm, 426mm) = 426mm$

The bending moment for the section located at 0.675m from the edge of the support:
$M_f = M_{Eg} + V_{f,trial}(1.2m - x - 0.15m/2) = 71.88kNm$

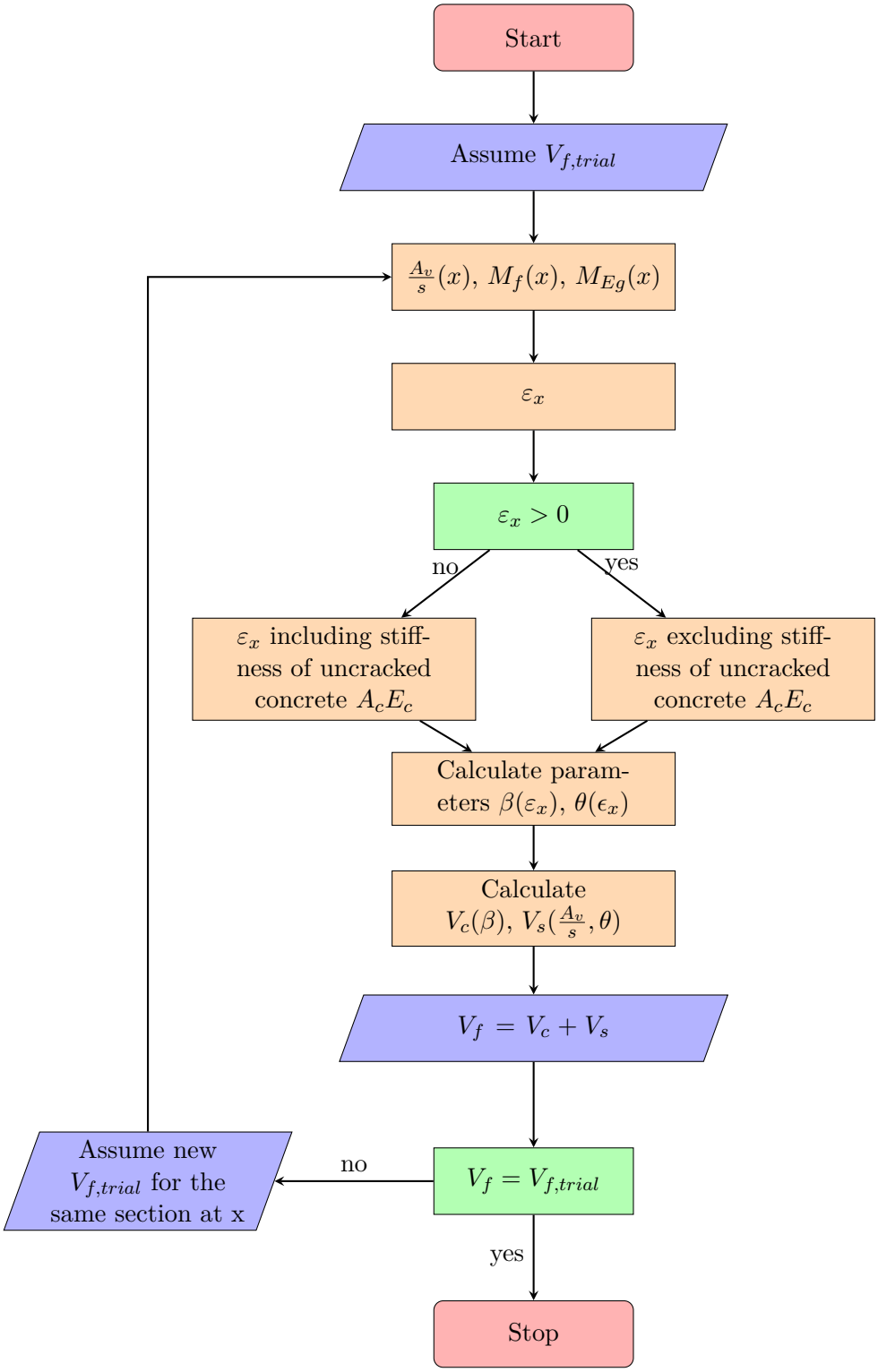

Figure 4-2: Flowchart for calculation of shear resistance acc. to the CSA code

The section is fully in compression which was found from the force in the longitudinal reinforcement at a crack:
$M_f/d_v + V_{f,trial} + V_{Eg} + 0.5N_{axial} = 71.88kNm/0.426m + 159.1kN + 2.689kN - 0.5 * 797kN = -67.835kN < 0$ thus in compression.

The longitudinal strain at the mid-height (average) is calculated including the stiffness of concrete on the flexural tension side of the member:
$\varepsilon_x = \frac{M_f/d_v + V_{f,trial} + V_{Eg} + 0.5N_{axial}}{2(E_s A_s + E_c A_{ct})} = \frac{71.88kN*m/0.426m + 159.1kN + 2.69kN - 0.5*797kN}{2(201100MPa*934mm^2 + 40300MPa*35560mm^2)} = -0.0000209$
Because of the fact that the amount of shear reinforcement is higher than the minimum, the crack spacing is 300mm. The factor β accounting for aggregate interlock in concrete is:
$\beta = \frac{0.4}{1+1500\varepsilon_x} \frac{1300}{1000+s_{ze}} = \frac{0.4}{1+1500*(-0.0000209)} \frac{1300}{1000+300} = 0.41$
The diagonal crack inclination θ:
$\theta = 29 + 7000\varepsilon_x = 28.85\,\text{deg}$

Now, the concrete and steel contribution to shear resistance can be calculated:
$V_c = \beta\sqrt{f'_c} b_w d_v = 0.41 * \sqrt{63.5} * 73mm * 426mm = 102.26kN$
$V_s = f_{yv} \frac{A_v}{s} d_v \cot\theta = 529MPa * 139.1mm^2/m * 426mm * \cot(28.85\,\text{deg}) = 56.856kN$

The total shear resistance: $V_f = V_c + V_s = 102.26kN + 56.856kN = 159.12kN$
which is exactly the value of the assumed $V_{f,trial}$, hence no further iterations are necessary.

Calculation of the shear resistance is determined assuming that the flexural capacity of the longitudinal reinforcement is sufficient to allow a shear failure. In addition to this, crushing of concrete compressive struts cannot occur.

Flexural failure:
$F_{lt} = A_s * f_y = 382.0kN \geq M_f/d_v + 0.5N_{axial} + (V_R - 0.5V_s)\cot\theta = 71.88kNm/0.426m - 0.5 * 797kN + (159.12kN - 0.5 * 56.856kN)\cot(28.85\,\text{deg}) = 7.553kN$, thus flexural failure does not occur.

Crushing of concrete struts:
$\frac{V_R}{b_w d_v} = \frac{159.1kN}{73mm*426mm} = 5.12N/mm^2 < 0.25\phi_c f'_c = 0.25 * 1 * 63.5N/mm^2 = 15.875N/mm^2$.
Neither the flexural capacity of the longitudinal reinforcement nor the crushing of concrete struts is governing hence the requirements are met. The governing failure mechanism is shear failure.

Analysis for the Critical Section in the Beam LB10

A similar procedure was carried out for the beam LB10. In this case, as opposed to the other beam, no variation of stirrups along the beam's length takes place. Nevertheless, a number of sections have to be check in order to determine the critical. Similarly to the preceding section, the calculations presented below are related to the critical section with the already known shear capacity found through the iterative procedure at a different distance from the edge of the support's face.

The critical section of beam LB10 is at the distance **x=425mm** from the edge of the loading plate. The shear resistance at this location is: $\boldsymbol{V_f = V_{f,trial} = 182.25kN}$

The uniformly distributed load from the block:
$q_{Eg1} = h * b_{ftop} * \gamma_{concrete} = 0.506m * 0.351m * 25kN/m^3 = 4.44kN/m$

Uniformly distributed load from the I shaped section:
$q_{Eg2} = A_g * \gamma_{concrete} = 0.0737m^2 * 25kN/m^3 = 1.842kN/m$

The reaction force at the west support resulting from the self-weight equals:
$R_A = 7.81kN$.

Bending moment from the self weight at the considered location:
$M_{Eg}(x) = 0.7m * q_{Eg1} * (0.350m + 0.410m + x) + (0.41m + x) * q_{Eg2} * (\frac{0.41m+x}{2}) - R_A * x$
$M_{Eg}(0.425m) = 1.00kN * m$
The shear force from the self-weight:
$V_{Eg}(x = 0.425m) = -\frac{d}{dx}(0.7m * q_{Eg1} * (0.350m + 0.410m + x) + (0.41m + x) * q_{Eg2} * (\frac{0.41m+x}{2}) - R_A * x) = 3.16kN$

The amount of shear reinforcement is constant in the entire test region: $A_v/s = 276.57mm^2/m$

The bending moment for the section located at 0.425m from the edge of the support:
$M_f(x = 0.425m) = M_{Eg} + V_{f,trial}(1.2m - x - 0.15m/2) = 1.00kNm + 182.25kN(1.2m - 0.425m - 0.075m) = 128.58kNm$

From:
$M_f/d_v + V_{f,trial} + V_{Eg} + 0.5N_{axial} = 128.58kNm/0.426m + 182.25kN + 3.16kN - 411kN = 76.45kN$
it can be seen that the section at the level of the longitudinal reinforcement is in tension. Under the conservative assumption of the General Method, the compressive strains are zeroed and consequently the longitudinal strain factor is calculated without the effect of the concrete stiffness $A_{ct}E_c$:
$\varepsilon_x = \frac{M_f/d_v+V_{f,trial}+V_{Eg}+0.5N_{axial}}{2(E_sA_s)} = \frac{128.58kNm/0.426m+182.25kN+3.16kN-0.5*822kN}{2(201100MPa*934mm^2)} = 0.000020351$
The amount of shear reinforcement is four times the minimum amount, therefore the crack spacing is again 300mm. Factor β accounting for the aggregate interlock in concrete is:
$\beta = \frac{0.4}{1+1500\varepsilon_x}\frac{1300}{1000+s_{ze}} = \frac{0.4}{1+1500*(0.000020351)}\frac{1300}{1000+300} = 0.31$
The diagonal crack inclination θ:
$\theta = 29 + 7000\varepsilon_x = 30.42\,\text{deg}$

The concrete and steel contribution to shear resistance can be calculated:
$V_c = \beta\sqrt{f'_c}b_wd_v = 0.31 * \sqrt{62.3} * 74mm * 426mm = 76.2kN$
$V_s = f_{yv}\frac{A_v}{s}d_v\cot\theta = 529MPa * 276.57mm^2/m * 426mm * \cot(30.42\,\text{deg}) = 106.05kN$

The total shear resistance:
$V_f = V_c + V_s = 76.2kN + 106.05kN = 182.25kN$
Because $V_f = V_{f,trial}$ no further iterations are needed.

To check if the above calculated shear failure mechanism is governing, the flexural capacity of the longitudinal reinforcement and crushing of compressive struts are checked.

Flexural failure:
$F_{lt} = A_s * f_y = 382.0kN \geq M_f/d_v + 0.5N_{axial} + (V_R - 0.5V_s)\cot\theta = 128.58kNm/0.426m - 0.5 * 822kN + (182.25kN - 0.5 * 106.53kN)\cot(30.42\,\text{deg}) = 73.48kN$, thus flexural failure does not occur.

Crushing of concrete struts:
$\frac{V_R}{b_wd_v} = \frac{182.25.kN}{74mm*426mm} = 6.51N/mm^2 < 0.25\phi_cf'_c = 0.25 * 1 * 62.3N/mm^2 = 15.575N/mm^2$ thus also not governing.

Analysis for the Critical Section in the Beam LB11

The test region essentially consists of two regions: Region 1 and Region 2. In the case of the beam LB11, to avoid a flexural-shear failure, stirrups were applied only in the Region 2 (near the support). As previously, a number of cross-sections are to be check to determine the critical. In this example, the cross-section at **x=0.575m** with the shear resistance of $\boldsymbol{V_f = 86.29kN}$ is considered.

The uniformly distributed load from the diaphragm block:
$q_{Eg1} = h * b_{ftop} * \gamma_{concrete} = 0.506m * 0.352m * 25kN/m^3 = 4.453kN/m$
Uniformly distributed load from the I shaped section:
$q_{Eg2} = A_g * \gamma_{concrete} = 0.0737m^2 * 25kN/m^3 = 1.843kN/m$

The reaction force at the west support from the vertical force equilibrium:
$0.70m * q_{Eg1} * 4.120m + 3.220m * q_{Eg2} * (\frac{3.220m}{2} + 0.550m) + 0.550m * q_{Eg1} * \frac{0.550m}{2} - \frac{(0.150m)^2}{2} * q_{Eg1} - R_A * 3.360m = 0 \longmapsto R_A = 0.9m * q_{Eg1} + 2.07m * q_{Eg2} = 7.824kN$

The bending moment for the self-weight:
$M_{Eg}(x = 0.575m) = 0.7m * q_{Eg1} * (0.350m + 0.410m + x) + (0.41m + x) * q_{Eg2} * (\frac{0.41m+x}{2}) - R_A * x = 0.557kNm$
The shear force from the self-weight:
$V_{Eg}(x = 0.575m) = -\frac{d}{dx}(0.7m * q_{Eg1} * (0.350m + 0.410m + x) + (0.41m + x) * q_{Eg2} * (\frac{0.41m+x}{2}) - R_A * x) = 2.89kN$

The amount of shear reinforcement at the critical section from the equation 4-1:
$A_v/s = 56.3mm^2/m$ which is lower than the minimum value:

$$A_{v,min} = 0.06\sqrt{f'_c}\frac{b_w}{f_{yv}} = 66.25mm^2/m$$

The total bending moment due to the applied load at x=0.575m from the edge of the support:
$M_f = M_{Eg} + V_{f,trial}(1.2m - x - 0.15m/2) = 0.557kNm + 86.29kN * (1.2m - 0.575m - 0.075m) = 48.01kNm$

Force in the longitudinal reinforcement is: $M_f/d_v + V_{f,trial} + V_{Eg} + 0.5N_{axial} = 48.01kNm/0.426m + 86.29kN + 2.89kN - 0.5 * 807kN = -201.5kN < 0$ thus in compression.

As a consequence, the longitudinal strain at the mid-depth includes the stiffness of concrete on the flexural tension side of the member:
$\varepsilon_x = \frac{M_f/d_v + V_{f,trial} + V_{Eg} + 0.5N_{axial}}{2(E_s A_s + E_c A_{ct})} = \frac{48.01kN*m/0.426m + 86.29kN + 2.89kN - 0.5*807kN}{2(201100MPa*934mm^2 + 37900MPa*36880mm^2)} = -6.36 * 10^{-5}$

The amount of shear reinforcement is lower than the minimum. For members without shear reinforcement the general method of shear design takes crack spacing s_z as the effective shear depth d_z.
Aggregate interlock is influenced by two major factors: a crack width and roughness of a crack plane. Cracks spaced in a larger distance from each other imply a reduced effect of the aggregate interlock as a results of larger crack widths. To account for an aggregate size, an effective crack spacing parameter is calculated with: $s_{ze} = \frac{35*d_v}{a_{g,adjusted}+15} = \frac{35*426}{7.7+15} = 656.4mm$ where $a_{g,adjusted}$ is the correction factor accounting for the cracks passing through aggregate particles rather than around them in concrete of higher strength. This in turn reduces the effect of the aggregate interlock. It follows from:

$$a_{g,adjusted} = \begin{cases} 0 & \text{for } f_c^{'} \geq 70MPa \\ a_g \frac{70-f_c^{'}}{10} & \text{for } 60MPa < f_c^{'} < 70MPa \\ a_g & \text{otherwise} \end{cases}$$

The factor β: $\beta = \frac{0.4}{1+1500\varepsilon_x}\frac{1300}{1000+s_{ze}} = \frac{0.4}{1+1500*(-0.0000636)}\frac{1300}{1000+656.37} = 0.35$

The diagonal crack inclination θ:
$\theta = 29 + 7000\varepsilon_x = 28.56\,\text{deg}$

As the results of not sufficient quantity of stirrups, the total shear resistance is equal to the contribution of concrete only:
$V_c = \beta\sqrt{f_c'}b_w d_v = 0.35 * \sqrt{62.3} * 74mm * 426mm = 86.29kN$
$V_s = 0$

Total shear resistance: $V_f = V_c = 86.29kN$
which is equivalent to the assumption $V_{f,trial}$.

Finally, the remaining possible failure mechanisms have to be checked:

Flexural failure:
$F_{lt} = A_s * f_y = 382.0kN \geq M_f/d_v + 0.5N_{axial} + (V_R - 0.5V_s)\cot\theta = 48.01kNm/0.426m - 0.5 * 807kN + (86.29kN)\cot(28.56\,\text{deg}) = -132.16kN$, thus flexural failure does not occur.

Crushing of concrete struts:
$\frac{V_R}{b_w d_v} = \frac{86.29kN}{74mm*426mm} = 2.73N/mm^2 \ll 0.25\phi_c f_c^{'} = 0.25 * 1 * 62.3N/mm^2 = 15.575N/mm^2$
thus also not governing.

4-3-2 Cumulative Results

The obtained results, Figures 4-3, 4-4 and 4-5 are generally in agreement with the results in [13] except for the results of the LB11. The critical sections found in [13] and in this report for the beams LB6 and LB10 coincide and the ultimate shear resistance is found to be almost the same (LB6: 159.12kN and 159.9kN; LB10:182.25kN and 183.2kN). Slightly higher values from [13] resulted probably from excluding the impact of the self-weight, which in fact turned out to be negligibly small. The locations of the critical section for each specimen is marked in the figures with a blue marker.
The only difference arises for the case LB11. It is most probably caused by the way in which the steel contribution was treated. In this thesis, the contribution of shear reinforcement for sections at which the amount of stirrups does not meet the minimum amount requirement was completely disregarded; resulting in a sudden drop of shear resistance visible in Figure 4-5. As opposed to that, the [13] considered the impact of stirrups even below the threshold of $A_{s,min}$.
From the comparison between the experimental and analytical solution results, it is apparent that the prediction of the shear capacity for region without shear reinforcement is substantially underestimated. The reason for this is presumably the fact that the code conservatively estimates the post-cracking shear strength (an ability of an element to bridge stresses across the crack plane through aggregate interlock) rather than the first cracking shear force which is much higher (as will be shown in the section devoted to the EC2).
It is interesting to note that the effect of a combination of axial force, shear force and bending

moment on an angle θ is the same as explained in section 2-1. The angle is flatter for sections in compression (LB6, LB11) and more open for sections in tension (LB10). Heavily reinforced members naturally are capable of withstanding higher values of shear forces before failure which translate to positive (tensile) strain in the "strain state" parameter ϵ_x on which θ in the method is dependent.
The critical section for the beam LB6 was determined at the distance 675 mm from the west support. The major crack observed in the test happened to be situated roughly at the same distance. The governing resistance for the beam LB10 was predicted at the distance d_v from the edge of the support which is often considered as the critical section. From the test observation, this region was extensively cracked with web shear cracks with the major crack situated approximately in the same area. Again, it can be concluded that the code's prediction is fairly good. For the beam LB11 the critical crack runs along the junction of the web and the upper flange with the largest crack width in the middle of the test region. This location does not exactly coincide with the prediction of the code but in both cases the critical section(s) is determined to be in the region unreinforced against shear.

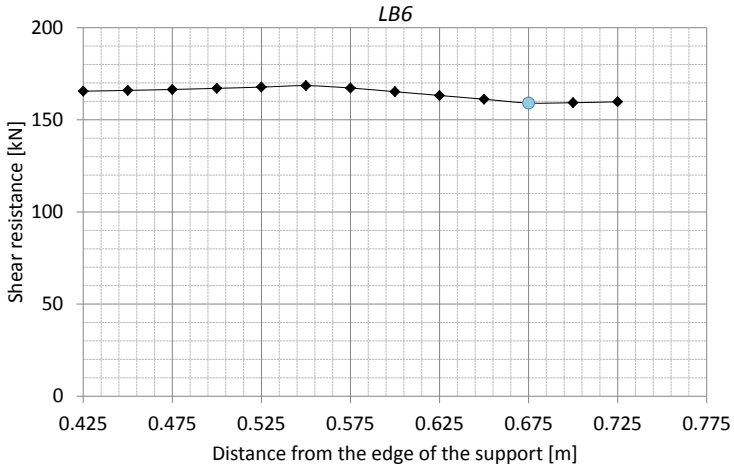

Figure 4-3: Shear capacity of the beam LB6 by CSA at different locations

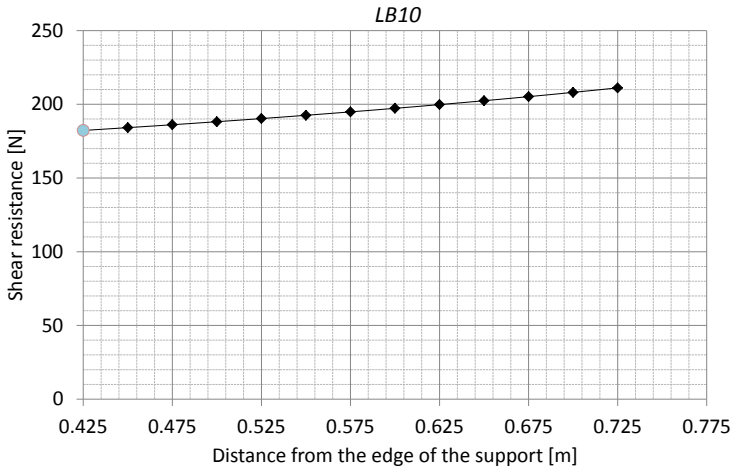

Figure 4-4: Shear capacity of the beam LB10 by CSA at different locations

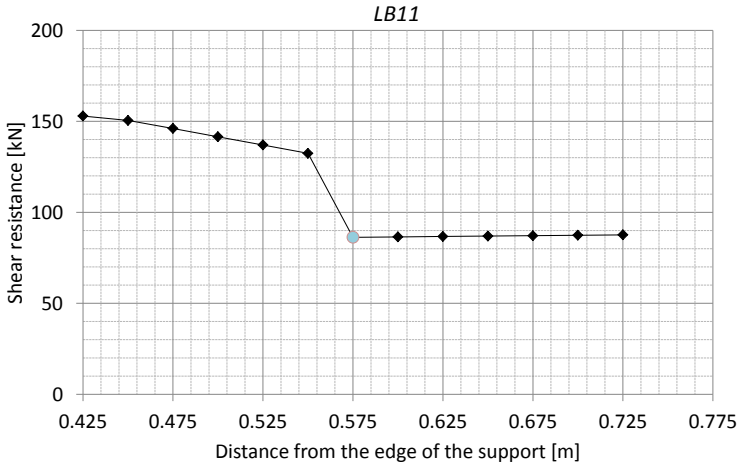

Figure 4-5: Shear capacity of the beam LB11 by CSA at different locations

4-3-3 Detailed Analyses

"More Accurate Calculations"

The method of the CSA code to determine the longitudinal strain conservatively assumes zero strain values in the flexural compression flange. This enables to conveniently take $\varepsilon_x = \varepsilon_t/2$. The simplification is supported by the fact that ε_c has usually small negative values thus might be assumed to be negligible.

This section investigate the shear resistances for the critical cross-sections obtained when the aforementioned conservative assumption is disregarded. The axial strain in the flanges is calculated directly from forces acting on the flanges and adopting the bilinear relationships shown in Figure 2-21. The average strain at the mid-depth is calculated as an average of strains at the top and bottom flanges. The procedure is iterative and apart from the way a section is considered, does not differ from the one explained in the preceding chapters.

Beam LB6
Predefined shear resistance and the location of the critical section: $V_{f,trial} = 168.06kN$ and $x = 0.7m$
The axial strain is calculated from the axial forces in the flanges.
$F_{TopChord} = V_f + V_{Eg} + M_f/d_v + N_{axial}/2 = 168.06kN + 2.643kN + 71,637kNm/0.426m - 797kN/2 = -59.52kN$ compression

$F_{BottomChord} = V_f + V_{Eg} - M_f/d_v + N_{axial}/2 = 168.06kN + 2.643kN + 71.637kNm/0.426m - 797kN/2 = -396.08kN$ compression

The cross-section is in compression hence strains are calculated with a combination of the concrete and steel stiffnesses.

$\varepsilon_{TopChord} = \frac{F_{TopChord}}{E_s A_s + E_c A_{ct}} = -1.84 * 10^{-5}$
$\varepsilon_{BottomChord} = \frac{F_{BottomChord}}{E_s A_s + E_c A_{ct}} = -1.22 * 10^{-4}$

The average strain, Figure 4-6:
$\varepsilon_x = \frac{\varepsilon_{TopChord} + \varepsilon_{BottomChord}}{2} = -7.03 * 10^{-5}$

The parameter β:
$\beta = \frac{0.4}{1+1500\varepsilon_x}\frac{1300}{1000+s_{ze}} = 0.447$

The angle θ:
$\theta = (29 + 7000\varepsilon_x) = 28.51\,\text{deg}$

The contributions of concrete and steel and the ultimate resistance:
$V_c = \beta\sqrt{f'_c}b_w d_v = 110.730kN$
$V_s = f_{yv}\frac{A_v}{s}d_v \cot\theta = 529MPa * 138.29mm^2/m * 426mm * \cot(28.51\,\text{deg}) = 57.336kN$
$V_f = V_c + V_s = 168.06kN$
The shear resistance calculated from the actual strain state is increased due to:
first, an increase of the factor β resulting in greater aggregate interlock and a higher concrete contribution, and
second, a slightly flattened inclination of compressive struts leading to a crack crossing a higher number of stirrups increasing effectiveness of applied shear reinforcement which translates to higher resistance attributed to steel.

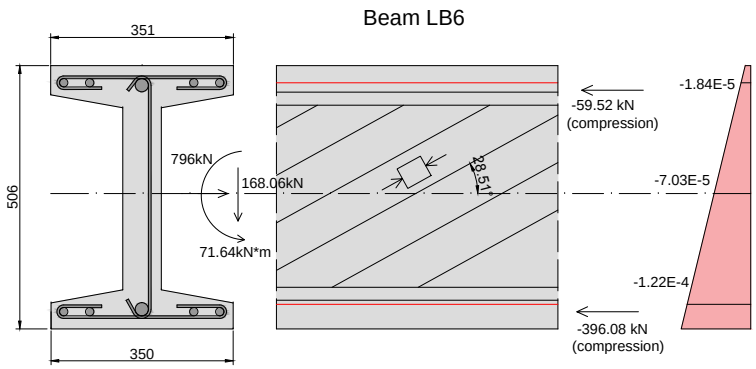

Figure 4-6: Calculated values of strain and forces for LB6

Beam LB10

Similar calculations have been performed for LB10:
Predefined shear resistance and the location of the critical section: $V_{f,trial} = 199.21kN$ and $x = 0.425m$.

$F_{TopChord} = V_f + V_{Eg} + M_f/d_v + N_{axial}/2 = 199.21kN + 3.162kN + 140.45kNm/0.426m - 822kN/2 = 121.31kN$ tension

$F_{BottomChord} = V_f - M_f/d_v + N_{axial}/2 = 199.21kN + 3.162kN - 140.45kNm/0.426m - 822kN/2 = -538.56kN$ compression

The top chord is in tension thus the strains are calculated taking only the reinforcement stiffness into account: $\varepsilon_{TopChord} = \frac{F_{TopChord}}{E_s A_s} = 3.23 * 10^{-4}$

The bottom chord is in compression; an effect of concrete stiffness is included:
$\varepsilon_{BottomChord} = \frac{F_{BottomChord}}{E_s A_s + E_c A_{ct}} = -1.71 * 10^{-4}$

The average strain, Figure 4-7:
$\varepsilon_x = \frac{\varepsilon_{TopChord} + \varepsilon_{BottomChord}}{2} = 7.61 * 10^{-5}$

The parameter β:
$\beta = \frac{0.4}{1+1500\varepsilon_x} \frac{1300}{1000+s_{ze}} = 0.359$

The angle θ:
$\theta = (29 + 7000\varepsilon_x) = 29.53\,\text{deg}$

The contribution of concrete and steel and the ultimate resistance:
$V_c = \beta\sqrt{f'_c} b_w d_v = 89.271kN$
$V_s = f_{yv}\frac{A_v}{s} d_v \cot\theta = 529MPa * 276.57mm^2/m * 426mm * \cot(29.53\,\text{deg}) = 109.94kN$
$V_f = V_c + V_s = 199.21kN$

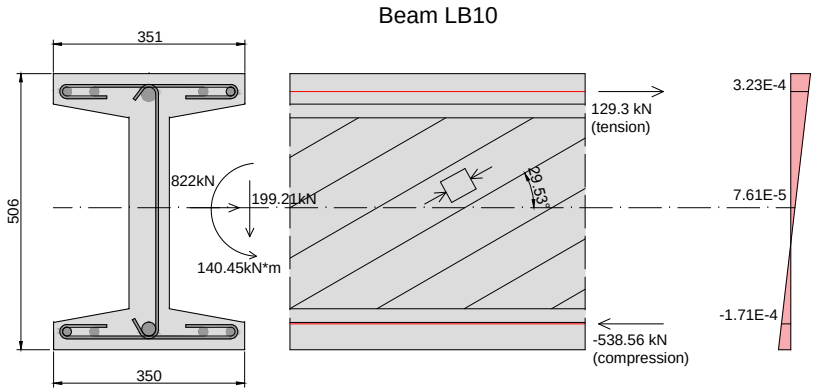

Figure 4-7: Calculated values of strain and forces for LB10

Beam LB11
Predefined shear resistance and the location of the critical section: $V_{f,trial} = 91.43kN$ and $x = 0.575m$.

$F_{TopChord} = V_f + V_{Eg} + M_f/d_v + N_{axial}/2 = 91.43kN + 2.89kN + 50.84kNm/0.426m - 807kN/2 = -189.7kN$ compression

$F_{BottomChord} = V_f + V_{Eg} - M_f/d_v + N_{axial}/2 = 91.43kN + 2.89kN - 50.84kNm/0.426m - 807kN/2 = -428.6kN$ compression

$\varepsilon_{TopChord} = \frac{F_{TopChord}}{E_s A_s + E_c A_{ct}} = -5.98 * 10^{-5}$
$\varepsilon_{BottomChord} = \frac{F_{BottomChord}}{E_s A_s + E_c A_{ct}} = -1.35 * 10^{-4}$

The average strain, Figure 4-8:
$\varepsilon_x = \frac{\varepsilon_{TopChord} + \varepsilon_{BottomChord}}{2} = -9.75 * 10^{-5}$
The parameter β:
$\beta = \frac{0.4}{1+1500\varepsilon_x} \frac{1300}{1000+\frac{35*d_v}{a_{g,adjusted}+15}} = 0.368$
The contribution of concrete and steel and the ultimate resistance:
$V_c = \beta\sqrt{f'_c} b_w d_v = 91.43kN$
$V_s = 0$
$V_f = V_c + V_s = 91.43kN$

In Figure 4-9 and Table 4-4 the "accurate method" is summarized. From the comparison between the methods, it can be concluded that the slight increase of the ultimate shear resistance mostly stems from a larger contribution of concrete and almost unnoticeable increase of

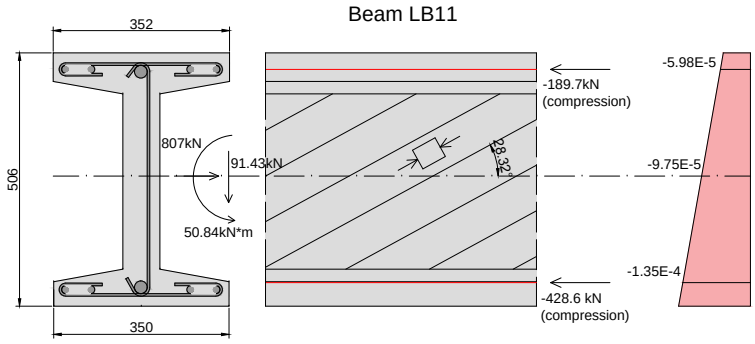

Figure 4-8: Calculated values of strain and forces for LB11

shear resistance from the stirrups. It would suggest that the method is only somewhat sensitive to small changes in longitudinal for sections in compression and moderately sensitive to sections in tension. For the design in which the benchmark shear resistances are not known beforehand, more detailed consideration might have a negative impact being more unconservative as it happened in this study for beam LB6. From Table 4-4, it can be seen that while for LB10 and LB11, "more accurate" analyses improved code's prediction, for beam LB6 the effect was opposite and the results unconservatively drifted away from the benchmark result.

Table 4-4: Summary of the predictions by the CSA code

Beam	**LB6**	**LB10**	**LB11**
CSA General Method	159.1 kN	182.25 kN	86.29 kN
CSA "More Accurate Method"	168.06 kN	199.1 kN	91.43
$V_{U,Experiment}$	155.8 kN	215.0 kN	142.8 kN
Exp./General Method	0.97	1.18	1.65
Exp./"More Accurate Method"	0.92	1.08	1.56

Influence of a Variable Angle θ

In [12], which covers the development of the shear provision for concrete structures, the bottom chord longitudinal force component resulting from shear is simplified by assuming that $0.5cot\theta$ is approximately equal to one. Conservativeness of this assumption has been analysed for the critical sections in all beams through adding a dependence of the shear strength on the angle of the compressive principal direction. It was found that when the conservative assumption is ignored, the shear resistance for the beam LB10 can be increased by around 6%. The impact of the variable angle of compressive struts on the shear resistance was not meaningful for the remaining cases; less than 1% for the LB6 and LB11. The reason why the impact on the beams LB6 and LB11 is so small is the fact that the longitudinal strain for the critical sections has a negative value, thus calculated taking the stiffness of concrete into account which greatly decreases the value. Therefore, it can be seen that the reduction of applied forces with $0.5cot\theta$ is diminished through the strain parameter ε_x. It is important to know that negative value of ε_x indicates that the crack width is much lower (the member is cracked! even for negative values of the longitudinal strain ε_x), though not

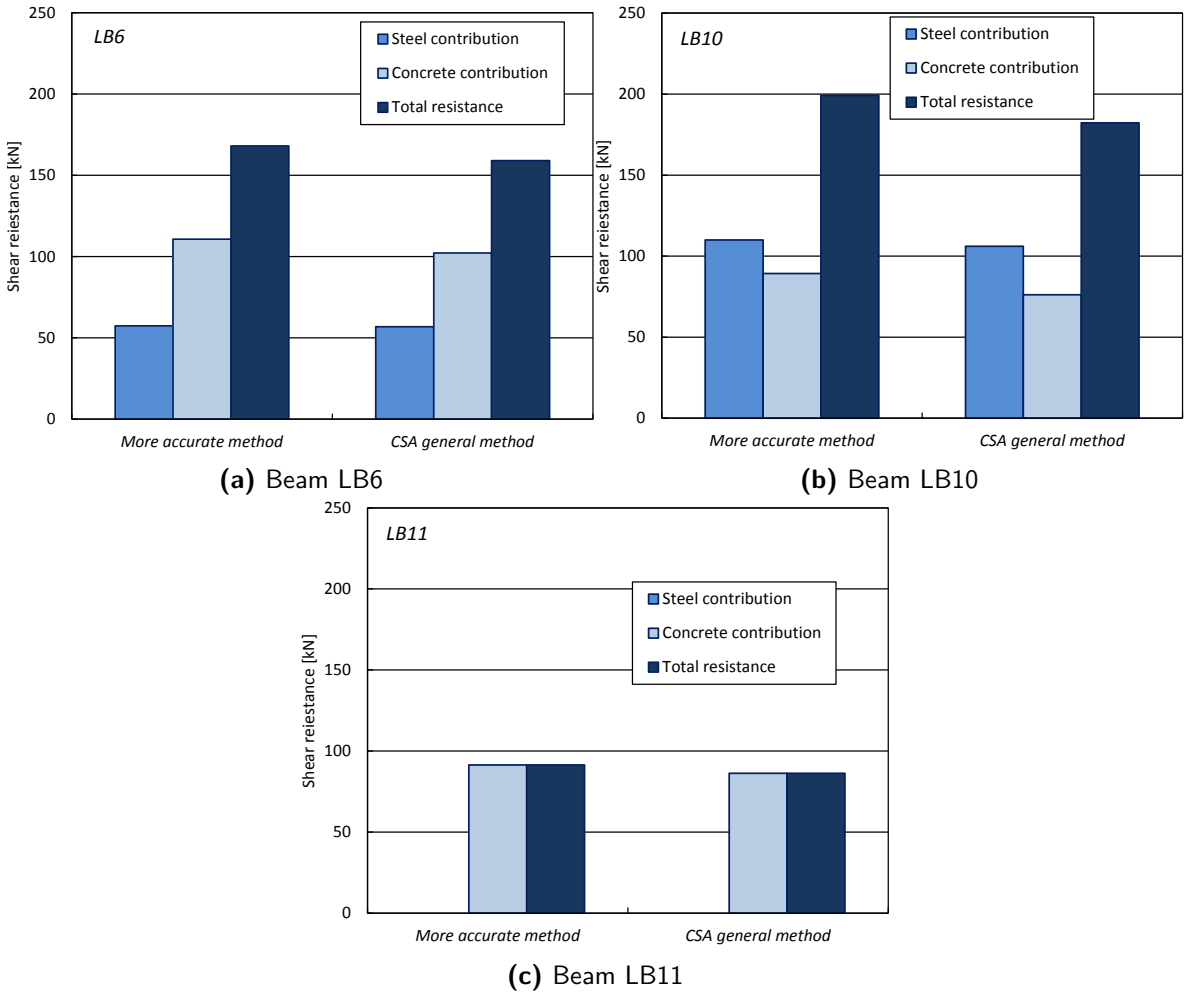

(a) Beam LB6

(b) Beam LB10

(c) Beam LB11

Figure 4-9: Contribution of concrete and steel to total resistance according to the General Method and "more accurate method"

negative. In [12], the authors mentioned that the method *"does not predict first cracking strength, but the strength in a member that is already cracked for whatever cause"*. A different situation occurs for the beam LB10 which is heavily reinforced with stirrups. Consequently, on a section act higher forces which results in a positive value of the longitudinal strain; a higher crack width controlled by the higher demand of shear reinforcement. The positive value of the longitudinal strain is calculated with only steel stiffness taken in the formula resulting in a greater impact of the forces on the strain parameter ε_x. This means that the reduction of the applied shear and moment by employing $0.5cot\theta$ would results in an increase of the ultimate shear strength as indicated in Table 4-5.

Table 4-5: Summary of the results for calculations with a variable angle θ.

Beam	ε_x	β	θ [deg]	V_c [kN]	V_s [kN]	V_f [kN]
LB6 with a variable angle θ	$-2.928 * 10^{-5}$	0.418	28.795	103.60	56.99	160.6
LB6	$-2.09 * 10^{-5}$	0.41	28.85	102.26	56.86	159.12
LB10 with a variable angle θ	$1.123 * 10^{-4}$	0.342	29.79	85.12	108.81	193.93
LB10	$2.034 * 10^{-4}$	0.31	30.42	76.198	106.05	182.25
LB11 with a variable angle θ	$-6.147 * 10^{-5}$	0.346	28.57	85.99	0	85.99
LB11	$-6.36 * 10^{-5}$	0.35	28.56	86.29	0	86.29

4-4 Analytical Solution *fib* Model Code 2010

The fib Model Code 2010 (MC 2010) introduces a significant advancement over the previous fib Model Code 1990 as it waives from standardized empirical methods. In the current MC2010 the approach referred as levels of approximation (LoA) is introduced. The method was already outlined in the chapter 2 to which reference is made for further information.
To analyse strength reserves of existing structures, the fib Model Code 2010 suggests the refined base level of approximation III for members including shear reinforcement [24], [25]. By virtue of consideration potential increases on the shear strength, a precise assessment can be achieved. The background of the fib MC 2010 explains that for members with shear reinforcement the method brings together the simplified MCFT and Generalized Stress Field approach, hence similarly to CSA A23.3 2004, the methods explicitly takes account of concrete contribution to the ultimate shear resistance. Moreover, as presented in previous sections, the procedure of determining shear resistance requires iterations with intermediate parameters dependent to the greatest extent on a strain parameter and an angle of compressive stress field; in this case minimum value of the angle. Because of the common background that the CSA code and Model Code 2010 have, even though differences in certain aspects occur, the methods are expected to yield similar results.

In the flowchart 4-10, the general procedure for members with shear reinforcement is demonstrated. For members without shear reinforcement in LoA II only the formula for parameter k_v changes. Examples explaining the calculations for the critical sections for both types of members are presented in the following sections of the report.

4-4-1 Shear Resistance of the Critical Sections

The MC 2010 specifies to check the shear resistance in the critical section which is generally taken in a distance d_v from the support but other potential critical section should be checked as well. In the calculations below, the critical section was searched for at the same intervals as for the CSA code. To maintain consistency with prior estimations an effective amount of reinforcement was calculated using relation 4-1.

In contrast with CSA A23.3 2004, calculation of effective shear depth was carried out by determining the centrelines of the top and the bottom chord, where the depth of the compression chord is calculated for the location of maximum bending and assumption of a stress

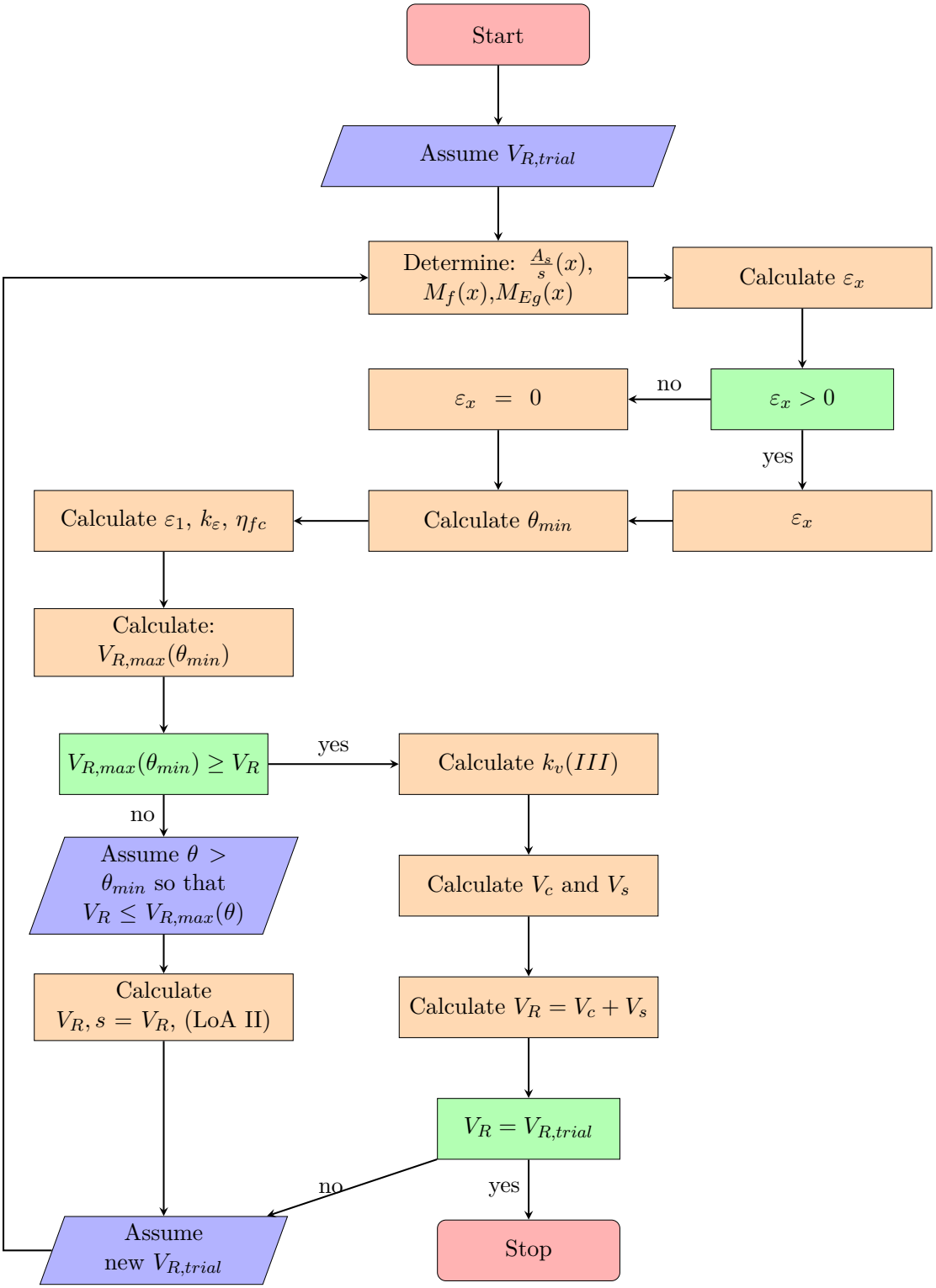

Figure 4-10: Flowchart for calculation of shear resistance in members with shear reinforcement

block [25]. It is only an alternative as the MC 2010 allows assuming the effective shear depth $z = 0.9d$.

Refer also to Appendix B for all results and Mathcad calculations

Analysis of the Critical Section in the Beam LB6

The calculations start with determining the self-weight of the beam. It was already described in the section devoted to the CSA code calculations for the critical sections thus the reference to this part of the report is made (section 4-3-1). In contrast to the CSA approach an effective shear depth was calculated from equilibrium assuming the bilinear stress distribution for a double reinforced section. Having calculated these values, an iterative procedure can be commenced.
Alike the CSA code computation, in these examples the critical sections are known as well as the $V_{R,trial}$. These are: $\boldsymbol{x = 0.7m}$ from the face of the supporting plate and $\boldsymbol{V_{R,trial} = 137.98kN}$.

The bending moment from the self-weight at the considered location:
$M_{Eg}(x = 0.7m) = 0.211kNm$
The value of the bending moment at x from effects' action:
$M_E = M_{Eg} + V_{R,trial}\left(1.2m - x - \frac{0.15m}{2}\right) = 0.211kNm + 137.98kN(1.2m - 0.7m - 0.075m) = 58.85kNm$

The force in the longitudinal reinforcement at the "tension side" at the crack:
$F_{lt,section} = \frac{M_E}{z} + V_{R,trial} + V_{Eg} + 0.5N_{axial} = \frac{58.85kNm}{0.448m} + 137.98kN + 2.64kN - 0.5 * 797kN = -126.42kN$ which indicates compression.

Commentary to the fib MC2010 in cl.7.3.3.1 explains that for sections in compression thus negative values of ε_x, it is conservatively assumed $\varepsilon_x = 0$.

The minimum angle of inclination θ_{min} and remaining parameters following suit are independent of the strain condition.
$\theta_{min} = 20 + 10000\varepsilon_x = 20\,\text{deg}$

The principal tensile strain:
$\varepsilon_1 = \varepsilon_x + (\varepsilon_x - \varepsilon_2) * (\cot(\theta_{min})^2) = 0 + (0 - 0.002)\cot(20\,\text{deg}) = 0.0151$

The strain effect parameter:
$k_\varepsilon = \frac{1}{1.2+55\varepsilon_1} = 0.493 \leq 0.65$

The strength reduction factor:
$k_c = k_\varepsilon \eta_{fc} = 0.493\left(\frac{30}{63.5}\right)^{1/3} = 0.384$

The strength limited by crushing of concrete at the θ_{min}.
$V_{R,max} = k_c f_{cm} b_w \sin(\theta)\cos(\theta) = 0.384 * 63.5MPa * 73mm * \sin(20\,\text{deg})\cos(20\,\text{deg}) = 255.87kN$
which is more than $V_{R,trial}$ thus in the LoA III, the concrete contribution can be accounted for with a factor k_v.
$k_v = \frac{0.4}{1+1500\varepsilon_x}\left(1 - \frac{V_{E,trial}}{V_{R,max(\theta_{min})}}\right) = \frac{0.4}{1+0}\left(1 - \frac{137.98kN}{255.87kN}\right) = 0.184$

The steel and concrete contributions are:
$V_{R,s} = \frac{A_v}{s} z f_{yw}\cot(\theta_{min}) = 138.28mm^2/m * 0.448m * 529MPa * \cot(20\,\text{deg}) = 89.98kN$

$V_{R,c} = k_v * \sqrt{f_{cm}} b_w z = 0.184 * \sqrt{63.5MPa} * 73mm * 448mm = 48.00kN$ The total shear resistance:
$V_R = V_{R,s} + V_{R,c} = 89.98kN + 48kN = 137.98kN$

Analysis of the Critical Section in the Beam LB10

The critical section is defined as: $\boldsymbol{x = 425mm}$ with the shear resistance $\boldsymbol{V_{R,trial} = 190.2kN}$.

The bending moment from the self-weight at the considered location:
$M_{Eg}(x = 0.425m) = 1.007kNm$

The value of the bending moment at x from effects' action:
$M_E = M_{Eg} + V_{R,trial}\left(1.2m - x - \frac{0.15m}{2}\right) = 1.007kNm + 190.2kN(1.2m - 0.425m - 0.075m) = 134.1kNm$

The force in the longitudinal reinforcement at the "tension side" at the crack:
$F_{lt,section} = \frac{M_E}{z} + V_{R,trial} + V_{Eg} + 0.5N_{axial} = \frac{134.1kNm}{0.446m} + 190.2kN + 3.15kN - 0.5 * 822kN = 82.78kN > 0$ hence in tension.

The value of the strain parameter:
$\varepsilon_x = \frac{1}{2E_s A_s}\left(\frac{M_E}{z} + V_{R,trial} + N_{axial}\left(\frac{1}{2} + \frac{\Delta e}{z}\right)\right) = \frac{1}{2*201100MPa*934mm^2}((\frac{134.1kNm}{0.446m} + 190.2kN - 822kN9(\frac{1}{2} + \frac{7.63mm}{446mm})) = 0.000183$

The minimum angle of inclination θ_{min} is dependent on the value of average strain.
$\theta_{min} = 20 + 10000\varepsilon_x = 20 + 10000 * 0.000183 = 21.83\,\text{deg}$

The principal tensile strain:
$\varepsilon_1 = \varepsilon_x + (\varepsilon_x - \varepsilon_2) * (\cot(\theta_{min})^2) = 0.000183 + (0.000183 - 0.002)\cot(21.83\,\text{deg}) = 0.014$

The strain effect parameter:
$k_\varepsilon = \frac{1}{1.2+55\varepsilon_1} = 0.511 \leq 0.65$

The strength reduction factor:
$k_c = k_\varepsilon \eta_{fc} = 0.511\left(\frac{30}{62.3}\right)^{1/3} = 0.4$

The strength limited by crushing of concrete at the θ_{min}.
$V_{R,max} = k_c f_{cm} b_w \sin(\theta)\cos(\theta) = 0.4 * 62.3MPa * 74mm * \sin(21.83\,\text{deg})\cos(21.83\,\text{deg}) = 284.4kN$
which is more than $V_{R,trial}$ thus in the LoA III, the concrete contribution can be accounted for with a factor k_v.
$k_v = \frac{0.4}{1+1500\varepsilon_x}\left(1 - \frac{V_{E,trial}}{V_{R,max(\theta_{min})}}\right) = \frac{0.4}{1+1500*0.000183}\left(1 - \frac{190.2kN}{284.4kN}\right) = 0.104$

The steel and concrete contributions are:
$V_{R,s} = \frac{A_v}{s} z f_{yw}\cot(\theta_{min}) = 276.57mm^2/m * 0.446m * 529MPa * \cot(21.83\,\text{deg}) = 163.1kN$
$V_{R,c} = k_v * \sqrt{f_{cm}} b_w z = 0.104 * \sqrt{62.3MPa} * 74mm * 446mm = 27.1kN$

The total shear resistance:
$V_R = V_{R,s} + V_{R,c} = 163.1kN + 27.1kN = 190.2kN$

Analysis of the Critical Section in the Beam LB11

The minimum demand for shear reinforcement is determined according to the equation 7.3-22 fib Model Code 2010 with help of which it is possible to determine whether a section qualifies as unreinforced against shear or not. For such sections, concrete is accounted for differently. In the considered example, the critical section happened to be located at $\boldsymbol{x = 0.525m}$ for the face of the support. The area of stirrups per running meter calculated with equation 4-1 for this sections is: $\frac{A_v}{s} = 83.63mm^2/m$.

The minimum required amount of shear reinforcement per running meter resulting from the aforementioned equation is: $\rho_{min} b_w = \left(0.08\frac{\sqrt{f_{cm}}}{f_{yw}}\right) * 74mm = 88.33mm^2/m$
which proves the point that the section should be calculated as unreinforced against shear.

The shear resistance at the considered location is equal to $\boldsymbol{V_{R,trial} = 87.51kN}$.

The bending moment from the self-weight at the considered location:
$M_{Eg}(x = 0.525m) = 0.703kNm$

The value of the bending moment at x from effects' actions:
$M_E = M_{Eg} + V_{R,trial}\left(1.2m - x - \frac{0.15m}{2}\right) = 0.703kNm + 87.51kN(1.2m - 0.525m - 0.075m) = 53.21kNm$

The force in the longitudinal reinforcement at the "tension side" at the crack:
$F_{lt,section} = \frac{M_E}{z} + V_{R,trial} + V_{Eg} + 0.5N_{axial} = \frac{53.21kNm}{0.446m} + 87.51kN + 2.89kN - 0.5 * 807kN = -194.8kN$ which indicates compression $\longmapsto \varepsilon_x = 0$

The minimum angle of inclination θ_{min}: $\theta_{min} = (20 + 10000\varepsilon_x) = 20\,\text{deg}$

The principal tensile strain:
$\varepsilon_1 = \varepsilon_x + (\varepsilon_x - \varepsilon_2) * (\cot(\theta_{min})^2) = 0 + (0 - 0.002)\cot(20\,\text{deg}) = 0.0151$

The strain effect parameter:
$k_\varepsilon = \frac{1}{1.2 + 55\varepsilon_1} = 0.493 \leq 0.65$

The strength reduction factor:
$k_c = k_\varepsilon \eta_{fc} = 0.493\left(\frac{30}{62.3}\right)^{1/3} = 0.39$

The strength limited by crushing of concrete at the θ_{min}.
$V_{R,max} = k_c f_{cm} b_w \sin(\theta)\cos(\theta) = 0.39 * 62.3MPa * 74mm * \sin(20\,\text{deg})\cos(20\,\text{deg}) = 255.4kN$
which is more than $V_{R,trial}$.
For LoA II, members without shear reinforcement, the factor k_v:
$k_v = \frac{0.4}{1 + 1500\varepsilon_x}\left(\frac{1300}{1300 + k_{dg}z}\right)$
where: $k_{dg} = \frac{32}{16 + d_g} = \frac{32}{16 + 10} = 1.23 \geq 0.75$
$k_v = \frac{0.4}{1}\left(\frac{1300}{1000 + 1.23 * 446mm}\right) = 0.336$

The total shear resistance is attributed to the concrete shear resistance:
$V_{R,c} = k_v * \sqrt{f_{cm}} b_w z = 0.336 * \sqrt{62.3MPa} * 74mm * 446mm = 87.51kN$
$V_R = V_{R,c} = 87.51kN$.

4-4-2 Cumulative Results

In Figures 4-11, 4-12 and 4-13 the shear resistances obtained from calculations are plotted. From the comparison with the results of the CSA code, it can be concluded that both methods yield similar results. The critical sections were found to be located in the same distances from the edge of the support – beam LB10 or the point of contraflexure – beams LB6 and LB11. For a more detailed comparison, see section 4-7.

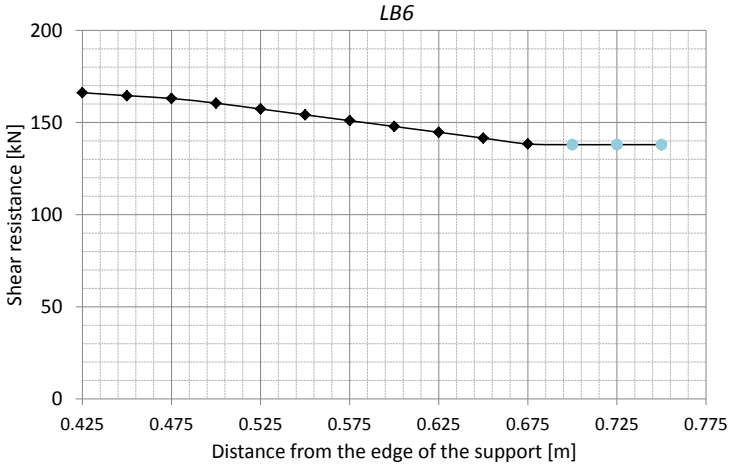

Figure 4-11: Shear capacity of the beam LB6 by fib MC 2010 at different locations

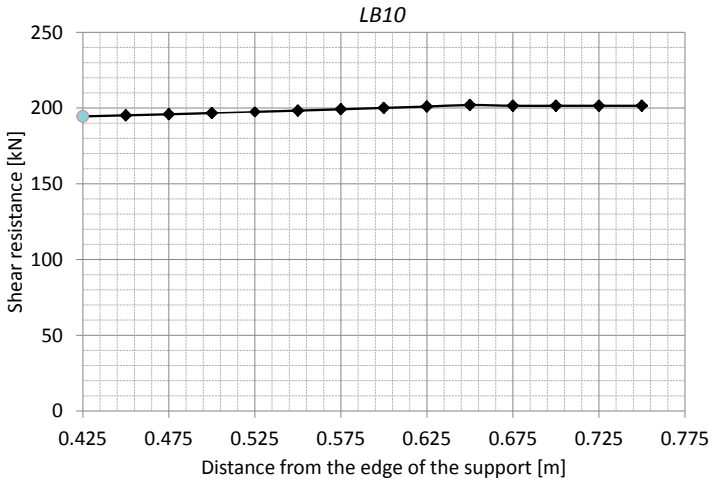

Figure 4-12: Shear capacity of the beam LB10 by fib MC 2010 at different locations

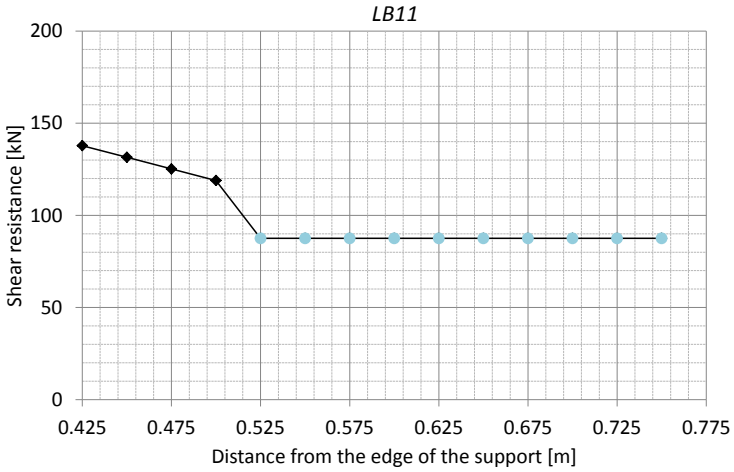

Figure 4-13: Shear capacity of the beam LB11 by fib MC 2010 at different locations

4-5 Analytical Solution EC2

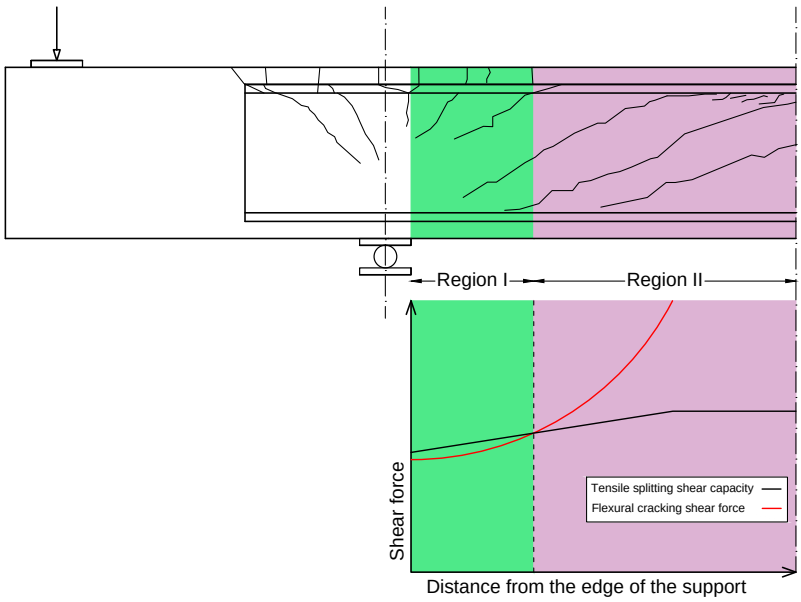

Figure 4-14: Crack pattern in regions cracked in flexure (Region I) and tensile splitting (Region II)

In the EC2, unlike the "strain dependent" codes, the applied procedure depends on whether the considered section is cracked or uncracked in flexure and whether the amount of shear reinforcement is higher than minimum or not. Both criteria determine the expected failure mechanism and accordingly different formulas are used to calculate shear resistance of a member. It was already described in the literature study, that in the case of prestressed members, two regions can be distinguished. In the first region where prestress is not enough to compensate for bending, thus where high bending moment and shear occur, flexural cracks initiate when the flexural tensile stress in the outer fibre of a section exceeds the tensile

strength of the concrete (Region I in Figure 4-14). In the second region, (Region II in Figure 4-14) possibly where high values of shear force and low bending moment occur, flexural tensile stresses are compensated for by prestressing. When the principal tensile stresses reach the concrete tensile strength, it is expected that tension shear failure is the governing mechanism.

4-5-1 General Procedure

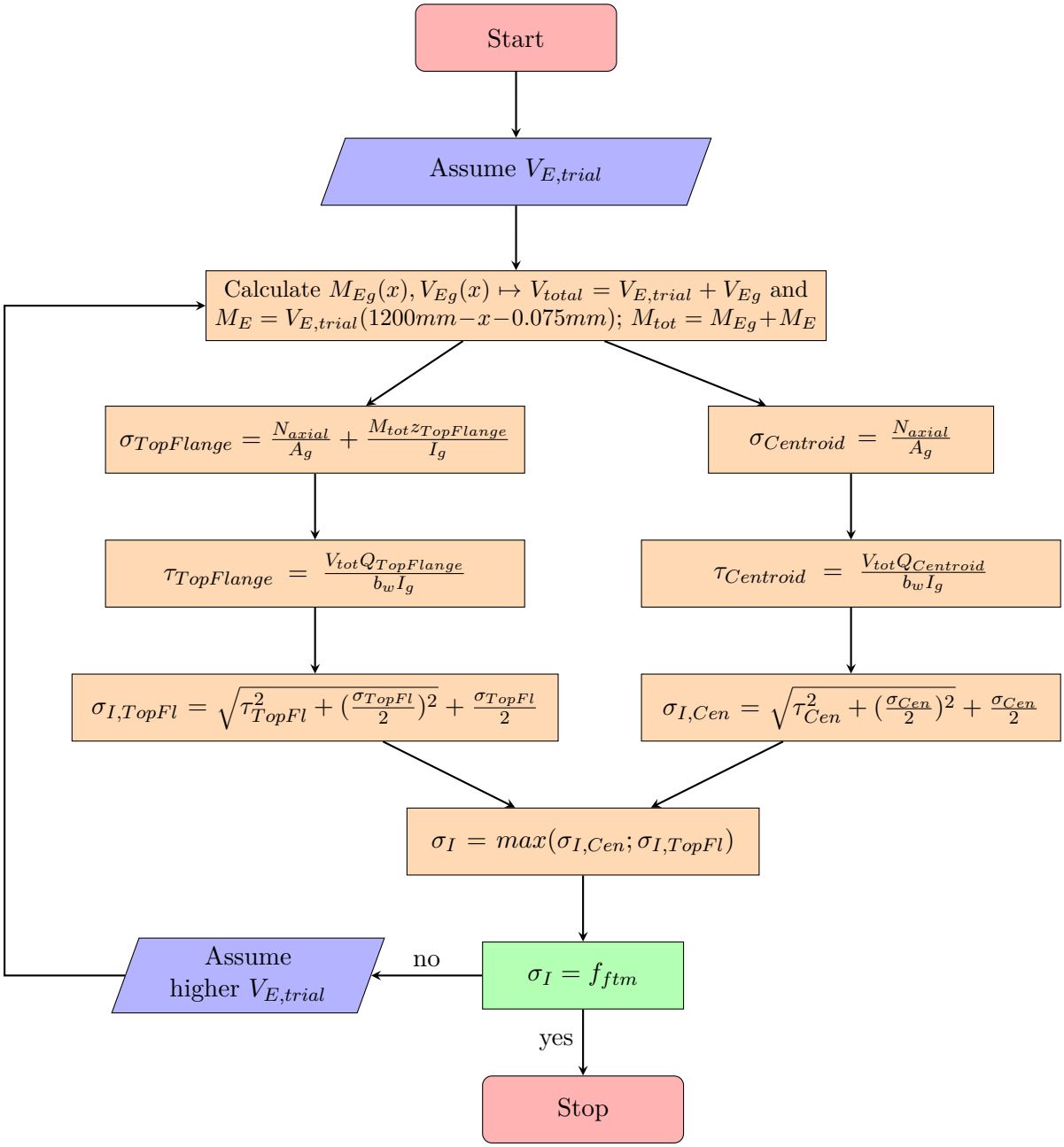

Figure 4-15: Determination of the critical tensile splitting shear force

Definition of the region cracked in flexure

The procedure of finding the shear resistance consisted of a collation of the shear force that would lead to the flexural shear failure and the shear force related to the shear tension failure. The smaller value of them would indicate the ultimate shear load the beam is able to withstand. As mentioned before, the flexural shear cracks are cracks which propagate from flexure cracks. Since the concrete is assumed to crack when the tensile stress in the outer fibre reaches the concrete tensile strength, the cracking bending moment as a function of the distance from the edge of the west loading plate could be found with the following relation:

$$\frac{N_{axial}}{A_g} + \frac{M_{cr} y_{0top}}{I_g} + \frac{M_{Eg}(x) y_{0top}}{I_g} = f_{ctm}$$

and subsequently after transformations:

$$M_{cr}(x) = \frac{I_g \left(\frac{N_{axial}}{A_g} - f_{ctm} + \frac{M_{Eg}(x) y_{0top}}{I_g} \right)}{y_{0top}}$$

The shear force due to the experimental setup is constant in the test region, thus the maximum shear force is obtained with:

$$V_E(1200 - x - 150mm/2) - M_{cr} = 0 \longmapsto V_E = \frac{M_{cr}(x)}{1200 - x - 150mm/2}$$

The values of the flexural cracking shear force (represented by the red curve in Figure 4-14) were compared with values of shear resistance against shear tension cracking in the web (a black line in Figure 4-14); followed from the Mohr's circle.

Definition of tensile splitting shear capacity

The proceedings of the method are shown in Figure 4-15. The procedure starts with an assumption of a shear force. For the assumed shear force value $V_{E,trial}$, the bending moment:

$$M_E = V_{E,trial} \left(1200mm - x - \frac{150mm}{2} \right)$$

increased by the effect of self weight was calculated.
Next, normal stresses at the junction of the web and the flange, normal stresses in the centroid as well as shear stresses are computed. Having all the components needed to calculate tensile stresses in the principal direction at the level of the junction of the web and the flange and the centroidal axis were checked. If for the initially assumed shear force, the principal stresses are lower than the tensile strength of the concrete, the resistance of the beam against the tensile splitting shear failure is larger and therefore the assumed shear force has to be increased. The iterations proceed until the strength of concrete is reached. Different locations x are to be checked.

Shear capacity of regions cracked uncracked in flexure

Another aforementioned influential aspect is whether an element is considered as with or without shear reinforcement. The minimum ratio of reinforcement is given by the expression 9.5N in EN 1992-1-1: 2004. For all elements that do not meet the requirement of the minimum ratio of reinforcement, irrespective of the crack type (i.e. flexural or shear tension crack), the

shear resistance is determined by the formula 6.2; therefore this shear resistance constitutes the "guaranteed" capacity of a member. Even though it is not directly stated in the code, the expression 6.2 can be used in the region that is not cracked in bending; meaning that the highest result of expressions 6.2 and 6.4 from the EC2 is the shear resistance of a beam in the region uncracked in bending. If the considered section uncracked in flexure contains shear reinforcement, its resistance should be also accounted for; an inclined crack initiated in an element's web intersects the stirrups which can provide resistance according to the formula 6.8 EC2.

Ultimate shear resistance

The maximum of 6.2 and 6.8 from the EC2 for the region cracked due to bending has to be compared with the minimum value resulting from the expression 6.4, or if $V_{6.4} < V_{6.2}$ or $V_{6.4} < V_{6.8}$, the resistance obtained with the expression 6.2 or 6.8. The minimum value of this comparison is the shear resistance of the beam. It can be represented with:

$$V_{Ultimate} = min[max(V_{6.2}, V_{6.4}, V_{6.8} \quad \text{for Region II}), max(V_{6.2}, V_{6.8} \quad \text{for Region I})] \tag{4-2}$$

where indices indicate the expression number in the code and the regions are depicted in Figure 4-14. For members without shear reinforcement the shear resistance is taken as the smallest value of results from the expressions 6.2 and 6.4.
It is important to mention that the higher values of the coefficient C and k_1 in the expression 6.2 of the EC2 were used: 0.163 (0.12 in EC2) for the coefficient C and 0.225 for k_1 (0.15 in EC2). The first increase originate from the study of Regan, 1993 which later was confirmed by König/Fischer. The **mean value** for 0.225 is the result of the currently ongoing research at the TU Delft.

As far as calculations from [13] are concerned, it can be concluded that the predictions given by the author were made without distinguishing between regions cracked in flexure and tension shear. Additionally, shear resistance against the web splitting tensile crack was not checked for different sections. Instead, from the results of the expressions 6.2, 6.4 and 6.8 in EN 1992-1-1, the lowest value of these estimations was taken as the governing shear resistance. Lastly, values of coefficient $C = 0.12$, $k_1 = 0.15$ were used as specified in the code, thus lower than in this project.

4-5-2 Example of Calculations for Beam LB6

Refer also to Appendix C for all results and Mathcad calculations

Shear resistance of region uncracked in flexure

In the first step, the procedure as shown in Figure 4-15 is used to determine shear resistance for beam LB6 in the section located $x = 0.2m$ from the edge of the support. The assumed shear force resistance is: $V_{trial} = 157.7kN$. It can be seen from Figure 4-16 that it is the lowest value in the region uncracked in flexure. Please bear in mind that the trial value of shear resistance in not known beforehand and it has to be found iteratively. Also the position of critical section is not prescribed to a certain distance from the edge of the support. Consequently, in order to determine the critical section, an iterative procedure has to performed at several locations.

Shear force and bending moment from the self-weight calculated with the equations as derived in section 4-3-1 at the location x are:
$V_{Eg} = 3.56kN$ and $M_{Eg} = 1.76kNm$.
The total shear force:
$V_{tot} = V_{trial} + V_{Eg} = 157.7kN + 3.56kN = 161.3kN$
The bending moment from the applied loads increased by the effect self-weight:
$M_{tot} = V_{trial} * (1200mm - x - 150mm/2) + M_{Eg} = 157.7kN * (1200mm - 200mm - 150mm/2) + 1.76kNm = 147.70kNm$
The axial stress from prestressing is:
$\sigma_{c,cen} = N_{axial}/A_g = -797kN/73225mm^2 = -10.884MPa$
The calculations of the principal stresses at the level of centroidal axis and the junction of flange and web are carried out separately.

Shear stress at the centroidal axis:
$\tau_{Centroid} = \frac{V_{tot}Q_{Centroid}}{b_w I_g} = \frac{161.3kN*6.32*10^6mm^3}{73mm*2.55*10^9mm^4} = 5.476MPa$
Stress in the principal direction:
$$\sigma_{I,Cen} = \sqrt{\tau_{Cen}^2 + \left(\frac{\sigma_{Cen}}{2}\right)^2} + \frac{\sigma_{Cen}}{2} = \sqrt{(5.476MPa)^2 + \left(\frac{-10.884MPa}{2}\right)^2} + \frac{-10.884MPa}{2} = 2.278MPa$$

Normal and shear stresses at the junction of the web and the flange:
$\sigma_{TopFl} = \frac{N_{axial}}{A_g} + \frac{M_{tot} * z_{TopFl}}{I_g} = -10.884 + \frac{147.70kN*m*0.18m}{2.55*10^{-3}mm^4} = -0.461MPa$
$\tau_{TopFl} = \frac{V_{tot} * Q_{Flange}}{b_w * I_g} = \frac{161.3kN*5.14*10^6mm^3}{73mm*2.55*10^9mm^4} = 4.453MPa$
Stress in the principal direction:
$$\sigma_{I,TopFl} = \sqrt{\tau_{TopFl}^2 + (\frac{\sigma_{TopFl}}{2})^2} + \frac{\sigma_{TopFl}}{2} = \sqrt{5.476^2 + \left(\frac{-0.461MPa}{2}\right)^2} + \frac{-0.461MPa}{2} = 4.229MPa$$

For the considered section as well as the magnitude of shear force $V_{trial} = 159.31kN$, tensile stress in the principal direction reached the concrete tensile strength $f_{ctm} = 4.229MPa$ at the level of web-flange junction. It is a governing depth in the section. No further iterations are necessary. Note: if for the assumed V_{trial}, $\sigma_I \neq f_{ctm}$, a different value of V_{trial} has to be assumed and calculations repeated till $\sigma_I = f_{ctm}$.

As indicated in equation 4-2, the above-obtained shear resistance has to be compared with resistance attributed to stirrups (6.8 EC2) at this location and shear resistance for members not requiring shear reinforcement (6.2 EC).
The amount of reinforcement at the specified location $x = 200mm$ from equation 4-1:
$A_s = 269.041mm^2/m$
Shear resistance of stirrups calculated for $\theta = 21.8°$:
$V_{R,s} = A_s f_{yw} z \cot(\theta) = 269.041mm^2/m * 0.448m * 529MPa * \cot(21.8°) = 159.31kN$
Shear resistance acc. 6.2 EC2 for members not requiring shear reinforcement:
$V_{R,c} = [C_{Rd,c} k (100\rho_l f_{cm})^{\frac{1}{3}} + k_1 \sigma_{cp}] b_w d = 0.163 * 1.65 * (2.0 * 63.6)^{1/3} * 0.225 * 10.884MPa * 74mm * 473mm = 131.247kN$
where:
$C_{Rc} = 0.163$;
$\sigma_{cp} = N_{axial}/A_g = 797kN/73225mm^2 = 10.884MPa$;
$k = 1 + \sqrt{\frac{200}{d}} = 1 + \sqrt{200/473mm} = 1.65$;

$\rho_l = min\left(\frac{A_s}{b_w d}, 0.02\right) = 0.02;$
$k_1 = 0.225$
The dictating criterion in expression 4-2 takes the highest value as the governing shear resistance: $V = max(157.7kN; 159.31kN; 131.247kN) = 159.31kN$

Shear resistance of region cracked in flexure

According to the assumed procedure, the governing ultimate shear resistance is the minimum value of regions uncracked and crack in flexure. In Figure 4-16, it can be observed that within the region limited by the blue line (cracked in flexure) the maximum shear reinforcement is related to resistance attributed to yielding of stirrups. The shear resistance therefore is:
$V_{R,s} = A_s/s f_{yw} z \cot(\theta) = 276.57mm^2/m * 0.448m * 529MPa * \cot(21.8°) = 163.77kN$
Note: for the derivation of z in the above formula, refer to Appendix B.

Shear resistance in the region cracked in flexure is equal to $max(6.2, 6.8)$ as explained in expression 4-2. Therefore the remaining flexural shear resistance acc. to 6.2 EC2:
$V_{R,c} = [C_{Rd,c} k (100\rho_l f_{cm})^{\frac{1}{3}} + k_1 \sigma_{cp}] b_w d = 0.163 * 1.65 * (2.0 * 63.6)^{1/3} * 0.225 * 10.884MPa * 74mm * 473mm = 131.247kN$
$V = max(163.77kN, 131.247) = 163.77kN$

Governing shear resistance

To finalize calculations, the governing resistances from both regions have to be compared and the minimum value according to equation 4-2 constitutes the ultimate shear resistance. It is therefore:
$V_{ultimate} = min(159.31kN; 163.77kN) = 159.31kN$
Due to the fact that the location corresponding to the shear resistance of 159.31kN is outside the region crack in flexure as indicated by a blue line in Figure 4-16, the failure mechanism is shear tension.

4-5-3 Results

In Figures 4-16, 4-17, 4-18 the predictions of shear resistance according to the EC2 are presented. The calculations were carried out at sections spaced 50 mm starting from the inner edge of the support. The values of the shear force causing flexural cracking are marked with a blue dashed line. It is important to remember that these are values of the shear force causing an onset of cracking in the outer top fibre i.e. due to bending, not the shear resistance. These cracks can further propagate into flexural shear cracks. The shear resistance within the test region is controlled by the stirrups with values obtained from the expression 6.8 EC2. The remaining lines are the resistances attributed to different formulas. The shape of the curve of shear tension resistance can be split in two branches. In the first branch (the sloped branch) values of shear resistances resulting from stresses at the web-flange junction reached the tensile concrete strength before stresses at the centroidal axis, thus decisive. In the second branch the situations is reversed with stresses at the centroid dictating the outcome; almost constant values of $V_{R,c6.4}$ are the effect of calculations being independent of the bending moment. The shear resistance for the critical section is indicated with a green marker. It can be see that for all specimens the critical section was found to be within the distance of 100-200 mm from the axis of the support. The summary containing the calculated shear resistance and governing failure mechanism is shown in Table 4-6.

Table 4-6: Results of the analysis according to the EC2

Beam	Shear resistance [kN]	Distance x [m]	Governing mechanism
LB6	159.31	0.2	Tension shear
LB10	160.2	0.15	Tension shear
LB11	163.143	0.15	Flexural shear

The shear resistances from the analysis for all beams are similar. Not only in terms of the magnitude but also the locations of the critical sections. They are either the values of a splitting shear capacity at the transition from flexural crack region (region I) or constant resistance attributed to stirrups in the Region I. For the specimens LB6, 10 and 11 these values happened to be very much alike. It is also aftermath of the short region I following from high compression applied to the beams.

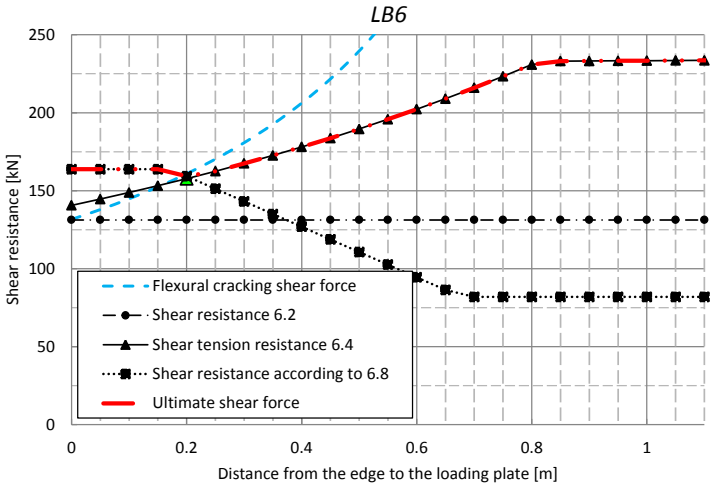

Figure 4-16: Shear resistance for the LB6 according to the EC2; $V_{Ultimate} = 159.31kN$

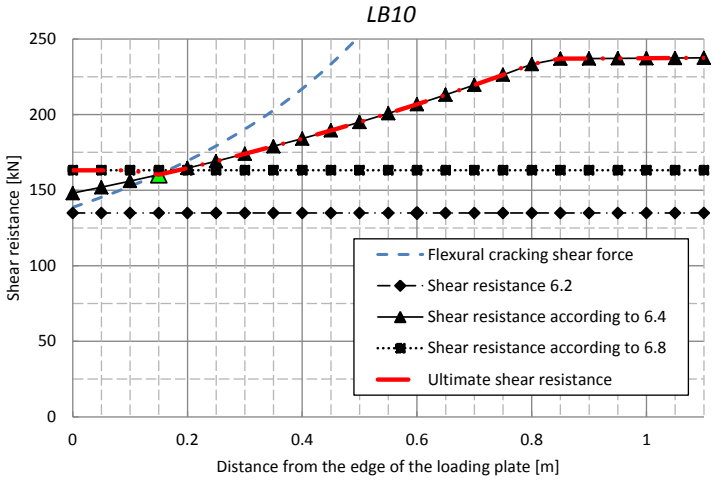

Figure 4-17: Shear resistance for the LB10 according to the EC2; $V_{Ultimate} = 160.2kN$

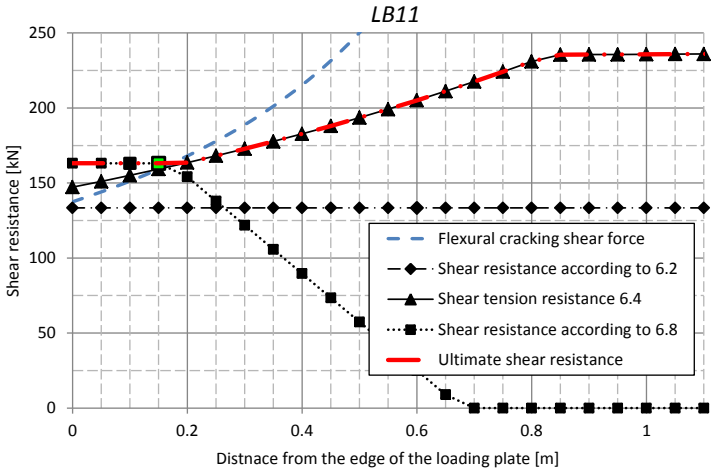

Figure 4-18: Shear resistance for the LB11 according to the EC2; $V_{Ultimate} = 163.143kN$

4-6 Analytical Solution RBK 1.1

4-6-1 General Procedure

The RBK (Richtlijnen Beoordeling Kunstwerken) are the guidelines for an assessment of structural safety of existing structures. Shear resistance is calculated as a sum of concrete and steel contributions. The contributions are obtained from the EC2 expression with adjustments applied. The total resistance acc. to RBK 6.2.1 (2):

$$V_{Rd} = V_{Rd,s} + V_{Rd,c} \tag{4-3}$$

where the steel contribution to the resistance for prestressed concrete is calculated with the expression 6.8 from the EC2 with an angle of struts inclination limited to 30 deg. The contribution from concrete acc. to 6.2.2 (1) follows from the modified expression 6.2 from the EC2:

$$V_{Rd,c} = [0.12k_{cap}k(100\rho_l f_{ck})^{(1/3)} + 0.15\sigma_{cp}]b_{wgem}d_e \tag{4-4}$$

with $k_{cap} = 1$ for members different than plates; b_{wgem} determined based on Figure 2.1 in the RBK 1.1 and cl. 6.2.2 (1) as $A_{projected}/d$ with the maximum of $1.25b_{min}$ and b_{min} being the smallest width of the projected cross-section with exclusion of ducts and prestressing cables. The areas of the projected sections are given in Figure 4-19.

4-6-2 Example of Calculations for Beam LB6

Refer also to Appendix D for all results and Mathcad calculations

The shear resistance according to the procedure from Figure 4-15 will be applied for beam LB6 in the section located $x = 0.7$ from the edge of the support. The assumed shear force resistance is: $V_{trial} = 216kN$. From the calculations it was recognized that the shear resistance for this section is governing.
Shear force and bending moment at this locations are:
$V_{Eg} = 2.64kN$ and $M_{Eg} = 0.21kN * m$.

Bending moment from the applied loads increased by the self-weight:
$M_tot = V_{trial} * (1200mm - x - 150mm/2) + M_{Eg} = 216kN * (1200mm - 700mm - 150mm/2) + 0.21kN * m = 92.01kN * m$
Axial stress from prestressing is:
$\sigma_{c,cen} = N_{axial}/A_g = -797kN/73225mm^2 = -10.884MPa$
This was general input. Now, the calculations for the junction of the web and the flange and at the centroid of the section will be considered separately.

Shear stress at the centroidal axis:
$\tau_{Centroid} = \frac{V_{tot}Q_{Centroid}}{b_w I_g} = \frac{218.6kN*6.32*10^6mm^3}{73mm*2.55*10^9mm^4} = 7.423MPa$
Stress in the principal direction:
$\sigma_{I,Cen} = \sqrt{\tau_{Cen}^2 + (\frac{\sigma_{Cen}}{2})^2} + \frac{\sigma_{Cen}}{2} = \sqrt{(7.423MPa)^2 + (\frac{-10.884MPa}{2})^2} + \frac{-10.884MPa}{2} = 3.762MPa$

Normal and shear stresses at the junction of the web and the flange:
$\sigma_{TopFl} = \frac{N_{axial}}{A_g} + \frac{M_{tot}*z_{TopFl}}{I_g} = -10.884MPa + \frac{92.01kNm*0.18m}{2.55*10^{-3}mm^4} = -4.39MPa$
$\tau_{TopFl} = \frac{V_{tot}*Q_{Flange}}{b_w*I_g} = \frac{218.6kN*5.14*10^6mm^3}{73mm*2.55*10^9mm^4} = 6.037MPa$
Stress in the principal direction:
$\sigma_{I,TopFl} = \sqrt{\tau_{TopFl}^2 + (\frac{\sigma_{TopFl}}{2})^2} + \frac{\sigma_{TopFl}}{2} = \sqrt{6.037^2 + (\frac{-4.39MPa}{2})^2} + \frac{-4.39MPa}{2} = 4.229MPa$

One can see that tensile stress in the principal direction at the considered location at the web-flange junction for the assumed shear force reached the concrete tensile strength. It means that the assumed shear force V_{trial} is equal to the shear resistance acc. to 6.4 EC2.

This shear resistance has to be compared with the shear resistance from combined contributions of steel and concrete.

Contribution of concrete:
the "mean" width:
$b_{wgem} = min(1.25b_w; \frac{A_{c,projected}}{d_e}) =$
$min(1.25 * 73mm; 42778mm^2/473mm) = min(91.25mm; 90.44mm) = 90.44mm$

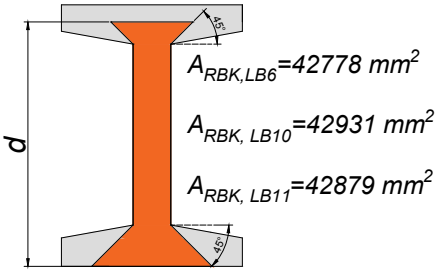

Figure 4-19: Projected section area according to RBK

Size effect factor: $k = 1 + \sqrt{\frac{200}{d_e}} = 1.65$
Reinforcement ratio: $\rho = \frac{A_s}{b_{wgem}*d_e} = \frac{934mm^2}{90mm*473mm} = 0.022$ and $\rho \leq 0.02 \longrightarrow \rho = 0.02$
The concrete contribution is therefore:
$V_{R,c} = \left[0.163 * 1 * 1.65 * (100 * 0.020 * 63.5)^{1/3} + 0.225\frac{797*10^3}{73225mm^2}\right] * 473mm * 90.44mm = 162.601kN.$

The resistance of stirrups that constitutes another source of strength to the ultimate shear resistance is calculated with equation 2-29 for $\theta = 30°$. For the amount of stirrups from equation 4-1, the resistance is:
$V_{R,s} = \frac{A_{sw} z f_{ywd} \cot\theta}{s} = 138.2857mm^2/m * 0.448m * 529MPa * \cot 30° = 56.726kN$

Total shear resistance:
$V_{tot} = V_{R,c} + V_{R,s} = +162.601kN + 56.726kN = 219.327kN$

From the comparison of $V_{tot} = 219.327kN$ and $V_{ShearTension} = 216kN$ can be deduced that because $219.327kN > 216kN$, the former is the governing shear resistance at this cross section. In conclusion: for the considered section at $x = 0.7m$ according to the assumed procedure for RBK 1.1 the beam fails in shear tension with governing ultimate shear resistance from the combined contributions of stirrups and concrete.

4-6-3 Results

The results of the RBK 1.1 code should be interpreted in the same way as the outcome of the EC2 calculations hence the reader is referred to the previous section. In Figure 4-20 through 4-22 the curves represent the results of different formulas. One can already see that the resistance attributed to concrete is significantly higher than that obtained from the EC2. An important role to the overall resistance plays concrete providing resistance which in the considered cases is even higher than that provided by stirrups (at the reduced angle $\theta = 30°$). In addition, the location of the governing resistance is shifted towards the point of contraflexure and equals roughly 500-700 mm from the axis of the west support plate.
The results are summerized in 3-2 and Figure 4-23.

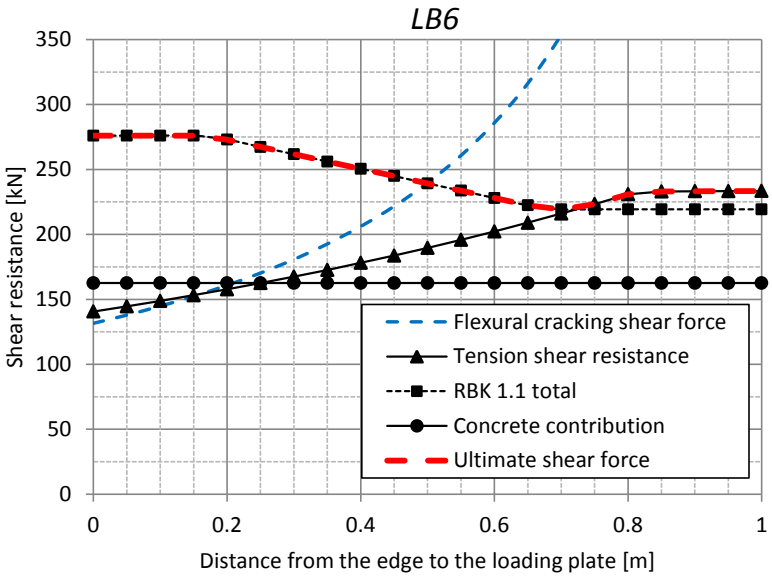

Figure 4-20: Shear resistance for the LB6 according to RBK 1.1; $V_{Ultimate} = 219.33kN$; governing mechanism: **shear tension**

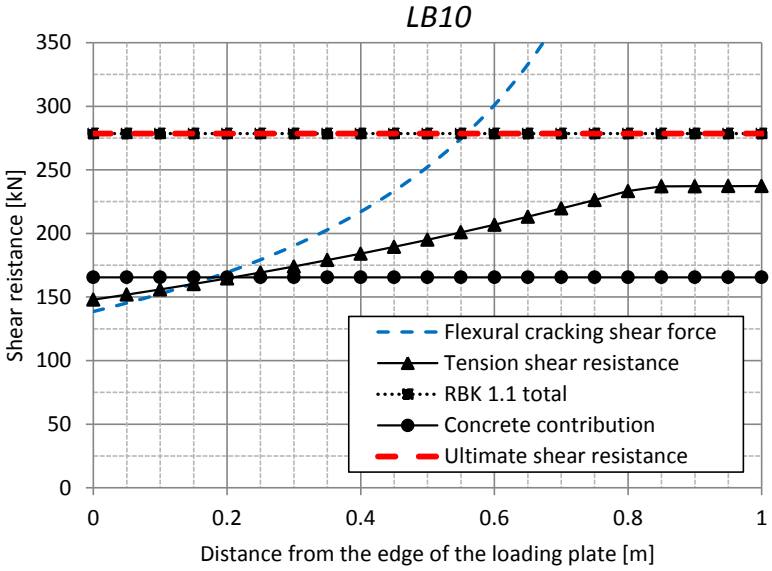

Figure 4-21: Shear resistance for the LB10 according to RBK 1.1; $V_{Ultimate} = 278.48kN$; governing mechanism: **shear tension/flexural shear**

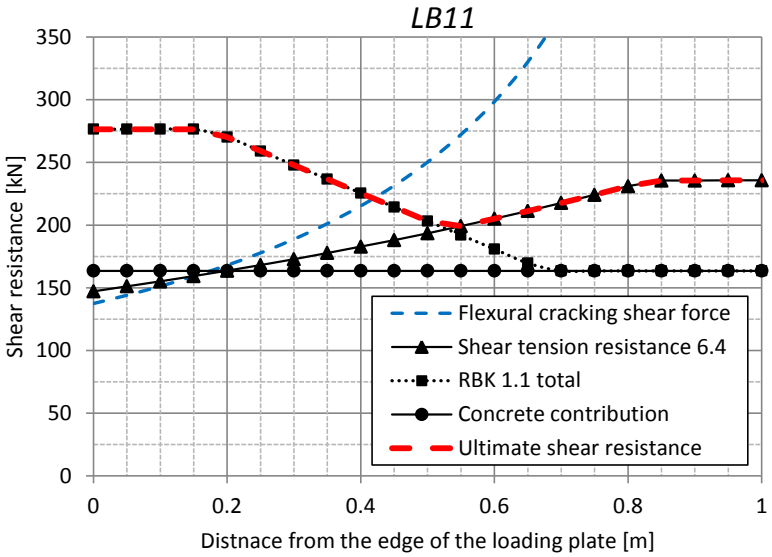

Figure 4-22: Shear resistance for the LB11 according to the RBK 1.1; $V_{Ultimate} = 199.2kN$; governing mechanism: **shear tension**

4-7 Comparison of the Theoretical and Experimental Results

Table 4-7 and Figure 4-23 summarize the predictions by different methods. To estimate which of the methods determines shear resistance the most accurately, the ratio between the experimental results and the shear resistances were calculated. The ratios the closest to unity, thus the best predictions, are highlighted.

The CSA "more accurate method" gives the best prediction for the beam LB10. For the beam LB6 it overestimates the capacity. The CSA General Method provides lower values

than the detailed analysis acc. to the CSA code. It predicts conservative results for beam LB10 and LB11 while for the LB6 the predicted shear capacity is very close to unity. The resistance predicted for LB11 was much lower than the experimental results. The reason for this deviation is the fact that the experimental ultimate load for LB11 was taken as the cracking load while the CSA code predicted the post-cracking shear strength which was low for beams without stirrups [13].
As expected due to the common background, the MC2010 yielded similar results to the CSA code. The prediction for the LB6 were slightly lower as compared to the CSA code. For the beam LB10, the MC2010 predicted the resistance more accurately than any other code except for the detailed method of the CSA. Similarly to the CSA code, the resistance for beams without shear reinforcement was much lower than the experimental results. It can be again justified by the code taking the post cracking shear strength.
The results from the EC2 were fairly satisfactory in terms of values *but not so much when the location of the crack is concerned.* The code predicted the resistance of the LB6 the most accurately out of all the codes. One the other hand, it slightly overestimates the resistance of the beam LB11. The critical section was determined to be located in the region crack in flexure thus by no means in agreement with the experimental observation. The resistance of the LB10 was conservatively underestimated.
Lastly, the RBK 1.1 proved to be overly unconservative (unsafe) for all specimens. Even though the location as well as the governing shear failure mechanism for beams LB6 and LB11 were predicted correctly, the ultimate shear strength was substantially overestimated by 29 and 28% for LB6 and LB11 respectively. The interpretation of the governing results of beam LB10 is ambiguous as the resistance is predicted to be constant across the beam therefore both in the region cracked in flexure as well as in the region where the shear tension failure might appear.
When the average of ratios as well as the coefficient of variation are concerned, the results of the CSA detailed method were the best; even though the shear resistance of LB6 was overreached by 8%. The remaining codes of practise result in similar coefficient of variation. It can be reasoned by stating that for each of the codes, one of the predictions was over or underestimated.

In Figure 4-24, the contributions of concrete and steel to the ultimate shear resistance at different sections are presented. Even though the methods have a similar background, a few dissimilarities can be observed. While comparing the charts, one can notice that in the CSA code, the contributions of steel and concrete are more levelled out. In contrast, the resistance in the MC2010 is mostly attributed to stirrups. The difference stems from the way in which the sections with the amount of stirrups higher than minimum are considered (for the sections without stirrups, the methods are the same). For these sections, unlike the CSA code, MC2010 assumes conservatively longitudinal strains equal to zero. Moreover, for sections in tension under the assumption of the same value of an average strain ε_x, the contribution of concrete according to MC2010 results in lower values as compared to the CSA code. To compensate for this, greater resistance has to be attributed to shear reinforcement. It can be achieved by virtue of reduced values of an angle θ. The θ calculated with the MC2010 provision is generally lower than θ estimated by the CSA code. It can be therefore reasoned that the function of the reduced angle in MC2010 is to compensate for the intentionally diminished contribution of concrete to the ultimate resistance. Naturally, the lower values of the angle of compressive struts result in a crack intersecting a higher number of stirrups thus higher

shear resistance originated from shear reinforcement.

Table 4-7: Summary of prediction by analysed methods

Specimen	LB6	LB10	LB11	Average	C.o.V
N [kN]	-797	-822	-809		
V_{u-exp} [kN]	155.8	215	142.8		
CSA General Method [kN]	159.1	182.25	86.29		
CSA Detailed Method [kN]	168.06	199.1	91.43		
MC2010 [kN]	137.98	190.2	87.51		
EC2 [kN]	159.31	160.2	163.143		
RBK 1.1 [kN]	219.33	278.48	199.2		
Exp/CSA General Method	0.98	1.18	1.65	1.27	27.30 %
Exp/CSA Detailed Method	0.92	**1.08**	1.56	1.19	27.85 %
Exp/MC2010	1.13	1.13	1.63	1.30	22.34 %
Exp/EC2	**0.98**	1.34	**0.88**[†]	1.07	23.02 %
Exp/RBK	0.71	0.77	0.72	0.73	4.62 %

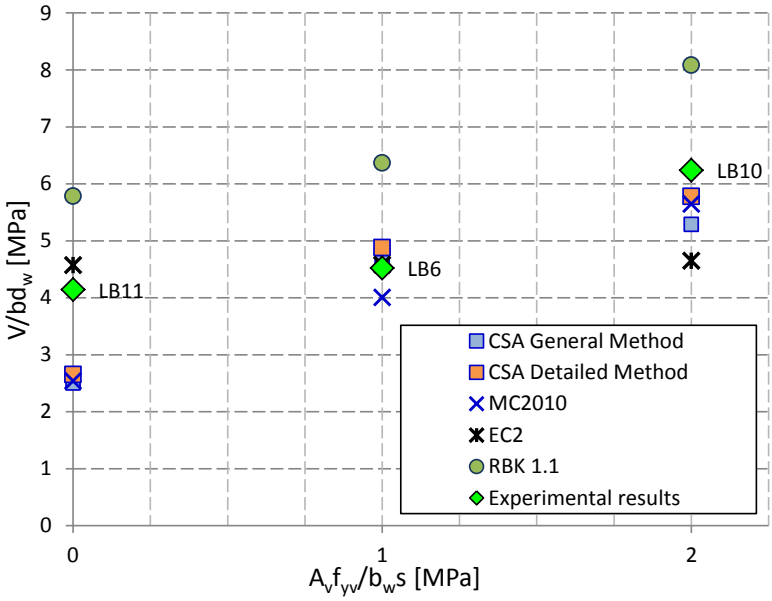

Figure 4-23: Normalized summary of predictions by analysed methods

To conclude the discussion, it is crucial to appreciate the most suitable method for assessing shear tension failure in existing bridges. The decision is made based on the following criteria:

- conservative methods are preferred over unconservative; overestimation of the shear resistance can lead to unexpected, abrupt failure which implies possible tragic consequences,

[†]the value of shear strength corresponds to the shear resistance calculated according to expression 6.4 EC2 which is in disagreement with the experimental research outcome.

- the code has to be consistent in terms of the predicted shear strength as well as the location of the critical section with experimental results; this means that the governing failure mechanism as well as the magnitude of failing shear force should be in agreement with the observations from the test,
- the results from the point above followed from the models should be as accurate as possible

Sieving out could begin by eliminating both RBK 1.1 and EC2. The results of RBK greatly overestimate the shear resistance while the EC2, despite of providing values close to the reality for beam LB6 and LB11, neither predict the correct failure mechanism nor the location which is claimed to be too close to the west support. The ratios close to unity for beam LB6 and 11 could be to thought to be coincidental. It can be explained by the fact that the prediction comes from the region reinforced against shear (near the support)thus attributed to stirrups while the beam failed in the region unreinforced with stirrups. At the same time the code is inconsistent for beam LB10 yielding an underestimated value.
As far as the "strain state" based methods are concerned the results are similar and here the most accurate prediction for the beam LB10 and a conservative prediction for LB6 seem to be decisive. The resistance for the specimen sparsely furnished with shear reinforcement is too conservative and even though special measures through scrutinizing the real strain state were undertaken, the results were not significantly improved. Concluding from the above considerations the results of the fib Model Code 2010 give the most accurate and the same time conservative shear resistances. The results according to this method are also the most consistent for members supplied with shear reinforcement.

Please note I: from the previous paragraph, it was concluded that none of the methods is appropriate to accurately evaluate members without shear reinforcement failing in shear tension. However, if a relation to the results of the expression 6.2 EC2 with mean values in section 4-5-3 is made, the resistance at the level of 133.42 kN and the ratio $V_{u-exp}/V_{Rc,6.2} = 142.8kN/133.42kN = 0.93$ is obtained. It implies that for members unreinforced against shear, the hereby assumed procedure (section 4-5-1) is not suitable and with a single formula the shear resistance can be predicted much more accurately. *

Please note II: the choice of the fib MC2010 as the most adequate shear provision was not obvious. It clearly suffers from a major drawback of inability to address the governing shear failure mechanism which is of high importance. Nevertheless the location of the predicted critical section can serve as an indirect indication of the possible failure mode. This, in a combination with good engineering judgement, might be sufficient in some cases.

*even though not directly expressed in the EC2, the formula EC2 can be applied in the region crack and uncracked in flexure. Moreover, the empirical expression was obtained based on the results of experiments of beams failing in flexural shear therefore the resulting values of the shear resistance assigned to shear tension failure might be coincidental

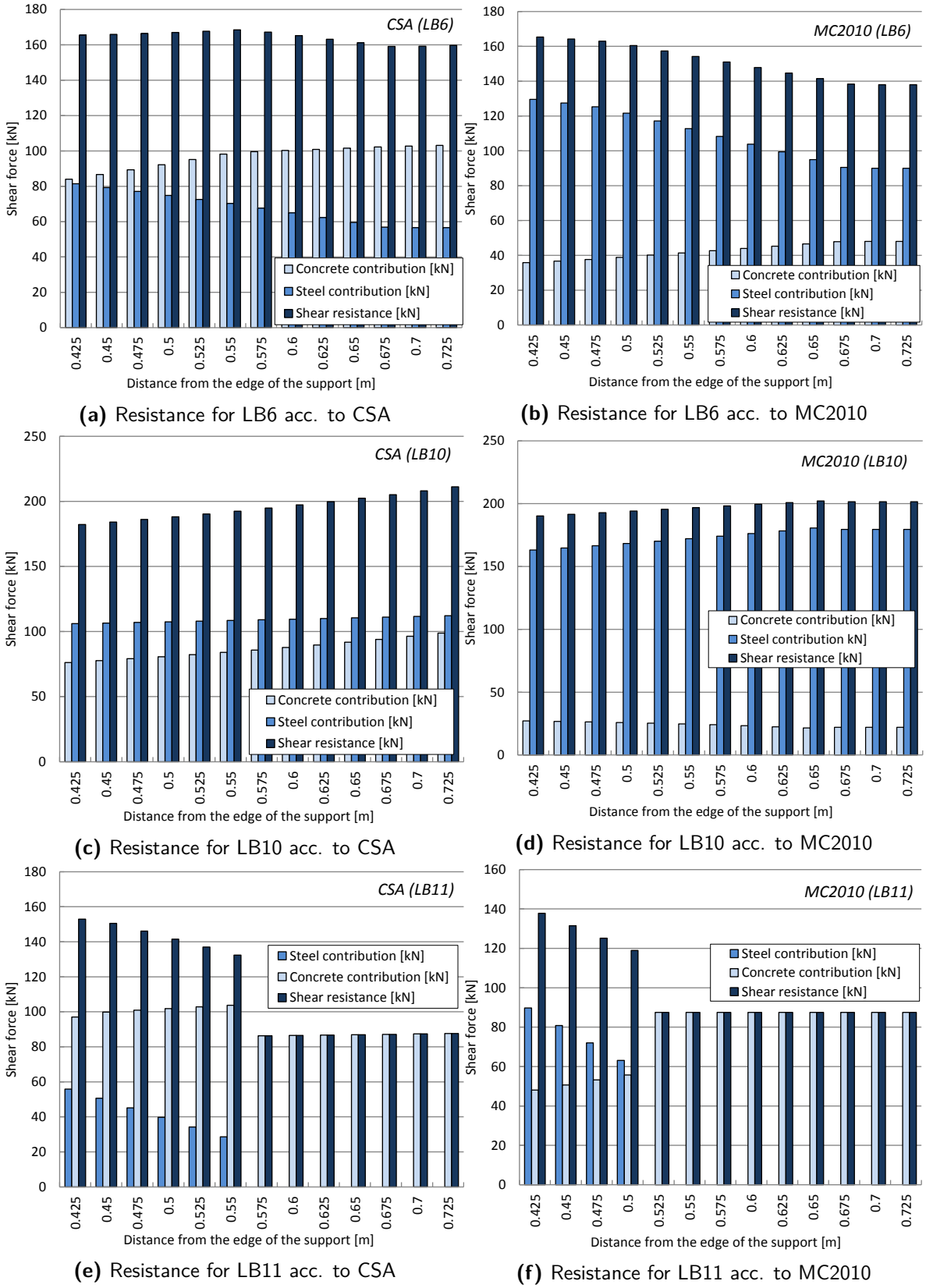

(a) Resistance for LB6 acc. to CSA

(b) Resistance for LB6 acc. to MC2010

(c) Resistance for LB10 acc. to CSA

(d) Resistance for LB10 acc. to MC2010

(e) Resistance for LB11 acc. to CSA

(f) Resistance for LB11 acc. to MC2010

Figure 4-24: Values of shear resistances according to CSA and MC2010 methods attributed to concrete and steel for individual sections

Chapter 5

Numerical Analysis of Benchmark Beam LB6, LB10, LB11

5-1 General Aspects of Numerical Modelling of Concrete

To model cracking, which is one of the most common types of nonlinearity in concrete structures, there are discrete crack or smeared crack approaches (with a fixed or with rotating fracture plane) available. The cracks accordingly can be taken as smeared all through an element or present at finite element boundaries for the discrete cracking. In this section, an attempt to explain basic concepts, and thereby the decisions taken throughout the process of modelling is made.

5-1-1 Discrete Crack Modelling

In the discrete crack concept cracks are modelled through a separation between element edges [27]. The discontinuity is modelled with an application of an interface element between e.g. plane stress elements; in this case line interface elements. These elements relate the forces acting on the interface (a traction vector) to the relative displacement of the two sides of the interface [28]. For a two-dimensional configuration the relative displacement vectors consist of a mode I opening component and a mode II sliding component. Further in [27], it is explained that this approach suffers from two drawbacks. The first drawback is the fact that separation of the element edges implies "a continuous change in nodal connectivity, which does not fit the nature of the finite element displacement method". Secondly, the crack propagates along the path predefined by a user by means of an interface element. The approach of discrete crack modelling may be undertaken when the location of the potential cracking is well-known.
Concrete structures are typically characterized by distributed fracture. Such a dispersed cracking is especially valid for reinforced concrete structures. Modelling of structures with discrete cracks is impractical. This provides the reason why it is appropriate and rational to consider the numerical models in the report with the smear crack approach explained below.

5-1-2 Smeared Crack Modelling

Modelling of reinforced concrete with dispersed cracking as a quasi-continuous material waives from a user defined crack location but instead, the cracks are idealized as being distributed over the whole element. The [27] explains that the procedure is attractive twofold. Firstly, it preserves the topology of the original finite element mesh and consequently no redefinition is needed and secondly, it does not restrain the orientation of the crack planes.
In principle, in the smear crack approach the material is initially considered as isotropic. Upon generation of one or more fractures in a representative area of an element that is attributed to an integration point, the fractures are translated into a reduction of stiffness and strength at integration point. The fractures are initiated when e.g. the condition of tensile stresses in the principal direction is violated. This implies that at the integration point which is where stresses and strains are calculated, the initially isotropic stress-strain relation is substituted with the orthotropic stress-strain relation. The axes of orthotropy are defined in direction normal and tangential to the crack at the angle ϕ to the global x, y coordinate system. With the angle ϕ the local components of stress and strain can be related to the global components in the x,y coordinate system through transformation matrices: $\boldsymbol{T}_{\varepsilon}(\phi)$ and $\boldsymbol{T}_{\sigma}(\phi)$:

$$\varepsilon_{ns} = \boldsymbol{T}_{\varepsilon}(\phi)\boldsymbol{\varepsilon}_{xy} \tag{5-1}$$

$$\sigma_{ns} = \boldsymbol{T}_{\sigma}(\phi)\boldsymbol{\sigma}_{xy} \tag{5-2}$$

$$\sigma_{xy} = \boldsymbol{T}_{\sigma}^{-1}(\phi)\boldsymbol{D}^{S}\boldsymbol{T}_{\varepsilon}(\phi)\varepsilon_{xy} \tag{5-3}$$

where $\boldsymbol{D}^{S}$ is a stiffness matrix accounting for a gradual reduction of the tensile carrying capacity (μ) and shear stiffness retention with β given by

$$D^{S} = \begin{bmatrix} \mu E & 0 & 0 \\ 0 & E & 0 \\ 0 & 0 & \beta G \end{bmatrix} \tag{5-4}$$

The reduced shear stiffness component $\beta G(0 \leq \beta \leq 1)$ depends upon the assumed stress-strain concept; fixed or coaxial (rotating) stress-strain concept. The shear as well as tensile behaviour of concrete is elaborated in subsequent sections.

5-1-3 Shear Reduction β

Upon cracking, the crack plane in a concrete element is defined as normal to the maximum principal stress direction. At the moment of cracking, shear stress and strain are zero as the crack plane coincides with the principal stress direction. As loading proceeds, the principal axes rotate and this eventually leads to initiation of a new crack. Now, two options are possible. As loading proceeds or/and due to potential redistribution of strains and stresses after a cracking onset, the principal axes rotate and this eventually leads to initiation of a new crack. As the already existing crack plane is regarded as being geometrically fixed (under the assumption of the fixed crack concept), the misalignment of a new orientation of the principal axes, therefore the newly formed crack, and the plane of existing crack gives a rise to shear stress resulting from being subjected to shear strain. Consequently, the fixed crack approach requires an explicit definition of shear transfer along the crack interface. It is furnished via

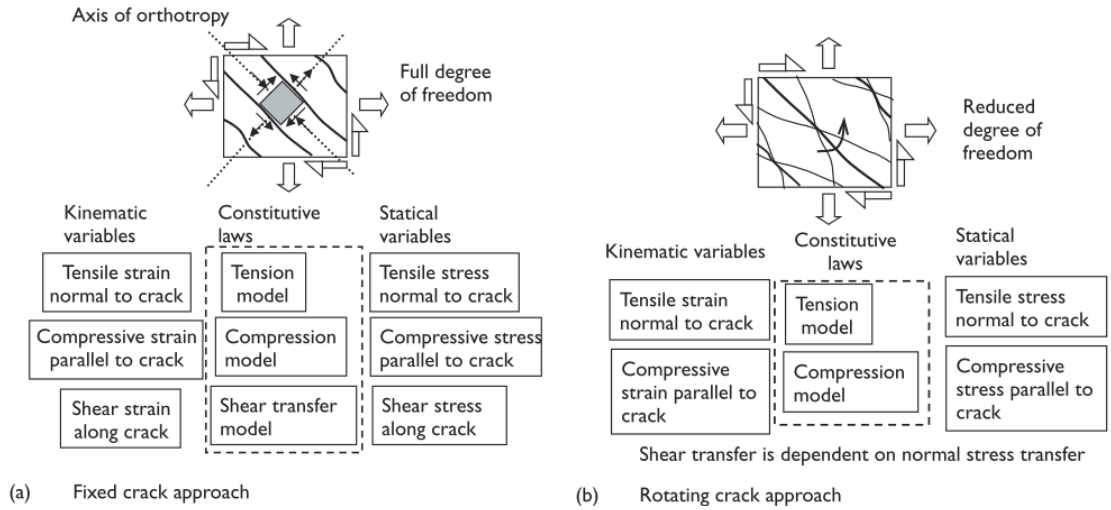

Figure 5-1: Classification of the smeared crack approach [14]

the shear retention factor β. A number of different approaches is available in FEA software packages. The approaches of interest in this report are: variable shear retention, damage based shear retention and aggregate size based shear retention; where shear retention means a reduction of the shear stiffness as a result of cracking. The behaviours are further analysed in the section devoted to evaluation of shear behaviour in total strain based fix crack models, section 5-5.

A different situation applies for the rotating crack concept. The rotating smeared crack approach primarily assumes that the crack direction coincides with the principal direction of average strain. Here only normal and parallel to the crack axis stress-strain relations need to be defined and shear stiffness vanishes.

The classification of the smeared crack approaches are summarized in Figure 5-1. The fixed crack approach is regarded as physically more appealing due to its ability to included shear stresses on the crack interpreted as aggregate interlocking. It is also closer to the reality that after a crack initiation, its orientation remains in place while only principal strains rotate. In the rotating crack approach, a crack plane is continually updated to align with principal strains which seems to be incorrect. Nevertheless, this proves to significantly simplify computation and still provide reasonably accurate results.

5-1-4 Tensile Behaviour

A concrete element prior to cracking is described as an isotropic linear-elastic material with Young's modulus E and Poisson's ratio v. Once the element is cracked, the behaviour of a crack is locally described by a stress-crack opening (traction/crack strain for the smeared cracking framework) relation whereas surrounding concrete continue with linear elasticity, Figure 5-2. The relation stress-crack opening applies to discrete cracking and as far as smeared cracking framework is concerned, it has to be translated into average stress-average strain relation. It can be done by smearing the cracks over a specified reference length/bandwidth which can be conveniently assumed as an element size [14]. To address a tensile behaviour of concrete after cracking, [27] specifies that the most versatile alternative in finite element

analysis is to use mode I fracture function representing tensile tension softening through the fracture energy parameter G_f and the shape of tensile-softening diagram. Fracture energy is the energy consumed per unit of crack propagation in the mode I while tension softening is defined as a decrease in the ability for concrete to bridge/resist the tensile stresses when a crack width increases. The possible diagram shapes that can be employed in the FEA vary from linear, bilinear to nonlinear exponential. The area under the softening curve is fracture energy for discrete cracking or when divided by the crack bandwidth, fracture energy for smeared crack formulation. In the matrix 5-4, a gradual reduction of the tensile strength is introduced via μ.

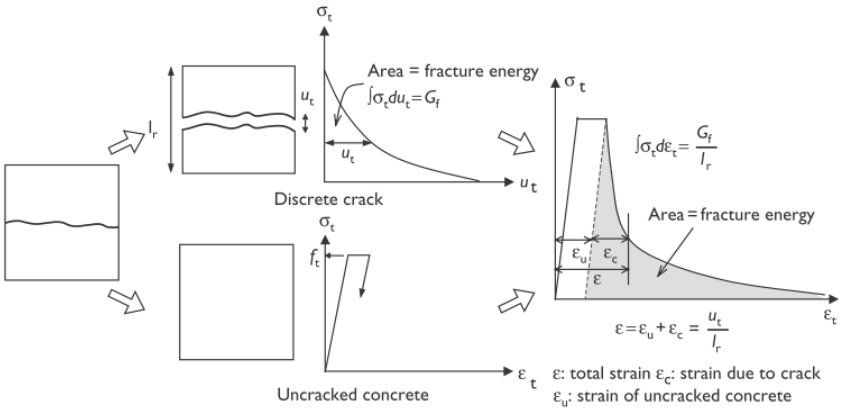

Figure 5-2: Softening behaviour of concrete [14]

5-2 Solution Methods in FEA

A credible assessment of strength and integrity of concrete structures requires non-linear modelling of materials and geometry. In such an analysis the relation between a force vector and displacement vector are nonlinear. To determine the state of equilibrium, the incremental-iterative solution procedure is used. The name stems from discretization not only in space (with finite elements) but also in time with the external load increments [28]. In each load increment the equilibrium is achieved by an iterative solution algorithm. The discretization with load increments is imposed to ensure convergence. The accuracy of the solution also depends on the size of the increments as the behaviour of the structures is often path dependent meaning that different stress states can be obtained depending on the way displacement/force was applied.

5-2-1 Incremental Procedure

The most elementary incremental procedures of applying an external load are the load and displacement control. As the names suggest, the first method applies a load in a number of increments while the second types imposes prescribed displacement onto a structure, also in an incremental manner. Which of these alternatives is selected depends primarily on the nature of a given problem.

5-2-2 Iterative Procedures

An incremental solution with equilibrium iterations after each step is a correction to a pure incremental procedure. In the pure incremental approach, Figure 5-3 material stiffness is updated after each load increment and the value corresponds to the displacement obtained in a previous increment. This however results in the calculated curve progressively drifting away from the correct curve. It is important to know that the correct curve is in fact unknown therefore the calculated error is unknown as well. The measure to eliminate this problem is the implementation of equilibrium iteration performed by the Newton-Raphson method. A force imbalance that is the difference between the applied force in an increment and the resisting force can be used to drive the displacement towards the correct value. Consider the example shown in Figure 5-4. In the first iteration that would enable to approach the correct solution, the tangent stiffness k_{ta} is used to solve the linear equation for Δu through $k_{ta}\ \Delta u = e_{PA}$. and then added to u_A. This displacement is now used to calculate a new tangent stiffness (reduced in case of softening) for the subsequent iteration. With a new force imbalance, the procedure is repeated until the force imbalance is considered by a convergence criterion small enough that a new force increment can be applied. The method in which the stiffness relation is evaluated for every iteration is called Regular Newton-Raphson. An alternative to Regular Newton-Raphson is the Modified Newton-Raphson. This method evaluates the stiffness relation only at the start of the increment. For every iteration, only the prediction of the iterative incremental displacements and the internal force vector have to be calculated.

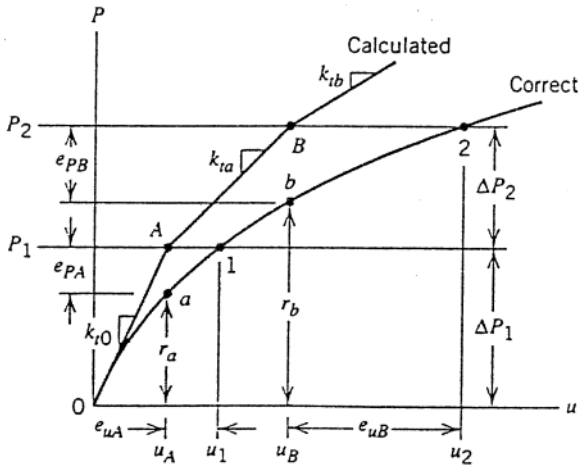

Figure 5-3: Pure incremental procedure [15]

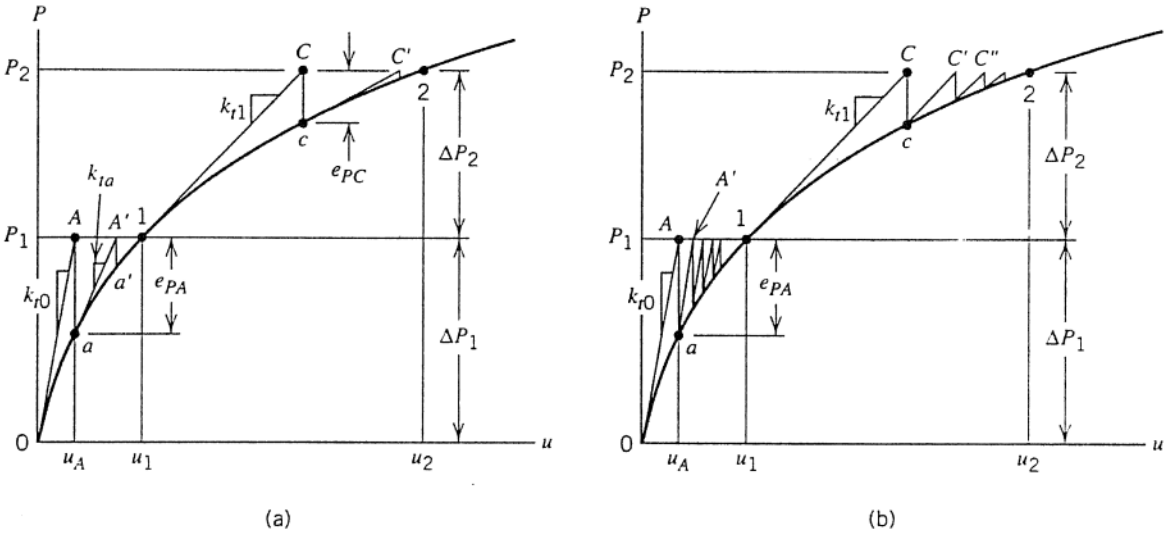

Figure 5-4: Incremental iterative procedure [15]; a) regular Newton-Raphson b)modified Newton-Raphson

5-3 Pre-processing

The objective of this part is to develop a finite element model that simulates the experiments as closely as possible through non-linear analyses. The non-linear finite element analyses according to the classification of the fib Model Code 2010 fall within the highest level of approximation IV. The hereby non-linear models were developed based on the Guidelines for Nonlinear Finite Element Analysis of Concrete Structures RTD 1016:2012 [29].

Please note that the recommendations of RTD 1016:2012 applied here are related to general procedures of treating girder members but ***do not apply to all material properties***. The material properties (if covered) employed in the models were as specified in the Liping Xie PhD dissertation [13]. In the remaining cases, the instructions from [29] were followed. By means of that, the intention is to adapt measures available in the software (i.e. different iterative procedure, shear retention functions etc.) according to RTD 1016:2012 to the specified material properties in [13].

5-3-1 Geometry

The test set-up was chosen to reproduce the loading condition of a continuous beam. The geometry with a longitudinal plane of symmetry, in-plane loading and boundary conditions allow for approximations to be made to the full three-dimensional beams. Additionally, according to the beam theory the stress in the out of plane direction is zero. Consequently, the beams were conveniently modelled as plane stress models. Such a measure enables significantly reduce pre and post processing as well as computational expenses without compromising the accuracy of results. The plane stress models were constructed using plane elements with a given thickness. The as-built geometry was used therefore deviations arisen at execution were not neglected.

5-3-2 Boundary Conditions

In Figure 5-5 the model of the beam LB6 is depicted. The fixed translations are located at the bottom side of the element. At the top, the prescribed displacement is applied. In order to avoid stress concentrations, the load and support reaction forces were introduced through steel loading plates. Due to occurrence of the discontinuous behaviour between steel plates and concrete, interface line elements have to be inserted. The very high dummy normal stiffness modulus was chosen:

$$k_n = 1000 * E_c/l_{element} = 1000 * 40300/50mm \approx 806000N/mm^3$$

where 50 mm stands for the length of initially assumed adjacent continuum element, E_c is the Young's modulus and small tangential stiffness $k_t = 100N/mm^3$. In further analysis the size of elements was more refined. The characteristics of the normal stiffness modulus of interface elements remained the same as they were deemed to be high enough to be consider dummy.

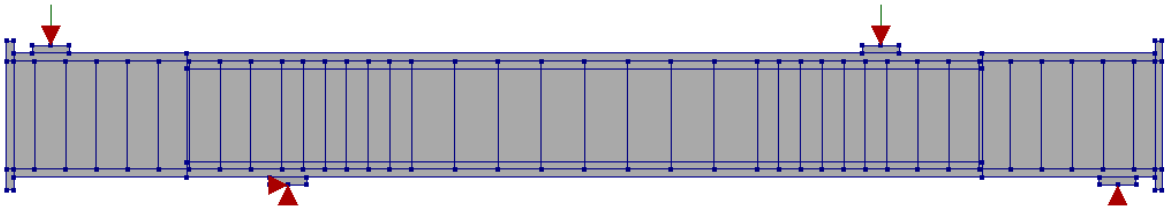

Figure 5-5: Applied boundary conditions and loading

Apart from the prescribed deformation, prestressing and self-weight loading were applied. The prestressing was introduced through unbonded strands anchored in the plate elements at the both ends of the members. The end steel plates spread across the whole section of a beam to avoid splitting of concrete in the web. The prestressing force in each of the 1-inch smooth bars was $797kN/2 * A_{1InchBar} = 786N/mm^2$ (please note that different values were used for specimens LB10 and LB11 because the values of prestressing force, although similar, were not exactly the same). As far as the value of prescribed deformation is concerned, it was specified as the maximum deflection from the readings of vertical LVDTs used in the test.

5-3-3 Material Properties and Material Behaviour

The input data used in the report relies to a large extend on the specified values in [13]. If the input required additional parameters not covered in [13], the recommendations from RTD 1016:2012 were exercised.

Concrete input data

The concrete compressive strengths used in the models were taken from the laboratory tests performed on cylinders at the test day. The cylinders were cured under the same condition as the specimens. The concrete tensile strength was not measured but derived from the concrete compressive strength.
The fracture energy G_f was calculated with:

$$G_F = G_{f0} \left(\frac{f_{cm}}{10} \right)^{0.7} Nmm/mm^2 \tag{5-5}$$

where $G_{f0} = 0.025$ for $d_a = 8mm$ [30].
The compressive fracture energy:

$$G_C = 250 G_F \tag{5-6}$$

Cl. 2.4.1.1 of [29] recommends to use a reduced Young's modulus with a reduction factor equal to 0.85 to account for initial cracking due to creep, shrinkage. The reduction was applied to the derived values of E_c specified in [13]. Young's modulus including the reduction is calculated in [29] as:

$$0.85 E_{ci} = 0.85 E_{c0} \left(\frac{f_{cm}}{f_{cm0}} \right)^{1/3}$$

and for e.g. LB6 it equals to:

$$0.85 * 22000 \left(\frac{63.5}{10} \right)^{1/3} = 34.63 GPa$$

which is a slightly larger value than listed in Table 5-1. Nevertheless, in the models the values as given in Table 5-1 were applied. It can questioned whether it is appropriate to use the reduction of Young's modulus in newly built structures as recommendations of RTD 1016: 2012 address existing structures. To argument the decision, in tests of [13] members were heavily reinforced against flexure. Due to a high level of restrain from the used steel, development of microcracks is expected to be greater which result in a reduction of material strength.

Table 5-1: Concrete input data

Beam		LB6	LB10	LB11
Linear material properties	Young's modulus $[N/mm^2]$	34255	32215	32215
	Poisson's ratio	0.15	0.15	0.15
Tensile behaviour	Tensile strength $[N/mm^2]$	2.63	2.60	2.60
	Fracture energy $[N/mm]$	0.091	0.090	0.090
Compressive behaviour	Compressive strength $[N/mm^2]$	63.5	62.3	62.3
	Compressive fracture stength $[N/mm]$	22.75	22.5	22.5

Steel for rebars and prestressing bars

The material properties for bars 10M, 15M, wires D4 and prestessing steel were provided in [13]. The simplified stress-strain relations are presented in Figure 5-6.
The test set-up was design such that the highest force in the prestressing smooth-rebars would not exceed the yield force therefore the prestressing steel was modelled as linear elastic. The steel properties are listed in Table 4-3 supplemented by the Poisson's ratio $v = 0.3$.

Constitutive Model for Concrete

The behaviour of reinforced concrete incorporated in the models is shown in Table 5-2. For the tensile behaviour after cracking, RTD 1016:2012 recommends models with an exponential softening diagram. The compressive behaviour of concrete should have a specified limit of maximum stresses. The parabolic stress strain diagram with a softening branch based on

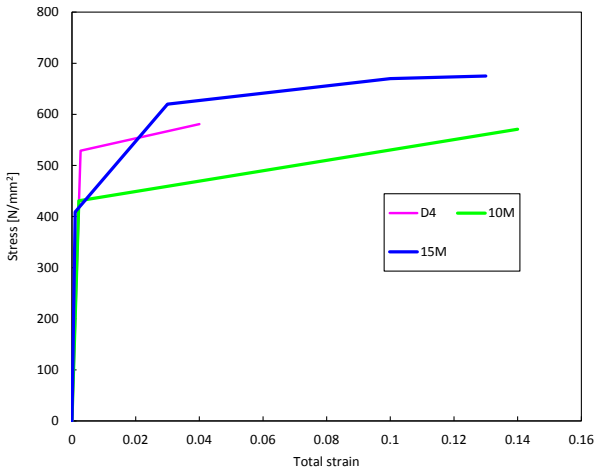

Figure 5-6: Stress-strain relation for steel used in the model

compressive fracture energy is recommended. For shear behaviour RTD 1016:2012 specifies a rotating crack model and a fixed crack model with variable shear retention as preferable.

The reduction of the Poisson's effect was applied as well. The general idea of the reduction is that when an finite element is a subject of cracking, the Poisson's effect ceases to exist. It means the element while being stretched no longer contracts in the direction perpendicular to the direction of stretching [28].

Table 5-2: Concrete Constitutive Model

Total strain based crack model	
Fixed/rotating	
Tensile behaviour	
Tensile curve	Exponential
Reduction due to later cracking	Vecchio and Collins 1993, lower bound reduction curve 0.6
Poisson's ratio reduction	Damage based
Compressive behaviour	
Compression curve	Parabolic
Shear behaviour	
Shear retention function	Damage based
	Variable

Steel behaviour

To model the behaviour of steel reinforcement an elastic-plastic stress-strain relationship with strain hardening hypothesis was selected, Figure 5-6. Yielding of steel is expressed with the von Mises yield criterion.

5-3-4 Element Selection and Discretization

The prestressed beams were modelled using the plane stress method. The eight-node quadrilater isoparametric plane stress elements based on quadratic interpolation and 3x3 Gaussian integration scheme were adopted for the concrete elements and the steel loading and support plates. The reinforcement was modelled with embedded reinforcement elements. A perfect bond between surrounding elements and the embedded reinforcement was specified. This implies that reinforcement strains are computed from the displacement field of the mother element. The embedded elements are integrated within a mother element using 2-pointed integration. The specified mesh size was 25mm.

5-4 Preliminary Analysis

The goal of the preliminary analysis was to check whether loading is applied correctly and forces are introduced to the test region as intended. It was also meant to ensure that the incremental-iterative procedure provides rational results.

Performing analysis with a prescribed displacement in Diana 10 requires imposing a constraint in the direction in which the displacement is applied i.e. application of an additional support to the same node which the load is applied to. For this reason, a model with an included effect of self-weight demanded a phased analysis. In such an analysis computations comprise of several calculation phases. In between each phase the model is updated by addition or removal of elements and constrains and for each phase a separate analysis is performed. At the beginning of each subsequent phase, results from previous phases are contained and used as initial conditions.

The analysed models comprised of three phases. In the first phase, supports were only applied to the bottom side of the beam and the beam was loaded with self-weight alone. In the second phase the beams were prestressed. Finally, the prescribed displacement at the constrained nodes at the upper side of a beam split into a number of increments was activated.

The preliminary analysis was performed on the beam LB6 because it combines the characteristics of the remaining beams. In this analysis the rotating total strain based crack model and the fixed total strain based crack model with the damage based shear retention function were used. Both constitutive models were selected as they do not require any additional user input (the models were described in chapter 5-1). The displacement controlled procedures was applied with the incremental step-size set as 0.005 of the total displacement (0.025mm). The iterative procedure was regular Newton-Raphson with the maximum of 50 iterations. The convergence tolerance was left as default thus 0.01 acc. to both displacement or force convergence norm. The convergence was attained when the equilibrium according to one of the norms was met.

The desired compressive stresses in the test region should be similar to those measured in the test and specified in Table 3-2. From Figure 5-7 it can be seen that for the specified prestressing force, the resulting normal stresses have slightly lower values in the region near the bottom flange which has a higher cross-sectional area than the top flange. The difference between the readings from the test and the model is approximately 4% hence can be considered as insignificant.

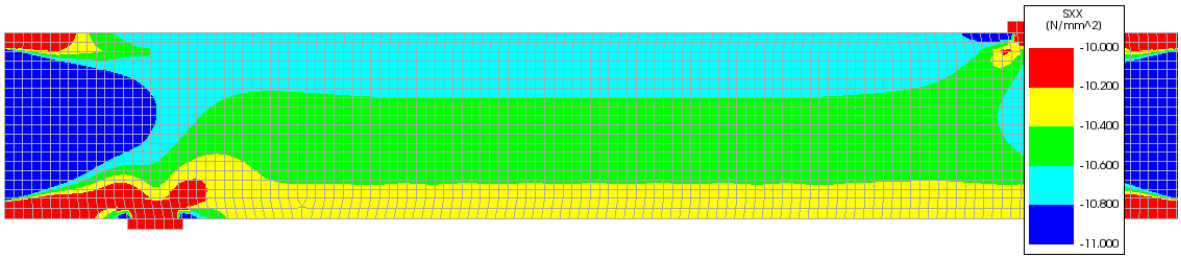

Figure 5-7: Compressive stresses SXX in the test region, beam LB6

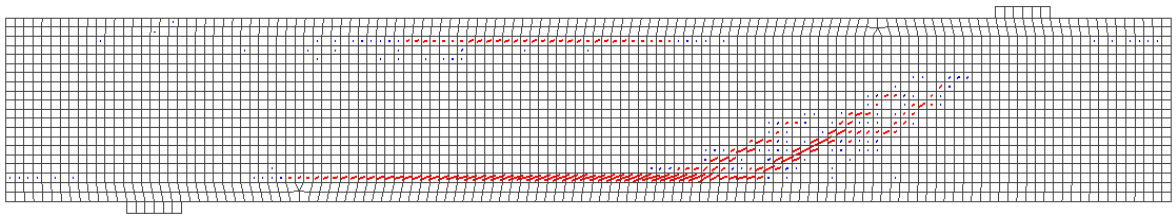

Figure 5-8: Crack pattern for rotating crack shear behaviour, beam LB6

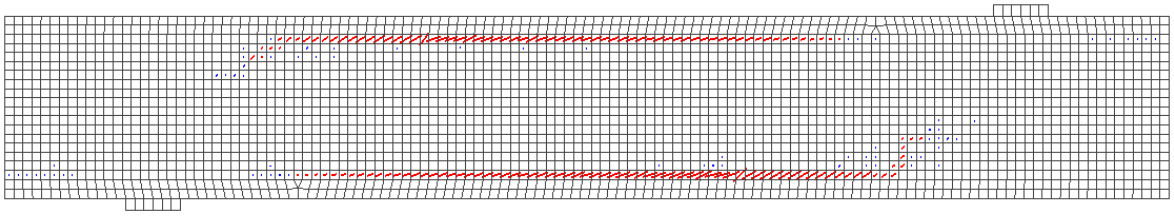

Figure 5-9: Crack pattern for fixed crack, damage based shear behaviour, beam LB6

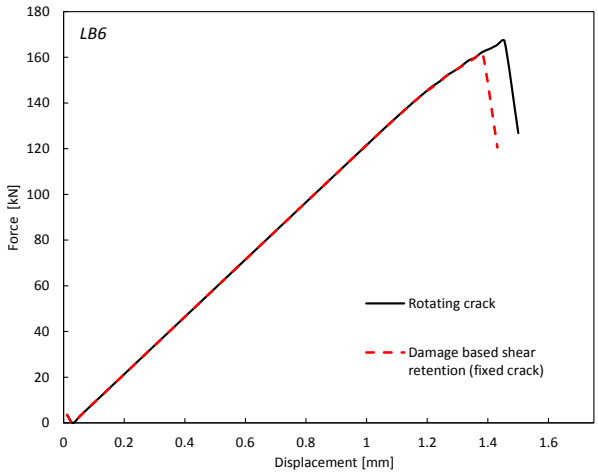

Figure 5-10: Displacement controlled procedure, shear force - displacement for beam LB6

From the observations of the preliminary analysis we can draw a few distinctive conclusions. First, the general behaviour until failure will be appreciated. When the applied load approaches the shear capacity of the beam, at the junction of the web and the flange at the tension side at the distance around d_v from the edge of the support a crack develops. Such

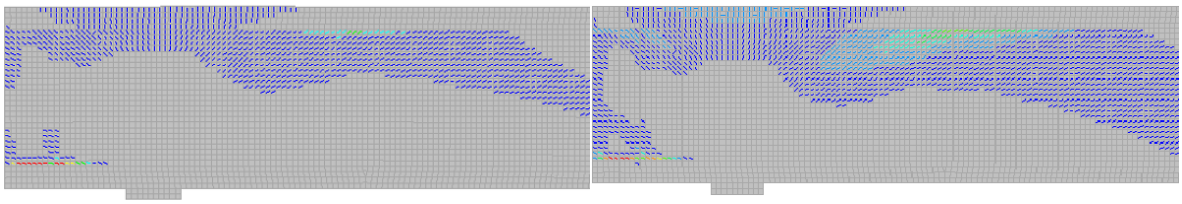

(a) Damage based fixed crack model **(b)** Rotating crack model

Figure 5-11: Crack patterns before failure for displacement control models

an initiation in both models occurs at the similar shear force, approximately 133 kN. The location is also related to the detrimental effect of tensile normal stresses from high bending moment combined with a shear force contributing to crack formation. With an increasing load, the crack further propagates into the critical crack until the beams capacity is reached. The failure mechanism is very abrupt and takes place within one load step. It is noticeable when two last steps of the analysis in figures 5-11 and 5-9 are compared. At the moment of failure i.e. during the last load step, the crack propagates further along the junction as well as diagonally towards the support following the principal compressive stresses. The critical crack is more prominently visible in the case of the rotating crack model than for the fixed crack behaviour. Furthermore, when stirrups along the critical crack yield at failure, the beam exhibits no further load-carrying capacity. It is important to mention that stresses in the shear reinforcement prior to failure were significantly lower than the yield stress. After the failure, stirrups yielded across the crack with the strain at the critical location equal almost to rupture strain. When the developed crack pattern and the fact that longitudinal rebars did not yield are considered, it can be concluded that the beams failed in shear tension. Lastly, the applied prescribed displacement produces reaction forces with the ratio of 1.8 which is in agreement with the ratio achieved from the transverse loading in the tests.
When the results of the benchmark beam LB6 from the experimental research and the obtained FEA results are compared, both similarities and deviations can be noticed. The primary common feature is undoubtedly the failure mechanism. In both cases the opening of one major shear crack crossing the web diagonally took place followed by the dissection at the web-flange junction. Even though formation of the major crack and the shear tension failure appeared in both experimental research and FEA models, the crack patterns obtained from the numerical analyses do not exactly resemble the crack patter from the test. It is visible when the crack pattern from Figure 3-5 is compared with either Figure 5-9 or 5-8. Moreover, the result obtained from the model with rotating crack behaviour tend to overestimate the web-shear capacity.

Table 5-3: Comparison of the results obtained from the preliminary numerical analysis and the experimental results

Loading procedure	Crack orientation	Shear behaviour	Ultimate shear force [kN]
Displacement controlled	Fixed	damage based	154.0
	Rotating	–	159.55
V_{U-exp}	–	–	155.8

From Table 5-3 it can be seen that the models with fixed crack orientation provided better

results than the rotating crack models. It is surprising as it was documented in various literature that fixed crack models typically provide higher values of shear resistance.
In subsequent sections models of LB10 and LB11 for a fixed crack orientation with different shear retention functions are further investigated. As an additional premise, cl.2.4.1.3 of RTD 1016:2012 specifies that for fixed crack models variable shear retention models are strongly recommended. Consequently, the selected shear behaviours are the damage based shear retention function, the variable shear retention function and the shear retention based on a mean aggregate size.

5-5 Evaluation of Shear Behaviour

Shear behaviour of the beams was modelled using the Total strain based constitutive model which is based on the modified compression field theory. Originally this model used an approximation that the principal strain and stress directions coincide for both elastic stress limit as well as after an onset of cracking thus known as the rotating crack model. Currently Diana offers a constitutive model in which the reference system of the crack does not follow the direction of the principal strains – the fixed crack concept. For the fixed crack concept a number of shear retention function can be selected. The guidelines RBT 1016:2012 do not specify which shear retention function should be chosen therefore, in order to determine whether it is possible to simulate the propagation of the crack as observed in the experiments, different set-ups were investigated.

To maintain consistency throughout the analyses, the following framework was used: for beams LB6 and 11, no. of iterations was set to 100 and 150 for LB10. For all the specimens force and displacement convergence norms with the convergence tolerance 0.01 were governing. In addition to that for the selected models an inclusion of energy norm with the tolerance of 0.01 was considered.

5-5-1 Total strain based fixed crack models

Variable shear retention

The recommended variable shear retention function is an improvement to the drawback that the approach with a constant value of the crack shear modulus suffers from. The first drawback is the arbitrariness of the selection for the value of retention. Further, because the shear stress can constantly increase, the principal stresses in the cracked elements rotate endlessly. The variable shear retention function, as explained in [27], relates the reduction of shear stiffness after cracking through the crack normal strain. It means that along with increasing crack width, the shear modulus decreases. This phenomenon can be interpreted as decline of the interlock of aggregate particles. The reduction of the elastic shear modulus G can be written as $G_{red} = \beta G$ with:

$$\beta = \left[1 - \frac{\varepsilon_{nn^{cr}}}{\varepsilon_u^{cr}}\right]^p \tag{5-7}$$

where ε_{nn}^{cr} is the crack normal strain at the beginning of the load increment, ε_u^{cr} is the ultimate strain and p is a constant. The stress-free crack normal strain ε_u^{cr} for the exponential softening is calculated with: $\varepsilon_u = \frac{G_F}{h_{eq} f_{ct}}$.

The shear retention function applied in the models are shown in Figure 5-12. The results of the analysis for different β functions do not differ very much from each other. The pre-peak behaviour up to the moment of cracking is linear for all the models and only the value of the ultimate shear resistance slightly increases along with a low value of the constant p. The response of the models with higher shear retention is therefore stiffer after cracking. The failure for all the cases is brittle and upon formation of the critical crack, the stirrups yield providing no additional capacity.

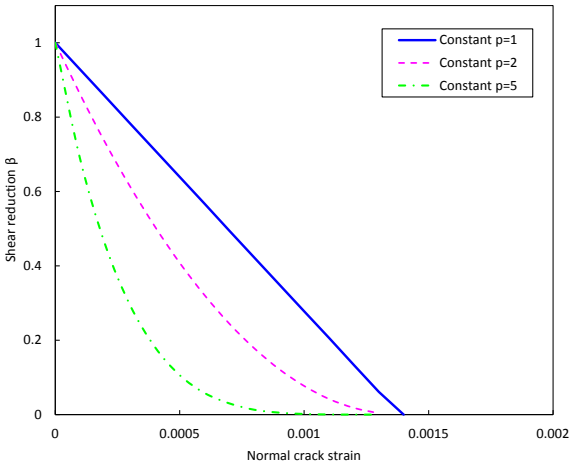

Figure 5-12: Shear retention function for beam LB6

The crack pattern for the beam LB6 is shown in Figure 5-13. The crack patterns were in essence very similar for all functions. It can be observed that the higher the shear retention, the slightly more developed the crack pattern as well as the ultimate resistance. Nevertheless in either case, the the major crack initiated at the distance roughly d_v from the support, in the subsequent loading step, propagates further along the web-flange junction and towards the support (or towards the east loading plate on the opposite side). *Please note that the depicted crack pattern represents general crack pattern with the stress-free (open) cracks in the colour different than dark blue.*

All the three models did not convergence at the failure. For the models with a power function of the constant $p = 2$ decay at the last step spurious kinematic modes were observed. The location of the spurious kinematic modes was the tip of the longitudinal crack along the bottom flange, near the point of contraflexure. In [27] it was stated that the constitutive models with the fixed crack concept are more susceptible to the spurious modes than models with the rotating crack concept. It is so because spurious modes of softening remain fixed throughout the analysis while for the later concept spurious modes may vanish in the subsequent steps due to the ability to rotate direction of material softening. In the models, except for the same location where spurious modes occurred, no excessive stress-locking was observed. The stress-locking is a phenomenon typically related to smeared crack approach as a consequence of displacement compatibility. It means that element which underwent cracking imposes strain on the adjacent elements causing tensile straining as the result of inseparability of the mesh. It can result in excessive tensile stresses of the element in the proximity of a crack resulting in spurious stiffening - overstiffening. Alternatively, when the tensile strength of the material is reached, an onset of crack takes place. This is also undesirable due to disruption of a crack localization, called spurious cracking [27]. When the ultimate shear force is compared to the results of the laboratory tests it can be concluded that the models are characterized as over-stiff in the pre-peak regime and display too brittle post-peak behaviour.

Similar shear retention functions were applied to the remaining beams LB10 and 11. It is important to remember that the shear retention acc. to 5-7 are a little different due to different values of f_{ct} and G_f for those beams. In Figure 5-17 only the crack pattern of the beam LB11 for shear retention with the constant k=5 is presented. The remaining beams displayed almost the same crack pattern up to failure due to insignificant influence of shear retention. All beams failed in a brittle manner with only a single critical crack along the top flange. The

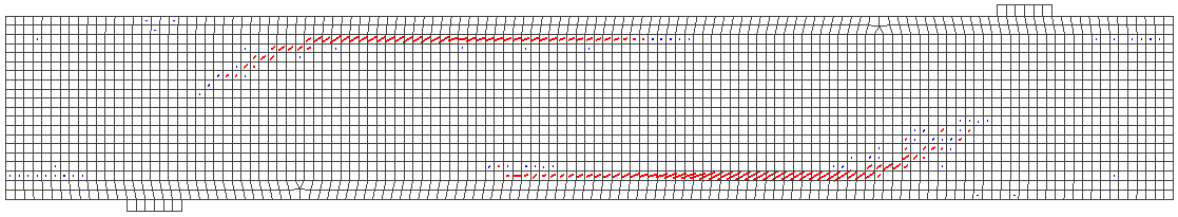

Figure 5-13: Crack pattern for LB6 with variable shear retention, constant k=2

crack was initiated in a distance approximately d_v from the support and propagated further along the flange till failure. The location of the critical crack at the top side is probably related to the asymmetric section with the top flange having a higher cross-sectional area, thus a lower value of compressive stresses from prestressing. As a consequence the tensile strength of the concrete in the principal direction is reached earlier than at the bottom side. From Figure 5-34 and Table 5-7 one can see that both beams LB6 and LB11 failed at approximately the same shear force in the test region. It is surprising as the beam LB6 had twice the minimum amount of stirrups in the test region while the beam LB11 none. Similar ultimate shear resistance can be justified by the fact that a higher value of prestressing acted on the beam LB11 which increased the concrete cracking shear force through diminishing the detrimental effect of tension from bending. While for the beam LB6 at failure stirrups at the bottom flange-web junction ruptured, for the beam LB11 no rupture strain of 0.04 was observed. The response prior to failure was almost constantly linear with no visible reduction of stiffness nor ductility.

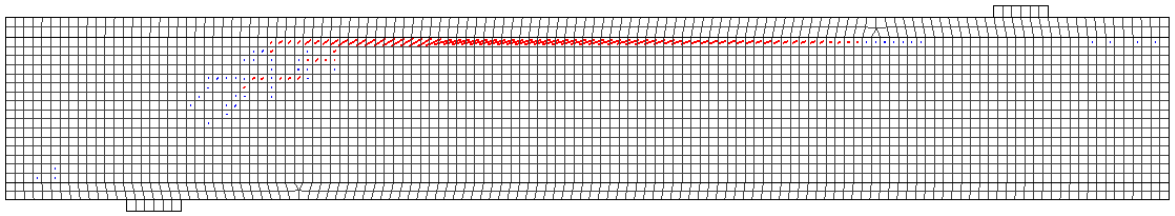

Figure 5-14: Crack pattern for LB11 with variable shear retention, constant k=5

Much more developed crack pattern was obtained for the beam LB10 containing a high amount of stirrups, Figures 5-16 and 5-17. One can notice three general observation. First, with an increase of shear retention formation of the critical crack is delayed (represented with the first snap and jump in Figure 5-15). As it turned out from the performed analysis, this also influenced the overall crack pattern. Delayed formation of the critical crack through a stiffer response of the member in the region with high bending moment and shear force enable development of crack across the beam's web. Nevertheless, the advancement of the major crack with increasing loading does not vary significantly. Another observations are improved shear resistance and ductility. Such improvements can be assigned to the shear stresses build-up on a crack plane even at an advanced stage of stirrups yielding.

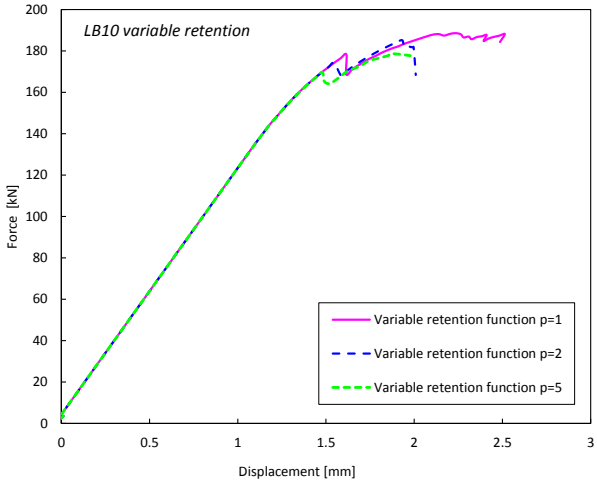

Figure 5-15: Shear force – displacement curve for variable retention shear behaviour

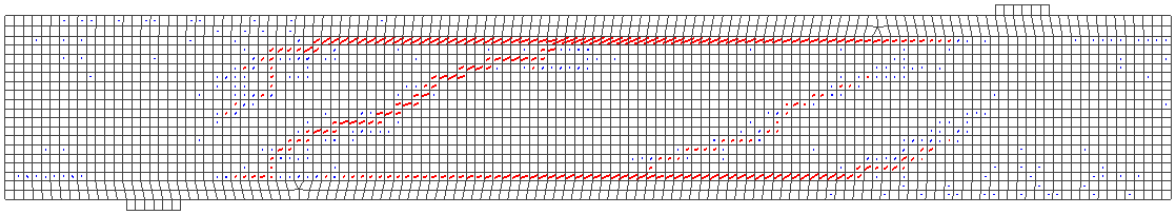

Figure 5-16: Crack pattern for LB10 with variable shear retention, constant k=1

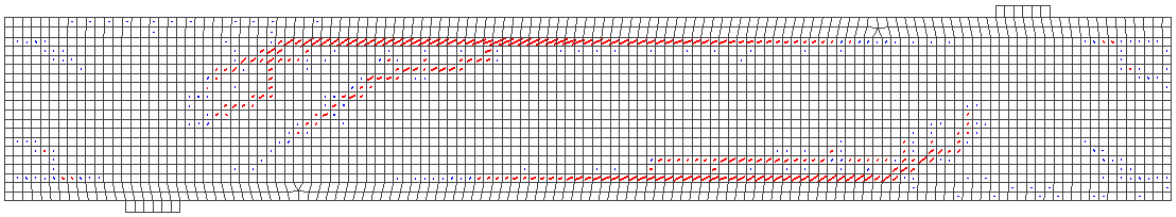

Figure 5-17: Crack pattern for LB10 with variable shear retention, constant k=5

Aggregate size based shear retention

In this shear retention model implemented in Diana the shear stiffness of a crack diminishes with opening of a crack equal to $w = \varepsilon_n h$ [28]. The linear relation reads:

$$\beta = 1 - \left(\frac{2}{d_{agg}}\right)\varepsilon_n h \quad (0 \leq \beta \leq 1) \tag{5-8}$$

It assumes no contact between a crack face thus no shear stiffness for the crack width wider than half the mean aggregate size. The formulation 5-8 would suggest that for the element size of 25mm, shear retention factor reaches 0 when the crack strain equals to 0.2 or equivalently a crack width 5mm. At first glance, it means that only for very large cracks the shear retention diminishes. To investigate the model's performance, the analyses of beams LB6, 10 and 11 were conducted. The resulting ultimate shear resistances are tabulated in Tables 5-4, 5-5, 5-6 and Figure 5-34.

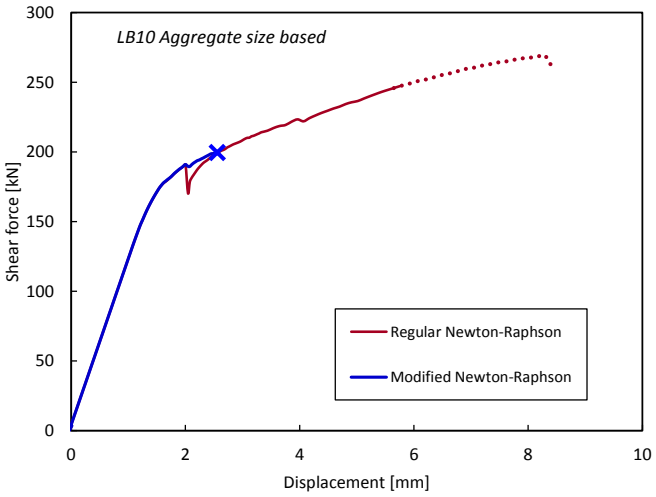

Figure 5-18: F-δ for beam LB10 with aggregate size shear retention and only force and displacement norms

The course of the crack propagation, apart from the failure mode, does not differ from the one explained in the proceeding section. The crack onset in the web comes into sight in the regions influenced by bending moment. Moreover, the crack appears earlier on the side of the cross section where the cross-sectional area is larger. As expected due to higher values of shear retention factor β, a build-up of shear stresses on the crack plane occurs; e.g. for the beam without shear reinforcement in the region I, prior to failure, crack shear stresses were twice as high as for the model with variable shear retention with the constant $p = 2$. Another conflicting observation as compared to the previous models regards failure mechanism which occurs roughly at the same shear force. It is therefore clear that the crack pattern is dependent on the applied shear retention function. One can see in Figures 5-22 and 5-23 that beams LB10 and 11 fail with the pronounce critical crack propagating across the web in the final stage. Such a behaviour resembles the crack pattern from exterimental research depicted in Figure 3-9 and 3-9. A possible remark concluding this observation is that shear retention based on the aggregate size substantially improves failure mechanism and at the same time does not deviate meaningfully from the ultimate shear resistance of the experimental research. Please note that this applies only to the models without energy convergence norm. The behaviour of the aggregate size based shear retention function was confirmed by user supplied input relation $\beta - \varepsilon_{nn}$ assuming the mean aggregate size equal to 8 mm. Predictably, the ultimate shear force as well as failure mechanisms were identical.

The analyses with force and displacement convergence norms and with an additional energy convergence norm were carried out using two different iterative procedure: regular (rNR) and modified Newton-Raphson (mNR). The results obtained with those methods differ substantially from each other for both beams LB6 and LB10. For beam LB11, the failure characteristics were rather consistent as the beam always fails in the region unreinforced in shear. The response of beam LB10 with rN-R (Figure 5-19b) exhibited a ductile behaviour with extensive yielding of the majority of stirrups eventually leading to crushing of concrete near the west support. It is important to mention that values of strain in individual stirrups at the critical crack exceeded the rupture strain which in reality should be accompanied by the failure due

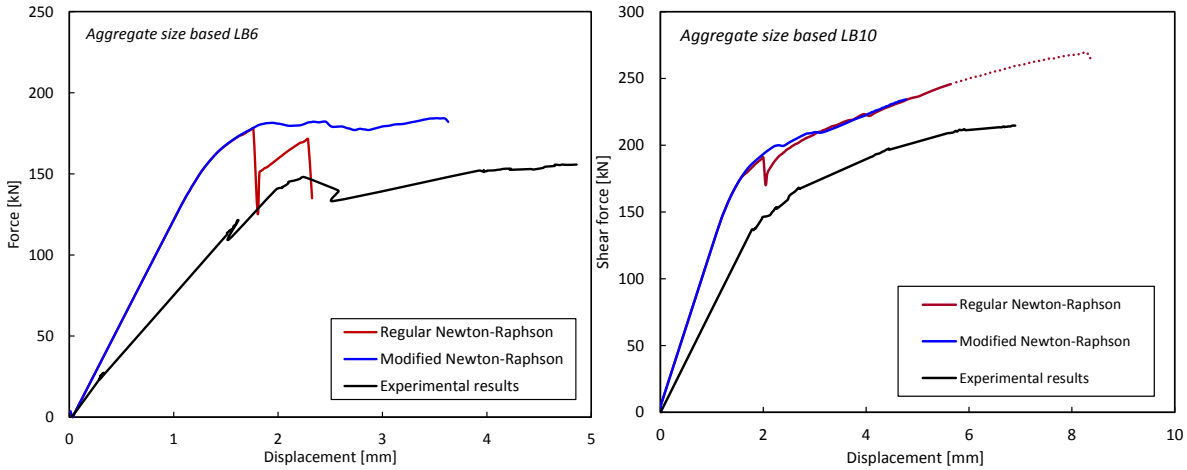

(a) Specimen LB6 **(b)** Specimen LB10

Figure 5-19: Comparison of force-displacement diagrams of specimens LB6 and LB10 calculated with energy convergence norm with the experimental results

to limited redundancy at a late loading stage. Contrary to that, the beam was able to withstand loading till a failure mode different than shear tension was developed. The response after reaching the rupture strain is depicted with a dotted line in Figure 5-19b. The possible explanation for this might be extrapolation of stress-strain relation for stirrups performed by the computer program after reaching the strain limit specified by a user. Calculations of LB10 with mN-R were terminated at much earlier load step resulting in a lower ultimate shear resistance which is closer to the ultimate shear resistance observed in the experimental research. The beam failed with a pronounced diagonal crack crossing the web. Prior to the onset of failure, stirrups in the crack location already yielded with the maximum strain of roughly 0.015.
The above description treats the set of analyses of LB10 with the energy convergence norm. Similar however applies to the analysis of LB10 without energy norm where abnormal elongation of stirrups occurred as well. It can observed in Figure 5-18.
As far a model of beam LB6 with the energy convergence norm is concerned, the shear resistance predicted with mN-R is higher than with rN-R, Figure 5-19a. The analysis using the former iterative method results in more realistic crack pattern with formation of a well-established major crack, Figures 5-20 and 5-21.
Finally, in the case of analyses of both beams LB6 and LB10 with mN-R, extensive distortion of mesh in the last step accompanied by numerous spurious nodes and stress-locking were monitored.

Damage based shear retention

In damage based shear retention, shear stiffness decays with a decay of normal stiffness beyond the cut-off stress [28]. It is done by relating the factor β to the strain in normal direction of a crack. In this case the decrease of the shear stiffness is based on the principle that along with an increase of a crack width, the shear stiffness decreases. The exact relation applied in Diana is however not given in the users' manual. A simplified strain-stress relation can be

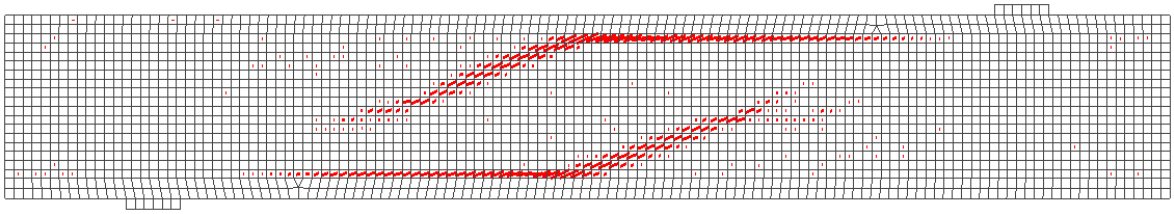

Figure 5-20: Crack pattern of LB6 with aggregate size based shear retention obtained with regular N-R iterative procedure and force, displacement and energy convergence norms, $V_{ultimate} = 171.4kN$

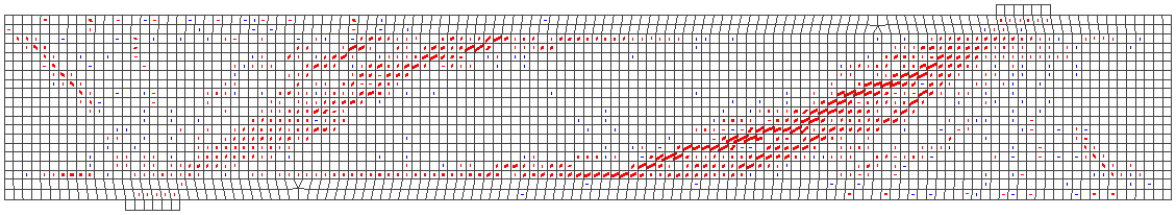

Figure 5-21: Crack pattern of LB6 with aggregate size based shear retention obtained with modified N-R iterative procedure and force, displacement and energy convergence norms, $V_{ultimate} = 184.3kN$

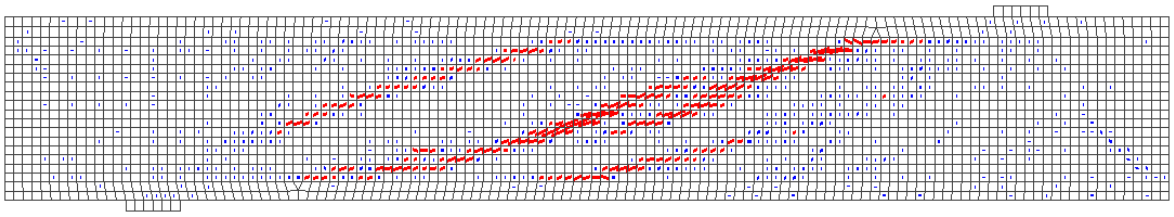

Figure 5-22: Crack pattern of LB10 with aggregate size based shear retention obtained with modified N-R iterative procedure and force, displacement and energy convergence norms, $V_{ultimate} = 234.22kN$

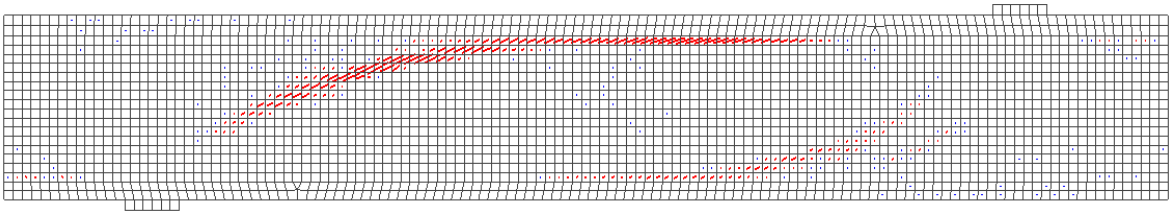

Figure 5-23: Crack pattern of LB11 with aggregate size based shear retention obtained with regular N-R iterative procedure and force and displacement convergence norm, $V_{ultimate} = 177.82kN$

represented with:

$$\sigma = (1 - d(\alpha))D^0\varepsilon \tag{5-9}$$

where the damage variable d is a function of an internal parameter α and grows from zero for undamaged state to unity at full disintegration. The internal parameter α is in turn a function of uniaxial strain determined based on formulation of the damage norms. The stiffness D^0 is the stiffness of the virgin material [31].

To start with, the obtained ultimate shear forces are considered. The results are generally in a good agreement with results from the test site. Likewise all the previous analyses the capacity of the beam LB6 and 11 are overestimated and underestimated for the LB10. However, this shear retention provides the most accurate (in terms of the average and coefficient of variation) results as far as the fixed crack models are concerned. The incremental-iterative procedure for the beam LB10 diverged at the shear force 199.7kN despite of an application of very small load steps equal to 0.0005.

The failure mechanism for beams with limited amount stirrups initiates in the location near the east support (the location of high bending moment and shear force). As soon as crack passes Region II supplied with stirrups, thus crack width controlled, the beam fails abruptly. Only beam LB10 is equipped with a sufficient amount of reinforcement to ensure some stresses redistribution therefore ductility. In this case a formation of critical crack takes place gradually.

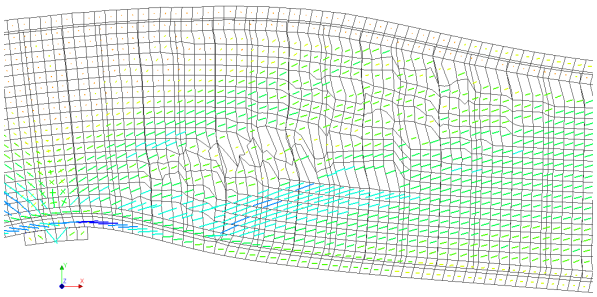

Figure 5-24: In-plane principal components at the critical crack at failure in LB10

The observable feature of beam LB6 and 11 is not well-developed crack pattern, Figure 5-9. The crack pattern in LB10 is much more expanded. Nevertheless the diagonal crack progressing through the web is not so well established as for the case with aggregate interlock shear retention, Figure 5-25. Moreover, at the several location along the major crack, strain concentration in the stirrups can be observed. The maximum crack width at failure, which occurred at approximately the same shear force, is almost twice as large as the crack width obtained with the aggregate size based shear retention. It would suggest that according to present model local strain concentration can be expected. Lastly, in Figure 5-24 the critical crack is depicted. It is apparent that the finite element mesh is distorted in unnatural way leading to stress concentration around the crack.
Side note: this type of behaviour was recognized in every other model calculated with mN-R iterative procedure.

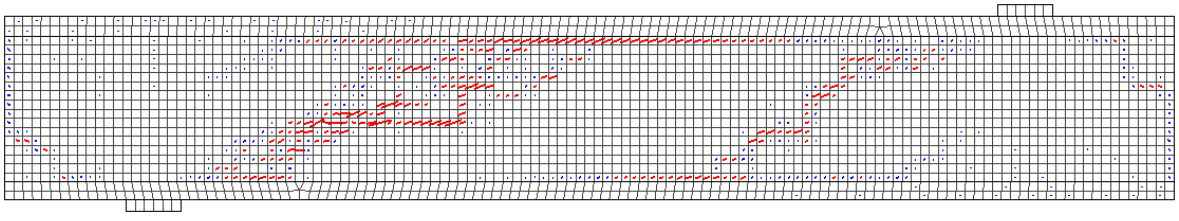

Figure 5-25: Crack pattern of LB10 with damage based shear retention

Rotating crack

The second recommended shear behaviour in RTD 1016:2012 [29] is that based on the rotating angle theory. The stress-strain mode II relation in the vector 5-4 now is:

$$\beta G = \frac{\sigma_{11} - \sigma_{22}}{2(\varepsilon_{11} - \varepsilon_{22})} \tag{5-10}$$

The general aspects of models with a rotating crack orientation were explained in section 5-1. Tables 5-4, 5-5, 5-6 and Figure 5-34 summarize the results of the analyses. From the comparison of main counterparts i.e. fixed crack model with aggregate size based shear retention and rotating crack model, it can be observed that shear stresses at the crack surface significantly influence both the crack pattern as well as the ultimate shear resistance. It is well observed when formation of the critical crack is examined for both models LB10. A lack of the stress build-up encourages crack propagation which is accompanied by higher values of normal crack strains in the already existing cracks. In this context, it is worthwhile to mention that the critical crack for the fixed crack model with the aggregate size based shear retention arose from a newly created crack in the zone with no moment and high shear stresses i.e. the centroidal axis at the point of contraflexure. On the other hand for the rotating crack model LB10, the major crack developed from the "first crack" at the distance d_v from the edge of the support. The crack subsequently propagates horizontally towards the centre of the test region in a search of a new equilibrium state. This equilibrium can be obtained by redistribution of forces to neighbouring stirrups in zones not affected by cracking. This in turn triggers formation of new cracks (and widening of existing) following the flow of principal stresses. Again, it is apparent that crack pattern is dependent on a selected shear behaviour. The presented in this section crack pattern in Figure 5-29, which most properly captured features observed in the crack pattern from tests, was obtained with application of energy convergence norm and mN-R iterative method.

As far as the value of ultimate shear force are concerned, apart from dependency on the applied iterative method, it is relevant to pay attention to the chosen convergence norm. In Figure 5-26, a comparison between results of the same rN-R analyses and a different selection of convergence norms are presented. According to the red curve (based on observation of results), calculations were terminated due to rupture of stirrups. While it was appropriately caught by this analyses, the model assigned to the green curve, thus with additional energy convergence norm, continuously converged until crushing of concrete appeared. Such a spurious yielding resulted in a overestimated prediction of failing shear force and an incorrect failure mechanism.

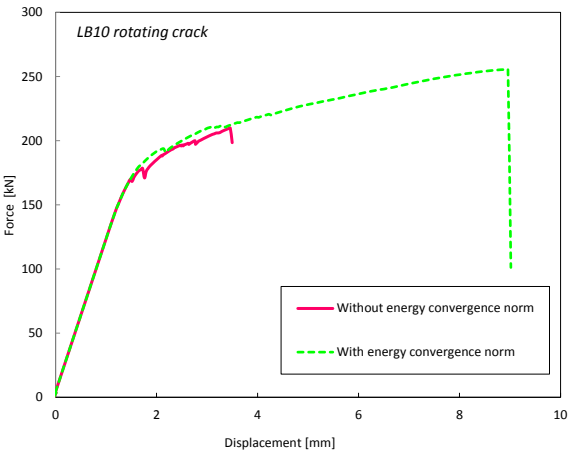

Figure 5-26: F-δ for beam LB10, rN-R iterative procedure

A shear transfer mechanism in beams containing a lower amount of stirrups (LB6 and LB11) can be easily portrayed when the analyses with only displacement and force convergences norms are considered. According to such models, the first critical crack thus the crack formed along the flange-web junction leads to failure. It was already mentioned that crack initiated at the distance d_v typically propagates further along the web-flange junction and diagonally towards the support following principal compressive stresses. In the case of beam LB11 failure occurs once the crack reaches the region unreinforced with stirrups. It is interesting to mentioned that the crack propagates into this region as far as the end of the zone controlled by the last stirrup. At this point a reference to expression 4-1 and Figure 4-1 is made. Once the crack goes out beyond this zone, abrupt failure occurs due to inability to redistribute

internal forces. The crack pattern for this particular case is shown in Figure 5-30. Such a failure exhibits a satisfactory resemblance to the observed failure mechanism depicted in Figure 3-9. A similar although slightly delayed failure mechanism applies to the specimen LB6. It can be well recognized in Figure 5-27. This small retardation does not translate to a higher shear force causing first crack formation but rather an ability to find the equilibrium after onset of major crack. One can only capitalise on it when the energy convergence norm is included into analyses. The response of the structure is depicted in Figure 5-31a whereas the crack pattern in Figure 5-28. It can be seen that for the rN-R analysis, after a few snap and jump, the lower level equilibrium could be found. This eventually resulted in a greatly overestimated ultimate shear resistance accompanied it substantial elongation of stirrups. Locally, the elongation exceeded the threshold value assigned to rupture which might result in a spurious behaviour. This observation i.e. the first excess of the rupture strain is represented by a dashed line in Figure 5-31. One can draw a few conclusions from the aforementioned figures. Fundamentally, for the respected cases the analyses with mN-R resulted in more smooth force displacement curves with no significant drops. This enabled to reach higher value of the shear force before the onset of the major crack. What is more, the analyses with mN-R iterative method were usually terminated at earlier load steps than the analyses with rN-R. The later, as already mentioned, usually resulted in extensive yielding of stirrups until a different failure mechanism occurred – crushing of concrete (in Figure 5-31 indicated by sudden drop of a shear force). It is important to remark that analyses according to mN-R iterative procedure also failed abruptly but the failure was caused by considerable widening of the major crack. It is highlighted by the drop for beam LB6 and marker at the end of the curve for beam LB10, Figure 5-31b. Lastly, from the comparison of responses between rotating crack models of beams LB6 and LB10 and experimental readings, it is apparent that if it was not for the initial overstiff response, the curves would resemble each other acceptably well in both pre first cracking as well as post first cracking regime. It is especially prominent in the case of beam LB10 in which similar hardening plateau and rupture of stirrups are displayed. As far as the specimen LB6 is concerned, an occurrence of the first critical cracking takes place at roughly the same displacement but a distinctly higher shear force.

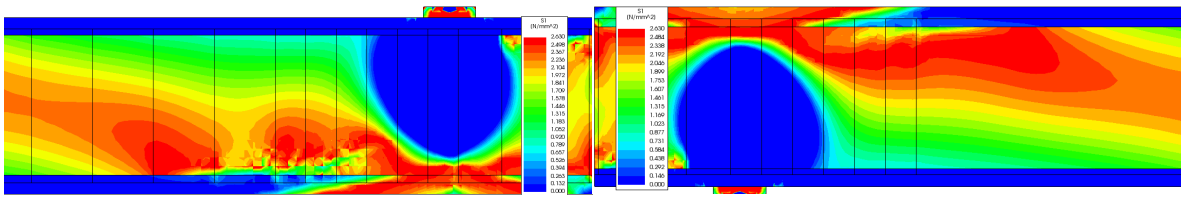

(a) σ_1 contour near east loading plate for specimen LB6 **(b)** σ_1 contour near west support plate for specimen LB11

Figure 5-27: Principal stresses prior to failure in the test region of beams LB6 and LB11

***Note**: in the present report, a detailed mesh sensitivity study has not been performed. From the performed analyses, it was recognised that the rupture strain can be reached at different load steps depending on a mesh size e.g. for the analysis with rNR and the mesh with an element size of 25mm, the rupture strain was surpassed right after onset of the first major crack whereas for the same analysis set-up but the mesh size of 45 mm, it occurred at much later stage, if occurred at all; Figure 5-32.*

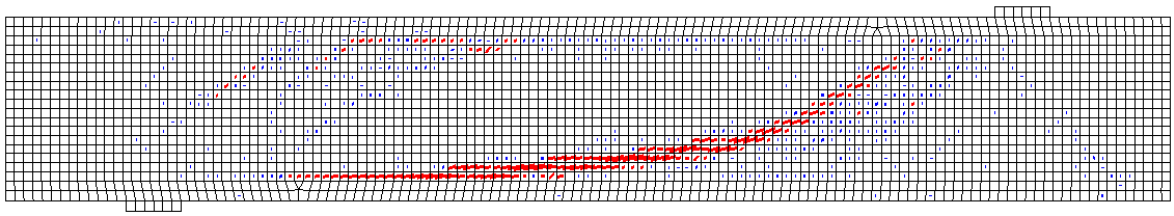

Figure 5-28: Crack pattern at failure of beam LB6 for rotating crack orientation, mN-R iterative method and energy norm convergence

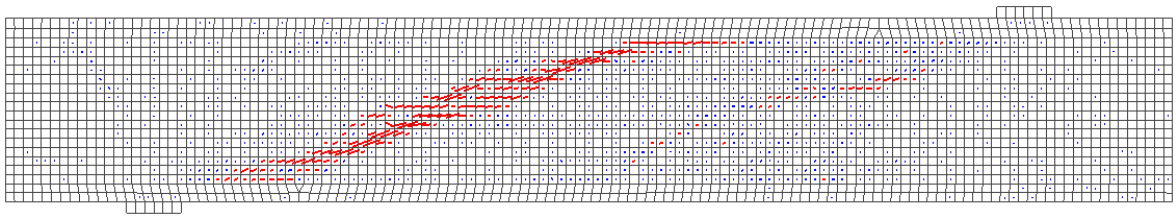

Figure 5-29: Crack pattern at failure of beam LB10 for rotating crack orientation, mN-R iterative method and energy norm convergence

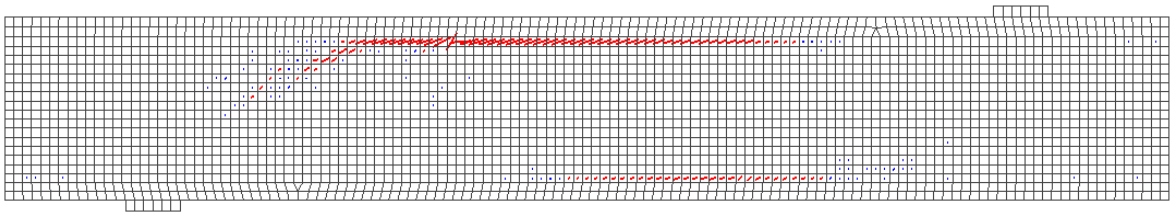

Figure 5-30: Crack pattern of LB11 for rotating crack, rNR

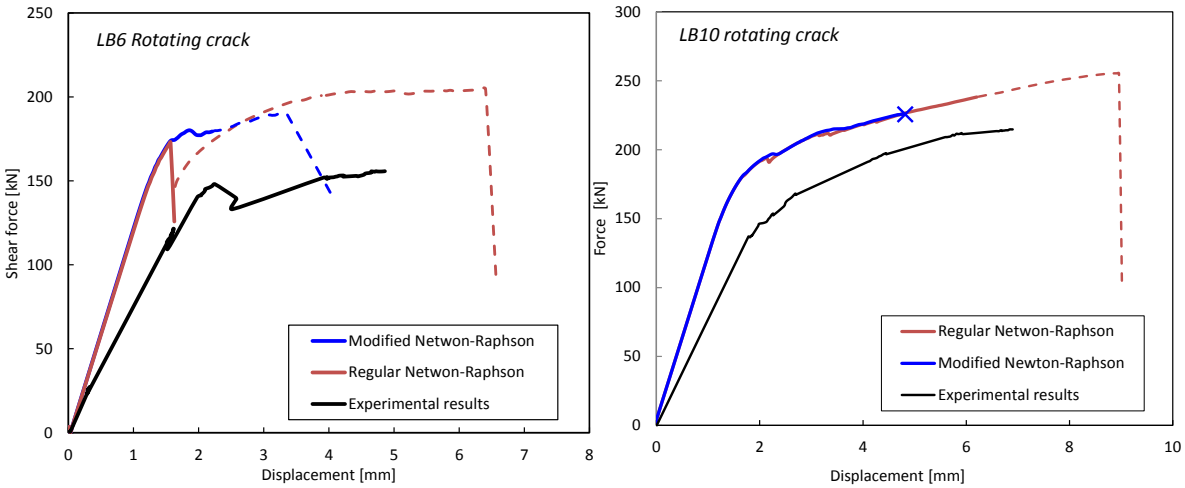

(a) Specimen LB6 **(b)** Specimen LB10

Figure 5-31: Comparison of force-displacement diagrams of specimens LB6 and LB10 with experimental results

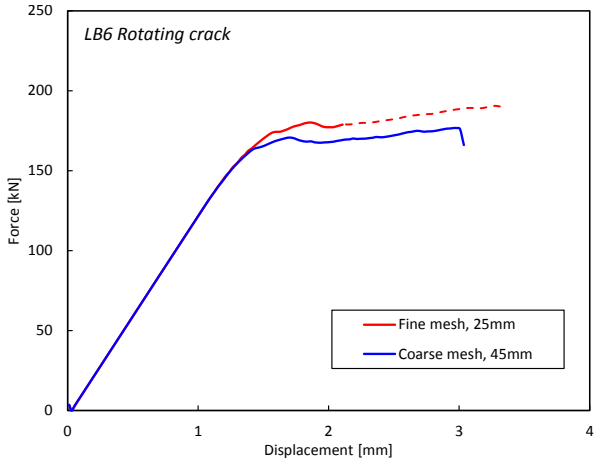

Figure 5-32: Comparison of results for LB6 with mesh element size 25mm and 45mm; dashed line represents the response after stirrups strain locally reached 0.04 corresponding to the rupture strain value

5-5-2 Influence of the Amount of Stirrups

In the study [13], the results of ultimate shear strength were obtained based on the finite element analysis using the program VecTor2 developed at the University of Toronto. From that results which are relatively similar to results listed in Table 5-7, an increase of shear capacity along with an increase of applied stirrups was experienced. The shear resistances from the FEA in [13] were 179kN for LB6, 201kN for LB10 and 167kN for LB11. This is conflicting with some of obtained results of shear strength for LB6 and LB11. An influence of shear reinforcement for beam LB10 was therefore investigated with two additional reinforcement ratios, namely: $\rho = 0.283\%$ and 0.566% thus an amount of reinforcement for LB6 and LB10 increased by 1.5. It is important to factor in that the spacing of reinforcement does not impact results significantly as concluded from the analysis on models with the amount of shear reinforcement of LB6 (0.1885%) but spaced 87.5 mm apart which is the original spacing decreased by the factor of two – beams having the same reinforcement ratio but different spacing of 175mm and 87.5mm failed at the same shear force.
From Figure 5-33 it is clear that a higher amount of shear reinforcement, confirming the presumption, increases the ultimate shear strength. The increase in strength is not however proportional and equal for different shear retention functions and is the most pronounced for the model with a rotating crack orientation. Also, based on the results, an increased in shear reinforcement by 50 % obviously does not lead to an increase in the ultimate shear strength by the same magnitude. It is incompatible with the outcome of the analytical expression such as e.g. equation 2-29 at which the growth of shear resistance is proportional to the added amount of stirrups. Please note that the analyses were conducted with force and displacement convergence norms only.
It is although distant from our current focus but not completely irrelevant to mention here that the beam with the reinforcement ratio of 0.566% and the rotating crack orientation failed due to crushing of concrete near the east loading plate. The completion of the remaining models' analyses with the same reinforcement ratio was necessitated due to divergence.

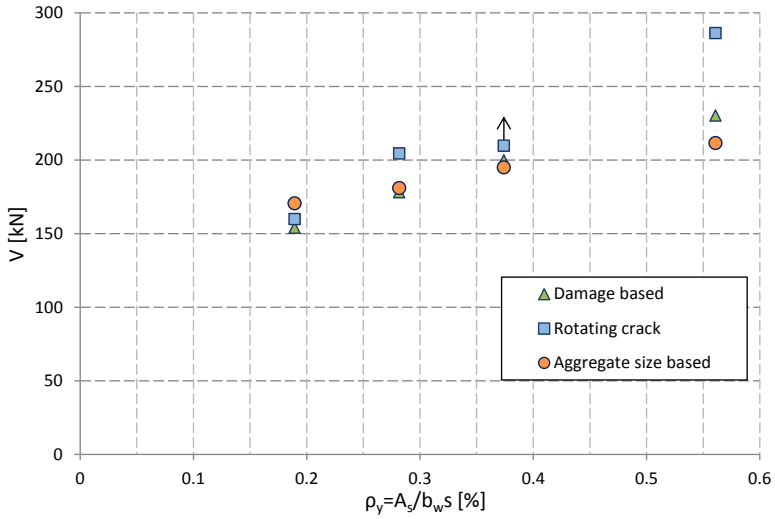

Figure 5-33: Influence of an increased amount of shear reinforcement illustrated with beam LB10[‡]

[‡]the arrow in Figure 5-33 indicates that the shear resistance for the considered case is most likely to be higher than obtained. The conclusion is drawn based on the observed relative out of balance force which was very close to fulfil the convergence norm which was set 0.01. The current result is taken to maintain the consistency with the remaining models' analysis settings.

5-6 Summary

Table 5-4: Summary of results for beam LB6

Shear resistance of beam LB6 [kN]			
	Iterative procedure		Convergence norm
	rNR	mNR	
Variable shear retention k=1	167.2	–	force & displacement
Variable shear retention k=2	165.5	–	force & displacement
Variable shear retention k=5	161.7	–	force & displacement
Damage based	154	–	force & displacement
Aggregate size based	170.5	168	force & displacement
	171.4	184.3	force, displacement & energy
Rotating crack	159.55	159.5	force & displacement
	207.49	190.17	force, displacement & energy

Table 5-5: Summary of results of beam LB10

Shear resistance for beam LB10 [kN]			
	Iterative procedure		Convergence norm
	rNR	mNR	
Variable shear retention k=1	188	–	force & displacement
Variable shear retention k=2	185.2	–	force & displacement
Variable shear retention k=5	178.9	–	force & displacement
Damage based	199.7	–	force & displacement
Aggregate size based	269.39	199.58	force & displacement
	269.7	234.22	force, displacement & energy
Rotating crack	209.75	201.77	force & displacement
	255	225.33	force, displacement & energy

Table 5-6: Summary of results of beam LB11

Shear resistance of beam LB11 [kN]			
	Iterative procedure		Convergence norm
	rNR	mNR	
Variable shear retention k=1	167.45	–	force & displacement
Variable shear retention k=2	165.2	–	force & displacement
Variable shear retention k=5	160.7	–	force & displacement
Damage based	160.7	–	force & displacement
Aggregate size based	177.82	176.66	force & displacement
	180	182.6	force, displacement & energy
Rotating crack	164.4	166.4	force & displacement
	164.4	166.97	force, displacement & energy

The objective of the present section is to target the question stated in section 1-2 concerning the aim of this study. It reads as follows: *is it possible model shear tension failure of the experiments numerically?*
To start with, to a certain extend implementation of numerical analysis can be used to reproduce the shear tension behaviour of tested specimens subjected to a mixed mode fracture (mode I and II). In the considerations two aspect were taken into account: the failure mechanism with a trajectory of the critical crack and the ultimate shear force in the test region. In Tables 5-5, 5-6 and 5-7 the results of different analyses are presented (the best records are highlighted in blue for the first group and cyan for the second group). The variables of the study were: shear retention functions, iterative method and convergence norms.
To formulate constructive conclusions from the conducted analyses, the results were categorized into two groups. The results of the first group are highlighted in Table 5-4. The group constitutes the outcome of the analyses which were performed with diverse shear retention functions and convergence regulated with force and displacement norms. From the outlined results one can see that for different shear retention functions, the obtained results do not deviate significantly from each other. From considerations in the previous section it could be concluded that the failure mechanism was highly dependent on the applied shear retention factor β and its relation with the crack normal strain.
The best representation of the crack pattern combined with values of shear tension resistance were obtained with the rotating crack orientation. Please recall that fully developed crack pattern could be only established when the energy norm convergence was included (it is elaborated in a further part of the section). Nevertheless for only force and displacement convergence norms, it was possible to capture the shear tension failure characteristics of each tested beam. The method provided sensible results for beams containing shear reinforcement but overestimated the capacity of the specimen without shear reinforcement. The average ratio of predicted values of shear resistance and readings from the experimental study is 0.97 with the relatively low c.o.v 8.4%.
Next to rotating crack models, accurate results were be obtained with the damage based shear retention function. The values of shear tension resistances support the tendency of the previous method thus the models predicted resistances of LB6 and LB10 with acceptable correctness while the shear capacity of LB11 was slightly overestimated. The average of results is almost equal to unity and the c.o.v equal to 9.6%. As far as the crack patterns are concerned, the shear retention function mapped them correctly. The exception may be beam LB6 for which, at failure, horizontal critical cracks arose along flanges.
The results from models with the aggregate size based shear retention typically overestimated shear tension capacity. It refers to models irrespective of the applied amount of reinforcement except of the LB10 computed with mN-R iterative method. An encountered pitfall was the analysis of beam LB10 with rN-R which exhibited greatly exaggerated resistance of 269.39 kN which is the highest deviation of all the results in this category. The characteristics of the crack pattern from tests were well reproduced.
Lastly, the variable shear retention from [27], not so commonly used in nowadays engineering practise, might well serve as visualization of the impact of shear retention on the ultimate shear resistance. It is clear from 5-4 that shear tension resistance increases for smaller reduction of shear stiffness G.
As far as crack formation is concerned a few mutual characteristics were observed. For all the beams the initial crack initiated at the distance roughly d_v from the support. In region (Region 2) the crack is controlled by stirrups spaced 87.5mm apart. The crack propagates

further towards Region 1. In the case of beam without shear reinforcement instantaneous failure occurs while for the remaining beams yielding of subsequent stirrups takes place. It can be seen that stirrups in the beam LB6 do not grant a reserve of load carrying capacity and the beams fail in a brittle manner. The similar values of resistance for LB6 and LB11 result probably from a higher value of prestressing force for beam LB11. The critical crack typically appeared on the side of where compressive stresses were diminished due to a larger area of flanges.
Regarding the effect of material parameters, the assumed concrete tensile strength $f_{ct} = 0.33(f_c')^{1/2}$ provided better estimates than the value of f_{ctm} acc. to the RTD 1016:2012. For the value of the concrete tensile strength according to the RTD 1016:2012 equal:

$$f_{ctm} = f_{ctk,0,m}\left(\frac{f_{ck}}{f_{ck,0}}\right)^{2/3} = 1.4MPa * \left(\frac{63.5MPa - 8MPa}{10MPa}\right)^{2/3} = 4.389MPa \qquad (5\text{-}11)$$

the cracking shear force as well as the ultimate shear resistance were extensively overestimated e.g. for the beam LB11 with rotating crack shear behaviour, the first cracking shear forces were 134 kN and 179.26 kN for the reduced concrete tensile strength and the tensile strength acc. to the RTD 1016 respectively. The ultimate shear forces were 164kN and 192.2kN thus also divergent.
In Figure 5-35 shear force in the test region against the displacement under the east support is plotted for all specimens. The pre-peak response for the assumed material properties of concrete in NLFEA is generally too stiff, even for the reduced value of Young's modulus by 15 %. In [32] a similar problem was encountered. A possible reason is the fact that Young's modulus of self compacting concrete is lower than for conventional concrete (Klug & Holschemacher 2003). The softer behaviour is explained by the lower amount of coarse aggregate in comparison with normal concrete. The extent of this effect is however uncertain. Additionally, the beams were heavily reinforced against flexure which could also be impactful due arose shrinkage cracks which reduce stiffness.

Table 5-7: Summary of results of numerical analyses with force and displacement convergence norms

Specimen	LB6	LB10	LB11	Average	C.o.V [%]
N [kN]	-797	-822	-809		
V_{u-exp} [kN]	155.8	215	142.8		
VecTor2 from [13] [kN]	179.0	201.0	167.0		
Rotating crack [kN]	159.55	209.75	164.4		
Damage based [kN]	154	199.7	160.7		
Variable shear retention p=1 [kN]	167.2	188.6	167.45		
Variable shear retention p=2 [kN]	165.5	185.2	165.2		
Variable shear retention p=5 [kN]	161.76	178.9	160.7		
Aggregate size based [kN]	170.5	199.58	176.66		
Exp/Rotating crack	0.98	1.025	0.87	0.97	8.4
Exp/Damage based	1.01	1.07	0.89	0.99	9.6
Exp/VSR, p=1	0.93	1.14	0.85	0.98	15.2
Exp/VSR, p=2	0.94	1.16	0.86	0.99	15.56
Exp/VSR, p=5	0.96	1.20	0.89	1.02	16.07
Exp/Aggregate size based	0.91	1.077	0.81	0.933	14.522

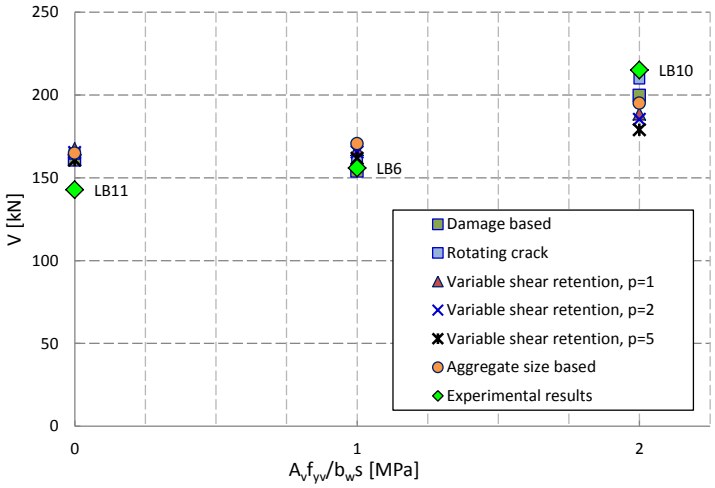

Figure 5-34: Summary of the numerical analysis results for different shear behaviours

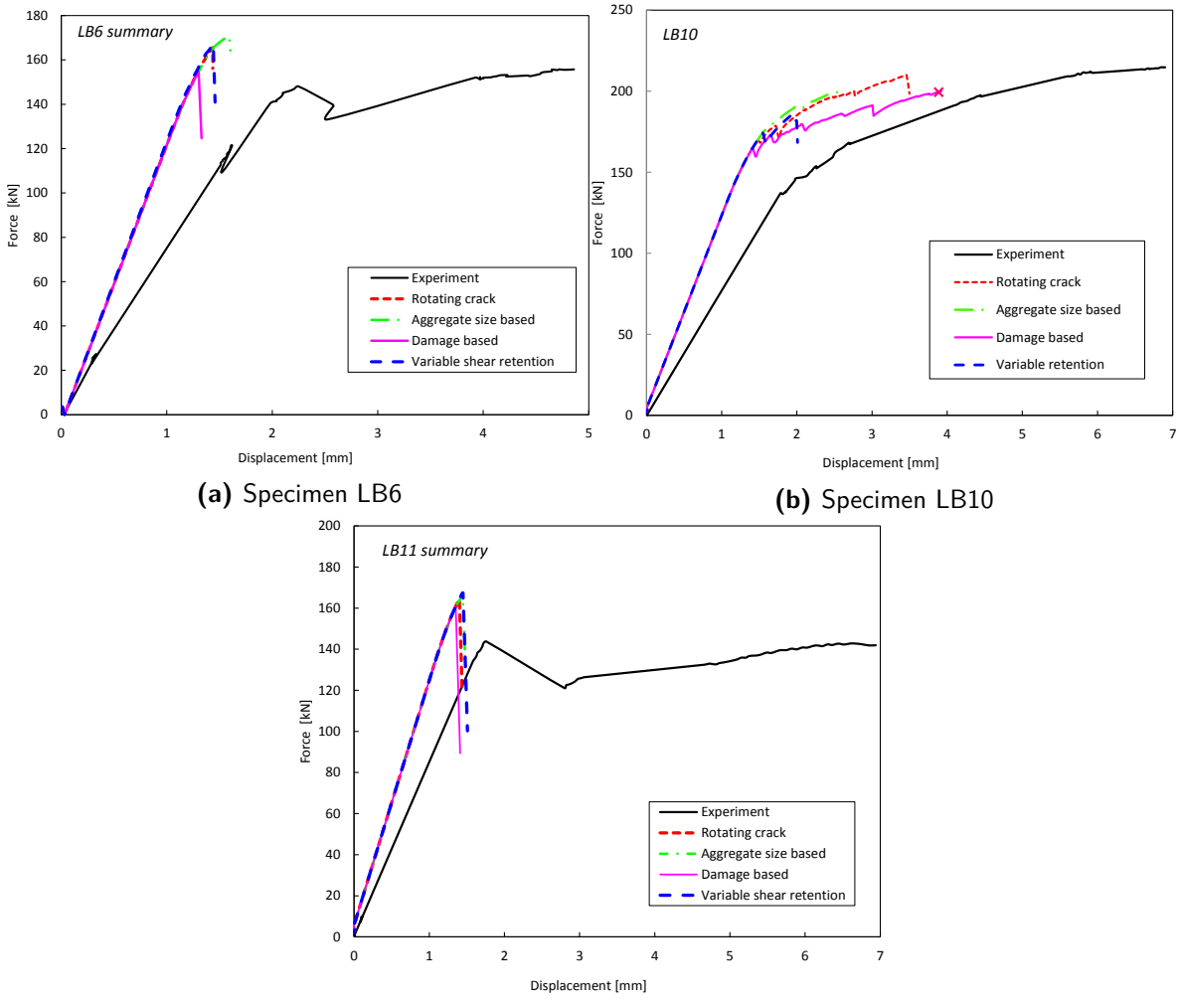

(a) Specimen LB6

(b) Specimen LB10

(c) Specimen LB11

Figure 5-35: Force-displacement diagrams for beams LB6, 10 and 11 corresponding to the results in Table 5-7.

The presented in previous sections crack patterns were typically obtained from the analyses with energy convergence norm of 0.01. By means of it, the analyses could further proceed (the equilibrium was found) after formation of major crack or in the stage of extensive yielding of reinforcement which is when the analyses corresponding to only force and displacement convergence norms terminated. The ultimate tension shear resistance values of these analyses are outlined in Table 5-8 and Figure 5-36. The corresponding force-displacement curves are plotted in Figures 5-19 for aggregate size based shear retention and 5-31 for rotating crack shear behaviour.
From the table it is rather difficult to distinguish a superior performance of one particular analysis set-up type. What can be concluded is that predicted shear resistances are overestimated for all possible combinations of amount of shear reinforcement, shear retention functions or iterative methods. For the case of a rotating crack orientation in both mN-R as well as rN-R, a distinction with respect to ultimate shear resistance between specimens with varying amounts of shear reinforcement can be made. In addition to that the trend of ratios of experimental and numerical analyses is consistent which is substantiated by a low value of c.o.v equal to 6.915 % and 5.739 % for rN-R and mN-R respectively.
While comparing the results of rN-R and mN-R, one can arrive at the conclusion that the latter iterative method furnishes better predictions. The values of shear resistance are lower than those obtained with rN-R. Another very relevant aspect is the consideration associated with spurious elongation of stirrups beyond the rupture threshold. From the force-displacement curves in section 5-5-1, it can be noticed that rN-R is much more susceptible to this phenomenon which potentially is the reason for exaggerated shear capacity. What is more, mN-R for the analysed specimens always resulted in shear failure. A different situation took place for individual analyses with rN-R which were terminated due to crushing of concrete in the location of either loading plate or a support. It was already mentioned that such a failure mechanism is succession of excessive extrapolated by program strains in stirrups. This leads to another essential aspect which is a crack pattern. In the majority of cases, reproducing a satisfactory crack was only possible with the mN-R iterative method. At this point, it is clear that it can be accomplished when the model fails in an anticipated manner – in shear tension. In conclusion, the results of the ultimate shear tension resistance as well as developed crack patterns proved that to be better for mN-R.

Table 5-8: Comparison of results for different iterative procedure

Specimen	LB6	LB10	LB11	Average	C.o.V [%]
N [kN]	-797	-822	-809		
V_{u-exp} [kN]	155.8	215	142.8		
Rotating crack rNR [kN]	204.77	269.7	164.0		
Rotating crack mNR [kN]	190	234.22	166.97		
Aggregate size based rNR [kN]	171.4	255	180		
Aggregate size based mNR [kN]	184.3	225.33	182.6		
Exp/Rotating crack rNR	0.761	0.797	0.871	0.81	6.915
Exp/Rotating crack mNR	0.820	0.918	0.855	0.864	5.739
Exp/Aggregate size based rNR	0.909	0.843	0.793	0.848	6.837
Exp/Aggregate size based mNR	0.845	0.954	0.782	0.861	10.117

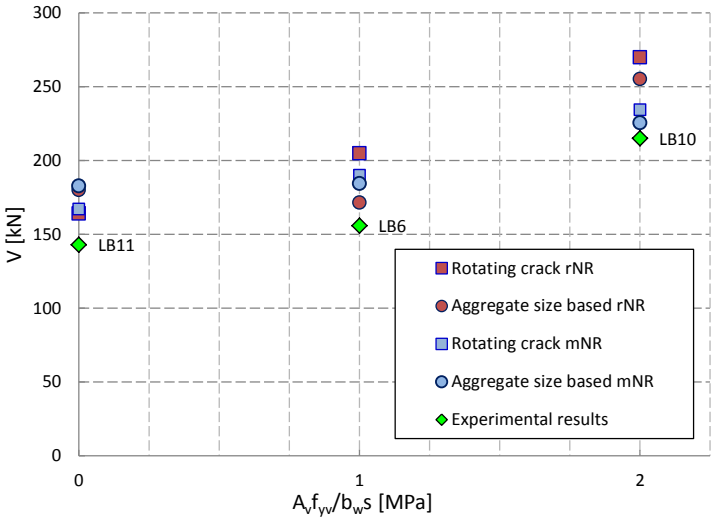

Figure 5-36: Summary of the numerical analysis results for different convergence norms and iterative procedures

Chapter 6

Conclusions and Recommendations

6-1 Analytical Analyses

The report contains analytical and numerical analyses of the benchmark specimens LB6, LB10 and LB11 tested as a part of the research on the influence of axial load and prestress on the shear strength of web-shear critical reinforced concrete elements [13]. The intention of the experiment set-up was to investigate shear tension behaviour at low moment regions in continuous reinforced concrete members under axial compression and tension away from the disturbed region near the support. At this locations the shear strength may be enhanced by strut action. The description of the research is summarized in Section 2. The selection of prestressed beams for the experiment i.e with a varying amount of shear reinforcement was meant to study a whole range of resistances (members with stirrups including those heavily reinforced against shear and members without shear reinforcement) according to a number of shear provisions in available designers' codes. The investigation was conduced in the context of the existing bridges therefore it was crucial to determine the shear strength as accurately as possible. It was executed by means of application of "real" (mean) material properties.
From the consideration on the analytical approaches, it was concluded that "strain state dependent" codes, namely the CSA and MC2010, give very good predictions for members supplied with stirrups. The differences between those codes were very small and only the criterion of conservativeness decided that the shear provision of fib Model Code 2010 is preferred over that of the CSA. It was also shown that despite of the shared background, the resistances attributed to the stirrups and concrete are assigned differently for individual standards. While for the CSA shear provision the contribution of stirrups and concrete was more levelled out, the fib Model Code 2010 assigns the majority of the shear resistance to shear reinforcement. The prediction according to the applied procedure of the EC2 provided a complicated analyses resulting in incorrect determination of the governing shear failure mechanism. The predictions of the tension shear capacity of the analysed standards for the beam without shear reinforcement were very poor. The predictions according to the fib MC2010 and the CSA code greatly underestimated the shear resistance as the resulting shear strength constitutes the post-cracking capacity while the experimental ultimate resistance was taken as the first

read cracking load. Lastly, the outcome of the analysis according to the RBK 1.1 yielded consistent results in terms of ratios of the calculated and observed in tests shear resistances as well as the governing failure mechanism yet extensively overestimated the shear tension capacity for all the considered specimens.

6-2 Numerical Analyses

In the second part of the study, an attempt to analyse the benchmark beams numerically was undertaken. From the conducted analysis the following main conclusions could be drawn:

- a prediction of the first cracking shear force and the ultimate shear resistance were substantially improved when the concrete tensile strength was determined according to $0.33\sqrt{f'_c}$; a similar observation of the decisive effect of concrete tensile strength was reported in [33] and [32] where despite being equipped with f_{ct} measured from splitting tests on concrete cylinders, an improved prediction of the initial crack development was obtained with a reduced value as shown above. As far as the ultimate shear resistance is concerned, the estimates based on the measured (thus not reduced) tensile strength in [33] were in a good agreement with experimental tests of beams failing in shear. [1]
- from the analysis on models of beams LB6 and LB11, the load corresponding to the onset of critical crack constituted the ultimate shear resistance for force and displacement norms; the results of analysis on LB10 heavily reinforced against shear displayed some ductility upon the formation of the major crack.
- analyses according to the displacement and force convergence norms provided accurate results nevertheless the observed in tests crack pattern could be better reproduced with an addition of the energy convergence norm. Despite of being more realistic, this approach provided overestimated results as compared to former analyses with only force and displacement convergence norms
- the most accurate as well as consistent results for all types of analyses (Table 5-7 and Table 5-8) could be obtained with a rotating crack orientation. It was also shown that the aggregate size based shear retention, despite overestimated predictions of shear tension resistance for members without shear reinforcement, provided sufficiently accurate results as well as correct crack patterns
- the results obtained with mN-R iterative procedure proved to yield more accurate values of shear resistance as well as a better representation of the crack pattern. The analyses according to rN-R suffered from extensive spurious stirrups elongation leading to incorrect results and a failure mechanism
- the pre-cracking response of FE models displays overstiff behaviour and deviates from the response from the tests' readings. This phenomenon potentially impacted the first cracking shear force as well the ultimate shear tension resistance

[1] concrete tensile strength reduction is recommended by Bresler and Scordelis [34] as explained in [33] and [32]; no access to item [34] was gained

6-3 Recommendations

Recent shear provisions in designers' codes relate shear design to calculations based on the strain state of a member. By means of that codes waive from expressions assigned to individual types of failure mechanisms or shear resistances attributed to steel or concrete separately. In this thesis, it was indicated that the shear provision of the CSA and the MC2010, while being correct for members with shear reinforcement, estimates the shear capacity of members sparsely reinforced with stirrups too conservatively. Moreover, from the performances of numerical models, it was concluded that the value of the first cracking shear force is significantly improved when f_{ct} is taken as $0.33\sqrt{f_c}$. At the same time, from the analytical solution of the EC2, it is clear that first cracking shear force as derived from the Mohr's circle with mean values of material properties according to the EC2 applied is typically overestimated. The question that might arise is: what would be the effect of exercising the reduced concrete strength $f_{ct} = 0.33\sqrt{f_c}$ in the expression for the first cracking shear force, 6.4 EC2?

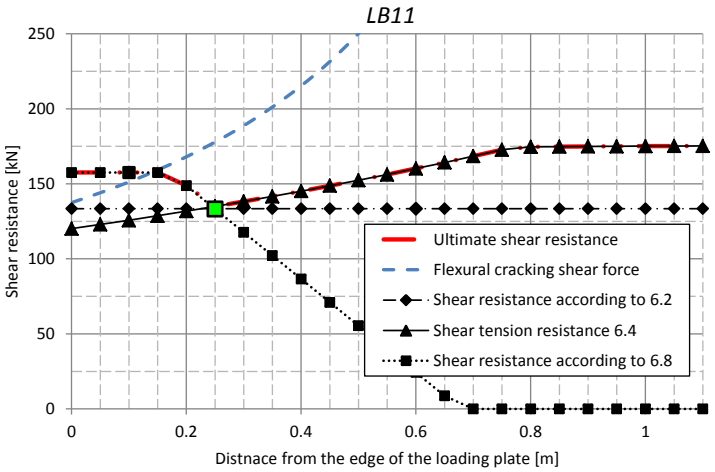

Figure 6-1: Shear resistance of beam LB11 without stirrups according to EC2 with the reduced value of concrete tensile strength

The answer to this question (the results of such an analysis) can be seen in Figure 6-1. Several aspects, some in relation to the numerical solution, should be considered. First, for the reduced values of concrete tensile strength, across the whole member's length, shear tension cracking is the governing failure mechanism. It is apparent as the values marked with a blue line in Figure 6-1 are always above the line assigned to Shear tension resistance 6.4. Secondly, according to the proposed procedure for the EC2, the ultimate shear resistance corresponds to the first cracking shear force according to 6.4 EC2 at the location of 250 mm which is roughly $d_v/2$. As far as the cross section of the beam is concerned, the crack is predicted at the depth of the web-flange junction. It is to some extend in agreement with the numerical analyses as the first cracking always initiated approximately d_v from the support at the level of the web-flange junction. From Figure 6-1, the value of shear resistance corresponding to d_v is approximately 150kN which is close to the failing shear force of the laboratory test, yet still slightly overestimated. Furthermore, from the numerical analysis, it could be observed that the first cracking shear force was typically 133kN which is exactly the value obtained in the calculations – 135kN. According to the code's predictions, the cracking shear force

indicates failure while from the numerical models it was noted that some residual strength was contained in an amount depending on the analysis type. Concluding from the last analysis in this document, one can see that the correlation between the cracking shear force from the numerical analyses and the analytical calculations is relatively strong. It was also possible to significantly improve the ratio of experimental and predicted values of shear resistance. To conclude more on this observation, further experiments/calculations have to undertaken. It is left as a recommendation for future researches. The similar recommendation i.e. a use of reduced concrete tensile strength applies to the calculations according to RBK 1.1. which tend to be unconservative for all studies beams.
Regarding members with shear reinforcement, the structural assessment according to the fib Model Code 2010 proved to be the most precise while still safe, therefore recommended. As far as additional potential future improvements are concerned, the method according to the RBK 1.1 provides some room for adjustments as it resulted in overestimated yet very consistent results (c.o.v of only 4.6%). The subject is currently under investigation therefore further advancement can be expected.
In [35] which treats structural assessment of bridge girders in shear, one can read that the highest level of precision can be obtained with a method derived from the Cracked Membrane Model. As a recommendation for further study, it would be interesting to investigate what level of accuracy can be obtained with application of elaborate analytical methods.

In connection with the numerical analysis little recommendations can be proposed. The conducted analyses can be considered as preliminary. Throughout the study is was noticed however that modelling shear behaviour numerically is yet another approximation and is highly dependent on the used input. In order to estimate its influence on the obtained results, much more in-depth sensitivity study should be performed. The aspects broached in the further study could possibly regard: spatial discretization to eliminate dimensional and directional bias, different crack model e.g. multi-directional crack model, different load control procedure (force control) or constitutive parameters. The last aspect is of special interest when the engineering practise is concerned. To visualize this thought, a reference to the current study and the Guidelines for NLFEA of Concrete Structures RTD 1016:2012 is made. The applied material properties in FE models developed in this thesis were taken as specified in the study [13] hence derived from measured concrete compressive strength obtained in concrete compressive tests, see section 5-3-3. It is e.g. for beam LB6 the concrete tensile strength of 2.63MPa. On the other hand, the suggested material properties of concrete in RTD 1016:2012 are different and might be higher in value. The equivalently calculated mean tensile strength acc. to RTD is equal 4.389MPa (equation 5-11). In a numerical assessment of existing bridges, an analyst would preferably follow the recommendation of RTD 1016 as they can be considered as "the best available practise" for nonlinear FEA of concrete structures. Recalling the conclusion stating that the tensile concrete strength acc. to $0.33\sqrt{f_c'}$ predicts cracking and ultimate shear force more accurately than the constitutive parameters according to RTD 1016, one can see that application of different material properties would lead to inaccurate results for this particular case. Moreover, the obtained in this report predictions of shear tension resistance generally exceeded those observed in experiments therefore a further increase would entail greater deviations. The extend is however unknown and should be advocated by an additional study.

Appendix A

Results of Calculations According to CSA A23.3 Shear Provision

The section contains calculations according to CSA A23.3 Shear provision of beam LB11 written in Mathcad. It was author's intention to include the analytical solution exclusively for LB11 as it comprises of steps that have to be undertaken for any other member considered in this report. The difference lies in an additional "if statement" for members which contain less stirrups than specified as the minimum. In such cases it takes only concrete contribution to the total resistance is considered. According to the method, a different crack spacing should be accounted for with an aggregate size adjustment depending on the concrete strength.
Members with shear reinforcement are calculated with the crack spacing of 300mm and contribution of both steel and concrete to the total capacity. For more information please refer to the main part of the report: section 2-4-3 for background or section 4-3 for an explicit solution of the critical sections. In the subsequent part of the appendix, the results for all beams are tabularized.

LB11 (Design according to CSA A23.3 2004)

Material properties from: Liping Xie, *Influence of Axial Load and Prestress on the Shear Strength of Web-Shear Critical Reinforced Concrete Elements*

References to material properties etc as in the source document of Liping Xie

- Concrete properties; reference Table 4.3 Concrete Compressive Strength

$f_c := 62.3MPa$ compressive strength at the test

$f_t := 2.6MPa$

$E_c := 37900MPa$

$\varepsilon_c := 2.27 \cdot 10^{-3}$

- Steel properties: reference Table 4.6 Reinforcement Properties in a Beam

$f_y := 409MPa$

$E_s := 201100MPa$

$f_{yv} := 529MPa$

$E_p := 199700MPa$

- Cross section dimensions (as-built)

$h := 506mm$ $b_w := 74mm$ $b_{ftop} := 352mm$ $h_{ftop} := 57mm$

$h_{fbot} := 49mm$ $h_1 := 25mm$ $h_2 := 25mm$ $d := 473mm$

$A_g := 73740mm^2$ $A_{ct} := 36880mm^2$ $I_g := 2.56 \cdot 10^9 mm^4$ $A_v := 24.2mm^2$

$A_{stop} := 934mm^2$ $A_{sbot} := 934mm^2$ $N_{axial} := -807kN$ *(Table 4.2)*

$A_s := 934mm^2$ $A_p := 507mm^2$ *(Table 4.6)*

$a_g := 10mm$ *(Table 4.13)*

$$a_{g.adjusted} := \begin{cases} 0 & \text{if } f_c \geq 70MPa \\ \left(70 - \frac{f_c}{MPa}\right) \cdot \frac{a_g}{10} & \text{if } 60MPa < f_c < 70MPa \\ a_g & \text{otherwise} \end{cases} = 7.7 \cdot mm$$

Stirrups: D4 spacing 175mm, 4-15M longitudinal bars, 1" High Strength Smooth Bar prestressing

$$s_v := \begin{pmatrix} 87.5mm \\ 0 \end{pmatrix}$$

$x_1 := 425mm - \frac{h}{2} = 0.172\,m$ $x_2 := 425mm + \frac{h}{2} = 0.678\,m$

$d_v := \max(0.72 \cdot h, 0.9d) = 0.426\,m$

$q_{Eg2} := A_g \cdot 25 \frac{kN}{m^3} = 1.843 \cdot \frac{kN}{m}$ $q_{Eg1} := h \cdot b_{ftop} \cdot 25 \frac{kN}{m^3} = 4.453 \cdot \frac{kN}{m}$

$$0.700m \cdot q_{Eg1} \cdot (4.120m) + 3.220m \cdot q_{Eg2} \cdot \left(\frac{3.220m}{2} + 0.550m\right) \ldots = 0$$

$$+ 0.550m \cdot q_{Eg1} \cdot \frac{0.550m}{2} - \frac{(0.150m)^2}{2} \cdot q_{Eg1} - R_A \cdot (3.360m)$$

$$R_A := 0.9 \cdot m \cdot q_{Eg1} + 2.07 \cdot m \cdot q_{Eg2} = 7.824 \cdot kN$$

$$R_B := 2 \cdot 700mm \cdot q_{Eg1} + 3200mm \cdot q_{Eg2} - R_A = 4.31 \cdot kN$$

$V_R(x) :=$

$V_{f.trial} \leftarrow 0$

for $i \in x$

while $V_{f.trial} \le V_f$

$V_{f.trial} \leftarrow V_{f.trial} + 0.001kN$

break if $V_{f.trial} = V_f$

$$A_{vPerUnitOfLength} \leftarrow \begin{cases} \dfrac{A_v}{s_{v_0}} & \text{if } x \le x_1 \\ \dfrac{A_v}{s_{v_0}} - \left(\left(\dfrac{A_v}{s_{v_0}}\right)\right) \cdot \dfrac{x - x_1}{x_2 - x_1} & \text{if } x_1 < x < x_2 \\ 0 & \text{if } x \ge x_2 \end{cases}$$

$$M_{Eg} \leftarrow 0.7m \cdot q_{Eg1} \cdot (0.350m + 0.410m + x) + (0.41 \cdot m + x) \cdot q_{Eg2} \cdot \left(\frac{0.41m + x}{2}\right) - R_A \cdot x$$

$$V_{Eg} \leftarrow -\frac{d}{dx}\left[0.7m \cdot q_{Eg1} \cdot (0.350m + 0.410m + x) + (0.41 \cdot m + x) \cdot q_{Eg2} \cdot \left(\frac{0.41m + x}{2}\right) - R_A \cdot x\right]$$

$$M_f \leftarrow M_{Eg} + V_{f.trial} \cdot \left(1200mm - x - \frac{150mm}{2}\right)$$

$$F_{section} \leftarrow \frac{M_f}{d_v} + V_{f.trial} + V_{Eg} + 0.5N_{axial}$$

$$\varepsilon_x \leftarrow \begin{cases} \dfrac{\dfrac{M_f}{d_v} + V_{f.trial} + 0.5 \cdot N_{axial} + V_{Eg}}{2 \cdot \left(E_s \cdot A_s\right)} & \text{if } F_{section} \ge 0 \\ \max\left[\dfrac{\dfrac{M_f}{d_v} + V_{f.trial} + 0.5 \cdot N_{axial} + V_{Eg}}{2 \cdot \left(E_s \cdot A_s + E_c \cdot A_{ct}\right)}, -0.20 \cdot 10^{-3}\right] & \text{otherwise} \end{cases}$$

$$A_{vmin} \leftarrow 0.06 \cdot \sqrt{\frac{f_c}{MPa}} \cdot MPa \frac{b_w}{f_{yv}}$$

$$s_{ze} \leftarrow \begin{cases} (300mm) & \text{if } A_{vPerUnitOfLength} \ge A_{vmin} \\ \left(\dfrac{35 \cdot \dfrac{d_v}{mm}}{\dfrac{a_{g.adjusted}}{mm} + 15}\right) mm & \text{otherwise} \end{cases}$$

$$\beta \leftarrow \frac{0.4}{\left(1 + 1500\varepsilon_x\right)} \cdot \frac{1300}{\left(1000 + \dfrac{s_{ze}}{mm}\right)}$$

$$\theta \leftarrow \left(29 + 7000 \cdot \varepsilon_x\right) \cdot \frac{2\pi}{360}$$

$$V_c \leftarrow \beta \cdot \sqrt{\frac{f_c}{MPa}} \cdot MPa \cdot b_w \cdot d_v$$

$$
\left|
\begin{array}{l}
V_s \leftarrow \left| \begin{array}{l} \left(f_{yv} \cdot A_{vPerUnitOfLength} \cdot d_v \cdot \cot(\theta)\right) \text{ if } A_{vPerUnitOfLength} \geq A_{vmin} \\ 0 \text{ otherwise} \end{array} \right. \\
V_f \leftarrow V_c + V_s \\
\left(A_{vPerUnitOfLength} \cdot N \cdot \frac{m}{mm^2} \quad \frac{M_{Eg}}{m} \quad V_{Eg} \quad \frac{M_f}{m} \quad F_{section} \quad \varepsilon_x \cdot N \quad s_{ze} \cdot \frac{N}{mm} \quad \beta \cdot N \quad \theta \cdot \frac{N}{deg} \quad V_c \quad V_s \quad V_f \right)^T
\end{array}
\right.
$$

The above function can only return a multiple rows/columns vector for values with the same unit. Therefore all the variable had to be reduced to a consistent unit (here Newtons). The units were later restored.

An auxiliary function which calls the main function with every element of the argument vector and collects the results in an n x <cols(R)> matrix.

$$
\text{calculateV}(xvec) := \left|
\begin{array}{l}
\text{for } x \in xvec \\
\quad R^{\langle \text{cols}(R) \rangle} \leftarrow V_R(x) \\
R^T
\end{array}
\right.
$$

$x := 425mm, 450mm .. 725mm$

The function produces results as shown in Table A-5.

$\text{Results} := \text{calculateV}(x) =$ N

	8	9	10	11
0	29.119	$9.699 \cdot 10^4$	$5.591 \cdot 10^4$	$1.529 \cdot 10^5$
1	28.98	$9.988 \cdot 10^4$	$5.067 \cdot 10^4$	$1.505 \cdot 10^5$
2	28.935	$1.009 \cdot 10^5$	$4.52 \cdot 10^4$	$1.461 \cdot 10^5$
3	28.891	$1.018 \cdot 10^5$	$3.97 \cdot 10^4$	$1.415 \cdot 10^5$
4	28.848	$1.028 \cdot 10^5$	$3.419 \cdot 10^4$	$1.37 \cdot 10^5$
5	28.806	$1.038 \cdot 10^5$	$2.865 \cdot 10^4$	$1.324 \cdot 10^5$
6	28.555	$8.629 \cdot 10^4$	0	$8.629 \cdot 10^4$
7	28.545	$8.65 \cdot 10^4$	0	...

$$
\text{VectorDist}(Range) := \left|
\begin{array}{l}
\text{Count} \leftarrow \text{ORIGIN} \\
\text{for } i \in Range \\
\quad \left| \begin{array}{l} vec_{Count} \leftarrow i \\ \text{Count} \leftarrow \text{Count} + 1 \end{array} \right. \\
vec
\end{array}
\right.
$$

$\text{VecDist} := \text{VectorDist}(x) =$ ·mm

	0
0	425
1	450
2	475
3	500
4	525
5	550
6	575
7	600
8	625
9	650
10	675
11	700
12	725

$$A_{stirrups} := \frac{\text{Results}^{\langle 0 \rangle}}{N} \cdot \frac{mm^2}{m}$$

$V_R := \text{Results}^{\langle 11 \rangle}$

$M_f := \text{Results}^{\langle 3 \rangle} \cdot m$

$V_s := \text{Results}^{\langle 10 \rangle}$

$$\theta := \frac{\text{Results}^{\langle 8 \rangle}}{N} \cdot deg$$

$V_{Rmin} := \min(V_R) = 86.285 \cdot kN$

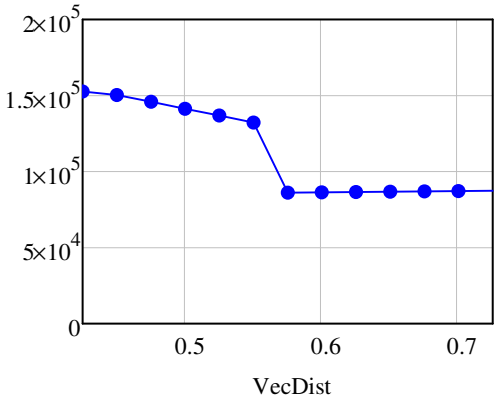

Flexural capacity and crushing of diagonal struts

Calculation of shear resistance is determined assuming that the flexural capacity of the longitudinal reinforcement is sufficient to allow a shear failure. In addition to this, crushing of concrete compressive struts cannot occur. To check if it is true to following equation has to be checked:

$$\text{Check}(z) := \left| \begin{array}{l} i \leftarrow \text{ORIGIN} \\ \text{for } i \in z \\ \quad \left| \begin{array}{l} F_{\text{RightSide}_i} \leftarrow \dfrac{M_{f_i}}{d_v} + 0.5 N_{\text{axial}} + \left(V_{R_i} - 0.5\, V_{s_i}\right)\cot\left(\theta_i\right) \\ f_{cc} \leftarrow \dfrac{V_{R_i}}{b_w \cdot d_v} \\ \phi_c \leftarrow 1 \\ \text{Check}_i \leftarrow \left| \begin{array}{l} \text{"Flexural failure"} \quad \text{if } F_{\text{RightSide}_i} \geq A_s \cdot f_y \\ \text{"Crushing of concrete"} \quad \text{if } f_{cc} \geq 0.25 \cdot \phi_c \cdot f_c \\ \text{"Shear Failure"} \quad \text{otherwise} \end{array} \right. \end{array} \right. \\ \left(F_{\text{RightSide}_i} \;\; A_s \cdot f_y \;\; f_{cc} \cdot \text{mm}^2 \;\; 0.25 \cdot \phi_c \cdot f_c \cdot \text{mm}^2 \;\; \text{Check}_i\right)^T \end{array} \right.$$

$$\text{calculateV1}(\text{xvec}) := \left| \begin{array}{l} \text{for } x \in \text{xvec} \\ \quad R^{\langle \text{cols}(R) \rangle} \leftarrow \text{Check}(x) \\ R^T \end{array} \right.$$

$$z := 0, 1 .. \text{rows}(\text{VecDist}) - 1$$

$\text{check} := \text{calculateV1}(z) =$ N

	0	1	2	3	4
0	$7.461 \cdot 10^4$	$3.82 \cdot 10^5$	4.854	15.575	'Shear Failure"
1	$6.348 \cdot 10^4$	$3.82 \cdot 10^5$	4.779	15.575	'Shear Failure"
2	$4.484 \cdot 10^4$	$3.82 \cdot 10^5$	4.636	15.575	'Shear Failure"
3	$2.664 \cdot 10^4$	$3.82 \cdot 10^5$	4.493	15.575	'Shear Failure"
4	$8.894 \cdot 10^3$	$3.82 \cdot 10^5$	4.349	15.575	'Shear Failure"
5	$-8.403 \cdot 10^3$	$3.82 \cdot 10^5$	4.204	15.575	'Shear Failure"
6	$-1.322 \cdot 10^5$	$3.82 \cdot 10^5$	2.739	15.575	'Shear Failure"
7	$-1.367 \cdot 10^5$	$3.82 \cdot 10^5$	2.746	15.575	'Shear Failure"
8	$-1.412 \cdot 10^5$	$3.82 \cdot 10^5$	2.753	15.575	'Shear Failure"
9	$-1.457 \cdot 10^5$	$3.82 \cdot 10^5$	2.76	15.575	'Shear Failure"
10	$-1.503 \cdot 10^5$	$3.82 \cdot 10^5$	2.767	15.575	...

"More accurate method "

$V_{Racc}(x) :=$ $V_{f.trial} \leftarrow 0$

for $i \in x$

while $V_{f.trial} \le V_f$

$V_{f.trial} \leftarrow V_{f.trial} + 0.001kN$

break if $V_{f.trial} = V_f$

$$A_{vPerUnitOfLength} \leftarrow \begin{cases} \frac{A_v}{s_{v_0}} & \text{if } x \le x_1 \\ \frac{A_v}{s_{v_0}} - \left(\left(\frac{A_v}{s_{v_0}}\right)\right) \cdot \frac{x - x_1}{x_2 - x_1} & \text{if } x_1 < x < x_2 \\ 0 & \text{if } x \ge x_2 \end{cases}$$

$$M_{Eg} \leftarrow 0.7m \cdot q_{Eg1} \cdot (0.350m + 0.410m + x) + (0.41 \cdot m + x) \cdot q_{Eg2} \cdot \left(\frac{0.41m + x}{2}\right) - R_A \cdot x$$

$$V_{Eg} \leftarrow -\frac{d}{dx}\left[0.7m \cdot q_{Eg1} \cdot (0.350m + 0.410m + x) + (0.41 \cdot m + x) \cdot q_{Eg2} \cdot \left(\frac{0.41m + x}{2}\right) - R_A \cdot x\right]$$

$$M_f \leftarrow M_{Eg} + V_{f.trial} \cdot \left(1200mm - x - \frac{150mm}{2}\right)$$

$$F_{sec.top} \leftarrow \frac{M_f}{d_v} + V_{f.trial} + V_{Eg} + 0.5N_{axial}$$

$$F_{sec.bot} \leftarrow \frac{-M_f}{d_v} + V_{f.trial} + V_{Eg} + 0.5N_{axial}$$

$$\varepsilon_{xtop} \leftarrow \begin{cases} \frac{\frac{M_f}{d_v} + V_{f.trial} + V_{Eg} + 0.5 \cdot N_{axial}}{2 \cdot (E_s \cdot A_s)} & \text{if } F_{sec.top} \ge 0 \\ \max\left[\frac{\frac{M_f}{d_v} + V_{f.trial} + V_{Eg} + 0.5 \cdot N_{axial}}{2 \cdot (E_s \cdot A_s + E_c \cdot A_{ct})}, -0.20 \cdot 10^{-3}\right] & \text{otherwise} \end{cases}$$

$$\varepsilon_{xbot} \leftarrow \begin{cases} \frac{\frac{-M_f}{d_v} + V_{f.trial} + V_{Eg} + 0.5 \cdot N_{axial}}{2 \cdot (E_s \cdot A_s)} & \text{if } F_{sec.bot} \ge 0 \\ \max\left[\frac{\frac{-M_f}{d_v} + V_{f.trial} + V_{Eg} + 0.5 \cdot N_{axial}}{2 \cdot (E_s \cdot A_s + E_c \cdot A_{ct})}, -0.20 \cdot 10^{-3}\right] & \text{otherwise} \end{cases}$$

$$\varepsilon_x \leftarrow \frac{\varepsilon_{xtop} + \varepsilon_{xbot}}{2}$$

$$A_{vmin} \leftarrow 0.06 \cdot \sqrt{\frac{f_c}{MPa}} \cdot MPa \frac{b_w}{f_{yv}}$$

$$s_{ze} \leftarrow \begin{cases} (300mm) & \text{if } A_{vPerUnitOfLength} \ge A_{vmin} \\ \left(35 \cdot \frac{d_v}{mm}\right)_{mm} & \text{otherwise} \end{cases}$$

$$\left\| \left(\frac{a_{g.adjusted}}{mm} + 15 \right) \right| mm \quad \text{otherwise}$$

$$\beta \leftarrow \frac{0.4}{\left(1 + 1500\varepsilon_x\right)} \cdot \frac{1300}{\left(1000 + \frac{s_{ze}}{mm}\right)}$$

$$\theta \leftarrow \left(29 + 7000 \cdot \varepsilon_x\right) \cdot \frac{2\pi}{360}$$

$$V_c \leftarrow \beta \cdot \sqrt{\frac{f_c}{MPa}} \cdot MPa \cdot b_w \cdot d_v$$

$$V_s \leftarrow \begin{cases} \left(f_{yv} \cdot A_{vPerUnitOfLength} \cdot d_v \cdot \cot(\theta)\right) & \text{if } A_{vPerUnitOfLength} \geq A_{vmin} \\ 0 & \text{otherwise} \end{cases}$$

$$V_f \leftarrow V_c + V_s$$

$$\left(s_{ze} \cdot \frac{N}{mm} \quad \frac{M_f}{m} \quad F_{sec.top} \quad F_{sec.bot} \quad \varepsilon_{xtop} \cdot N \quad \varepsilon_{xbot} \cdot N \quad \varepsilon_x \cdot N \quad \beta \cdot N \quad \theta \cdot \frac{N}{deg} \quad V_c \quad V_s \quad V_f \right)^T$$

$$\text{calculateV}_{acc}(xvec) := \begin{array}{l} \text{for } x \in xvec \\ \quad R^{\langle cols(R) \rangle} \leftarrow V_{Racc}(x) \\ R^T \end{array}$$

The function produces results as shown in Table A-6

$$\text{Results2} := \text{calculateV}_{acc}(x) = \quad \text{N}$$

	6	7	8	9	10	11
0	$3.832 \cdot 10^{-5}$	0.424	28.732	$1.055 \cdot 10^{5}$	$5.681 \cdot 10^{4}$	$1.623 \cdot 10^{5}$
1	$-5.69 \cdot 10^{-5}$	0.437	28.602	$1.087 \cdot 10^{5}$	$5.147 \cdot 10^{4}$	$1.602 \cdot 10^{5}$
2	$7.502 \cdot 10^{-5}$	0.451	28.475	$1.121 \cdot 10^{5}$	$4.607 \cdot 10^{4}$	$1.581 \cdot 10^{5}$
3	$7.802 \cdot 10^{-5}$	0.453	28.454	$1.126 \cdot 10^{5}$	$4.043 \cdot 10^{4}$	$1.531 \cdot 10^{5}$
4	$7.971 \cdot 10^{-5}$	0.454	28.442	$1.13 \cdot 10^{5}$	$3.477 \cdot 10^{4}$	$1.477 \cdot 10^{5}$
5	$8.141 \cdot 10^{-5}$	0.456	28.43	$1.133 \cdot 10^{5}$	$2.91 \cdot 10^{4}$	$1.424 \cdot 10^{5}$
6	$-9.75 \cdot 10^{-5}$	0.368	28.318	$9.143 \cdot 10^{4}$	0	$9.143 \cdot 10^{4}$
7	$9.751 \cdot 10^{-5}$	0.368	28.317	$9.143 \cdot 10^{4}$	0	$9.143 \cdot 10^{4}$
8	$9.752 \cdot 10^{-5}$	0.368	28.317	$9.144 \cdot 10^{4}$	0	$9.144 \cdot 10^{4}$
9	$9.754 \cdot 10^{-5}$	0.368	28.317	$9.144 \cdot 10^{4}$	0	...

Table A-1: Results from calculations of LB6 acc. to CSA A23.3

Location [m]	Area of stirrups per unit of length $[mm^2/m]$	Moment from self-weight [Nm]	Shear force from self-weight [N]	Moment due to applied load [Nm]	Force in longitudinal reinforcement at crack, including effect of shear [N]	Longitudinal strain	Crack spacing [mm]	Factor β to account for aggregate interlock in concrete member	Diagonal crack inclination θ [deg]	Concrete contribution to shear resistance [N]	Steel contribution to shear resistance [N]	Total shear resistance [N]
0.425	207.43	1006.70	3146.50	116870.00	44686.00	1.19E-04	300.00	0.34	29.83	84056.00	81456.00	165510.00
0.45	200.60	928.62	3100.70	112940.00	35861.00	9.55E-05	300.00	0.35	29.67	86647.00	79299.00	165950.00
0.475	193.76	851.68	3054.90	109050.00	27183.00	7.24E-05	300.00	0.36	29.51	89355.00	77104.00	166460.00
0.5	186.93	775.88	3009.20	105190.00	18657.00	4.97E-05	300.00	0.37	29.35	92187.00	74868.00	167060.00
0.525	180.10	701.22	2963.40	101350.00	10280.00	2.74E-05	300.00	0.38	29.19	95149.00	72594.00	167740.00
0.55	173.27	627.71	2917.60	97532.00	2056.10	5.47E-06	300.00	0.40	29.04	98248.00	70281.00	168530.00
0.575	166.43	555.34	2871.90	92540.00	-11002.00	-3.39E-06	300.00	0.40	28.98	99561.00	67682.00	167240.00
0.6	159.60	484.11	2826.10	87228.00	-25541.00	-7.88E-06	300.00	0.40	28.94	100240.00	64988.00	165230.00
0.625	152.77	414.03	2780.30	82015.00	-39861.00	-1.23E-05	300.00	0.41	28.91	100920.00	62285.00	163200.00
0.65	145.94	345.10	2734.60	76899.00	-53958.00	-1.66E-05	300.00	0.41	28.88	101590.00	59575.00	161170.00
0.675	139.11	277.30	2688.80	71882.00	-67835.00	-2.09E-05	300.00	0.41	28.85	102260.00	56856.00	159120.00
0.7	138.29	210.66	2643.00	67906.00	-77056.00	-2.38E-05	300.00	0.41	28.83	102720.00	56567.00	159280.00
0.725	138.29	145.15	2597.30	64048.00	-85694.00	-2.64E-05	300.00	0.42	28.82	103140.00	56611.00	159750.00

Table A-2: Results from calculations of LB6 acc. to CSA A23.3 "More accurate method"

Location [m]	Moment due to applied load [Nm]	Force in the top flange[N]	Force in the bottom flange[N]	Strain in the top flange	Strain in the bottom flange	Mid-depth strain	Factor β to account for aggregate interlock in concrete member	Diagonal crack inclination θ [deg]	Concrete contribution to shear resistance [N]	Steel contribution to shear resistance [N]	Total shear resistance [N]
0.425	126170.00	79816.00	-512930.00	2.12E-04	-1.58E-04	2.71E-05	0.3844	29.19	95182.00	83616.00	178800.00
0.45	121320.00	67933.00	-502030.00	1.81E-04	-1.55E-04	1.30E-05	0.3924	29.09	97161.00	81191.00	178350.00
0.475	116510.00	56192.00	-491200.00	1.50E-04	-1.52E-04	-9.69E-07	0.4006	28.99	99199.00	78741.00	177940.00
0.5	111750.00	44590.00	-480440.00	1.19E-04	-1.48E-04	-1.48E-05	0.4091	28.90	101300.00	76267.00	177560.00
0.525	107040.00	33127.00	-469750.00	8.82E-05	-1.45E-04	-2.84E-05	0.4178	28.80	103460.00	73769.00	177220.00
0.55	102360.00	21800.00	-459110.00	5.80E-05	-1.42E-04	-4.18E-05	0.4268	28.71	105680.00	71248.00	176930.00
0.575	97726.00	10611.00	-448520.00	2.82E-05	-1.38E-04	-5.51E-05	0.4360	28.61	107970.00	68702.00	176670.00
0.6	93076.00	-667.29	-437950.00	-2.06E-07	-1.35E-04	-6.77E-05	0.4452	28.53	110240.00	66124.00	176360.00
0.625	87266.00	-17021.00	-427010.00	-5.25E-06	-1.32E-04	-6.85E-05	0.4458	28.52	110390.00	63308.00	173700.00
0.65	81590.00	-33063.00	-416380.00	-1.02E-05	-1.28E-04	-6.93E-05	0.4464	28.51	110550.00	60492.00	171040.00
0.675	76048.00	-48790.00	-406070.00	-1.51E-05	-1.25E-04	-7.02E-05	0.4470	28.51	110700.00	57674.00	168380.00
0.7	71637.00	-59516.00	-396080.00	-1.84E-05	-1.22E-04	-7.03E-05	0.4471	28.51	110730.00	57336.00	168060.00
0.725	67371.00	-69580.00	-386100.00	-2.15E-05	-1.19E-04	-7.03E-05	0.4471	28.51	110730.00	57336.00	168060.00

Table A-3: Results from calculations of LB10 acc. to CSA A23.3

Location [m]	Area of stirrups per unit of length $[mm^2/m]$	Moment from self-weight [Nm]	Shear force from self-weight [N]	Moment due to applied load [Nm]	Force in longitudinal reinforcement at crack, including effect of shear [N]	Longitudinal strain	Crack spacing [mm]	Factor β to account for aggregate interlock in concrete member	Diagonal crack inclination θ [deg]	Concrete contribution to shear resistance [N]	Steel contribution to shear resistance [N]	Total shear resistance [N]
0.425	276.57	1000.90	3160.10	128580.00	76449.00	0.00020351	300.00	0.31	30.42	76198.00	106050.00	182250.00
0.45	276.57	922.44	3114.00	125230.00	70439.00	0.00018751	300.00	0.31	30.31	77625.00	106530.00	184160.00
0.475	276.57	845.17	3068.00	121830.00	64387.00	0.00017140	300.00	0.32	30.20	79117.00	107010.00	186130.00
0.5	276.57	769.05	3021.90	118380.00	58294.00	0.00015518	300.00	0.32	30.09	80679.00	107500.00	188180.00
0.525	276.57	694.07	2975.90	114880.00	52157.00	0.00013884	300.00	0.33	29.97	82315.00	108000.00	190310.00
0.55	276.57	620.25	2929.80	111330.00	45977.00	0.00012239	300.00	0.34	29.86	84031.00	108500.00	192530.00
0.575	276.57	547.58	2883.80	107710.00	39755.00	0.00010583	300.00	0.35	29.74	85833.00	109010.00	194850.00
0.6	276.57	476.06	2837.80	104040.00	33487.00	0.00008914	300.00	0.35	29.62	87727.00	109530.00	197260.00
0.625	276.57	405.69	2791.70	100300.00	27174.00	0.00007234	300.00	0.36	29.51	89723.00	110060.00	199780.00
0.65	276.57	336.48	2745.70	96485.00	20812.00	0.00005540	300.00	0.37	29.39	91827.00	110590.00	202420.00
0.675	276.57	268.41	2699.60	92599.00	14402.00	0.00003834	300.00	0.38	29.27	94049.00	111130.00	205180.00
0.7	276.57	201.49	2653.60	88635.00	7944.70	0.00002115	300.00	0.39	29.15	96400.00	111680.00	208080.00
0.725	276.57	135.73	2607.50	84587.00	1436.30	0.00000382	300.00	0.40	29.03	98891.00	112240.00	211130.00

Table A-4: Results from calculations of LB10 acc. to CSA A23.3 "More accurate method"

Location [m]	Moment due to applied load [Nm]	Force in the top flange[N]	Force in the bottom flange[N]	Strain in the top flange	Strain in the bottom flange	Mid-depth strain	Factor β to account for aggregate interlock in concrete member	Diagonal crack inclination θ [deg]	Concrete contribution to shear resistance [N]	Steel contribution to shear resistance [N]	Total shear resistance [N]
0.425	140450.00	121310.00	-538560.00	3.23E-04	-1.71E-04	7.61E-05	0.3590	29.53	89271.00	109940.00	199210.00
0.45	136350.00	113040.00	-527560.00	3.01E-04	-1.67E-04	6.68E-05	0.3636	29.47	90397.00	110230.00	200630.00
0.475	132210.00	104710.00	-516410.00	2.79E-04	-1.64E-04	5.75E-05	0.3682	29.40	91560.00	110520.00	202080.00
0.5	128010.00	96319.00	-505110.00	2.56E-04	-1.60E-04	4.81E-05	0.3731	29.34	92762.00	110820.00	203580.00
0.525	123770.00	87859.00	-493650.00	2.34E-04	-1.57E-04	3.87E-05	0.3781	29.27	94004.00	111120.00	205120.00
0.55	119490.00	79326.00	-482030.00	2.11E-04	-1.53E-04	2.92E-05	0.3832	29.20	95290.00	111420.00	206710.00
0.575	115150.00	70723.00	-470250.00	1.88E-04	-1.49E-04	1.96E-05	0.3886	29.14	96620.00	111730.00	208350.00
0.6	110750.00	62045.00	-458280.00	1.65E-04	-1.45E-04	9.93E-06	0.3941	29.07	97999.00	112040.00	210040.00
0.625	106300.00	53289.00	-446130.00	1.42E-04	-1.41E-04	1.97E-07	0.3999	29.00	99429.00	112350.00	211780.00
0.65	101790.00	44456.00	-433790.00	1.18E-04	-1.38E-04	-9.60E-06	0.4058	28.93	100910.00	112670.00	213580.00
0.675	97225.00	35537.00	-421240.00	9.46E-05	-1.34E-04	-1.95E-05	0.4120	28.86	102450.00	112990.00	215450.00
0.7	92591.00	26534.00	-408470.00	7.06E-05	-1.30E-04	-2.94E-05	0.4185	28.79	104050.00	113320.00	217370.00
0.725	87889.00	17439.00	-395480.00	4.64E-05	-1.25E-04	-3.95E-05	0.4252	28.72	105720.00	113650.00	219370.00

Table A-5: Results from calculations of LB11 acc. to CSA A23.3

Location [m]	Area of stirrups per unit of length $[mm^2/m]$	Moment from self-weight [Nm]	Shear force from self-weight [N]	Moment due to applied load [Nm]	Force in longitudinal reinforcement at crack, including effect of shear [N]	Longitudinal strain	Crack spacing [mm]	Factor β to account for aggregate interlock in concrete member	Diagonal crack inclination θ [deg]	Concrete contribution to shear resistance [N]	Steel contribution to shear resistance [N]	Total shear resistance [N]
0.425	138.29	1011.00	3167.00	108000.00	6367.00	0.000016950	300.00	0.39	29.12	96990.00	55910.00	152900.00
0.45	124.62	932.64	3121.00	102600.00	-8922.00	-0.000002814	300.00	0.40	28.98	99880.00	50670.00	150500.00
0.475	110.96	855.19	3075.00	95790.00	-29350.00	-0.000009255	300.00	0.41	28.94	100900.00	45200.00	146100.00
0.5	97.29	778.89	3029.00	89240.00	-49300.00	-0.000015550	300.00	0.41	28.89	101800.00	39700.00	141500.00
0.525	83.63	703.74	2983.00	82900.00	-68790.00	-0.000021690	300.00	0.41	28.85	102800.00	34190.00	137000.00
0.55	69.96	629.74	2937.00	76770.00	-87800.00	-0.000027690	300.00	0.42	28.81	103800.00	28650.00	132400.00
0.575	56.30	556.90	2891.00	48010.00	-201500.00	-6.36E-05	656.37	0.35	28.56	86290.00	0.00	86290.00
0.6	42.63	485.20	2845.00	45900.00	-206300.00	-0.000065070	656.37	0.35	28.55	86500.00	0.00	86500.00
0.625	28.97	414.66	2799.00	43780.00	-211100.00	-0.000066580	656.37	0.35	28.53	86720.00	0.00	86720.00
0.65	15.30	345.28	2752.00	41640.00	-216000.00	-0.000068110	656.37	0.35	28.52	86940.00	0.00	86940.00
0.675	1.64	277.04	2706.00	39500.00	-220800.00	-0.000069640	656.37	0.35	28.51	87160.00	0.00	87160.00
0.7	0.00	209.95	2660.00	37350.00	-225700.00	-0.000071180	656.37	0.35	28.50	87390.00	0.00	87390.00
0.725	0.00	144.02	2614.00	35190.00	-230600.00	-0.000072720	656.37	0.35	28.49	87620.00	0.00	87620.00

Table A-6: Results from calculations of LB11 acc. to CSA A23.3 "More accurate method"

Location [m]	Moment due to applied load [Nm]	Force in the top flange[N]	Force in the bottom flange[N]	Strain in the top flange	Strain in the bottom flange	Mid-depth strain	Factor β to account for aggregate interlock in concrete member	Diagonal crack inclination θ [deg]	Concrete contribution to shear resistance [N]	Steel contribution to shear resistance [N]	Total shear resistance [N]
0.425	114600.00	31300.00	-507300.00	8.33E-05	-1.60E-04	-3.83E-05	0.42400	28.73	105500.00	56810.00	162300.00
0.45	109100.00	16050.00	-496400.00	4.27E-05	-1.57E-04	-5.69E-05	0.43700	28.60	108700.00	51470.00	160200.00
0.475	103600.00	1182.00	-485800.00	3.15E-06	-1.53E-04	-7.50E-05	0.45100	28.48	112100.00	46070.00	158100.00
0.5	96450.00	-20840.00	-474000.00	-6.57E-06	-1.50E-04	-7.80E-05	0.45300	28.45	112600.00	40430.00	153100.00
0.525	89340.00	-42900.00	-462700.00	-1.35E-05	-1.46E-04	-7.97E-05	0.45400	28.44	113000.00	34770.00	147700.00
0.55	82510.00	-64350.00	-452000.00	-2.03E-05	-1.43E-04	-8.14E-05	0.45600	28.43	113300.00	29100.00	142400.00
0.575	50840.00	-189700.00	-428600.00	-5.98E-05	-1.35E-04	-9.75E-05	0.36800	28.32	91430.00	0.00	91430.00
0.6	48490.00	-195300.00	-423100.00	-6.16E-05	-1.33E-04	-9.75E-05	0.36800	28.32	91430.00	0.00	91430.00
0.625	46130.00	-200900.00	-417600.00	-6.34E-05	-1.32E-04	-9.75E-05	0.36800	28.32	91440.00	0.00	91440.00
0.65	43780.00	-206500.00	-412100.00	-6.51E-05	-1.30E-04	-9.75E-05	0.36800	28.32	91440.00	0.00	91440.00
0.675	41430.00	-212000.00	-406700.00	-6.69E-05	-1.28E-04	-9.76E-05	0.36800	28.32	91440.00	0.00	91440.00
0.7	39070.00	-217600.00	-401200.00	-6.86E-05	-1.27E-04	-9.76E-05	0.36800	28.32	91440.00	0.00	91440.00
0.725	36720.00	-223200.00	-395700.00	-7.04E-05	-1.25E-04	-9.76E-05	0.36800	28.32	91440.00	0.00	91440.00

Appendix B

Results of Calculations According to fib Model Code 2010

The Appendix B contains the algorithm used to calculate beam LB11. The decision to present beam LB11 only was advocated by the fact that calculations in the form of a loop contain expressions for beams with and without stirrups controlled by "if statements". Recall that beam LB11 contained stirrups spaced 87.5 mm near the west support and east loading plate to control the region influence by high bending moment against flexural shear cracks. Due to that a part of the test region is calculated as members reinforced against shear. Where the effect of stirrups is diminished, the member is calculated as a beam without shear reinforcement. For more information please refer to the main part of the report: section 2-4-2 for background or section 4-4 for an explicit solution of the critical sections. In the subsequent part of the appendix, the results for all beams are tabularized.

LB11 (Design according to fib Model Code 2010)

Material properties from: Liping Xie, *The Influence of Axial Load and Prestress on the Shear Strength of Web-Shear Critical Reinforced Concrete Elements* :

- Concrete properties: reference *Table 4.3 Concrete Compressive Strength*

$f_{cm} := 62.3MPa$

$E_c := 37900MPa$

- Steel properties: reference Table 4.6 Reinforcement Properties in a Beam

$f_y := 409MPa$

$E_s := 201100MPa$

$f_{yw} := 529MPa$

- Cross section dimensions (as-built)

$h := 506mm$ $b_w := 74mm$ $b_{fbot} := 350mm$ $h_{fbot} := 49mm$

$b_{ftop} := 352mm$ $h_{ftop} := 57mm$ $h_1 := 25mm$ $h_2 := 25mm$

$d := 473mm$ $A_g := 73740mm^2$ $I_g := 2.56 \cdot 10^9 mm^4$ $y_{0top} := 247mm$

$y_{0bot} := 259mm$ $A_{stop} := 934mm^2$ $A_{sbot} := 934mm^2$ $A_{sw} := 24.2mm^2$

$N_{Ed} := -809kN$ *(Table 4.2)*

$d_g := 10mm$ *(Table 4.13)*

$A_s := 934mm^2$ (*Table 4.6*)

Stirrups: D4 spacing 175mm, 4-15M longitudinal bars, 1" High Strength Smooth Bar prestressing

$$s_v := \begin{pmatrix} 87.5mm \\ 0 \end{pmatrix}$$

Solution

$x_1 := 425mm - \frac{h}{2} = 0.172\,m$ $x_2 := 425mm + \frac{h}{2} = 0.678\,m$

The minimum reinforcement ratio is calculated with: $\rho_w := 0.08 \cdot \frac{\sqrt{\frac{f_{cm}}{MPa}} \cdot MPa}{f_{yw}} = 0.119 \cdot \%$

Bending moment from the self-weight

$q_{Eg2} := A_g \cdot 25\frac{kN}{m^3} = 1.843 \cdot \frac{kN}{m}$ $q_{Eg1} := h \cdot b_{ftop} \cdot 25\frac{kN}{m^3} = 4.453 \cdot \frac{kN}{m}$

$0.700m \cdot q_{Eg1} \cdot (4.120m) + 3.220m \cdot q_{Eg2} \cdot \left(\frac{3.220m}{2} + 0.550m\right) \ldots = 0$

$+ 0.550m \cdot q_{Eg1} \cdot \frac{0.550m}{2} - \frac{(0.150m)^2}{2} \cdot q_{Eg1} - R_A \cdot (3.360m)$

$R_A := 0.9 \cdot m \cdot q_{Eg1} + 2.07 \cdot m \cdot q_{Eg2} = 7.824 \cdot kN$

$R_B := 2 \cdot 700mm \cdot q_{Eg1} + 3200mm \cdot q_{Eg2} - R_A = 4.31 \cdot kN$

$$M_{Eg}(x) := 0.7m \cdot q_{Eg1} \cdot (0.350m + 0.410m + x) + (0.41 \cdot m + x) \cdot q_{Eg2} \cdot \left(\frac{0.41m + x}{2} \right) - R_A \cdot x$$

Maximum spacing of stirrups

$$s_w := \min(0.75d, 500mm) = 0.355\,m$$

Internal lever arm calculation from the horizontal forces equilibrium

$$\eta := 1.0 - \frac{\frac{f_{cm}}{MPa} - 50}{200} = 0.938$$

$$\lambda := 0.8 - \frac{\frac{f_{cm}}{MPa} - 50}{400} = 0.769$$

$$\varepsilon_{cu3} := \frac{2.6 + 35 \cdot \left(\frac{90 - \frac{f_{cm}}{MPa}}{100} \right)^4}{1000} = 2.806 \times 10^{-3}$$

$$\varepsilon_{c3} := \frac{1.75 + 0.55 \cdot \left(\frac{\frac{f_{cm}}{MPa} - 50}{40} \right)}{1000} = 1.919 \times 10^{-3}$$

Assumption: bottom steel is not yielding (in compression), top steel is yielding (in tension)

$$\left| N_{Ed} \right| - A_{sbot} \cdot E_s \cdot \frac{C_{NA} - 33mm}{C_{NA}} \cdot \varepsilon_{cu3} + A_{stop} \cdot f_y - \eta \cdot f_{cm} \cdot b_{fbot} \cdot \lambda \cdot C_{NA} = 0$$

$$C_{NA} := 0.061m = 61 \cdot mm \qquad F_{cc} := C_{NA} \cdot \lambda \cdot \eta \cdot b_{fbot} \cdot f_{cm} = 960.258 \cdot kN$$

$$\varepsilon_{sbot} := \frac{C_{NA} - 33mm}{C_{NA}} \cdot \varepsilon_{cu3} = 1.288 \times 10^{-3}$$

$$\varepsilon_s := \frac{f_y}{E_s} = 2.034 \times 10^{-3} \quad \text{yielding strain}$$

$$\varepsilon_{stop} := \frac{d - C_{NA}}{C_{NA}} \cdot \varepsilon_{cu3} = 0.019$$

$$check(\varepsilon) := \begin{cases} \text{"steel is yielding"} & \text{if } \varepsilon \geq \varepsilon_s \\ \text{"steel is not yielding"} & \text{if } \varepsilon < \varepsilon_s \end{cases}$$

$check(\varepsilon_{sbot}) = \text{"steel is not yielding"}$ OK

$check(\varepsilon_{stop}) = \text{"steel is yielding"}$ OK

Because C_{NA}>flange height, the neutral line is located in the web thus:

Assumption: $x_u := 69mm$

$$x_I := \frac{x_u \cdot (\varepsilon_{cu3} - \varepsilon_{c3})}{\varepsilon_{cu3}} = 0.022\,m$$

$F_1 := x_I \cdot b_{fbot} \cdot f_{cm} = 475.553 \cdot kN$

$$f_{ccWebLocation} := \frac{f_{cm} \cdot \left(x_u - h_{fbot}\right)}{x_u - x_I} = 26.404 \cdot MPa$$

$$F_2 := \left(h_{fbot} - x_I\right) \cdot b_{fbot} \cdot \frac{f_{cm} + f_{ccWebLocation}}{2} = 422.084 \cdot kN$$

$h_{inc} := x_u - h_{fbot} = 20 \cdot mm$

$$A_{c\_Inclined} := \frac{b_{fbot} + \left[\left[\frac{\left(b_{fbot} - b_w\right)}{2} \cdot \left(h_2 - h_{inc}\right)}{h_2}\right] \cdot 2 + b_w\right]}{2} \cdot h_{inc} = 4.792 \times 10^3 \cdot mm^2$$

$F_3 := A_{c\_Inclined} \cdot f_{ccWebLocation} \cdot 0.5 = 63.263 \cdot kN$

$\sum F = 960.9 \cdot kN$ $\quad$ $Check := \frac{F_{cc}}{\sum F} = 0.999$ $\quad$ thus the equilibrium is met

$\lambda \cdot x_u = 53.078 \cdot mm$ $\quad$ $\eta \cdot f_{cm} = 58.469 \cdot MPa$

$$z := d - \frac{\lambda \cdot x_u}{2} = 0.446\,m$$

$y_{Cg} := 259.03mm$

$$\Delta e := y_{Cg} - \left(\frac{z}{2} + \frac{\lambda \cdot x_u}{2}\right) = 9.26 \cdot mm$$

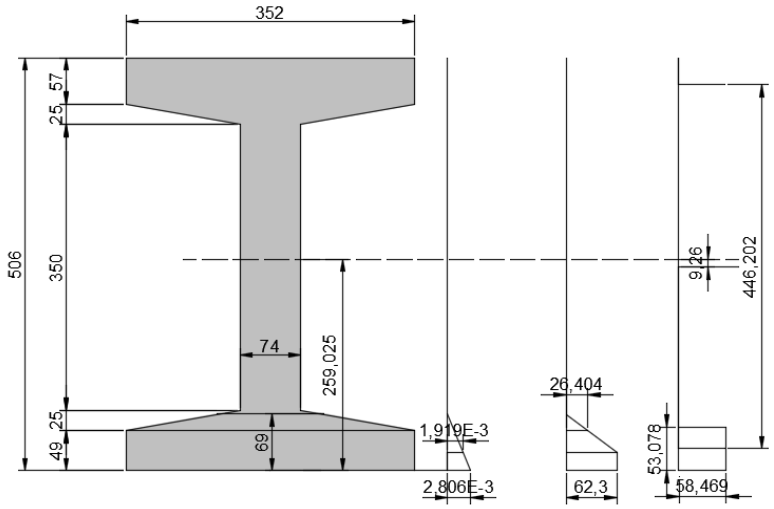

Shear resistance

$V_{Resistance}(x) :=$

$V_{E.trial} \leftarrow 0$

for $i \in x$

while $V_{E.trial} \le V_R$

$V_{E.trial} \leftarrow V_{E.trial} + 0.001kN$

break if $V_{E.trial} = V_R$

$$A_{swPerUnitOfLength} \leftarrow \begin{cases} \frac{A_{sw}}{s_{v_0}} & \text{if } x \le x_1 \\ \frac{A_{sw}}{s_{v_0}} - \left(\frac{A_{sw}}{s_{v_0}}\right)\cdot\frac{x - x_1}{x_2 - x_1} & \text{if } x_1 < x < x_2 \\ 0 & \text{if } x \ge x_2 \end{cases}$$

$$M_{Eg} \leftarrow 0.7m\cdot q_{Eg1}\cdot(0.350m + 0.410m + x) + (0.41\cdot m + x)\cdot q_{Eg2}\cdot\left(\frac{0.41m + x}{2}\right) - R_A\cdot x$$

$$M_E \leftarrow M_{Eg} + V_{E.trial}\cdot\left(1200mm - x - \frac{150mm}{2}\right)$$

$$V_{Eg} \leftarrow -\frac{d}{dx}\left[0.7m\cdot q_{Eg1}\cdot(0.350m + 0.410m + x) + (0.41\cdot m + x)\cdot q_{Eg2}\cdot\left(\frac{0.41m + x}{2}\right) - R_A\cdot x\right]$$

$$F_{section} \leftarrow \frac{M_E}{z} + V_{E.trial} + V_{Eg} + 0.5N_{Ed}$$

$$\varepsilon_x \leftarrow \begin{cases} \frac{1}{2\cdot E_s\cdot A_s}\cdot\left[\frac{M_E}{z} + V_{E.trial} + V_{Eg} + N_{Ed}\cdot\left(\frac{1}{2} + \frac{\Delta e}{z}\right)\right] & \text{if } F_{section} \ge 0 \\ 0 & \text{otherwise} \end{cases}$$

$$k_{dg} \leftarrow \frac{32}{16 + \frac{d_g}{mm}}$$

$$\theta_{min} \leftarrow (20 + 10000\cdot\varepsilon_x)deg$$

$$\varepsilon_1 \leftarrow \varepsilon_x + (\varepsilon_x + 0.002)\cdot(\cot(\theta_{min}))^2$$

$$k_{\varepsilon Prime} \leftarrow \frac{1}{1.2 + 55\cdot\varepsilon_1}$$

$$k_\varepsilon \leftarrow \begin{cases} k_{\varepsilon Prime} & \text{if } k_{\varepsilon Prime} \le 0.65 \\ 0.65 & \text{otherwise} \end{cases}$$

$$k_c \leftarrow k_\varepsilon\cdot\left(\frac{30MPa}{f_{cm}}\right)^{\frac{1}{3}}$$

$$V_{Rmax\theta min} \leftarrow k_c\cdot f_{cm}\cdot b_w\cdot z\cdot\sin(\theta_{min})\cos(\theta_{min})$$

$$s_{max} \leftarrow \frac{A_{sw}}{b_w\cdot\left(0.08\cdot\frac{\sqrt{\frac{f_{cm}}{MPa}}\cdot MPa}{f_{yw}}\right)}$$

$$
\left|\begin{array}{l}
k_v \leftarrow \left\| \begin{array}{l} \dfrac{0.4}{1+1500\varepsilon_x}\cdot\left(1-\dfrac{V_{E.trial}}{V_{Rmax\theta min}}\right) \text{ if } A_{swPerUnitOfLength} \geq \dfrac{A_{sw}}{s_{max}} \\ \left(\dfrac{0.4}{1+1500\cdot\varepsilon_x}\cdot\dfrac{1300}{1000+k_{dg}\cdot\dfrac{z}{mm}}\right) \text{ otherwise} \end{array}\right. \\
V_c \leftarrow k_v\cdot\sqrt{\dfrac{f_{cm}}{MPa}}MPa\cdot b_w\cdot z \\
V_s \leftarrow \left\| \begin{array}{l} A_{swPerUnitOfLength}\cdot z\cdot f_{yw}\cdot\cot(\theta_{min}) \text{ if } A_{swPerUnitOfLength} \geq \dfrac{A_{sw}}{s_{max}} \\ 0 \text{ otherwise} \end{array}\right. \\
V_R \leftarrow V_c + V_s \\
\left(\dfrac{M_E}{m}\ F_{section}\ \varepsilon_x\cdot N\ \theta_{min}\cdot\dfrac{N}{deg}\ \varepsilon_1\cdot N\ k_{\varepsilon Prime}\cdot N\ k_\varepsilon\cdot N\ k_c\cdot N\ V_{Rmax\theta min}\ k_v\cdot N\ V_c\ V_s\ V_R\right)^T
\end{array}\right.
$$

The above function can only return a multiple rows/columns vector for values with the same unit. Therefore all the variable had to be reduced to a consistent unit (here Newtons).

An auxiliary function which calls the main function with every element of the argument vector and collects the results in an n x <cols(R)> matrix.

$$
\text{calculateV}(xvec) := \left|\begin{array}{l} \text{for } x \in xvec \\ \quad R^{\langle cols(R)\rangle} \leftarrow V_{Resistance}(x) \\ R^T \end{array}\right.
$$

$x := 425mm, 450mm .. 750mm$

The function produces results as shown in Table B-3.

Results := calculateV(x)

Results = N

	4	5	6	7	8	9	10	11	12
0	0.015	0.493	0.493	0.386	$2.554\cdot10^5$	0.184	$4.804\cdot10^4$	$8.973\cdot10^4$	$1.378\cdot10^5$
1	0.015	0.493	0.493	0.386	$2.554\cdot10^5$	0.194	$5.061\cdot10^4$	$8.087\cdot10^4$	$1.315\cdot10^5$
2	0.015	0.493	0.493	0.386	$2.554\cdot10^5$	0.204	$5.318\cdot10^4$	$7.2\cdot10^4$	$1.252\cdot10^5$
3	0.015	0.493	0.493	0.386	$2.554\cdot10^5$	0.214	$5.575\cdot10^4$	$6.313\cdot10^4$	$1.189\cdot10^5$
4	0.015	0.493	0.493	0.386	$2.554\cdot10^5$	0.336	$8.751\cdot10^4$	0	$8.751\cdot10^4$
5	0.015	0.493	0.493	0.386	$2.554\cdot10^5$	0.336	$8.751\cdot10^4$	0	$8.751\cdot10^4$
6	0.015	0.493	0.493	0.386	$2.554\cdot10^5$	0.336	$8.751\cdot10^4$	0	$8.751\cdot10^4$
7	0.015	0.493	0.493	0.386	$2.554\cdot10^5$	0.336	$8.751\cdot10^4$	0	$8.751\cdot10^4$
8	0.015	0.493	0.493	0.386	$2.554\cdot10^5$	0.336	$8.751\cdot10^4$	0	$8.751\cdot10^4$
9	0.015	0.493	0.493	0.386	$2.554\cdot10^5$	0.336	$8.751\cdot10^4$	0	$8.751\cdot10^4$
10	0.015	0.493	0.493	0.386	$2.554\cdot10^5$	0.336	$8.751\cdot10^4$	0	$8.751\cdot10^4$
11	0.015	0.493	0.493	0.386	$2.554\cdot10^5$	0.336	$8.751\cdot10^4$	0	$8.751\cdot10^4$
12	0.015	0.493	0.493	0.386	$2.554\cdot10^5$	0.336	$8.751\cdot10^4$	0	...

Table B-1: Results from calculations of LB6 acc. fib Model Code 2010

Location [m]	Area of stirrups per unit of length [mm2̂/m]	Moment from the self-weight [N*m]	Moment due to the applied load [N*m]	Force in longitudinal reinforcement at a crack	Longitudinal strain	Diagonal crack inclination [deg]	Principal tensile strain	Strain factor [unitless]	Strength reduction factor for concrete [unitless]	Maximum shear resistance [N]	Factor accounting for strain effect and member size [N]	Concrete contribution to shear resistance [N]	Steel contribution to shear resistance [N]	Total shear resistance [N]
0.425	207.4286	1006.80	116750.00	30754.00	7.70E-05	20.7704	0.0145	0.5004	0.3897	268190.00	0.1375	35813.00	129530.00	165340.00
0.45	200.5963	928.69	111750.00	18370.00	4.41E-05	20.4407	0.0148	0.4971	0.3871	262930.00	0.1409	36703.00	127470.00	164170.00
0.475	193.7640	851.75	106780.00	6037.80	1.12E-05	20.1124	0.0150	0.4937	0.3845	257670.00	0.1446	37652.00	125320.00	162970.00
0.5	186.9317	775.95	101070.00	-9255.50	0.00E+00	20.0000	0.0151	0.4925	0.3836	255870.00	0.1491	38838.00	121640.00	160480.00
0.525	180.0994	701.30	95092.00	-25824.00	0.00E+00	20.0000	0.0151	0.4925	0.3836	255870.00	0.1541	40124.00	117190.00	157320.00
0.55	173.2671	627.79	89269.00	-42034.00	0.00E+00	20.0000	0.0151	0.4925	0.3836	255870.00	0.1590	41410.00	112750.00	154160.00
0.575	166.4348	555.43	83605.00	-57892.00	0.00E+00	20.0000	0.0151	0.4925	0.3836	255870.00	0.1639	42697.00	108300.00	151000.00
0.6	159.6025	484.20	78100.00	-73392.00	0.00E+00	20.0000	0.0151	0.4925	0.3836	255870.00	0.1689	43983.00	103860.00	147840.00
0.625	152.7702	414.13	72754.00	-88538.00	0.00E+00	20.0000	0.0151	0.4925	0.3836	255870.00	0.1738	45270.00	99410.00	144680.00
0.65	145.9379	345.19	67568.00	-103330.00	0.00E+00	20.0000	0.0151	0.4925	0.3836	255870.00	0.1788	46556.00	94964.00	141520.00
0.675	139.1056	277.41	62540.00	-117760.00	0.00E+00	20.0000	0.0151	0.4925	0.3836	255870.00	0.1837	47843.00	90518.00	138360.00
0.7	138.2857	210.76	58853.00	-126420.00	0.00E+00	20.0000	0.0151	0.4925	0.3836	255870.00	0.1843	47997.00	89984.00	137980.00
0.725	138.2857	145.26	55338.00	-134320.00	0.00E+00	20.0000	0.0151	0.4925	0.3836	255870.00	0.1843	47997.00	89984.00	137980.00
0.75	138.2857	80.90	51824.00	-142210.00	0.00E+00	20.0000	0.0151	0.4925	0.3836	255870.00	0.1843	47997.00	89984.00	137980.00

Table B-2: Results from calculations of LB10 acc. fib Model Code 2010

Location [m]	Area of stirrups per unit of length [mm2̂/m]	Moment from the self-weight [N*m]	Moment due to the applied load [N*m]	Force in longitudinal reinforcement at a crack	Longitudinal strain	Diagonal crack inclination [deg]	Principal tensile strain	Strain factor [unitless]	Strength reduction factor for concrete [unitless]	Maximum shear resistance [N]	Factor accounting for strain effect and member size [N]	Concrete contribution to shear resistance [N]	Steel contribution to shear resistance [N]	Total shear resistance [N]
0.425	276.5710	1007.00	134100.00	82780.00	1.83E-04	21.8300	0.0140	0.5110	0.400	284400.00	0.104	27110.00	163100.00	190200.00
0.45	276.5710	928.06	130200.00	75200.00	1.63E-04	21.6280	0.0140	0.5090	0.399	281200.00	0.103	26750.00	164700.00	191500.00
0.475	276.5710	850.73	126200.00	67510.00	1.42E-04	21.4230	0.0140	0.5070	0.397	278000.00	0.101	26340.00	166500.00	192800.00
0.5	276.5710	774.54	122100.00	59700.00	1.22E-04	21.2150	0.0140	0.5050	0.396	274700.00	0.099	25880.00	168300.00	194100.00
0.525	276.5710	699.51	118000.00	51750.00	1.00E-04	21.0040	0.0140	0.5030	0.394	271400.00	0.097	25350.00	170100.00	195500.00
0.55	276.5710	625.62	113800.00	43660.00	7.88E-05	20.7880	0.0150	0.5010	0.392	268000.00	0.095	24760.00	172100.00	196800.00
0.575	276.5710	552.89	109500.00	35410.00	5.69E-05	20.5690	0.0150	0.4980	0.391	264500.00	0.092	24100.00	174100.00	198200.00
0.6	276.5710	481.31	105200.00	27010.00	3.45E-05	20.3450	0.0150	0.4960	0.389	260900.00	0.090	23340.00	176200.00	199500.00
0.625	276.5710	410.88	100800.00	18440.00	1.17E-05	20.1170	0.0150	0.4940	0.387	257300.00	0.086	22490.00	178300.00	200800.00
0.65	276.5710	341.60	96350.00	9682.00	-1.16E-05	19.8840	0.0150	0.4910	0.385	253500.00	0.083	21520.00	180600.00	202100.00
0.675	276.5710	273.47	90940.00	-3128.00	0.00E+00	20.0000	0.0150	0.4930	0.386	255400.00	0.084	22010.00	179500.00	201500.00
0.7	276.5710	206.50	85840.00	-14610.00	0.00E+00	20.0000	0.0150	0.4930	0.386	255400.00	0.084	22010.00	179500.00	201500.00
0.725	276.5710	140.67	80730.00	-26080.00	0.00E+00	20.0000	0.0150	0.4930	0.386	255400.00	0.084	22010.00	179500.00	201500.00
0.75	276.5710	75.99	75630.00	-37550.00	0.00E+00	20.0000	0.0150	0.4930	0.386	255400.00	0.084	22010.00	179500.00	201500.00

Table B-3: Results from calculations of LB11 acc. fib Model Code 2010

Location [m]	Area of stirrups per unit of length [mm2/m]	Moment from the self-weight [N*m]	Moment due to the applied load [N*m]	Force in longitudinal reinforcement at a crack	Longitudinal strain	Diagonal crack inclination [deg]	Principal tensile strain	Strain factor [unitless]	Strength reduction factor for concrete [unitless]	Maximum shear resistance [N]	Factor accounting for strain effect and member size [N]	Concrete contribution to shear resistance [N]	Steel contribution to shear resistance [N]	Total shear resistance [N]
0.425	138.2860	1011.00	97450.00	-45290.00	0.00E+00	20.0000	0.0150	0.4930	0.39	255400.00	0.184	48040.00	89730.00	137800.00
0.45	124.6210	932.64	89680.00	-69040.00	0.00E+00	20.0000	0.0150	0.4930	0.39	255400.00	0.194	50610.00	80870.00	131500.00
0.475	110.9570	855.19	82220.00	-92080.00	0.00E+00	20.0000	0.0150	0.4930	0.39	255400.00	0.204	53180.00	72000.00	125200.00
0.5	97.2920	778.89	75080.00	-114400.00	0.00E+00	20.0000	0.0150	0.4930	0.39	255400.00	0.214	55750.00	63130.00	118900.00
0.525	83.6270	703.74	53210.00	-194800.00	0.00E+00	20.0000	0.0150	0.4930	0.39	255400.00	0.336	87510.00	0.00	87510.00
0.55	69.9630	629.74	50950.00	-199900.00	0.00E+00	20.0000	0.0150	0.4930	0.39	255400.00	0.336	87510.00	0.00	87510.00
0.575	56.2980	556.90	48690.00	-205000.00	0.00E+00	20.0000	0.0150	0.4930	0.39	255400.00	0.336	87510.00	0.00	87510.00
0.6	42.6340	485.20	46430.00	-210100.00	0.00E+00	20.0000	0.0150	0.4930	0.39	255400.00	0.336	87510.00	0.00	87510.00
0.625	28.9690	414.66	44170.00	-215300.00	0.00E+00	20.0000	0.0150	0.4930	0.39	255400.00	0.336	87510.00	0.00	87510.00
0.65	15.3040	345.28	41910.00	-220400.00	0.00E+00	20.0000	0.0150	0.4930	0.39	255400.00	0.336	87510.00	0.00	87510.00
0.675	1.6400	277.04	39660.00	-225500.00	0.00E+00	20.0000	0.0150	0.4930	0.39	255400.00	0.336	87510.00	0.00	87510.00
0.7	0.0000	209.95	37400.00	-230500.00	0.00E+00	20.0000	0.0150	0.4930	0.39	255400.00	0.336	87510.00	0.00	87510.00
0.725	0.0000	144.02	35150.00	-235600.00	0.00E+00	20.0000	0.0150	0.4930	0.39	255400.00	0.336	87510.00	0.00	87510.00
0.75	0.0000	79.24	32900.00	-240700.00	0.00E+00	20.0000	0.0150	0.4930	0.39	255400.00	0.336	87510.00	0.00	87510.00

Appendix C

Results of Calculations According to Eurocode 2

LB11 (Design according to EN 1992-1-1: 2004)

Material properties from: Liping Xie, *The Influence of Axial Load and Prestress on the Shear Strength of Web-Shear Critical Reinforced Concrete Elements* :

- Concrete properties: reference *Table 4.3 Concrete Compressive Strength*

$f_{cm} := 62.3MPa$

Analytical relation from EN 1992-1-1: 2004, Table 3.1 *Strength and deformation characteristics for concrete*

$$f_{ctm} := 2.12 \cdot \ln\left(1 + \frac{\frac{f_{cm}}{MPa}}{10}\right) \cdot MPa = 4.194 \cdot \frac{N}{mm^2}$$

- Steel properties: reference *Table 4.6 Reinforcement Properties in a Beam*

$f_y := 409MPa$ yield strength of rebars 15M

$f_{yw} := 529MPa$ yield strength of shear links D4

- Cross section dimensions (as-built)

$h := 506mm$ $b_w := 74mm$ $b_{ftop} := 352mm$ $h_{ftop} := 57mm$

$h_1 := 25mm$ $d := 473mm$ $A_g := 73740mm^2$ $A_{sw} := 24.2mm^2$

$z := 446mm$ *Calculated in fMC 2010 for the beam LB11*

$I_g := 2.56 \cdot 10^9 mm^4$ $Q_{flange} := 5.34 \cdot 10^6 mm^3$ $Q_{cen} := 6.35 \times 10^6 mm^3$ $N_{axial} := -809kN$

$y_{0bot} := 259mm$ $y_{0top} := 247mm$ $z_{tf} := y_{0top} - h_1 - h_{ftop} = 0.165\,m$ *(Table 4.2)*

$A_p := 507mm^2$ $A_s := 934mm^2$ *(Table 4.6)*

- Self weight value:

$$q_{Eg2} := A_g \cdot 25\frac{kN}{m^3} = 1.843 \cdot \frac{kN}{m} \qquad q_{Eg1} := h \cdot b_{ftop} \cdot 25\frac{kN}{m^3} = 4.453 \cdot \frac{kN}{m}$$

$l_{TestRegion} := 2400mm$ the region between the supports B and C

Solution

Shear resistance attributed to the stirrups:

$$s_v := \begin{pmatrix} 87.5mm \\ 0mm \end{pmatrix}$$

$$x_1 := 425mm - \frac{h}{2} = 0.172\,m$$

$$x_2 := 425mm + \frac{h}{2} = 0.678\,m$$

Shear resistance according to EN 1992-1-1:2004 eq. 6.8 for members with vertical shear reinforcement including variation of the stirrups along the span (*see function* $A_{swPerUnitofLength}$)

$$V_{R.s6.8}(x) := \left| \begin{array}{l} \text{for } i \in x \\ \quad \left| \begin{array}{l} \theta \leftarrow 21.8\text{deg} \\ A_{swPerUnitOfLength} \leftarrow \left| \begin{array}{ll} \frac{A_{sw}}{s_{v_0}} & \text{if } i \le x_1 \\ \frac{A_{sw}}{s_{v_0}} - \left(\frac{A_{sw}}{s_{v_0}}\right) \cdot \frac{i - x_1}{x_2 - x_1} & \text{if } x_1 < i < x_2 \\ 0 & \text{if } i \ge x_2 \end{array} \right. \\ V_R \leftarrow A_{swPerUnitOfLength} \cdot z \cdot f_{yw} \cdot \cot(\theta) \end{array} \right. \\ V_R \end{array} \right.$$

$$f_{ck} := f_{cm} - 4\text{MPa} = 58.3 \cdot \text{MPa}$$

$$\sigma_{cp} := \left| \frac{N_{axial}}{A_g} \right| = 10.971 \cdot \text{MPa}$$

$$\alpha_{cw} := \left| \begin{array}{ll} 1 + \frac{\sigma_{cp}}{f_{cm}} & \text{if } 0 < \sigma_{cp} \le 0.25 \cdot f_{cm} \\ 1.25 & \text{if } 0.25 \cdot f_{cm} < \sigma_{cp} \le 0.5 \cdot f_{cm} \\ \left[2.5\left(1 - \frac{\sigma_{cp}}{f_{cm}}\right)\right] & \text{if } 0.5 \cdot f_{cm} < \sigma_{cp} < 1 \cdot f_{cm} \end{array} \right. = 1.176$$

$$V_{Rmax} := \text{for } \theta \in 21.8\text{deg} = 383.629 \cdot \text{kN}$$

$$\frac{\alpha_{cw} \cdot b_w \cdot z \cdot 0.6 \cdot \left(1 - \frac{\frac{f_{ck}}{\text{MPa}}}{250}\right) \cdot f_{cm}}{\cot(\theta) + \tan(\theta)}$$

Support reactions from the self-weight

$$0.700\text{m} \cdot q_{Eg1} \cdot (4.120\text{m}) + 3.220\text{m} \cdot q_{Eg2} \cdot \left(\frac{3.220\text{m}}{2} + 0.550\text{m}\right) \ldots = 0$$

$$+ 0.550\text{m} \cdot q_{Eg1} \cdot \frac{0.550\text{m}}{2} - \frac{(0.150\text{m})^2}{2} \cdot q_{Eg1} - R_A \cdot (3.360\text{m})$$

$$R_A := 0.9 \cdot \text{m} \cdot q_{Eg1} + 2.07 \cdot \text{m} \cdot q_{Eg2} = 7.824 \cdot \text{kN}$$

$$R_B := 2 \cdot 700\text{mm} \cdot q_{Eg1} + 3200\text{mm} \cdot q_{Eg2} - R_A = 4.31 \cdot \text{kN}$$

$$M_{Eg}(x) := 0.7\text{m} \cdot q_{Eg1} \cdot (0.350\text{m} + 0.410\text{m} + x) \ldots + \left[(0.41 \cdot \text{m} + x) \cdot q_{Eg2} \cdot \left(\frac{0.41\text{m} + x}{2}\right) - R_A \cdot x\right]$$

Bending moment from prestressing

$$M_{vrsp} := 0$$

Shear resistance according to the equation (6.2) EN 1991-1-2

$V_{6.4}(x) :=$ $V_{E.trial} \leftarrow 0$

while $\sigma_1 \le f_{ctm}$

$V_{E.trial} \leftarrow V_{E.trial} + 0.001kN$

break if $\sigma_1 = f_{ctm}$

$V_{Eg} \leftarrow \frac{d}{dx}\left[0.7m \cdot q_{Eg1} \cdot (0.350m + 0.410m + x) + (0.41 \cdot m + x) \cdot q_{Eg2} \cdot \left(\frac{0.41m + x}{2}\right) - R_A \cdot x\right]$

$M_{Eg} \leftarrow 0.7m \cdot q_{Eg1} \cdot (0.350m + 0.410m + x) \ldots + \left[(0.41 \cdot m + x) \cdot q_{Eg2} \cdot \left(\frac{0.41m + x}{2}\right) - R_A \cdot x\right]$

$V_{tot} \leftarrow V_{E.trial} + V_{Eg}$

$M_E \leftarrow V_{E.trial} \cdot \left(\frac{l_{TestRegion}}{2} - x - \frac{150mm}{2}\right)$

$M_{tot} \leftarrow M_{Eg} + M_E$

$\sigma_{cptf} \leftarrow \frac{N_{axial}}{A_g} + \frac{M_{tot} \cdot z_{tf}}{I_g}$

$\tau_{tf} \leftarrow \frac{V_{tot} \cdot Q_{flange}}{b_w \cdot I_g}$

$\sigma_{cpcen} \leftarrow \frac{N_{axial}}{A_g}$

$\tau_{cen} \leftarrow \frac{V_{tot} \cdot Q_{cen}}{b_w \cdot I_g}$

$\sigma_{1cen} \leftarrow \sqrt{\tau_{cen}^2 + \left(\frac{\sigma_{cpcen}}{2}\right)^2} + \frac{\sigma_{cpcen}}{2}$

$\sigma_{1tf} \leftarrow \sqrt{\tau_{tf}^2 + \left(\frac{\sigma_{cptf}}{2}\right)^2} + \frac{\sigma_{cptf}}{2}$

$\sigma_1 \leftarrow \max(\sigma_{1tf}, \sigma_{1cen})$

$\left(V_{tot} \quad \frac{M_{tot}}{m} \quad \sigma_{cptf} \cdot mm^2 \quad \tau_{tf} \cdot mm^2 \quad \sigma_{cpcen} \cdot mm^2 \quad \tau_{cen} \cdot mm^2 \quad \sigma_{1cen} \cdot mm^2 \quad \sigma_{1tf} \cdot mm^2 \quad \sigma_1 \cdot mm^2 \quad V_{E.trial}\right)^T$

The above function can only return a multiple rows/columns vector for values with the same unit. Therefore all the variable had to be reduced to a consistent unit (here Newtons). The units were later restored.

An auxiliary function which calls the main function with every element of the argument vector and collects the results in an n x <cols(R)> matrix.

$x := 0mm, 50mm .. 1200mm$

$calculateV(xvec) :=$ for $x \in xvec$

$R^{\langle cols(R) \rangle} \leftarrow V_{6.4}(x)$

R^T

Results := calculateV(x)

Results = N

	2	3	4	5	6	7	8	9
19	-8.338	6.706	-10.971	7.975	4.194	3.728	4.194	$2.357 \cdot 10^5$
20	-9.104	6.706	-10.971	7.975	4.194	3.553	4.194	$2.358 \cdot 10^5$
21	-9.87	6.706	-10.971	7.975	4.194	3.392	4.194	$2.359 \cdot 10^5$
22	-10.636	6.706	-10.971	7.975	4.194	3.241	4.194	$2.36 \cdot 10^5$
23	-11.403	6.706	-10.971	7.975	4.194	3.101	4.194	$2.361 \cdot 10^5$
24	-12.17	6.706	-10.971	7.975	4.194	2.971	4.194	...

$V_{Resistance6.4.} := Results^{\langle 9 \rangle}$

Shear resistance of members not requiring shear reinforcement according to EN 1992-1-1: 2004 eq. 6.2.a. **Please note: in the formulation mean values of C_{Rc} and k_1 are used.**

$$V_{Resistance6.2} := \left| \begin{array}{l} C_{Rc} \leftarrow 0.163 \\ \sigma_{cp} \leftarrow \frac{N_{axial}}{A_g} \\ k \leftarrow 1 + \sqrt{\frac{200}{\frac{d}{mm}}} \\ \rho_l \leftarrow \min\left(\frac{A_s}{b_w \cdot d}, 0.02\right) \\ k_1 \leftarrow 0.225 \\ V_R \leftarrow \left[C_{Rc} \cdot k \cdot \left(100 \cdot \rho_l \cdot \frac{f_{cm}}{\frac{N}{mm^2}} \right)^{\frac{1}{3}} + k_1 \cdot \left| \sigma_{cp} \right| \cdot \frac{mm^2}{N} \right] \cdot b_w \cdot d \cdot \frac{N}{mm^2} \end{array} \right.$$

$V_{Resistance6.2} = 133.427 \cdot kN$

Definition of a region uncracked and cracked in flexure

Flexural cracking is expected in the most tensile fiber when stresses from the applied load exceed the concrete tensile strength:

$$\frac{N_{axial}}{A_g} + \frac{M_{cr} \cdot y_{0top}}{I_g} + \frac{M_{Eg}(x) \cdot y_{0top}}{I_g} = f_{ctm} \quad \text{with: } N_{axial} = -8.09 \times 10^5 \, N$$

a negative sign - compression

After transformations flexural cracking bending moment is:

$$M_{cr}(x) := -\frac{I_g \cdot \left(\frac{N_{axial}}{A_g} - f_{ctm} + \frac{y_{0top} \cdot M_{Eg}(x)}{I_g} \right)}{y_{0top}}$$

Applied shear force causing flexural cracking in concrete. Please note: due to the experimental set-up, shear force is constant in the test region.

$$V_E \cdot \left(1200 \cdot mm - x - \frac{150mm}{2}\right) - M_{cr}(x) = 0$$

$$V_E(x) := \frac{M_{cr}(x)}{1200mm - x - \frac{150mm}{2}}$$

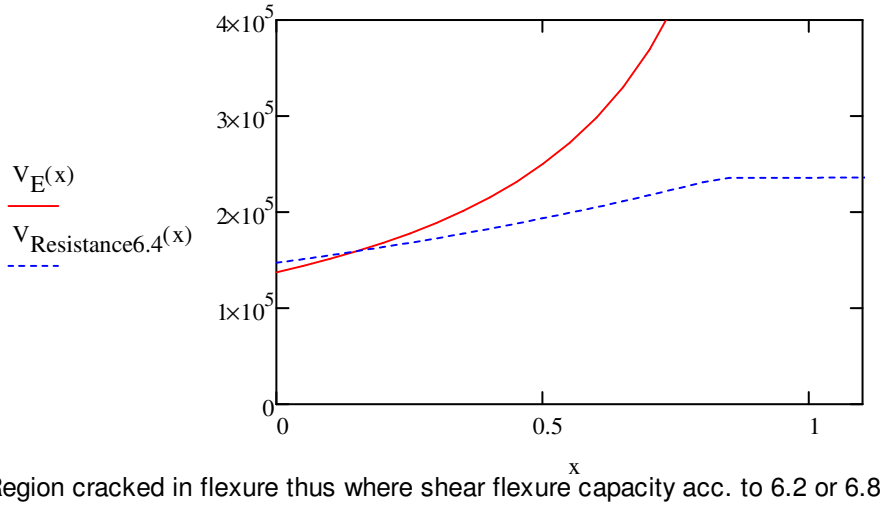

Region cracked in flexure thus where shear flexure capacity acc. to 6.2 or 6.8 EC2 is governing is presented above. The definition of this region is based on the assumption that the lowest value of shear resistances i.e. shear flexure resistance and shear tension resistance determines the manner in which a member fails.

$$V_{Regions}(x_1, x_2, x_{end}) := \left| \begin{array}{l} i \leftarrow ORIGIN \\ j \leftarrow ORIGIN \\ \text{for } x \in x_1, x_2 .. x_{end} \\ \quad \left| \begin{array}{l} V_{ultimate_{i,j}} \leftarrow \left| \begin{array}{ll} \text{"flexural"} & \text{if } V_E(x) < V_{Resistance6.4}(x) \\ \text{"tension shear"} & \text{otherwise} \end{array} \right. \\ V_{ultimate_{i,j+1}} \leftarrow \left| \begin{array}{ll} \max\left(V_{Resistance6.2}, V_{R.s6.8}(x)\right) & \text{if } V_{ultimate_{i,j}} = \text{"flexural"} \\ \max\left(V_{Resistance6.4}(x), V_{R.s6.8}(x), V_{Resistance6.2}\right) & \text{otherwise} \end{array} \right. \\ i \leftarrow i + 1 \end{array} \right. \\ V_{ultimate} \end{array} \right.$$

$V_{Regions}(0mm, 50mm, 1000mm) =$ ·kN

	0	1
0	"flexural"	163.143
1	"flexural"	163.143
2	"flexural"	163.143
3	"flexural"	163.143
4	"tension shear"	163.613
5	"tension shear"	168.129
6	"tension shear"	172.824
7	"tension shear"	177.703
8	"tension shear"	...

Table C-1: Results of calculations acc. to EC2 for beam LB6

Location [mm]	Shear force from self-weight [N]	Total shear force [N]	Bending moment due to self-weight [N*m]	Total bending moment [N*m]	Normal stress in concrete at the web-flange junction [MPa]	Shear stress in concrete at the web-flange junction [MPa]	Compressive normal stress due to prestressing [MPa]	Shear stress at the centroid [MPa]	Principal tensile stress at the centroid [MPa]	Principal stress at the web-flange junction	Max. value of principal stress equal to tensile strength [Mpa]	Shear force resistance 6.4 [kN]	Flexural cracking shear force $M_{cr}/(1200mm - x - 75mm)$	Shear force resistance 6.8 [kN]	Shear resistance 6.2 [kN]	Total shear resistance [kN]
0	3923	144600	2505	160700	0.461	3.992	-10.884	4.908	1.886	4.229	4.229	140.6	131.587	163.765	131.247	163.765
0.05	3831	148500	2311	157800	0.254	4.1	-10.884	5.041	1.976	4.229	4.229	144.6	137.888	163.765	131.247	163.765
0.1	3740	152600	2122	154700	0.033	4.212	-10.884	5.179	2.071	4.229	4.229	148.8	144.798	163.765	131.247	163.765
0.15	3648	156800	1937	151300	-0.205	4.33	-10.884	5.324	2.171	4.229	4.229	153.2	152.413	163.765	131.247	163.765
0.2	3556	161300	1757	147700	-0.461	4.453	-10.884	5.476	2.278	4.229	4.229	157.7	160.847	159.306	131.247	159.306
0.25	3465	166000	1581	143800	-0.737	4.582	-10.884	5.634	2.391	4.229	4.229	162.5	170.239	151.199	131.247	162.5
0.3	3373	170800	1410	139600	-1.033	4.717	-10.884	5.8	2.511	4.229	4.229	167.5	180.763	143.092	131.247	167.5
0.35	3282	175900	1244	135000	-1.352	4.858	-10.884	5.973	2.638	4.229	4.229	172.6	192.64	134.985	131.247	172.6
0.4	3190	181300	1082	130200	-1.695	5.005	-10.884	6.154	2.773	4.229	4.229	178.1	206.149	126.877	131.247	178.1
0.45	3099	186800	924.825	124900	-2.065	5.159	-10.884	6.343	2.916	4.229	4.229	183.7	221.652	118.77	131.247	183.7
0.5	3007	192700	772.173	119300	-2.463	5.32	-10.884	6.541	3.067	4.229	4.229	189.6	239.628	110.663	131.247	189.6
0.55	2916	198700	624.098	113200	-2.892	5.488	-10.884	6.747	3.226	4.229	4.229	195.8	260.723	102.556	131.247	195.8
0.6	2824	205100	480.599	106700	-3.355	5.663	-10.884	6.963	3.395	4.229	4.229	202.3	285.827	94.449	131.247	202.3
0.65	2733	211700	341.677	99610	-3.853	5.846	-10.884	7.188	3.574	4.229	4.229	209	316.207	86.341	131.247	209
0.7	2641	218600	207.331	92010	-4.39	6.037	-10.884	7.423	3.762	4.229	4.229	216	353.724	81.882	131.247	216
0.75	2550	225900	77.562	83820	-4.968	6.236	-10.884	7.668	3.961	4.229	4.229	223.3	401.233	81.882	131.247	223.3
0.8	2458	233400	-47.631	75000	-5.59	6.444	-10.884	7.923	4.17	4.229	4.229	230.9	463.346	81.882	131.247	230.9
0.85	2367	235500	-168.247	63930	-6.371	6.502	-10.884	7.994	4.229	4.055	4.229	233.1	548.03	81.882	131.247	233.1
0.9	2275	235500	-284.287	52180	-7.201	6.502	-10.884	7.994	4.229	3.832	4.229	233.2	670.33	81.882	131.247	233.2
0.95	2183	235500	-395.75	40430	-8.03	6.502	-10.884	7.994	4.229	3.626	4.229	233.3	862.489	81.882	131.247	233.3
1	2092	235500	-502.636	28670	-8.861	6.502	-10.884	7.994	4.229	3.437	4.229	233.4	1.21E+03	81.882	131.247	233.4
1.05	2000	235500	-604.946	16910	-9.691	6.502	-10.884	7.994	4.229	3.263	4.229	233.5	2.02E+03	81.882	131.247	233.5
1.1	1909	235500	-702.679	5136	-10.522	6.502	-10.884	7.994	4.229	3.103	4.229	233.6	6.05E+03	81.882	131.247	233.6

Table C-2: Results of calculations acc. to EC2 for beam LB10

Location [mm]	Shear force from self-weight [N]	Total shear force [N]	Bending moment due to self-weight [N*m]	Total bending moment [N*m]	Normal stress in concrete at the web-flange junction [MPa]	Shear stress in concrete at the web-flange junction [MPa]	Compressive normal stress due to prestressing [MPa]	Shear stress at the centroid [MPa]	Principal tensile stress at the centroid [MPa]	Principal stress at the web-flange junction	Max. value of principal stress equal to tensile strength [Mpa]	Shear force resistance 6.4 [kN]	Flexural cracking shear force $M_{cr}/(1200mm - x - 75mm)$	Shear force resistance 6.8 [kN]	Shear resistance 6.2 [kN]	Total shear resistance [kN]
0	3945	152000	2517	169000	-0.132	4.259	-11.158	5.093	1.975	4.194	4.194	148	138.624	163.143	134.899	163.143
0.05	3853	155800	2322	165600	-0.352	4.366	-11.158	5.222	2.062	4.194	4.194	151.9	145.253	163.143	134.899	163.143
0.1	3761	159800	2132	162000	-0.588	4.478	-11.158	5.355	2.154	4.194	4.194	156	152.525	163.143	134.899	163.143
0.15	3669	163900	1946	158200	-0.839	4.594	-11.158	5.494	2.251	4.194	4.194	160.2	160.537	163.143	134.899	160.2
0.2	3577	168200	1765	154100	-1.108	4.715	-11.158	5.639	2.353	4.194	4.194	164.6	169.411	163.143	134.899	164.6
0.25	3485	172700	1588	149700	-1.395	4.841	-11.158	5.789	2.461	4.194	4.194	169.2	179.293	163.143	134.899	169.2
0.3	3393	177400	1416	145000	-1.701	4.972	-11.158	5.946	2.575	4.194	4.194	174	190.368	163.143	134.899	174
0.35	3301	182300	1249	139900	-2.029	5.109	-11.158	6.109	2.694	4.194	4.194	179	202.865	163.143	134.899	179
0.4	3209	187300	1086	134600	-2.38	5.251	-11.158	6.279	2.82	4.194	4.194	184.1	217.08	163.143	134.899	184.1
0.45	3117	192600	928.035	128800	-2.754	5.398	-11.158	6.455	2.953	4.194	4.194	189.5	233.395	163.143	134.899	189.5
0.5	3024	198100	774.51	122700	-3.155	5.552	-11.158	6.639	3.093	4.194	4.194	195	252.312	163.143	134.899	195
0.55	2932	203800	625.589	116100	-3.584	5.711	-11.158	6.83	3.24	4.194	4.194	200.8	274.511	163.143	134.899	200.8
0.6	2840	209700	481.273	109100	-4.043	5.877	-11.158	7.028	3.395	4.194	4.194	206.8	300.93	163.143	134.899	206.8
0.65	2748	215800	341.561	101600	-4.533	6.05	-11.158	7.235	3.557	4.194	4.194	213.1	332.901	163.143	134.899	213.1
0.7	2656	222200	206.453	93520	-5.057	6.229	-11.158	7.449	3.727	4.194	4.194	219.6	372.384	163.143	134.899	219.6
0.75	2564	228800	75.95	84930	-5.617	6.415	-11.158	7.671	3.906	4.194	4.194	226.3	422.383	163.143	134.899	226.3
0.8	2472	235700	-49.949	75760	-6.216	6.607	-11.158	7.901	4.094	4.194	4.194	233.3	487.752	163.143	134.899	233.3
0.85	2380	239400	-171.244	65000	-6.917	6.71	-11.158	8.024	4.194	4.09	4.194	237	576.875	163.143	134.899	237
0.9	2288	239400	-287.934	53060	-7.697	6.71	-11.158	8.024	4.194	3.887	4.194	237.1	705.589	163.143	134.899	237.1
0.95	2196	239400	-400.02	41110	-8.476	6.71	-11.158	8.024	4.194	3.698	4.194	237.2	907.826	163.143	134.899	237.2
1	2104	239400	-507.501	29150	-9.256	6.71	-11.158	8.024	4.194	3.523	4.194	237.3	1272	163.143	134.899	237.3
1.05	2011	239400	-610.378	17190	-10.036	6.71	-11.158	8.024	4.194	3.361	4.194	237.4	2121	163.143	134.899	237.4
1.1	1919	239400	-708.651	5228	-10.817	6.71	-11.158	8.024	4.194	3.21	4.194	237.5	6367	163.143	134.899	237.5

Table C-3: Results of calculations acc. to EC2 for beam LB11

Location [mm]	Shear force from self-weight [N]	Total shear force [N]	Bending moment due to self-weight [N*m]	Total bending moment [N*m]	Normal stress in concrete at the web-flange junction [MPa]	Shear stress in concrete at the web-flange junction [MPa]	Compressive normal stress due to prestressing [MPa]	Shear stress at the centroid [MPa]	Principal tensile stress at the centroid [MPa]	Principal stress at the web-flange junction	Max. value of principal stress equal to tensile strength [Mpa]	Shear force resistance 6.4 [kN]	Flexural cracking shear force $M_{cr}/(1200mm - x - 75mm)$	Shear force resistance 6.8 [kN]	Shear resistance 6.2 [kN]	Total shear resistance [kN]
0	3945	152000	2517	169000	-0.132	4.259	-11.158	5.093	1.975	4.194	4.194	148	138.624	163.143	134.899	163.143
0.05	3853	155800	2322	165600	-0.352	4.366	-11.158	5.222	2.062	4.194	4.194	151.9	145.253	163.143	134.899	163.143
0.1	3761	159800	2132	162000	-0.588	4.478	-11.158	5.355	2.154	4.194	4.194	156	152.525	163.143	134.899	163.143
0.15	3669	163900	1946	158200	-0.839	4.594	-11.158	5.494	2.251	4.194	4.194	160.2	160.537	163.143	134.899	163.143
0.2	3577	168200	1765	154100	-1.108	4.715	-11.158	5.639	2.353	4.194	4.194	164.6	169.411	163.143	134.899	164.6
0.25	3485	172700	1588	149700	-1.395	4.841	-11.158	5.789	2.461	4.194	4.194	169.2	179.293	163.143	134.899	169.2
0.3	3393	177400	1416	145000	-1.701	4.972	-11.158	5.946	2.575	4.194	4.194	174	190.368	163.143	134.899	174
0.35	3301	182300	1249	139900	-2.029	5.109	-11.158	6.109	2.694	4.194	4.194	179	202.865	163.143	134.899	179
0.4	3209	187300	1086	134600	-2.38	5.251	-11.158	6.279	2.82	4.194	4.194	184.1	217.08	163.143	134.899	184.1
0.45	3117	192600	928.035	128800	-2.754	5.398	-11.158	6.455	2.953	4.194	4.194	189.5	233.395	163.143	134.899	189.5
0.5	3024	198100	774.51	122700	-3.155	5.552	-11.158	6.639	3.093	4.194	4.194	195	252.312	163.143	134.899	195
0.55	2932	203800	625.589	116100	-3.584	5.711	-11.158	6.83	3.24	4.194	4.194	200.8	274.511	163.143	134.899	200.8
0.6	2840	209700	481.273	109100	-4.043	5.877	-11.158	7.028	3.395	4.194	4.194	206.8	300.93	163.143	134.899	206.8
0.65	2748	215800	341.561	101600	-4.533	6.05	-11.158	7.235	3.557	4.194	4.194	213.1	332.901	163.143	134.899	213.1
0.7	2656	222200	206.453	93520	-5.057	6.229	-11.158	7.449	3.727	4.194	4.194	219.6	372.384	163.143	134.899	219.6
0.75	2564	228800	75.95	84930	-5.617	6.415	-11.158	7.671	3.906	4.194	4.194	226.3	422.383	163.143	134.899	226.3
0.8	2472	235700	-49.949	75760	-6.216	6.607	-11.158	7.901	4.094	4.194	4.194	233.3	487.752	163.143	134.899	233.3
0.85	2380	239400	-171.244	65000	-6.917	6.71	-11.158	8.024	4.194	4.09	4.194	237	576.875	163.143	134.899	237
0.9	2288	239400	-287.934	53060	-7.697	6.71	-11.158	8.024	4.194	3.887	4.194	237.1	705.589	163.143	134.899	237.1
0.95	2196	239400	-400.02	41110	-8.476	6.71	-11.158	8.024	4.194	3.698	4.194	237.2	907.826	163.143	134.899	237.2
1	2104	239400	-507.501	29150	-9.256	6.71	-11.158	8.024	4.194	3.523	4.194	237.3	1272	163.143	134.899	237.3
1.05	2011	239400	-610.378	17190	-10.036	6.71	-11.158	8.024	4.194	3.361	4.194	237.4	2121	163.143	134.899	237.4
1.1	1919	239400	-708.651	5228	-10.817	6.71	-11.158	8.024	4.194	3.21	4.194	237.5	6367	163.143	134.899	237.5

Appendix D

Results of Calculations According to RBK 1.1

LB11 (Design according to RBK 1.1)

Material properties from: Liping Xie, *The Influence of Axial Load and Prestress on the Shear Strength of Web-Shear Critical Reinforced Concrete Elements* :

- Concrete properties: reference *Table 4.3 Concrete Compressive Strength*

$f_{cm} := 62.3MPa$

Analytical relation from EN 1992-1-1: 2004, Table 3.1 *Strength and deformation characteristics for concrete*

$$f_{ctm} := 2.12 \cdot \ln\left(1 + \frac{\frac{f_{cm}}{MPa}}{10}\right) \cdot MPa = 4.194 \cdot \frac{N}{mm^2}$$

- Steel properties: reference *Table 4.6 Reinforcement Properties in a Beam*

$f_y := 409MPa$ yield strength of rebars 15M

$f_{yw} := 529MPa$ yield strength of shear links D4

- Cross section dimensions (as-built)

$h := 506mm$ $b_w := 74mm$ $b_{ftop} := 352mm$ $h_{ftop} := 57mm$

$h_1 := 25mm$ $d := 473mm$ $A_g := 73740mm^2$ $A_{sw} := 24.2mm^2$

$z := 446mm$ *Calculated in fMC 2010 for the beam LB11*

$I_g := 2.56 \cdot 10^9 mm^4$ $Q_{flange} := 5.34 \cdot 10^6 mm^3$ $Q_{cen} := 6.35 \times 10^6 mm^3$ $N_{axial} := -809kN$

$y_{0bot} := 259mm$ $y_{0top} := 247mm$ $z_{tf} := y_{0top} - h_1 - h_{ftop} = 0.165\,m$ *(Table 4.2)*

$A_p := 507mm^2$ $A_s := 934mm^2$ *(Table 4.6)*

- Self weight value:

$$q_{Eg2} := A_g \cdot 25\frac{kN}{m^3} = 1.843 \cdot \frac{kN}{m} \qquad q_{Eg1} := h \cdot b_{ftop} \cdot 25\frac{kN}{m^3} = 4.453 \cdot \frac{kN}{m}$$

$l_{TestRegion} := 2400mm$ the region between the supports B and C

Solution

Shear resistance attributed to the stirrups:

$$s_v := \begin{pmatrix} 87.5mm \\ 0mm \end{pmatrix}$$

$$x_1 := 425mm - \frac{h}{2} = 0.172\,m$$

$$x_2 := 425mm + \frac{h}{2} = 0.678\,m$$

Shear resistance according to RBK 1.1 for members with vertical shear reinforcement including variation of the stirrups along the span (*see function* $A_{swPerUnitofLength}$) and θ in prestressed concrete = 30 degrees.

$$V_{R.s6.8}(x) := \left| \begin{array}{l} \text{for } i \in x \\ \quad \left| \begin{array}{l} \theta \leftarrow 30\text{deg} \\ A_{swPerUnitOfLength} \leftarrow \left| \begin{array}{ll} \dfrac{A_{sw}}{s_{v_0}} & \text{if } i \le x_1 \\ \dfrac{A_{sw}}{s_{v_0}} - \left(\dfrac{A_{sw}}{s_{v_0}}\right) \cdot \dfrac{i - x_1}{x_2 - x_1} & \text{if } x_1 < i < x_2 \\ 0 & \text{if } i \ge x_2 \end{array} \right. \\ V_R \leftarrow A_{swPerUnitOfLength} \cdot z \cdot f_{yw} \cdot \cot(\theta) \end{array} \right. \\ V_R \end{array} \right.$$

Please note: total shear resistance according to RBK 1.1 consists of steel and concrete contributions. The above expression has to be supplemented with the resistance attributed to concrete $V_{Resistance6.2}$

$$f_{ck} := f_{cm} - 4\text{MPa} = 58.3 \cdot \text{MPa}$$

$$\sigma_{cp} := \left| \frac{N_{axial}}{A_g} \right| = 10.971 \cdot \text{MPa}$$

$$\alpha_{cw} := \left| \begin{array}{ll} 1 + \dfrac{\sigma_{cp}}{f_{cm}} & \text{if } 0 < \sigma_{cp} \le 0.25 \cdot f_{cm} \\ 1.25 & \text{if } 0.25 \cdot f_{cm} < \sigma_{cp} \le 0.5 \cdot f_{cm} \\ \left[2.5\left(1 - \dfrac{\sigma_{cp}}{f_{cm}}\right)\right] & \text{if } 0.5 \cdot f_{cm} < \sigma_{cp} < 1 \cdot f_{cm} \end{array} \right. = 1.176$$

$$V_{Rmax} := \text{for } \theta \in 30\text{deg} = 481.762 \cdot \text{kN}$$

$$\frac{\alpha_{cw} \cdot b_w \cdot z \cdot 0.6 \cdot \left(1 - \dfrac{\dfrac{f_{ck}}{\text{MPa}}}{250}\right) \cdot f_{cm}}{\cot(\theta) + \tan(\theta)}$$

Support reactions from the self-weight

$$0.700\text{m} \cdot q_{Eg1} \cdot (4.120\text{m}) + 3.220\text{m} \cdot q_{Eg2} \cdot \left(\frac{3.220\text{m}}{2} + 0.550\text{m}\right) \ldots = 0$$

$$+ 0.550\text{m} \cdot q_{Eg1} \cdot \frac{0.550\text{m}}{2} - \frac{(0.150\text{m})^2}{2} \cdot q_{Eg1} - R_A \cdot (3.360\text{m})$$

$$R_A := 0.9 \cdot \text{m} \cdot q_{Eg1} + 2.07 \cdot \text{m} \cdot q_{Eg2} = 7.824 \cdot \text{kN}$$

$$R_B := 2 \cdot 700\text{mm} \cdot q_{Eg1} + 3200\text{mm} \cdot q_{Eg2} - R_A = 4.31 \cdot \text{kN}$$

$$M_{Eg}(x) := 0.7\text{m} \cdot q_{Eg1} \cdot (0.350\text{m} + 0.410\text{m} + x) \ldots + \left[(0.41 \cdot \text{m} + x) \cdot q_{Eg2} \cdot \left(\frac{0.41\text{m} + x}{2}\right) - R_A \cdot x\right]$$

Bending moment from prestressing

$M_{vrsp} := 0$

Shear resistance according to the equation (6.2) EN 1991-1-2

$V_{6.4}(x) :=$ $V_{E.trial} \leftarrow 0$

while $\sigma_1 \le f_{ctm}$

$V_{E.trial} \leftarrow V_{E.trial} + 0.001kN$

break if $\sigma_1 = f_{ctm}$

$V_{Eg} \leftarrow -\frac{d}{dx}\left[0.7m \cdot q_{Eg1} \cdot (0.350m + 0.410m + x) + (0.41 \cdot m + x) \cdot q_{Eg2} \cdot \left(\frac{0.41m + x}{2}\right) - R_A \cdot x\right]$

$M_{Eg} \leftarrow 0.7m \cdot q_{Eg1} \cdot (0.350m + 0.410m + x) \ldots + \left[(0.41 \cdot m + x) \cdot q_{Eg2} \cdot \left(\frac{0.41m + x}{2}\right) - R_A \cdot x\right]$

$V_{tot} \leftarrow V_{E.trial} + V_{Eg}$

$M_E \leftarrow V_{E.trial} \cdot \left(\frac{l_{TestRegion}}{2} - x - \frac{150mm}{2}\right)$

$M_{tot} \leftarrow M_{Eg} + M_E$

$\sigma_{cptf} \leftarrow \frac{N_{axial}}{A_g} + \frac{M_{tot} \cdot z_{tf}}{I_g}$

$\tau_{tf} \leftarrow \frac{V_{tot} \cdot Q_{flange}}{b_w \cdot I_g}$

$\sigma_{cpcen} \leftarrow \frac{N_{axial}}{A_g}$

$\tau_{cen} \leftarrow \frac{V_{tot} \cdot Q_{cen}}{b_w \cdot I_g}$

$\sigma_{1cen} \leftarrow \sqrt{\tau_{cen}^2 + \left(\frac{\sigma_{cpcen}}{2}\right)^2} + \frac{\sigma_{cpcen}}{2}$

$\sigma_{1tf} \leftarrow \sqrt{\tau_{tf}^2 + \left(\frac{\sigma_{cptf}}{2}\right)^2} + \frac{\sigma_{cptf}}{2}$

$\sigma_1 \leftarrow \max(\sigma_{1tf}, \sigma_{1cen})$

$\left(V_{tot} \quad \frac{M_{tot}}{m} \quad \sigma_{cptf} \cdot mm^2 \quad \tau_{tf} \cdot mm^2 \quad \sigma_{cpcen} \cdot mm^2 \quad \tau_{cen} \cdot mm^2 \quad \sigma_{1cen} \cdot mm^2 \quad \sigma_{1tf} \cdot mm^2 \quad \sigma_1 \cdot mm^2 \quad V_{E.trial}\right)^T$

$x := 0mm, 50mm .. 1200mm$

calculateV(xvec) :=

for $x \in xvec$

$R^{\langle cols(R) \rangle} \leftarrow V_{6.4}(x)$

R^T

Results := calculateV(x)

Results = N

	5	6	7	8	9
0	5.067	1.982	4.194	4.194	$1.472 \cdot 10^5$
1	5.193	2.068	4.194	4.194	$1.511 \cdot 10^5$
2	5.325	2.159	4.194	4.194	$1.551 \cdot 10^5$
3	5.462	2.255	4.194	4.194	$1.593 \cdot 10^5$
4	5.604	2.357	4.194	4.194	$1.636 \cdot 10^5$
5	5.753	2.463	4.194	4.194	$1.681 \cdot 10^5$
6	5.907	2.576	4.194	4.194	...

$V_{Resistance6.4.} := Results^{\langle 9 \rangle}$

Shear resistance of members not requiring shear reinforcement according to RBK 1.1, cl.6.2.2 (1)

$V_{Resistance6.2} :=$

$C_{Rc} \leftarrow 0.163$

$k_{cap} \leftarrow 1$

$d_e \leftarrow 473mm$

$A_{b.pro} \leftarrow 42879mm^2$

$b_{wgem} \leftarrow \min\left(1.25b_w, \frac{A_{b.pro}}{d_e}\right)$

$k \leftarrow 1 + \sqrt{\frac{200}{\frac{d_e}{mm}}}$

$\rho_l \leftarrow \min\left(\frac{A_s}{b_{wgem} \cdot d_e}, 0.02\right)$

$k_1 \leftarrow 0.225$

$\sigma_{cp} \leftarrow \min\left(\frac{N_{axial}}{A_g}, 0.2 \cdot f_{cm}\right)$

$V_R \leftarrow \left[C_{Rc} \cdot k_{cap} \cdot k \cdot \left(100 \cdot \rho_l \cdot \frac{f_{cm}}{\frac{N}{mm^2}}\right)^{\frac{1}{3}} + k_1 \cdot \left|\sigma_{cp}\right| \cdot \frac{mm^2}{N}\right] \cdot b_{wgem} \cdot d_e \cdot \frac{N}{mm^2}$

$V_{Resistance6.2} = 163.454 \cdot kN$

Definition of a region uncracked and cracked in flexure

Flexural cracking is expected in the most tensile fiber when stresses from the applied load exceed the concrete tensile strength:

$\frac{N_{axial}}{A_g} + \frac{M_{cr} \cdot y_{0top}}{I_g} + \frac{M_{Eg(x)} \cdot y_{0top}}{I_g} = f_{ctm}$ with: $N_{axial} = -8.09 \times 10^5 N$ a negative sign - compression

After transformations flexural cracking bending moment is:

$$M_{cr}(x) := -\frac{I_g \cdot \left(\frac{N_{axial}}{A_g} - f_{ctm} + \frac{y_{0top} \cdot M_{Eg}(x)}{I_g} \right)}{y_{0top}}$$

Applied shear force causing flexural cracking in concrete. Please note: due to the experimental set-up, shear force is constant in the test region.

$$V_E \cdot \left(1200 \cdot mm - x - \frac{150mm}{2} \right) - M_{cr}(x) = 0 \qquad \text{therefore} \qquad V_E(x) := \frac{M_{cr}(x)}{1200mm - x - \frac{150mm}{2}}$$

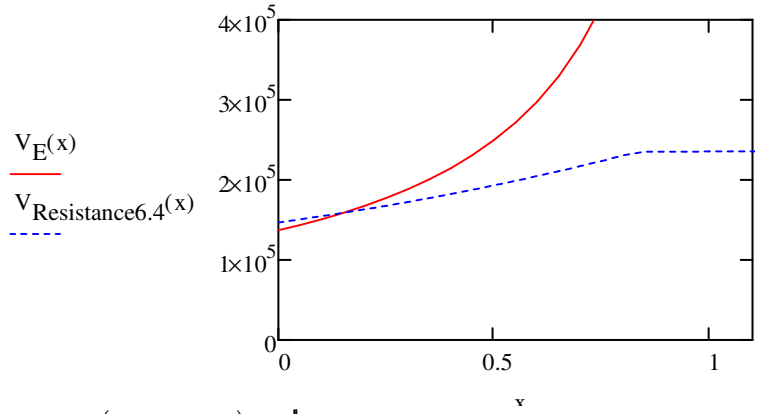

$$V_{Ultimate}(x_1, x_2, x_{end}) := \left| \begin{array}{l} i \leftarrow ORIGIN \\ j \leftarrow ORIGIN \\ \text{for } x \in x_1, x_2 .. x_{end} \\ \quad V_{ultimate_{i,j}} \leftarrow \begin{cases} \text{"flexural"} & \text{if } V_E(x) < V_{Resistance6.4}(x) \\ \text{"tension shear"} & \text{otherwise} \end{cases} \\ \quad V_{ultimate_{i,j+1}} \leftarrow \begin{cases} V_{Resistance6.2} + V_{R.s6.8}(x) & \text{if } V_{ultimate_{i,j}} = \text{"flexural"} \\ \max\left(V_{Resistance6.4}(x), V_{R.s6.8}(x) + V_{Resistance6.2}\right) & \text{otherwise} \end{cases} \\ \quad i \leftarrow i + 1 \\ V_{ultimate} \end{array} \right.$$

Function produces results of the ultimate shear resistance as given in **Table D-3**

$V_{Ultimate}(0mm, 50mm, 1000mm) =$ ·kN

	0	1
0	"flexural"	276.475
1	"flexural"	276.475
2	"flexural"	276.475
3	"flexural"	276.475
4	"tension shear"	270.221
5	"tension shear"	259.053
6	"tension shear"	...

Table D-1: Results of calculations acc. to RBK 1.1 for beam LB6

Location [mm]	Shear force from self-weight [N]	Total shear force [N]	Bending moment due to self-weight [N*m]	Total bending moment [N*m]	Normal stress in concrete at the web-flange junction [MPa]	Shear stress in concrete at web-flange junction [MPa]	Compressive normal stress due to prestressing [MPa]	Shear stress at the centroid [MPa]	Principal tensile stress at centroid [MPa]	Principal stress at the web-flange junction	Max. value of principal stress equal to tensile strength [MPa]	Shear force resistance [kN]	Flexural cracking shear force $M_{cr}/(1200mm - x - 75mm)$	Shear force resistance 6.8 [N]	Shear resistance 6.2 [N]	RBK 1.1 Total shear resistance	Total shear resistance [kN]
0	3923	144600	2505	160700	0.461	3.992	-10.884	4.908	1.886	4.229	4.229	140.6	131.587	113.452	162.601	276.053	276.053
0.05	3831	148500	2311	157800	0.254	4.1	-10.884	5.041	1.976	4.229	4.229	144.6	137.888	113.452	162.601	276.053	276.053
0.1	3740	152600	2122	154700	0.033	4.212	-10.884	5.179	2.071	4.229	4.229	148.8	144.798	113.452	162.601	276.053	276.053
0.15	3648	156800	1937	151300	-0.205	4.33	-10.884	5.324	2.171	4.229	4.229	153.2	152.413	113.452	162.601	276.053	276.053
0.2	3556	161300	1757	147700	-0.461	4.453	-10.884	5.476	2.278	4.229	4.229	157.7	160.847	110.363	162.601	272.964	272.964
0.25	3465	166000	1581	143800	-0.737	4.582	-10.884	5.634	2.391	4.229	4.229	162.5	170.239	104.746	162.601	267.347	267.347
0.3	3373	170800	1410	139600	-1.033	4.717	-10.884	5.8	2.511	4.229	4.229	167.5	180.763	99.13	162.601	261.731	261.731
0.35	3282	175900	1244	135000	-1.352	4.858	-10.884	5.973	2.638	4.229	4.229	172.6	192.64	93.513	162.601	256.114	256.114
0.4	3190	181300	1082	130200	-1.695	5.005	-10.884	6.154	2.773	4.229	4.229	178.1	206.149	87.897	162.601	250.498	250.498
0.45	3099	186800	924.825	124900	-2.065	5.159	-10.884	6.343	2.916	4.229	4.229	183.7	221.652	82.281	162.601	244.882	244.882
0.5	3007	192700	772.173	119300	-2.463	5.32	-10.884	6.541	3.067	4.229	4.229	189.6	239.628	76.664	162.601	239.265	239.265
0.55	2916	198700	624.098	113200	-2.892	5.488	-10.884	6.747	3.226	4.229	4.229	195.8	260.723	71.048	162.601	233.649	233.649
0.6	2824	205100	480.599	106700	-3.355	5.663	-10.884	6.963	3.395	4.229	4.229	202.3	285.827	65.431	162.601	228.032	228.032
0.65	2733	211700	341.677	99610	-3.853	5.846	-10.884	7.188	3.574	4.229	4.229	209	316.207	59.815	162.601	222.416	222.416
0.7	2641	218600	207.331	92010	-4.39	6.037	-10.884	7.423	3.762	4.229	4.229	216	353.724	56.726	162.601	219.327	219.327
0.75	2550	225900	77.562	83820	-4.968	6.236	-10.884	7.668	3.961	4.229	4.229	223.3	401.233	56.726	162.601	219.327	223.3
0.8	2458	233400	-47.631	75000	-5.59	6.444	-10.884	7.923	4.17	4.229	4.229	230.9	463.346	56.726	162.601	219.327	230.9
0.85	2367	235500	-168.247	63930	-6.371	6.502	-10.884	7.994	4.229	4.055	4.229	233.1	548.03	56.726	162.601	219.327	233.1
0.9	2275	235500	-284.287	52180	-7.201	6.502	-10.884	7.994	4.229	3.832	4.229	233.2	670.33	56.726	162.601	219.327	233.2
0.95	2183	235500	-395.75	40430	-8.03	6.502	-10.884	7.994	4.229	3.626	4.229	233.3	862.489	56.726	162.601	219.327	233.3
1	2092	235500	-502.636	28670	-8.861	6.502	-10.884	7.994	4.229	3.437	4.229	233.4	1.21E+03	56.726	162.601	219.327	233.4
1.05	2000	235500	-604.946	16910	-9.691	6.502	-10.884	7.994	4.229	3.263	4.229	233.5	2.02E+03	56.726	162.601	219.327	233.5
1.1	1909	235500	-702.679	5136	-10.522	6.502	-10.884	7.994	4.229	3.103	4.229	233.6	6.05E+03	56.726	162.601	219.327	233.6

Table D-2: Results of calculations acc. to RBK 1.1 for beam LB10

Location [mm]	Shear force from self-weight [N]	Total shear force [N]	Bending moment due to self-weight [N*m]	Total bending moment [N*m]	Normal stress in concrete at the web-flange junction [MPa]	Shear stress in concrete at web-flange junction [MPa]	Compressive normal stress due to prestressing [MPa]	Shear stress at the centroid [MPa]	Principal tensile stress at centroid [MPa]	Principal stress at the web-flange junction	Max. value of principal stress equal to tensile strength [MPa]	Shear force resistance [kN]	Flexural cracking shear force $M_{cr}/(1200mm - x - 75mm)$	Shear force resistance 6.8 [N]	Shear resistance 6.2 [N]	RBK 1.1 Total shear resistance	Total shear resistance [kN]
0	3945	152000	2517	169000	-0.132	4.259	-11.158	5.093	1.975	4.194	4.194	148	138.624	113.021	165.458	278.479	278.479
0.05	3853	155800	2322	165600	-0.352	4.366	-11.158	5.222	2.062	4.194	4.194	151.9	145.253	113.021	165.458	278.479	278.479
0.1	3761	159800	2132	162000	-0.588	4.478	-11.158	5.355	2.154	4.194	4.194	156	152.525	113.021	165.458	278.479	278.479
0.15	3669	163900	1946	158200	-0.839	4.594	-11.158	5.494	2.251	4.194	4.194	160.2	160.537	113.021	165.458	278.479	278.479
0.2	3577	168200	1765	154100	-1.108	4.715	-11.158	5.639	2.353	4.194	4.194	164.6	169.411	113.021	165.458	278.479	278.479
0.25	3485	172700	1588	149700	-1.395	4.841	-11.158	5.789	2.461	4.194	4.194	169.2	179.293	113.021	165.458	278.479	278.479
0.3	3393	177400	1416	145000	-1.701	4.972	-11.158	5.946	2.575	4.194	4.194	174	190.368	113.021	165.458	278.479	278.479
0.35	3301	182300	1249	139900	-2.029	5.109	-11.158	6.109	2.694	4.194	4.194	179	202.865	113.021	165.458	278.479	278.479
0.4	3209	187300	1086	134600	-2.38	5.251	-11.158	6.279	2.82	4.194	4.194	184.1	217.08	113.021	165.458	278.479	278.479
0.45	3117	192600	928.035	128800	-2.754	5.398	-11.158	6.455	2.953	4.194	4.194	189.5	233.395	113.021	165.458	278.479	278.479
0.5	3024	198100	774.51	122700	-3.155	5.552	-11.158	6.639	3.093	4.194	4.194	195	252.312	113.021	165.458	278.479	278.479
0.55	2932	203800	625.589	116100	-3.584	5.711	-11.158	6.83	3.24	4.194	4.194	200.8	274.511	113.021	165.458	278.479	278.479
0.6	2840	209700	481.273	109100	-4.043	5.877	-11.158	7.028	3.395	4.194	4.194	206.8	300.93	113.021	165.458	278.479	278.479
0.65	2748	215800	341.561	101600	-4.533	6.05	-11.158	7.235	3.557	4.194	4.194	213.1	332.901	113.021	165.458	278.479	278.479
0.7	2656	222200	206.453	93520	-5.057	6.229	-11.158	7.449	3.727	4.194	4.194	219.6	372.384	113.021	165.458	278.479	278.479
0.75	2564	228800	75.95	84930	-5.617	6.415	-11.158	7.671	3.906	4.194	4.194	226.3	422.383	113.021	165.458	278.479	278.479
0.8	2472	235700	-49.949	75760	-6.216	6.607	-11.158	7.901	4.094	4.194	4.194	233.3	487.752	113.021	165.458	278.479	278.479
0.85	2380	239400	-171.244	65000	-6.917	6.71	-11.158	8.024	4.194	4.09	4.194	237	576.875	113.021	165.458	278.479	278.479
0.9	2288	239400	-287.934	53060	-7.697	6.71	-11.158	8.024	4.194	3.887	4.194	237.1	705.589	113.021	165.458	278.479	278.479
0.95	2196	239400	-400.02	41110	-8.476	6.71	-11.158	8.024	4.194	3.698	4.194	237.2	907.826	113.021	165.458	278.479	278.479
1	2104	239400	-507.501	29150	-9.256	6.71	-11.158	8.024	4.194	3.523	4.194	237.3	1272	113.021	165.458	278.479	278.479
1.05	2011	239400	-610.378	17190	-10.036	6.71	-11.158	8.024	4.194	3.361	4.194	237.4	2121	113.021	165.458	278.479	278.479
1.1	1919	239400	-708.651	5228	-10.817	6.71	-11.158	8.024	4.194	3.21	4.194	237.5	6367	113.021	165.458	278.479	278.479

Table D-3: Results of calculations acc. to RBK 1.1 for beam LB11

Location [mm]	Shear force from self-weight [N]	Total shear force [N]	Bending moment due to self-weight [N*m]	Total bending moment [N*m]	Normal stress in concrete at the web-flange junction [MPa]	Shear stress in concrete at web-flange junction [MPa]	Compressive normal stress due to prestressing [MPa]	Shear stress at the centroid [MPa]	Principal tensile stress at centroid [MPa]	Principal stress at the web-flange junction	Max. value of principal stress equal to tensile strength [MPa]	Shear force resistance [kN]	Flexural cracking shear force $M_{cr}/(1200mm - x - 75mm)$	Shear resistance 6.8 [N]	Shear resistance 6.2 [N]	RBK 1.1 Total shear resistance	Total shear resistance [kN]
0	3951	151200	2524	168100	-0.135	4.261	-10.971	5.067	1.982	4.194	4.194	147.2	137.467	113.021	163.454	276.475	276.475
0.05	3859	154900	2329	164700	-0.354	4.367	-10.971	5.193	2.068	4.194	4.194	151.1	144.042	113.021	163.454	276.475	276.475
0.1	3766	158900	2138	161100	-0.587	4.478	-10.971	5.325	2.159	4.194	4.194	155.1	151.255	113.021	163.454	276.475	276.475
0.15	3674	162900	1952	157200	-0.836	4.593	-10.971	5.462	2.255	4.194	4.194	159.3	159.202	113.021	163.454	276.475	276.475
0.2	3582	167200	1771	153100	-1.102	4.713	-10.971	5.604	2.357	4.194	4.194	163.6	168.004	106.767	163.454	270.221	270.221
0.25	3490	171600	1594	148700	-1.386	4.838	-10.971	5.753	2.463	4.194	4.194	168.1	177.806	95.599	163.454	259.053	259.053
0.3	3398	176200	1422	144000	-1.69	4.967	-10.971	5.907	2.576	4.194	4.194	172.8	188.791	84.431	163.454	247.885	247.885
0.35	3306	181000	1254	139000	-2.014	5.102	-10.971	6.067	2.694	4.194	4.194	177.7	201.187	73.263	163.454	236.717	236.717
0.4	3213	186000	1091	133600	-2.36	5.243	-10.971	6.234	2.819	4.194	4.194	182.8	215.287	62.094	163.454	225.548	225.548
0.45	3121	191200	932.644	127900	-2.73	5.389	-10.971	6.408	2.95	4.194	4.194	188	231.469	50.926	163.454	214.38	214.38
0.5	3029	196500	778.888	121700	-3.125	5.54	-10.971	6.588	3.087	4.194	4.194	193.5	250.232	39.758	163.454	203.212	203.212
0.55	2937	202100	629.742	115200	-3.548	5.698	-10.971	6.776	3.232	4.194	4.194	199.2	272.251	28.59	163.454	192.044	199.2
0.6	2845	208000	485.204	108200	-3.999	5.862	-10.971	6.971	3.385	4.194	4.194	205.1	298.455	17.422	163.454	180.876	205.1
0.65	2752	214000	345.275	100700	-4.482	6.032	-10.971	7.173	3.544	4.194	4.194	211.2	330.166	6.254	163.454	169.708	211.2
0.7	2660	220300	209.954	92690	-4.997	6.209	-10.971	7.383	3.712	4.194	4.194	217.6	369.327	0	163.454	163.454	217.6
0.75	2568	226800	79.243	84150	-5.547	6.392	-10.971	7.601	3.888	4.194	4.194	224.2	418.92	0	163.454	163.454	224.2
0.8	2476	233500	-46.86	75030	-6.135	6.582	-10.971	7.826	4.072	4.194	4.194	231	483.757	0	163.454	163.454	231
0.85	2384	237900	-168.354	64600	-6.807	6.706	-10.971	7.975	4.194	4.117	4.194	235.5	572.154	0	163.454	163.454	235.5
0.9	2292	237900	-285.24	52730	-7.572	6.706	-10.971	7.975	4.194	3.915	4.194	235.6	699.819	0	163.454	163.454	235.6
0.95	2199	237900	-397.516	40850	-8.338	6.706	-10.971	7.975	4.194	3.728	4.194	235.7	900.409	0	163.454	163.454	235.7
1	2107	237900	-505.184	28970	-9.104	6.706	-10.971	7.975	4.194	3.553	4.194	235.8	1.26E+03	0	163.454	163.454	235.8
1.05	2015	237900	-608.243	17080	-9.87	6.706	-10.971	7.975	4.194	3.392	4.194	235.9	2.10E+03	0	163.454	163.454	235.9
1.1	1923	237900	-706.694	5193	-10.636	6.706	-10.971	7.975	4.194	3.241	4.194	236	6.32E+03	0	163.454	163.454	236

Bibliography

[1] Wikipedia.com, *Autosnelweg*.

[2] E. J. O'Brien, A. S. Dixon, and E. Sheils, *Reinforced and prestressed concrete design to EC2: the complete process*. Spon Press, 2012.

[3] R. I. Gilbert and N. C. Mickleborough, *Design of prestressed concrete*. CRC Press, 1990.

[4] M. P. Collins and D. Mitchell, *Prestressed concrete structures*, vol. 9. Prentice Hall Englewood Cliffs, NJ, 1991.

[5] J. C. Walraven, *Aggregate interlock: a theoretical and experimental analysis*. PhD thesis, TU Delft, Delft University of Technology, 1980.

[6] S. Sun, *Shear Behavior and Capacity of Large Scale Prestressed High Strength Concrete Bulb-Tee Girders*. ProQuest, 2007.

[7] M. P. Collins, D. Mitchell, P. Adebar, and F. J. Vecchio, "A general shear design method," *ACI Structural Journal*, vol. 93, no. 1, pp. 36–45, 1996.

[8] J. Walraven and C. Braam, "Prestressed concrete," 2013.

[9] T. T. Hsu and Y.-L. Mo, *Unified theory of concrete structures*. John Wiley & Sons, 2010.

[10] J. Jacobs, "Eurocode 2–commentary," *European Concrete Platform ASBL, Brussels*, 2008.

[11] L. Taerwe, S. Matthys, *et al.*, "fib model code for concrete structures 2010," 2013.

[12] E. C. Bentz and M. P. Collins, "Development of the 2004 canadian standards association (csa) a23. 3 shear provisions for reinforced concrete," *Canadian Journal of Civil Engineering*, vol. 33, no. 5, pp. 521–534, 2006.

[13] L. Xie, *The influence of axial load and prestress on the shear strength of web-shear critical reinforced concrete elements*. PhD thesis, 2009.

[14] K. Maekawa, H. Okamura, and A. Pimanmas, *Non-linear mechanics of reinforced concrete*. CRC Press, 2003.

[15] R. D. Cook, *Finite element modeling for stress analysis*. Wiley, 1994.

[16] M. Holicky, J. Markova, and M. Sykora, "Assessment of deteriorating reinforced concrete road bridges," in *Proceedings of European Safety and Reliability Conference (ESREL 2009)*, pp. 1–3, 2010.

[17] F. J. Vecchio and M. P. Collins, "The modified compression-field theory for reinforced concrete elements subjected to shear.," *ACI J.*, vol. 83, no. 2, pp. 219–231, 1986.

[18] R. K. Dhir and E. B. Jones, M Roderick; article's authors: M.P. Collins, *Innovation in Concrete Structures: Design and Construction: Proceedings of the International Conference Held at the University of Dundee, Scotland, UK on 8-10 September 1999; article: Investigating Shear Failure in Reinforced Concrete Structures*. Thomas Telford, 1999.

[19] J. G. Van Mier, *Fracture processes of concrete*, vol. 12. CRC press, 1996.

[20] Y. Yang, *Shear Behaviour of Reinforced Concrete Members without Shear Reinforcement: a New Look at an Old Problem*. TU Delft, Delft University of Technology, 2014.

[21] P. Adebar and M. P. Collins, "Shear strength of members without transverse reinforcement," *Canadian journal of civil engineering*, vol. 23, no. 1, pp. 30–41, 1996.

[22] B. S. Institution, *Eurocode 2: Design of Concrete Structures: Part 1-1: General Rules and Rules for Buildings*. British Standards Institution, 2004.

[23] D. A. Kuchma and M. P. Collins, "Advances in understanding shear performance of concrete structures," *Progress in Structural Engineering and Materials*, vol. 1, no. 4, pp. 360–369, 1998.

[24] V. Sigrist, E. Bentz, M. F. Ruiz, S. Foster, and A. Muttoni, "Background to the fib model code 2010 shear provisions–part i: beams and slabs," *Structural Concrete*, vol. 14, no. 3, pp. 195–203, 2013.

[25] V. Sigrist, "Assessment of structural concrete members using the fib modelcode 2010 shear provisions," in *IABSE Symposium Report*, vol. 99, pp. 1687–1693, International Association for Bridge and Structural Engineering, 2013.

[26] C. H. B. D. Code, "and commentary on can/csa s6 06. 2006," *CSA Special Publication S*, vol. 6, pp. 1–06.

[27] J. G. Rots, *Computational modeling of concrete fracture*. PhD thesis, Technische Hogeschool Delft, 1988.

[28] J. Manie, W. Kikstra, and T. D. BV, "Diana-9.4. 4 userâĂŹs manualâĂŤmaterial library," 2012.

[29] M. Hendriks, J. den Uijl, A. De Boer, P. Feenstra, B. Belletti, and C. Damoni, "Guidelines for nonlinear finite element analysis of concrete structures," *Rijkswaterstaat Technisch Document (RTD), Rijkswaterstaat Centre for Infrastructure, RTD*, vol. 1016, p. 2012, 2012.

[30] C.-F. M. Code, "Model code for concrete structures," *Bulletin D'Information*, no. 117-E, 1990.

[31] P. Feenstra, "Implementing an isotropic damage model in diana. use-case for the user-supplied subroutine usrmat," in *Proceedings of the Third DIANA World Conference*, pp. 89–97, 2002.

[32] N. Bicanic, H. Mang, G. Meschke, a. a. P. H. de Borst, René, and J. Kollegger, *Computational modelling of concrete structures, article: Numerical simulation of shear behaviour of reinforced concrete beams with and without flanges*. CRC Press, 2014.

[33] J. Sagaseta and R. Vollum, "Non-linear finite element analysis of shear critical high strength concrete beams," *Architecture Civil Engineering Environment*, vol. 2, pp. 95–105, 2009.

[34] B. Bresler and A. C. Scordelis, "Shear strength of reinforced concrete beams," in *Journal Proceedings*, vol. 60, pp. 51–74, 1963.

[35] V. S. Britta Hackbarth, "Structural assessment of bridge girders in shear," *fib Symposium PRAGUE 2011*, 2011.